Australian Water Recycling
Centre of Excellence

Project Report

National Validation Guidelines for Water Recycling: Reverse Osmosis Membranes

A Report of a study funded by the
Australian Water Recycling Centre of Excellence

The University of Queensland, September 2015

National Validation Guidelines for Water Recycling: Reverse Osmosis Membranes

Project Leader

Marie-Laure Pype
Advanced Water Management Centre
University of Queensland
Level 4, Gehrmann Building, Research Road
Saint Lucia QLD 4072, AUSTRALIA

Contact: Marie-Laure Pype   m.pype@awmc.uq.edu.au

Partners

The University of Queensland
The University of New South Wales
Curtin University
Victoria University
West Australian Water Corporation

About the Australian Water Recycling Centre of Excellence

Disclaimer

Executive summary

Validation and monitoring of treatment by high pressure membranes (reverse osmosis - RO, and nanofiltration - NF) is critical to ensure the risk to public health associated with pathogens is adequately managed. To-date, there is no accepted Australian or international validation protocol for this type of membranes despite conventional monitoring techniques, such as electrical conductivity (EC; only for RO), total organic carbon (TOC) or sulfate rejection, having been used for this purpose albeit based on ad-hoc approval by regulators. An agreed validation protocol establishing a correlation between log removal value (LRV) and indirect continuous online monitoring would provide confidence to recycled water treatment plant operators and project developers. In particular the ability to accredit LRV of three and above could reduce the investment costs and simplify treatment process trains by removing unnecessary treatment barriers.

The NatVal 2.2 sub-project 2 aimed to create a framework based on literature review, operational experience from stakeholders, experimental results, scientific knowledge and manufacturer software to develop validation and verification monitoring protocols for the rejection of pathogens (in particular viruses) using online monitoring and challenge testing techniques for RO/NF. This document compiles all experimental data produced under the sub-project 2 necessary to develop the validation framework.

This report is composed of five main sections and two appendices. After a brief introduction, the first part of the document provides an overview of the three types of removal mechanisms by RO/NF membranes and especially the ones involved in virus removal. This section also introduces the existing monitoring techniques and their correlation with virus surrogate (MS2 phage) from data gathered from the literature. The second part of the report presents the results of the study conducted to understand the impact of the operating conditions on surrogates' rejection. The third main section identifies spiked salt as a new surrogate. Finally, Sections four and five present the impact of fouling/ageing cycles on the rejection of MS2 phage and EC. The two appendices are studies conducted in parallel on: (i) the development of a new electrochemical sensor for online measurement of sulfate; and (ii) testing the commercially available sensor S::CAN in full-scale.

Literature review

High pressure membranes are the most effective physical barrier to remove inorganic and organic contaminants including pathogens such as viruses. Viruses are the smallest pathogens and the ones found in wastewater can be as small as 24 nm. High pressure membranes are using three different types of removal mechanisms: size exclusion, charge repulsion and adsorption/diffusion. The main removal mechanism for viruses is size exclusion, and charge repulsion improves their removal. Membrane studies generally used MS2 phage as virus model due to its characteristics being similar to enteric viruses (size and surface charge). The advantages of this surrogate are the possibility to culture in high quantity and the fact that it is harmless to human health. However, its quantification is time consuming (24h) and not practical in full-scale application. Hence, it is advantageous to find a non-biological surrogate to avoid the risk involved in performing challenge test with native viruses. Moreover, the use of non-biological surrogate allows online or near online measurement which is currently not possible with live organism such as bacteriophages.

The USEPA Long Term 2 Enhanced Surface Water Treatment Rule (LT2ESWTR) has driven many of the requirements regarding membrane monitoring. According to this rule, both indirect and direct integrity testings are required. The membrane filtration guidance manual (USEPA, 2005a) defines a direct integrity test as "a physical test applied on each membrane unit and monitored on a daily basis in order to identify and/or isolate integrity breaches" including pressure- and marker-based methods. Indirect integrity test is the "monitoring of some aspect of filtrate water quality that is indicative of the removal of particle matter at a frequency of no less than once every 15 minutes" (USEPA, 2005a). To date, different direct and indirect monitoring techniques are used in full-scale using specific surrogates. According to the Australian Guidelines for Water Recycling (NRMMC *et al.*, 2008), a surrogate is defined as a "parameter or combination of parameters that can be used to assess the quality of water; a specific contaminant, group of contaminants or constituent that signals the presence of something else (e.g. the presence of *Escherichia coli* can be taken to indicate the likely presence of pathogenic bacteria)". The surrogates and monitoring techniques found in the literature are briefly described below.

Rhodamine WT (R-WT)

Rhodamine WT is a non-reactive dye chemical approved by the USEPA for use in drinking water (Zornes *et al.*, 2010). It has a molecular weight (MW) of 487 g·mol^{-1} and a pKa of 5.1. Thus, this marker should be well removed by high pressure membranes due to its larger size than the membrane cavities (size exclusion mechanism) and its negative charge at a typical feedwater pH (charge repulsion mechanism). For these reasons, and also due to its low cost and ease to quantify by fluorescence, R-WT is considered an appropriate non-microbiological alternative to MS2 phage. Its rejection by RO membrane ranged from 2.8 - 4 LRV.

Pulsed marker technique

This technique is a deviation of the R-WT monitoring technique. A high concentration of dye is pulse-spiked in the feed side and monitored online by fluorescence detection in the permeate side. This technique permits validating RO membrane for 3.3 – 4.3 LRV using uranine (Surawanvijit *et al.*, 2015). Uranine is also a non-reactive, non-toxic tracer dye (Smart and Laidlaw, 1977; Behrens *et al.*, 2001) having a MW of 332 g·mol^{-1}, which is lower than R-WT.

TRASAR^{TM}

TRASAR^{TM} (Nalco company) is a fluorescent tracer dye attached to an antiscalant and it is also gaining interest (Kelle Zeiher *et al.*, 2003; Portillo, 2015). The cities of San Diego (California, USA) and Big Spring (Texas, USA) conducted a study comparing MS2 phage and TRASAR$^{®}$ integrity monitoring techniques (MWH, 2007; Steinle-Darling *et al.*, 2015). TRASAR$^{®}$ was dosed continuously as pure chemical to the RO feed and the permeate concentration was determined using a portable microprocessor-based analyser (TRASAR$^{®}$ Pen Fluorometer, Nalco). Under this condition, the TRASAR$^{®}$ marker achieved more than 4 LRV.

Total organic carbon (TOC)

Total organic carbon measurement is one of the current online techniques used in full-scale to monitor RO membranes but it can only be used to validate LRVs typically below 3 due to the limited rejection of organics by the RO process (Adham *et al.*, 1998a; Adham *et al.*, 1998b; Kitis *et al.*, 2003a; Kumar *et al.*, 2007). It can also be argued that TOC rejection varies during operation as it is a function of the organic composition. Nevertheless, TOC compounds are smaller than viruses by at least an order of magnitude and thus TOC will always be more conservative than virus measurement.

Electrical conductivity (EC)

Electrical conductivity is one of the current online techniques used to monitor the integrity of the RO process. It measures all the ions present in the feed and permeate water. This technique can currently validate this process for 1.4 - 2 LRV (Zornes *et al.*, 2010; Pype, 2013b).

Sulfate

Sulfate (SO_4^{2-}) is already used in some plants to monitor the integrity of RO membranes. To date, sulfate is measured offline by ion chromatography as there is no online monitoring technique. The advantage of sulfate is its natural presence in feed water which can be used to validate up to 3 LRV (Kruithof *et al.*, 2001b). In the case of low sulfate feed concentration, $MgSO_4$ can be spiked into the feed water to theoretically obtain 3 LRV. Appendix 1 of this report refers to research conducted within this project to develop a new online sulfate sensor using electrochemical techniques. Different tests have been carried using a commercially available ionophore which binds to sulfate ions. The ionophore helps to transfer sulfate from one phase (the RO feed or permeate) into the sensor phase. A sulfate sensor prototype was developed with a limit of detection (LOD) of 0.6 µM using this commercially available ionophore combined to a pre-concentration step. Selectivity studies for a range of anions (PO_4^{3-}, $H_2PO_4^-$, SO_3^{2-}, NO_3^-, CH_3COO^-, OH^-, Cl^- and SCN^-) were carried out which showed potential interferences by the ions PO_4^{3-}, NO_3^-, OH^-, Cl^-. To date, chloride ions interfere in the sulfate measurement, but this might be reduced using electrolysis to remove chloride, and the use of new, improved ionophores.

Dissolved organic matter (DOM)

Dissolved organic matter (DOM) is a heterogeneous mixture of aromatic and aliphatic hydrocarbon structures containing different functional groups. In the last decade, the use of excitation-emission matrix fluorescence (EEM) has been widely studied to analyse DOM in aquatic samples (Chen *et al.*, 2003; Leenheer and Croue, 2003; Her *et al.*, 2008; Singh *et al.*, 2009; Hambly *et al.*, 2010; Peiris *et al.*, 2010a; Peiris *et al.*, 2010b). Recently, two research groups demonstrated the feasibility to monitor the integrity of RO process using DOM rejection analysed by EEM (Singh *et al.*, 2012; Pype *et al.*, 2013). With this technique, it is feasible to obtain 1.9 – 2.7 log credit.

S::CAN

S::CAN is a commercially available UV/visible spectrometer sensor able to monitor different water quality parameters including TOC, EC, turbidity and total suspended solids (TSS) as well as specific groups of organic contaminants. This sensor is of interest in the context of validation as it is able to measure up to eight parameters simultaneously, which could support the online monitoring of RO/NF integrity. Thus in the context of the NatVal project, this sensor has been tested to measure specific operational parameters including TOC, R-WT and some organic contaminants and indicator compounds such as metolachlor, trifluralin, metformin, carbamazepine and N-Nitrosodimethylamine in RO water. The findings of this study are presented in Appendix 2, and briefly summarised as follows:

- Due to the S::CAN low sensitivity and selectivity, it was not possible to directly measure organic contaminants at concentration limits described within drinking water guidelines, except for the pharmaceutical carbamazepine (NHMRC and NRMMC, 2011). S::CAN was only able to demonstrate 3 LRV for R-WT under standard challenge testing conditions and an online fluorescence probe would be better suited to demonstrate 4 LRV of R-WT.
- TOC monitoring using S::CAN was compared to a more conventional online Sievers TOC analyser. It was difficult to correlate the results from these two instruments as the varying offsets between the two trends could either be a function of the instrument, substrate or calibration issues.

Conclusions

The aim of the NatVal project was not to develop a new surrogate or a new monitoring technique, but to provide all the information necessary to support a validation framework. Several surrogates and membrane integrity monitoring are found in the literature and have been described previously. Electrical conductivity, TOC and sulfate are already used in full-scale to monitor the integrity of RO membranes. Dissolved organic matter is another surrogate naturally present in feed water gaining interest. From the literature data, a correlation study has been conducted in order to determine the best potential surrogate for MS2 phage. This correlation study proved that R-WT is a good substitute to MS2 phage in contrast to EC. Sulfate and DOM have the potential to be used to validate the RO/NF process up to 3 LRV, which is lower than MS2 phage but higher than EC. Thus, they are of high interest in the context of NF/RO validation and have been selected for further research.

Impact of operating conditions

The rejection of surrogates depends on their own properties, but also on the operating conditions (e.g. feed pressure, cross-flow velocity, etc.), the type of membranes and the feed water quality (Antony *et al.*, 2012). It is important to ensure that the selected surrogates are not better rejected than viruses in order to remain conservative, but also to understand the influence of these factors to select the best conditions to conduct process validation.

The rejections of MS2 phage, R-WT, DOM, sulfate and EC were studied as a function of cross-flow velocity, permeate flux, recovery, membrane types, feed temperature, pH and ion strength within the operating range determined by membrane manufacturers. The benchmark conditions were at permeate flux 20 L·m^2·h, cross-flow velocity 0.1 m·s^{-1}, 22 ± 0.5^{0}C and pH 7 using a flat-sheet cross-flow bench-scale filtration system with concentrate and permeate recirculation. The recovery experiment was conduct with a single 4" spiral wound module membrane.

Table 1 summarises the results of this study. Overall, the removal of MS2 phage was not influenced by changes in operating conditions and membrane types. Under all conditions, the LRV was higher than 4, which is the maximum LRV Australian regulators will credit to a single process (NRMMC *et al.*, 2008). In general, only the solutes (sulfate and EC) were significantly impacted by changes in operating conditions.

Table 1. Impact of operating conditions on surrogates' rejection.

Operating conditions	Rejection					
	MS2 phage	R-WT	DOM		Sulfate	EC
↗ Permeate flux	→	→	→		↗	↗
↗ Cross-flow velocity	→	→	Membrane dependant		↗	↗
↗ Recovery	→	↘	↗		↗	↗
pH ↗ from 3 to 5	→	→	→		↗	↗
pH ↗ from 5 to 8	→	↗	→		→	↗
pH ↗ from 8 to 10	N/A	→	→		↘	↘
↗ Temperature	→	↘	↘		↗	↘

↗: increase   ↘: decrease   →: no impact.
N/A: not applicable.

Identification of target pathogens or surrogates – spiked salt rejection through electrical conductivity

Spiked salt conductivity is a simple test employed as quality assurance testing for RO membrane integrity, recommended by manufacturers. Commonly this test involves spiking 2000 ppm NaCl for a brackish water RO membrane or $MgSO_4$ for a NF membrane and challenge testing at an applied pressure of 7 – 15 bar. The type of salts, concentration and operating pressures may vary for different manufacturers. Performance of spiked salt testing on a regular basis during operation would enable the comparison of current against benchmarked initial performance. Although the separation behaviour of salt is independent of MS2 or any other specific pathogen of concern, its rejection efficiency can be taken as a more conservative indication of the state of the membrane. Also, spiked salt rejection can be especially useful when the feedwater conductivity is low (i.e. the LRV_{EC} able to be demonstrated is limited by sensitivity of permeate conductivity meters). In addition, already installed online conductivity sensors can be used for membrane performance. For pristine and aged RO membranes tested in this study, LRV_{NaCl} was up to 4 times lower than the corresponding LRV_{MS2} and also correlated well. Given the significantly smaller size of NaCl (the hydrated size of Na^+ is 0.36 nm and Cl^- is 0.33 nm compared with the diameter of MS2 - 26 nm) and the correlation observed in this study, spiked salt rejection can be considered as a highly conservative procedure for confirmation of LRV_{MS2}. A correlation of LRV_{MS2} and LRV_{NaCl} values obtained for RO membrane tested at different levels of ageing during four different cyclic ageing experiments is presented in Figure 1.
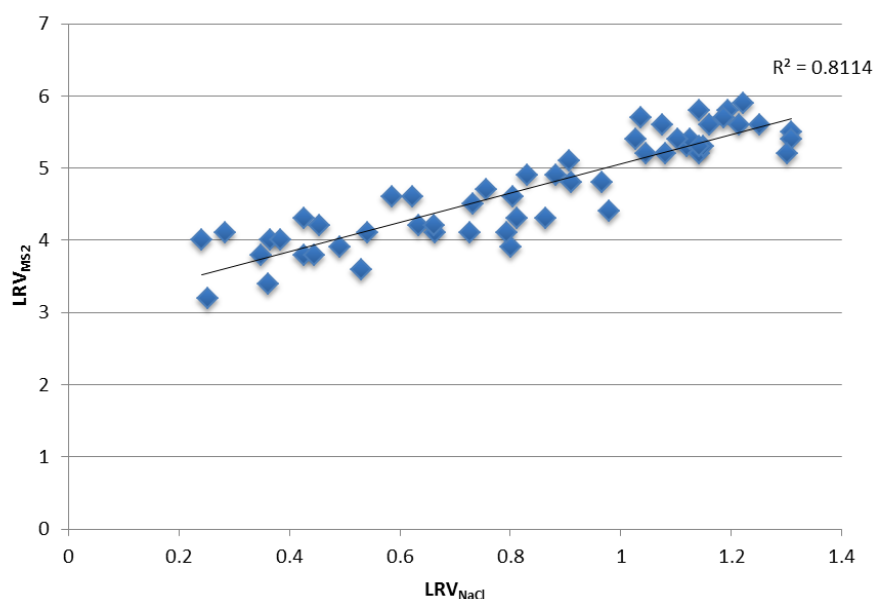

Figure 1. Correlation between LRV$_{NaCl}$ and LRV$_{MS2}$ for RO membrane tested at different degree of ageing during four cycling experiments.

Influencing factors of RO membrane performance - ageing

Although membrane ageing is known to change the physicochemical properties of the membrane active layer, the virus rejection efficiency was observed to remain consistent, under certain conditions. In a controlled lab experiment, LRV_{MS2} for virgin RO membrane was > 6.2 with salt rejection of 97% (2000 ppm NaCl); aged membranes, featuring salt rejection as low as 80%, consistently resulted on LRV_{MS2} values greater than 4. Also, industrially aged membranes of 2 - 5 years, tested in this study, were still a resilient barrier for MS2 sized particles, LRV_{MS2} always greater than 4.6. For the industrially aged membranes tested, when compared with aged virgin membranes, a higher LRV_{MS2} was observed at equivalent conductivity removal, but permeability was lower, suggesting development of an irreversible fouling layer. The irreversible fouling layer may assist with preservation of virus rejection, however, the reduction in conductivity removal and permeability decline would likely trigger membrane replacement, prior to significant reductions in LRV. Therefore, the potential risk of membranes losing their integrity as a mechanical barrier to pathogens (considering the smallest virus size is 24 nm) due to ageing is considered to be marginal.

Conclusions

In the context of validation
Two indicators are generally used for challenge testing:
- MS2: the operating conditions do no influence its removal.
- R-WT: Table 1 showed that operating condition impacts on its rejection. Thus, the RO process should select the operating conditions giving the lowest LRV_{R-WT}:
  - pH < 5
  - high temperature
  - high permeate recovery

In the context of operation monitoring
The following parameters should be monitored:
- Permeate flux
- Cross-flow velocity
- Recovery
- pH
- Temperature

In the context of Integrity monitoring
Several indicators can be used depending on how many LRVs the RO process aims to demonstrate.
- EC (1-1.5 LRV; online measurement)
- TOC (~2 LRV; online measurement)
- DOM (~2 LRV; offline measurement)
- Sulfate (~2.5 LRV; offline measurement)

The LRV of these indicators can be limited by the detection limit of the analytical instrument or the feed water concentration. Thus, indicator spiking such as sulfate or salt in the RO feed can increase its LRV.

Monitor RO process at around 4 LRV is feasible by using R-WT and TRASAR dyes, but it is more costly. TRASAR is a monitoring technique gaining interest, and more studies are needed to correlation its rejection to virus rejection.

In the context of revalidation
Operating condition might change over the year, due to the need of increasing water production for example. Revalidation of the RO process will depend on the type of indicator used to initially validate the RO process. A revalidation will not be necessary when using MS2 phage as its rejection is not impacted within the operating condition range determined by membrane manufacturer.

Table of Contents

List of Figures

List of Tables

List of Abbreviations

AGWR	Australian Guidelines for Water Recycling
AWRP	advanced water recycling plant
BOD	bio-chemical oxygen demand
BTPPA$^+$	bis(triphenylphosphoranyliden)ammonium
BTX	mixture of benzene, toluene, and the three xylene isomers
COD	chemical oxygen demand
CP	concentration polarisation
C:	cyclic voltammetry
DCE	1,2-dichloroethane
DCH	1,6-dichlorohexane
DCM	DCM Process Control Ltd, specialist supplier for S::CAN and Spectro::lyser™ probes
DI	deionized water
DOC	dissolved organic carbon
DOM	dissolved organic matter
DWG	drinking water guidelines
Eff	effluent
IC	ion chromatography
Ip	Isoelectric point
LC	liquid chromatography
LRV	log removal value
LT2ESWTR	long term 2 enhanced surface water treatment rule
MF	microfiltration
MW	molecular weight
MWCO	molecular weight cut-off
NB	nitrobenzene
NF	nanofiltration
NO$_3$-N	nitrogen as nitrates
NPOE	o-nitrophenyl octyl ether
PA	polyamide
PES	polyethersulfone
RO	reverse osmosis
R-WT	rhodamine WT
S-I	sulfate-ionophore I
SV	stripping voltammetry
TPBCl$^-$	tetrakis(4-chlorophenyl)borate
TEA$^+$Cl$^-$	tetraethylammonium chloride
TMP	transmembrane pressure
TOC	total organic carbon
TSS	total suspended solids
UF	ultrafiltration
USEPA	US Environmental Protection Agency
UV$_{254}$	UV signal measured at 254 nm
UV/Vis	Ultraviolet/visible absorption spectroscopy
WWTP	wastewater treatment plant

List of Nomenclature

Π	osmotic pressure (bar)
ε	attenuation coefficient ($L \cdot mol^{-1} \cdot cm^{-1}$)
Ψ	electrical potential ($J \cdot C^{-1}$)
θ	contact angle (°)
a	activity of the solutes
C	compound concentration ($mg \cdot L^{-1}$)
Da	dalton
F	Faraday constant ($C \cdot mol^{-1}$)
J_w	permeate flux ($L \cdot h^{-1} \cdot m^{-2}$)
K	constant characteristic of active layer membrane material
K_w	water permeability ($L \cdot h^{-1}$)
K_{ow}	octanol-water partition coefficient
ML/d	megalitres per day
NDP	net driving pressure (bar)
O	organic
P	pressure (bar)
pKa	logarithm of the ionisation constant Ka
R	gas constant ($J \cdot mol^{-1} \cdot K^{-1}$)
$R_\%$	compound rejection (%)
$R_{\%p}$	product recovery (%)
S	membrane area (m^2)
T	temperature (K or °C)
TCF	temperature coefficient factor
TMP	transmembrane pressure (bar)
W	water
z	valence of the ion

Subscripts

A	cation
aq	aqueous phase
B	anion
Don	Donnan
f	bulk feed solution
m	membrane surface
p	permeate
org	organic phase

1. Introduction

As communities are increasingly turning to recycled water to ease ongoing water shortages, membrane filtration of secondary effluent is fast becoming a commonly used tertiary treatment process for the production of fit-for-purpose recycled water. The Australian Guidelines for Water Recycling (AGWR) provide a framework for producing recycled water that is fit-for-purpose (NRMMC *et al.*, 2006). In the case of reducing the risk associated with microbial pathogens the guidelines prescribe a performance target based on a log reduction in the pathogen concentration from the raw water to the final product water. These guidelines, based on the risk assessment from sewage to the exposure scenario of indirect potable reuse (IPR), require a log removal above 9.5 for pathogenic viruses and a log removal above 8 for pathogenic bacteria and two protozoa: *Giardia* and *Cryptosporidium* (NRMMC *et al.*, 2006, 2008).

While the AGWR provide guidance on the use of treatment barriers, such as filtration, and preventative measures, such as controlled access, it is the responsibility of State Governments to assign log removal values (LRV) to these barriers and preventative measures. While there are adequate guidelines and/or regulations available for low pressure membrane systems used in water treatment for the removal of protozoan cysts and oocysts, established guidelines for validation and integrity monitoring of high pressure membrane systems like RO in water recycling or drinking water applications are limited. The LRVs are established through validation using a product specific challenge test, generally with MS2 phage and verified by operational monitoring tests. Other than challenge test data established prior to going into full scale operation, there is no information available on the correlation between the integrity tests performed and long-term virus removal (Antony *et al.*, 2012).

The RO process must be continuously monitored to ensure its correct operation to prove the log rejection that it has been validated for. To monitor the integrity of RO membranes and continuously assess their rejection performance, online electrical conductivity (EC) and total organic carbon (TOC) measurement are generally used to measure performance of critical control points (CCPs) (Adham *et al.*, 1998a; Kumar *et al.*, 2007). CCPs are validated preventive measures associated with removal of target criteria (such as viruses). The performance (sometimes expressed by 'log removal') of CCPs can be validated by once-off challenge testing using the target contaminant or a surrogate (such as a virus or virus-like particle), and this performance is then related to a set-point for the operational performance measure (usually EC) that can be measured online. This operational performance set-point is referred to as the critical limit for the process, which needs to be maintained to reduce risks to acceptable levels (NRMMC *et al.*, 2008).

EC is a good surrogate measurement for rejection of ions by the membrane, which is typically 1.4 - 2 log removal value (LRV; 96 - 99%). A major disadvantage is that rejection of ions measured by EC tends to underestimate the performance of RO membranes with regards to the rejection of microorganisms including viruses (Kitis *et al.*, 2003a). Other monitoring techniques have been studied to improve the monitoring of microorganisms rejection. In this sense, online TOC monitoring (2.3 - 3 LRV) has shown to be a better measure of their rejection than online EC (Adham *et al.*, 1998b). Nowadays, for full-scale RO plants, rhodamine WT (R-WT; 2.75 - 4 LRV depending on its concentration in feed water among other things) has been successfully used during initial plant validation and online EC, online TOC and offline sulfate measurement (2.4 - 2.8 LRV) are used for operational monitoring of integrity (Zornes *et al.*, 2010).

In order to establish the removal efficiency of a RO process, challenge test and direct integrity testing are used. Membrane integrity tests are used periodically to assure the correct performance of the system and are classified into direct[1] and indirect[2] methods. These tests have been described in different reports and review publications (USEPA, 2005a; ASTM, 2010; Antony *et al.*, 2012; Frenkel *et al.*, 2014), and are briefly described in the following parts. The system should be periodically verified by direct method testing and continuously by indirect method. The existing integrity methods are reliable and sensitive only for particle matter larger than 1 µm for low and high pressure membrane operations. The maximum removal credit of the system is the lower value of the removal efficiency determined by the challenge testing or the maximum LRV that can be verified by direct monitoring (USEPA, 2005a). However, to protect public health from microbial risk, it is essential to understand the virus removal mechanism to develop a monitoring test able to detect a loss of RO membrane integrity responsible for virus passage.

---

[1] Direct method: "a physical test applied to a membrane unit in order to identify and/or isolate integrity breaches" (USEPA 2005).

[2] Indirect method: "monitoring some aspect of filtrate water quality that is indicative of the removal of particulate matter" (USEPA 2005).

2. Literature review

2.1. Removal mechanism by high pressure membranes

High pressure membranes are made of three layers. The first (top) layer is a semi-permeable membrane made of polyamide (PA), which is pH resistant, rough, slightly negatively charged and has hydrophilic character (Figure 2). This layer is responsible for the passage of water and the rejection of dissolved species. Reverse osmosis (RO) membrane is generally made of a few hundred nanometres fully aromatic polymer, whereas nanofiltration (NF) is composed of a thinner either fully or semi aromatic polymer (Petersen, 1993; Freger *et al.*, 2002; Tang *et al.*, 2009). This difference in structure characterise the difference between RO and NF membranes. RO membranes have a tighter structure than NF permitting the rejection of smaller and less charged solute; whereas, NF has higher water permeability than RO. The second layer is a thick and spongy layer made of polyethersulfone (PES), which permits high water permeability. It serves as structural support for the first layer. Finally, the last layer is a fabric backing, which gives stiffness to the membrane.

Size exclusion and charge repulsion are the principal removal mechanisms of RO/NF membranes. However, depending on the compound properties, adsorption and diffusion mechanisms can also play a role for its rejection.
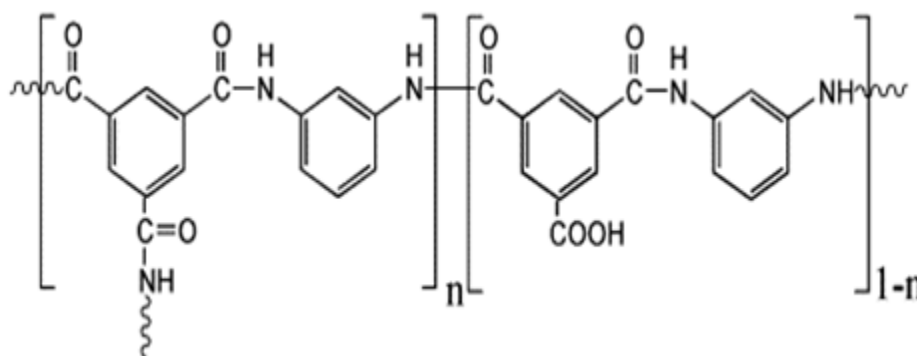
Figure 2. Fully aromatic PA layer (Tang et al., 2009).

2.1.1. Size exclusion

RO/NF membranes are non-porous membrane, but possess polymer material-free void spaces with various shapes (circular or not) possibly forming a continuous and interconnected network (Meares, 1976; Kamide and Iijima, 1994; Košutić *et al.*, 2000). The size of the material-free void spaces is not unique, but follows a log normal distribution (Košutić *et al.*, 2000) and its characterised by the molecular weight cut off (MWCO). The MWCO of a membrane is determined by the molecular weight (MW) of a solute that the membrane removes by 90% (Van der Bruggen *et al.*, 1999). Thus, the principal mechanism to remove compounds with a MW greater than the MWCO of the membrane is size exclusion. The MWCO of RO is in the range of 100 - 300 Dalton (Da) for organic molecules and it rejects in theory around 99% or greater of inorganic ionic solutes (Wilf, 2010). NF has a MWCO in the range of 150 - 2000 Da and is able to remove well multivalent ions such as calcium and sulfate but monovalent ions only to a lesser degree. However, the MWCO estimates only the sieving effect because MW does not take into account the hydrophobicity, the charge and the geometry of the molecule, although these properties impact on rejection (Kiso *et al.*, 2001). Moreover, taking the MW parameter for organic molecule having a MW smaller than the MWCO is not relevant for determining its rejection (Van der Bruggen *et al.*, 1999). It is well accepted that the Stokes radius is a better parameter for organics with a spherical shape (Davidson and Deen, 1988). For other organic molecules having non-spherical shapes, software such as Hyperchem can help to determine their dimensions (Van der Bruggen *et al.*, 1999).

Concerning ions rejection, it is the hydrated radius of the ion which plays an import role (Tansel *et al.*, 2006). Hydration free energy ($kJ \cdot mol^{-1}$) determines the stability of a hydrated ion in aqueous solution. Thus, this energy has an impact on the hydrated radius of an ion by modifying the number of water molecule in its hydrated shell (Tansel *et al.*, 2006). Hence, a low hydration free energy reduces the hydrated radius of the ions. Finally, the pH of the feed solution plays a role on the membrane structure.

Indeed, depending on the pH, the functional groups are ionised or not. Thus, repulsion charge between functional groups can increase the size of the polymer void space (Braghetta, 1995). In contrast, stronger electrostatic interactions can shrink the void space size (López-Muñoz *et al.*, 2009).

2.1.2. Charge or electrostatic repulsion

Charge repulsion might play a more important role in NF membrane than RO membrane for the rejection of charged solute due to the bigger size of NF PA cavities. Because of the presence of functional groups such as carboxylic (pKa$_{COOH}$ = 4.2) in the polymer, PA membranes are negatively charged at typical pH in water recycling and desalination applications (pH 5 - 9). Thus, PA membrane removes negatively charged solutes by charge repulsion. However, RO membrane has a higher surface charge than NF membrane, which lower the rejection of polar molecule by directing their dipole toward the cavities (Van der Bruggen *et al.*, 1998; Fujioka *et al.*, 2012a).

During the filtration of an electrolyte solution, the concentration of anions called co-ions is lower at the membrane surface than in the solution because of the charge repulsion effect. Whereas, the concentration of cations called counter-ions is higher on the surface membrane than in the solution (Peeters *et al.*, 1998). Hence, because of the difference of ions concentration, an electrical potential called Donnan potential is created between the solution and the membrane in order to maintain an electrochemical equilibrium between them. This potential causes the repulsion of anions and the attraction of the cations and Figure 3 introduces this concept (Bartels *et al.*, 2005). This attraction and accumulation of cations on the membrane create a surface layer neutralizing the negativity of the membrane. Therefore, an increase of the Donnan potential would result on a reduction of salt passage (Peeters *et al.*, 1998; Ong *et al.*, 2002). At very low salt concentration, the Donnan potential is very limited. However, by increasing the concentration of salt in the bulk solution, the Donnan potential increases until the cationic layer causes a decrease of salt passage. This phenomenon has a greater impact with membrane having strong negative surface charge (Elimelech *et al.*, 1994; Bartels *et al.*, 2005). To conclude, the Donnan potential depends on the concentration of salt, the valence of the anions and cations and the membrane charge (Equation 1; (Peeters *et al.*, 1998)). Thus, if the valence of the cations is higher than the anions, the concentration of anions will increase at the surface membrane.

$$\Psi_{Don} = \Psi^m - \Psi^f = \frac{RT}{z_A F} ln \frac{a_A}{a_A^m} = \frac{RT}{z_B F} ln \frac{a_B}{a_B^m} \tag{1}$$

Where Ψ_{Don} is the Donnan potential (J·C^{-1}), Ψ the electrical potential (J·C^{-1}) at the membrane surface 'm' and in the bulk solution 'f', R the gas constant (J·mol^{-1}·K^{-1}), T the temperature (K), z the valence of the cation (A) and anion (B), F the Faraday constant (C·mol^{-1}) and "a" the activity of the solutes.

The pH of the feed solution has also a variable impact on charged solute rejection. Indeed, depending on the feed solution pH, the amine, hydroxyl and carboxylic functional groups of the membrane ionise, which can affect its properties and modify the rejection of charged solute. In aqueous solution, molecules are ionised depending on their pKa, which is the negative logarithm of the ionisation constant Ka. The value of the pKa is intrinsic to a molecule and its charge is linked to the pH of the aqueous solution. Therefore, at pH > pKa, acid groups are negatively charged which will increase the rejection of acidic molecule (negatively charged) by increasing the charge repulsion mechanism.
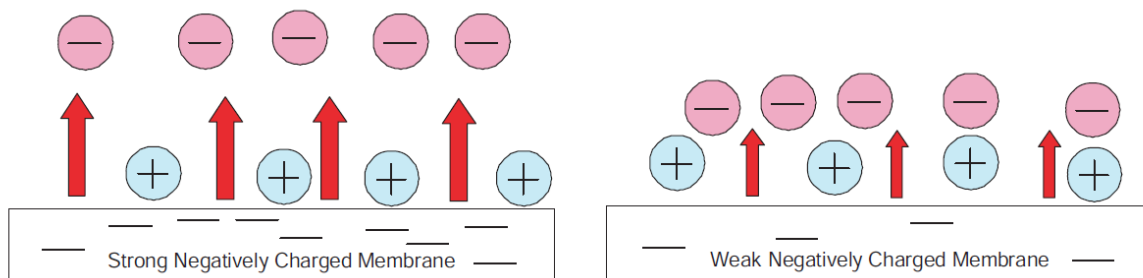
Figure 3. Donnan potential created by the repulsion of anions and cations by a negatively charged membrane. The membrane with a strong negative charge will produce a greater repulsive force with a weak negative charge (Bartels et al., 2005).

2.1.3. Adsorption

Hydrophobic interactions can occur during filtration process resulting on the adsorption of hydrophobic (non-polar) compounds on a hydrophobic membrane. The hydrophobicity of a compound is determined by its octanol-water partition coefficient (K_{ow}). K_{ow} is the ratio of the concentration of a compound in n-octanol and in water at equilibrium. Compounds with a high log K_{ow} have a higher probability to be adsorbed onto the membrane. Contact angle is the technique used to determine the hydrophobicity/hydrophilicity of a membrane by measuring the contact angle of a water droplet onto the membrane surface (Kim *et al.*, 2010). Hydrophilic membranes have a small contact angle ($\theta < 90°$) because of the presence of hydrogen bonds between water and membrane. Hydrophobic interactions are not the only adsorption mechanism occurring in RO/NF membrane filtration processes. Adsorption of compounds onto the membrane can also occur due to van der Waals forces and hydrogen bonding (Doederer, 2014). However, the number of adsorption site is limited in PA membranes. It is well accepted that the influence of adsorption on compounds rejection is time-dependant (Kimura *et al.*, 2003; Shan *et al.*, 2009; Fujioka *et al.*, 2012b). In the first step, the rejection of compounds increases due to the adsorption of compounds onto the membrane causing an overestimation of retention until the membrane reaches its equilibrium when adsorption equals desorption on feed and permeate side. Change of operating conditions can cause desorption of the compounds (Chang *et al.*, 2003) and the sorption-diffusion model has been used to describe the adsorption of a compound into the membrane and its transport by diffusion (Wiesner and Buckley, 1996; Williams *et al.*, 1999). Furthermore, other constituents present in the feed water can also impact negatively or positively on the compound's rejection. The interaction between two molecules can improve their rejection by size exclusion or charge repulsion mechanisms (Jin *et al.*, 2010). On the other hand, a molecule may improve the adsorption of another molecule onto the membrane and its diffusion through it resulting in a reduction of the rejection (Tödtheide *et al.*, 1997).

2.2. Virus removal mechanism by membrane processes

Virus rejection by membrane process is predominantly achieved by size exclusion mechanism, influenced by the physicochemical properties of the membrane, the surface properties of the virus (electrostatic and hydrophobic interactions) and the solution environment, which involves charge repulsion mechanism (Antony *et al.*, 2012). Virus rejection by low pressure membrane has been widely studied, but only few studies have been done using RO membrane. Bacteriophages[3] are generally used as model viruses avoiding the use of native viruses due to their complexity to use (e.g. lack of analysis methodology, pathogenic, etc.). Model viruses have also similar inactivation and adsorption behaviours than the native ones. A summary of the studies conducted on virus removal by high pressure membrane is presented in Table 2.

A first study done by Sorber (1972) on virus rejection (coliphage T2 and poliovirus) by cellulose acetate RO and UF membranes demonstrated the need to evaluate the virus removal using typical virus concentrations found in feed water. In fact, the higher the virus concentration in the feed water is, the higher is the possibility to obtain virus aggregates causing an increase of the measured LRV. However, the use of low virus concentration requires concentrating samples to be able to determine the LRV of the system. Therefore, the recovery of the sample concentration step can be low and thus, impacts on the final result. This study also mentioned that high feed pressure can force viruses to go through membrane imperfection. However, a variation of the feed pressure up to 20 bar does not impact on MS2 phage removal (Lozier *et al.*, 2003). In contradiction to the study conducted by Sorber (1972), Lovins III *et al.* (2002) suggested that the microorganism LRV was more dependent on the type of membrane than the organism size and concentration used in the challenge test by studying the rejection of different protozoan (*Cryptosporidium parvum* oocysts and *Gardia lamblia* cysts), bacteria (*Clostridium perfringens* spore) and viruses (MS2 phage and PRD1) by five membranes (two low pressure membranes: one MF and one UF; three high pressure membranes: NF). The effect of membrane composition (cellulose acetate or PA RO membranes) on MS2 phage rejection was also shown by Adham *et al.* (1998b).

Other studies using MF membranes applicable to high pressure membranes have been reported. The sorption of virus onto the membrane is facilitated by the presence of salt in the effluent (Huang *et al.*, 2012), which improves the hydrophobic interactions (van Voorthuizen *et al.*, 2001). However, depending on the salt composition, the virus type and the membrane type, the hydrophobic interactions can increase, do not change, or decrease (Lukasik *et al.*, 2000). Moreover, Herath *et al.* (1999) suggested a

---

[3] Bacteriophage: a virus that infects and replicates within bacteria. They are not pathogenic for human.

close relationship between isoelectric point (pI) and rejection. In this study, four coliphages with different pI value (Qβ, MS2, *fr* and T4) were filtered through a MF membrane (nucleopore UPH-25K, Advantec) at different feed pH (3.7 - 10.5) and water composition (different concentration of broth, bovine serum albumin protein and NaCl). Thus, it has been suggested that a pI near to the pH of the aqueous solution improves the virus rejection because of the equal positive and negative charge around the virus (zwitterionic form) which permits virus-virus and virus-impurity coagulation, and reduce the charge repulsion mechanism. However at pH around 6, the change of conductivity does not impact on Qβ and MS2 rejection. The impact of conductivity on the rejection of *fr* and T4 has not been studied. MS2 phage-impurity coagulation has been recently suggested by Huang *et al.* (2012). They demonstrated that in the presence of effluent organic matter and on a fouled membrane, the LRV of MS2 phage increased due to the formation of virus-impurity aggregates (increase of the virus size) and the obstruction of the membrane cavities. Recently, a particle tracking model was developed to assess virus passage through compromised low pressure membranes (MF and UF) in a stirred-cell test using MS2 and PRD1 bacteriophages (Pontius *et al.*, 2011). The conclusion of this study is that the influence of the hole on the virus rejection is depending on the hydrodynamics (flux and hole flow), which are principally functions of transmembrane pressure (TMP), water temperature and membrane resistance.

Although, it seems logical that the principal mechanism of virus rejection is size exclusion, the details of the process and what impacts of the response of the system to a defect on a membrane is difficult to understand and not well-established as it is a multi-factorial system. It is not only depending on the virus properties such as the pI and the size, but also depending on the type of membrane, the characteristics of the membrane operation such as flux and water composition. Thus, it is important to properly understand the mechanism in order to better understand the impact of the different membrane/process impairments on the virus removal and to be able to monitor the membrane integrity. To find a non-biological alternative would be advantageous given the risk involved in performing the challenge tests with viruses or other human pathogens and other related difficulties in using live organisms such as bacteriophages.

Table 2. LRV of MS2 phage by RO membrane reported in the literature.

Feed water	Scale	Membrane	S	Integrity	Pressure	Flux	J_w	T	pH	$C_{virus, feed}$	LRV	Reference
Secondary effluent	Pilot	RO SG/Ag 4040								N/A	6.7	(Madireddi *et al.*, 1997b)
Seeded DI water	Bench	RO (PA-TFC)								1E5-1E6	>6.5	(Adham *et al.*, 1998b)
		RO (PA-TFC)									5.6	
		RO (PA-TFC)									2.7	
		RO (CA)									>4.9	
		RO (CA)									4.6	
Surface water	Full	RO								1.8-3E4	3-4.8	(Kruithof et al., 2001b)
2g/L NaCl + 2g/L Na2SO4 + MS2	3 cells in parallel flat-sheet cross-flow setup	ESPA1	0.0139		4,3 - 14	0.2 - 1.6	2.95-23.6	25	6.1	1E8	5.0 - 7.0	(Lozier *et al.*, 2003)
					6.9 -13.8					1E6-1E7	>6	
				air entrainment			17.7-47.1			1E8	6.9 - >8	
										6E6	>6.8	
				scratch			4.7-23.6			1E6	>5.7	
				pinhole cell 1	7.1 - 13.7	0.6 - 1.5	5.9-23.6			1E6	> 4.7	
				pinhole cell 2 (biggest imperfection)	6 - 12.9	1.7 - 3				1E6	0.1- 1.3	
				pinhole cell 3 (particle obstructing imperfection)	5.2 - 12	0.3 - 1.3				1E6	3.1 - >4.7	
2g/L NaCl + MS2	Single 2.5" module	BW30HP	2.45						5.5-6.5	1E2 - 1E7	>2 - >7	
				1000 ppm·h chlorine	6.9 - 26.9		3.18-16.1			1E6 -1E8	>6	
		ESPA1	2.6		5 - 15.4					1E2 - 1E8	>2.1 - 7	
2g/L NaCl + Virus + 10mg/L microsphere					5.3 - 15.4					1E8 - 1E9	6.7 - 7.9	
				O-ring cracked	5.3 - 15.4					1E8	6.2 - 7	

Table 3. LRV of MS2 phage by RO membrane reported in the literature (continued).

Feed water	Scale	Membrane	S	Integrity	Pressure	Flux	J_w	T	pH	$C_{virus, feed}$	LRV	Reference
Permeate full-scale + 1.5g/L NaCl (total 1.52g/L) + MS2	single 4" module	ESPA1					7.7 - 11.8	~32		8E2 - 1E6	>2.9 - >6.1	(Lozier *et al.*, 2003)
Wastewater, no recycling mode + virus + R-WT + microsphere	Pilot: 2x(1x4" PV) in series; Head PV: ESPA1 RO; Tail PV: TFCS NF			pinhole							2.9	
				pinhole/fouled							7.0	
				pinhole/fouled/cleaned							2.8	
				O-ring cracked							>6.8	
				O-ring cut 1mm							>6.8	
Wastewater, no recycling mode + virus + R-WT + microsphere	Pilot: 3x(3x4" PV) in parallel	ESPA1		intact						1E7	5.3	
				pinhole lead position							2.3	
				pinhole trailing position							4.2	
				pinhole/fouled							>7.5	
				pinhole/fouled/cleaned							5.3	
				O-ring cut 2mm (lead)							2.3	
				O-ring cut 2mm (trailing)							>5.3	

N/A = not available.

S = membrane area (m^2).

J_w = permeate flux ($L \cdot h^{-1} \cdot m^{-2}$).

T = temperature (°C).

$C_{virus, feed}$ = concentration of virus in feed water ($PFU \cdot mL^{-1}$).

LRV = log removal value.

2.3. Existing monitoring techniques

The correct operation of the RO process must be continuously monitored to prove that the system can reach the log rejection it has been validated for. Table 3 presents the direct and indirect integrity testings currently available to monitor RO processes. The USEPA defines a direct integrity test as "a physical test applied on each membrane unit and monitored on a daily basis in order to identify and/or isolate integrity breaches" and an indirect integrity test as the "monitoring of some aspect of filtrate water quality that is indicative of the removal of particle matter at a frequency of no less than once every 15 minutes" (USEPA, 2005a).

2.3.1. Direct integrity test

Direct methods include pressure- and marker-based methods (USEPA, 2005a), and are standardised (ASTM, 2010). Pressure-based methods are offline techniques which assess the state of the membrane by monitoring pressure or air/water displacement under high pressure or vacuum (USEPA, 2005a; Frenkel et al., 2014). The vacuum decay test is the common method used in RO process. This test is performed on spiral-wound module elements to check the permeability of the wet membrane to air and thus to detect membrane leaks and imperfections (Adham et al., 1998a; Guo et al., 2010). However, this test is generally not used for full-scale practice, because of the inability to continuously monitor the integrity of the process and the difficulty to remove the air after test completion for example (USEPA, 2005a).

Marker-based methods spike a particulate or a molecule marker in the feed water. The marker is directly quantified to assess the LRV of the process. This type of testing must meet requirement criteria such as resolution, sensitivity and frequency (USEPA, 2005a). Ideally, the RO process would be validated for pathogen removal using MS2 phage before commissioning and at least yearly depending on the regulation. MS2 phage is one of the most used virus surrogates in virus removal studies performing challenge tests at lab- and pilot-scale. It has been reported as the best process surrogate because of its small size (~ 26 nm), ease to culture in large quantities and its non-pathogenic nature towards humans (Golmohammadi et al., 1993; UNESCO and WRQA, 2009; Michen and Graule, 2010). Its negative surface charge at circumneutral pH (6 - 8) favours electrostatic repulsion with negative charged membranes. Due to its low isoelectric point compared to other viruses, MS2 phage does not aggregate avoiding the increase of the LRV by size exclusion due to cluster formation (IAWPRC, 1991; Langlet et al., 2008a; Michen and Graule, 2010). Unfortunately, the implementation of this test at full-scale is impractical due to the high cost and effort required to culture and plate sufficient quantity of MS2 phage. For the very same reasons it is even less so feasible to conduct this testing at full-scale at the frequency required for operational monitoring. Moreover, the techniques used to detect this phage can be time-consuming (24 - 48 h by plaque-assay) and overall considerable expertise is required to avoid cross-contamination and conduct appropriate quality control.

A good alternative to MS2 phage is rhodamine WT (R-WT), which is a non-reactive tracer chemical approved by the US Environmental Protection Agency (USEPA) for use in drinking water (Zornes et al., 2010). This dye has a molecular weight of 487 g·mol^{-1} and it is expected to be well removed by RO membranes, because it is considerably larger than the molecular weight cut-off (MWCO). The MWCO of a membrane is determined by the molecular weight (MW) of a solute that the membrane removes by 90% and is in the range of 100 - 300 Da (dalton) for organic molecules (Van der Bruggen et al., 1999). Moreover, R-WT (pKa = 5.1) is negatively charged at water pH and thus it is expected to be removed by charge repulsion in addition to size exclusion. For these reasons, and also due to its low cost and ease to quantify by fluorescence, R-WT has been suggested as a non-microbiological alternative to MS2 phage. Several studies have demonstrated a very good correlation between the LRV of R-WT (up to 4 LRV at pilot-scale, only up to 2.8 LRV at full-scale) and the LRV of MS2 phage (Lozier et al., 2003; Zornes et al., 2010). An alternative to the conventional spiking of R-WT in feed water is the pulsed marked membrane integrity monitoring technique (PM-MIM) (Surawanvijit et al., 2015). Basically, a high concentration of dye (uranine in the previously cited study) is spiked in the system and its concentration is measured in the permeate side determining the LRV. This approach allows validating RO system for up to 4.3 LRV. The advantage of this system is the avoidance of adsorption of the marker to the membrane. Finally TRASAR^{TM} (Nalco company), a fluorescent tracer dye attached to an antiscalant, is also gaining of interest (Kelle Zeiher et al., 2003).

2.3.2. Indirect integrity test

Indirect monitoring testing does not test physically a membrane module or unit, but monitor some aspect of permeate water quality (e.g. turbidity, conductivity, etc.) similarly to challenge tests or marker-based tests of the direct integrity testing. In fact, a decrease of permeate water quality may indicate an integrity problem. The advantages of this technique are the capability to monitor a membrane process in a continuous and online mode, without to be specific to one plant (i.e. technique proposed for national guidelines) (USEPA, 2005a).

To-date, conductivity and total organic carbon (TOC) are the two online techniques allowing the indirect continuous assessment of the RO membrane rejection performance at critical control points (CCPs) (Adham *et al.*, 1998a; Kumar *et al.*, 2007). In theory, continuous measurement of polyvalent ion rejection such as sulfate, calcium or magnesium monitoring would also be an applicable technique providing a sensitivity increase compared to conductivity monitoring; however, there are currently no available economic instruments for online measurement. Appendix 1 presents the research conducted under the NatVal project to develop an electrochemical sensor able to measure sulfate online. The main issue of these techniques is that conductivity, TOC and polyvalent ions such as sulfate cannot demonstrate the integrity of the membrane to remove virus effectively. Indeed, according to the literature, RO membranes are able to remove virus by up to 5 - 7 log whereas the previously mentioned techniques can only ascertain a limited LRV, typically below 3 due to their limited presence in RO effluent (Adham *et al.*, 1998a; Adham *et al.*, 1998b; Kitis *et al.*, 2003a; Kumar *et al.*, 2007). It can be argued that TOC rejection varies during operation as it is function of the TOC composition. Nevertheless, TOC compounds are smaller than viruses by order of magnitude. Hence, the control alarm reached with TOC measurement would fluctuate but would always be more conservative than the one obtained via virus measurement. Appendix 2 presents the study determining the potential application of the S::CAN sensor for membrane integrity testing, by monitoring TOC, R-WT and other organic contaminants such as carbamazepine.

According to the USEPA membrane filtration guidance manual (USEPA, 2005a), the system should be periodically verified by direct integrity testing and continuously by indirect integrity testing. However, the actual direct methods do not allow a continuous monitoring of the RO system and the current indirect monitoring methods are too conservative to accredit accurately the log removal value for viruses. Therefore, to protect public health from microbial risk, it is essential to develop a test in order to continuously monitor and detect a loss of integrity of the RO membrane responsible for virus passage.

Table 3. Indirect and direct membrane integrity tests used in RO process.

Method	Test	Advantage	Disadvantage	LRV	Ref
Direct	Vacuum decay test	Sensitive to membrane breaches Results can be correlated to marker-based challenge test results Established ASTM standard method exists Suitable for large pathogens such as protozoa	Requires system shutdown and draining of membrane elements Lacking broad-range of LRV correlation LRV against marker-based challenge tests Limited to large integrity breaches able to be detected by 1 bar difference Difficulty to remove the air		
	MS2 phage	Model of enteric viruses	Cost Time-consuming (preparation and detection) Expertise	Up to 7	(Lozier *et al.*, 2003)
	Rhodamine WT	Simple detection method Inexpensive	Membrane sorption at high concentration	Up to 2.8	(Zornes *et al.*, 2010)
Indirect	Conductivity	Online detection Inexpensive Effective at detecting gross membrane failure	Not representative of virus rejection Insensitive to minor membrane breaches Sensitivity depends on feed salinity	~ 1.5	(Zornes *et al.*, 2010)
	TOC	Improved detection limit of TOC monitoring devices improving resolution and sensitivity More sensitive than conductivity monitoring	Instrument maintenance Sensitivity depends on feed water quality Currently no correlation between TOC removal and virus removal	> 2	(Adham *et al.*, 1998a)
	Sulfate	More sensitive than conductivity monitoring Higher LRV than conductivity	Offline measurement Insensitive to minor membrane breaches Sensitivity depends on feed water quality	Up to 3	(Kruithof et al., 2001a)

LRV obtained in full-scale plant.
Adapted from (Frenkel *et al.*, 2014).

2.4. Correlation study

As mentioned previously, MS2 phage is the challenge test having the closest relationship with enteric virus. However, its measurement is costly and time consuming. Several studies analysed MS2 phage rejection in parallel to other surrogates such as conductivity and R-WT. This section correlates the LRV of MS2 phage with the LRV of the other surrogates selected with intact and impaired membranes (e.g. fouling, pinhole) or system (e.g. o-ring cut) based on published data set (Kitis *et al.*, 2003c; Lozier *et al.*, 2003; Mi *et al.*, 2004; Pype, 2013b). Table 4 summarises the LRV of the selected surrogates reported from RO studies. This correlation helps to select the best substitute of MS2 phage to monitor RO membrane integrity. The Pearson's correlation coefficient (*r*) between two surrogates was determined by the function correlation (cor.test) of the R program. The closer the value of *r* to 1 the greater is the correlation between the two variables. Although there is no unanimously accepted way to do this, classification in five groups depending on the *r* value can be useful (Onwuegbuzie *et al.*, 2007):

- Weak or no correlation: *r* = 0 - 0.2;
- Weak correlation: *r* = 0.2 - 0.4;
- Moderate correlation: *r* = 0.4 - 0.6;
- Strong correlation: *r* = 0.6 - 0.8;
- Very strong correlation: *r* = 0.8 - 1.

Moreover, the *p-value* associated with the Pearson's correlation allows determination of the significance of a correlation. Thus, if the *p-value* is lower than 0.01 (*p-value* < 0.01), the correlation is significant at the 1% level.

Table 4. Comparison of the virus surrogates LRV (average) depending on ESPA membrane integrity (Lozier et al., 2003; Pype, 2013b).

Membrane integrity	Compound				
	MS2 phage	R-WT	Conductivity	Sulfate	DOM II
Intact[1]	5.2-6.8 (6.0)	3.7-4.1 (3.7)	1.4-1.5 (1.4)		
Pinhole[1] (lead position)	2.3-2.8	2.2	1.3		
O-ring[1] (2mm cut lead position)	2.8-3	2.7	1.4		
Compromised/Fouling[1]	7.5-8.0	3.8-4.5	1.4		
Intact[2]	>5.5	2.8-3.5	1.9	>2.5	2.1-2.5
Organic fouling[2]	>5.7	3.6-3.7	1.9-2	>2.5	2.4-2.6
Scaling[2]	>5.5	2.7-2.9	1.9	>2.5	2.1-2.4
Ageing[2]	4.2-5.7	2.2-2.4	1.2-1.5	1.9-2.3	1.6-1.9

[1] Pilot: 3 PV in parallel, 3x4" membrane modules/PV, P_f = 4.1 - 4.5 bar, J_w = 20 L·h^{-1}·m^{-2}, T = 25 - 27°C (Lozier *et al.*, 2003).
[2] Flat-sheet cross-flow set-up, P_f = 7.5 bar, cross-flow velocity = 0.1 m·s^{-1}, T = 25 - 30°C (normalised at 25°C) (Pype, 2013b).
<u>Organic fouling</u>: created from a mixture of three organic foulants in DI water: 5 mg C·L^{-1} humic acid, 0.25 mg C·L^{-1} bovine serum albumin (BSA, protein model foulant) and 0.25 mg C·L^{-1} sodium alginate (polysaccharide model foulant) (Pype, 2013b).
<u>Scaling</u>: created from synthetic RO feed solution (mix of salt reconstituting natural RO feed without organic matter) without recirculating the permeate line (Pype, 2013b).
<u>Ageing</u>: membrane soaking in a solution of sodium hypochlorite at 560 mg·L^{-1} (ppm), pH 7 for 16 h, targeting a total chlorine exposure of 9000 ppm·h (Pype, 2013b).
<u>DOM II</u>: λ_{ex} / λ_{em} 320 - 350 / 405 - 440 nm (Pype, 2013b).

2.4.1. MS2 phage vs conductivity

Commonly, the rejection of MS2 phage was studied by RO system with deionised water and NaCl or treated secondary effluent. Hence, its rejections were measured at the same time as salt rejection (measured by electrical conductivity EC). In the book "microbial removal and integrity monitoring of high pressure membranes", Lozier *et al.* (2003) presented a long study on the rejection of MS2 phage by several intact and impaired RO/NF processes at different set-up scales from flat-sheet cross-flow set-up to multi-stage pilot. Figure 4 presents the scatter plot of MS2 phage LRV with salt LRV obtained from three different pilot configurations with intact, pinholed, pinholed/fouled, pinholed/fouled/cleaned membranes and faulty O-ring. Pearson's correlation coefficient (*r*) proves that the rejections of MS2 phage and salt are significantly moderately correlated (*r* = 0.54, *p-value* < 0.01).
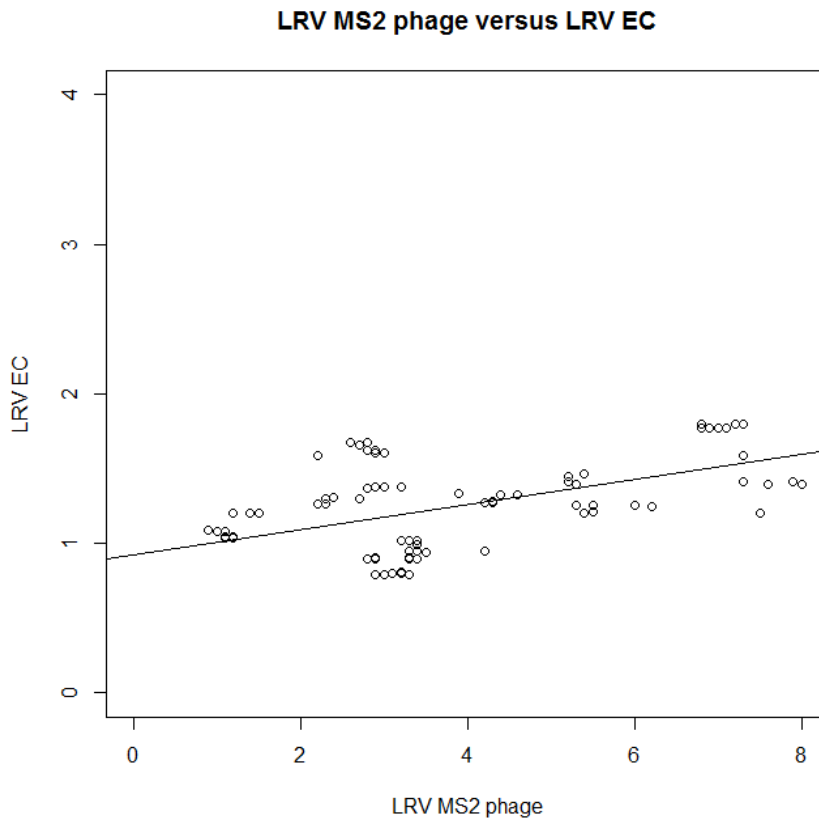
Figure 4. MS2 LRV and salt LRV scatter plot with linear regression from Lozier et al. (2003) data set. Pearson's correlation coefficient r = 0.54, *p-value = 5.958 10^{-09}.*

2.4.2. MS2 phage vs R-WT

The correlation between MS2 phage LRV and R-WT LRV presented in Figure 5 was produced from Lozier *et al.* (2003) data set. These results were obtained by three pilots with several membrane integrities. The characteristics and operating conditions are presented in Table 5. According to these experiments, R-WT rejection correlates very well with MS2 phage rejection (r = 0.81, *p-value* < 0.01).

LRV MS2 phage versus LRV R-WT
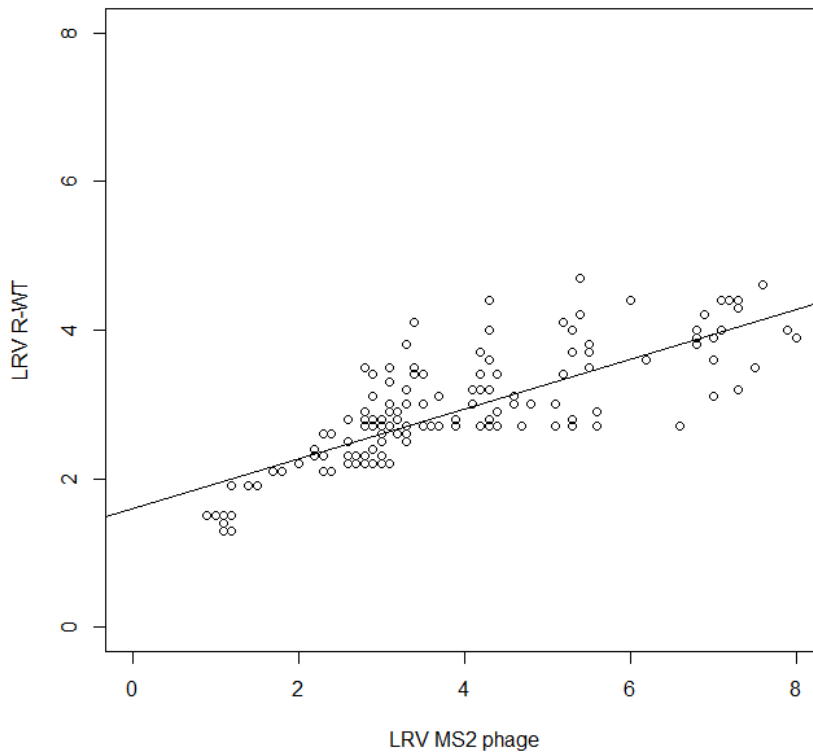
Figure 5. MS2 LRV and R-WT LRV scatter plot with linear regression from Lozier et al. (2003) ESPA1 membrane data set. Pearson's correlation coefficient r = 0.81, p-value < 2.2 10^{-16}.

Table 5. Characteristics and operating conditions of the three pilots of Lozier et al. study (2003).

	DETU	MVTU	MSTU
N of PV	2	3	6
N of module/PV	1 (4 inch)	3 (4 inch)	3 (4 inch)
N of stage	2	1	2
Membrane type	Head PV: ESPA1 (RO) Tail PV: TFCS (NF)	RO ESPA1 (Hydranautics) NF TFCS (Koch Fluid systems)	
Membrane integrity	Intact Pinholed Pinholed/fouled Pinholed/fouled/cleaned O-ring cracked O-ring cut (1 mm)	Intact Pinholed - Lead Pinholed - Trailing Pinholed/fouled Pinholed/fouled/cleaned O-ring cut 2 mm – Lead O-ring cut 2 mm - Trailing	Intact Pinholed - Position PV 1 to 6 O-ring cut 2 mm - Position PV 1 to 6
Effluent type	NaCl + MS2 phage or R-WT	Treated river + MS2 phage + R-WT + microsphere	Microfiltered 2^{ary} effluent + MS2 phage + R-WT+ microsphere
Feed pressure	4.5 - 4.8 bar	4.1 - 4.5 bar	9.9 bar
Recovery	15%	45%	75%
Target flux	117.7 L·m^{-2}·h^{-1}	20.4 L·m^{-2}·h^{-1}	17.7 L·m^{-2}·h^{-1}
Permeate flow rate	147.6 L·h^{-1}	499.7 L·h^{-1}	2498 - 2521 L·h^{-1}

DETU: dual-element test unit. Two 4" single membrane pressure vessel in series.
MVTU: multi-vessel test unit. Three parallel 4" pressure vessels holding three membranes each.
MSTU: multi-stage test unit. Six 4" pressure vessels holding three membranes each arranged in two stages.

2.4.3. Correlation between RWT, DOM, sulfate and salt

Table 6 summarises the Pearson's correlation coefficients 'r' for each combination of surrogates. According to the correlation coefficients, the LRV of DOM I, DOM II and DOM III are very strongly correlated ($r \geq 0.94$ for all combinations, *p-value* < 2.2 10^{-16}, n = 140). DOM I to III correspond to three different regions of the map obtained by fluorescence EEM (region I: λ_{ex} / λ_{em} 300 - 325 / 375 - 405 nm, region II: λ_{ex} / λ_{em} 320 - 350 / 405 - 440 nm defined as 'humic-like' by Coble *et al.* (1996) and region III: λ_{ex} / λ_{em} 230 - 260 / 380 - 470 nm). These results suggest that DOM I to III have similar behaviour during RO filtration process. Baghoth *et al.* (2011) reported strong correlation between different fluorescence EEM peaks such as tryptophan-like (λ_{ex} / λ_{em} < 250 / 360 nm) and tyrosine-like (λ_{ex} / λ_{em} 270 / 306 nm), and also with DOC and LC-OCD fractions in water samples from a drinking water treatment plant. Thus, the LRV of DOM II is used to interpret the general DOM LRV data. The choice of DOM II is due to its higher rejection tendency than the other DOM regions. The Pearson's correlation coefficient between each LRV duo of salt, sulfate and DOM II (r > 0.89) are very strong. The LRV of R-WT has lower correlations with the LRV of other surrogates (r = 0.46 – 0.63). This suggests that R-WT behave differently during RO membrane filtration than the other surrogates.

Table 6. Pearson's cross-correlation matrix for each combination of surrogates (LRV). Significant r *value (*p-value < *0.01).*

	DOM I	DOM II	DOM III	Salt	Sulfate
R-WT	0.63	0.61	0.61	0.63	0.46
DOM I	1	0.96	0.98	0.85	0.84
DOM II		1	0.94	0.89	0.89
DOM III			1	0.84	0.80
Salt				1	0.90

2.4.4. Conclusion

From the correlation analyses it can be concluded that R-WT is a very good virus surrogate and can be a substitute for MS2 phage. Both surrogates are rejected mainly by size exclusion ($MW_{MS2\ phage}$ = 3.6 10^{6} Da; MW_{R-WT} = 487 g·mol^{-1}) and charge repulsion mechanisms ($Ip_{MS2\ phage}$ = 3.1 - 3.9; pKa_{R-WT} = 5.1). The main advantage of R-WT to compare to MS2 phage is its easy detection by (potentially online) fluorescence and its low cost.

DOM, salt and sulfate are less well correlated to R-WT. Salt is a mixture of cations and anions. Their sizes are generally small, which limit the size exclusion mechanism. Sulfate is a smaller molecule than R-WT and MS2 phage. Despite its double negative charge, this anion is less rejected by RO membrane. Thus, a small defect on the membrane might have a greater impact on sulfate rejection than R-WT and MS2 phage. Finally, DOM is a heterogeneous mixture of aliphatic and aromatic hydrocarbon structures containing different functional groups. Thus, this variability of size, charge and composition impacts on DOM rejection. The monitoring of these surrogates to validate RO process underestimates its efficiency. However, their main advantage is their natural presence in the feed water and can be a good alternative to MS2 phage if the plant has to be validated for 1 or 2 LRV only.

To date, electrical conductivity (EC), sulfate and total organic carbon (TOC) online monitoring techniques are used to validate RO processes with those surrogates being rejected for 1.7 - 2, 2.4 - 2.8 and 2.3 - 3 LRV, respectively (Adham *et al.*, 1998a; Kumar *et al.*, 2007; Zornes *et al.*, 2010). However, operating conditions can affect the above cited techniques, but operating condition may not necessary affect organic compounds rejection such as virus and dissolved organic matter (DOM). In a previous paper (Pype *et al.*, 2013), we showed that salt rejection measured by electrical conductivity decreased stage by stage of a RO train and we compared this to DOM rejection measured by fluorescence excitation-emission matrix (EEM) which was constant along the train. Whereas, Ochando-Pulido *et al.* (Ochando-Pulido *et al.*, 2012) showed that the modification of RO membrane operating conditions varied the rejection of dissolved organic carbon (DOC) in contrast to phenols which were completely removed during all the experiments. There is also a lack of study showing the impact of operating condition on the rejection of DOM, R-WT and DOC.

3. Factors influencing surrogate removal

RO membrane is an efficient barrier to remove organic and inorganics contaminants. Previous studies (Wang *et al.*, 2005; Hoang *et al.*, 2010; Tu *et al.*, 2010; Ochando-Pulido *et al.*, 2012; Negaresh *et al.*, 2013) demonstrated that operating conditions play a role on RO removal efficiency for inorganic compounds. For example, studies showed an increase of salt rejection when increasing the permeate flux (Wang *et al.*, 2005) or decreasing the temperature (Tu *et al.*, 2010). The purpose of the NatVal 2.2 SP2 project is to develop a national guideline to validate RO processes in water recycling. Therefore, it is important to highlight the parameters influencing the removal of surrogates. Thus, in this study the effect of operating parameters (permeate flux, cross-flow velocity, permeate recovery) and the solution environment (feed temperature, pH and composition) on the rejection of virus surrogate (MS2 phage), conventional surrogates (salt, sulfate and R-WT) and new surrogates (DOM) were studied. This project considered RO application within the operating condition range determined by membrane manufacturer, in order to avoid unnecessary re-validation of an RO process due to the change of its operating conditions. Furthermore, NF membranes, which are the second type of high pressure membrane, should also be considered.

3.1 Theory

In high pressure system, feed pressure, cross-flow velocity and permeate flux are important parameters to produce high quality water. These operating parameters in combination with feed temperature, ionic strength, pH and composition impact on contaminants' rejection for a given membrane system (Berg *et al.*, 1997; Kiso *et al.*, 2000; Kimura *et al.*, 2003; Nghiem *et al.*, 2005; Hu *et al.*, 2007; Uyak *et al.*, 2008; Fujioka *et al.*, 2012b; Doederer *et al.*, 2014).

The principle of high pressure membrane is to apply an external pressure on the feed side to force the pure water to go through the membrane and retain the dissolved species. The water permeability (K_w) and salt rejection ($R_{salt\%}$) are expressed following Equations (2) and (5), respectively. Temperature changes water viscosity and by consequence impacts on water permeability.

$$K_w = \frac{J_w}{S} \times \frac{1}{NDP \times TCF} \tag{2}$$

$$NDP = P_f - 0.5 \times TMP - \pi_f \tag{3}$$

$$TCF = \left(\frac{1}{\exp\left(K \times \left(\frac{1}{273} + T\right) - \left(\frac{1}{298}\right)\right)} \right) \tag{4}$$

$$R_{salt\%} = \left(1 - \frac{c_p}{c_f}\right) \times 100 \tag{5}$$

where J_w is the permeate flux ($L \cdot h^{-1} \cdot m^{-2} \cdot bar^{-1}$), S the membrane area ($m^2$), NDP the net driving pressure (bar), TCF the temperature coefficient factor, P_f the feed pressure (bar), TMP the transmembrane pressure (bar), π_f the feed osmotic pressure (bar), K a constant characteristic of active layer membrane material, T the temperature (°C) at time t and C the salt concentration ($mg \cdot L^{-1}$) in feed (f) and permeate (p) (Hydranautics, 2001; Mi *et al.*, 2004; Wilf, 2010).

Along a spiral-wound module:

- Feed pressure diminishes due to friction;
- Ionic strength increases due to the concentration of the solutes, which is caused by the passage of pure water in the permeate side;
- Osmotic pressure increases due to the rise of solutes concentration, which declines the water permeation;
- Cross-flow velocity decreases due to a reduction of the turbulence, which increases the concentration polarisation causing a reduction of the solute rejection.

Concentration polarisation (CP) is a layer of higher concentrated solute on the membrane surface than on the bulk solution (Amjad, 1993). Thus, this layer increases the osmotic pressure at the membrane surface causing a decrease of the water flux. CP increases the concentration gradient causing an

increase of the solute passage. Finally, CP forms scale when the surface concentration exceeds the maximum level of solubility. CP is reduced when the membrane surface is well mixed, which can be achieved by working at high cross-flow velocity or by optimising turbulence promoters for example (Williams, 2003).

Contaminants rejection is also a function of the percentage of water recovery. Indeed, Chellam and Taylor (2001) have shown that the rejection of contaminants decreased as the permeate water recovery is increased due to the increase of the gradient concentration across the membrane. Finally and as described previously, pH of the feed water plays a role on contaminants rejection by impacting on membrane swelling, membrane surface charge and contaminants charge (Braghetta, 1995).

3.2 Materials and Methods

In this part, the physicochemical properties of surrogates, the experimental apparatus including experimental systems and membrane, the analytical techniques and the data analyses used at AWMC/UQ are described in detail.

3.2.1 Surrogates

Tests were performed with one model virus (MS2 phage) and four non-biological surrogates (R-WT, salts, DOM and sulfate). MS2 phage and R-WT were spiked to feed water. In order to determine the impact of ionic strength and dissolved organic carbon (DOC) concentration, five types of water were used in the feed composition experiments and their characteristics are detailed in Table 7. Water A was a RO feed water obtained from one advanced water treatment plant (AWTP) in South East Queensland (SEQ) and was used as a baseline unless otherwise stated. Water B is a RO feed water from the same AWTP than water A, but with a lower conductivity. Waters C and D are 50/50 (v/v) of water B and de-ionised water, and de-ionised plus salt, respectively. Finally water E is a mix of 50% water A and 50% pre-filtered raw water (0.45 μm) from a SEQ water treatment plant selected because of its high DOC.

Table 7. Feed water characteristics.

Technique	Ion/ element	A (n = 12)	B (n = 3)	C (n = 3)	D (n = 3)	E (n = 3)
pH		7.2 – 7.6	7.7	7.7	7.5	7.6
Conductivity ($\mu S \cdot cm^{-1}$)		2519 ± 258	1477 ± 17	927 ± 78	1327 ± 29	851 ± 21
DOC ($mg \cdot L^{-1}$)		9.6 ± 0.8	8.5 ± 0.2	6.0 ± 0.6	4.6 ± 0.1	13.9 ± 3.7
IC ($mg \cdot L^{-1}$)	Cl^-	553.3 ± 132.3	322.8 ± 3.1	162.9 ± 8.5	300.4 ± 4.6	179.1 ± 1.4
	SO_4^{2-}	118.7 ± 34.8	89.9 ± 0.8	159.7 ± 65.9	75.0 ± 2.4	48.8 ± 0.6
ICP-OES ($mg \cdot L^{-1}$)	Ca	35.5 ± 3.8	31.8 ± 0.8	15.6 ± 0.5	27.9 ± 0.7	18.0 ± 0.6
	K	26.8 ± 5.6	19.7 ± 0.6	9.8 ± 0.3	22.7 ± 1.4	11.6 ± 0.4
	Mg	43.5 ± 18.3	22.8 ± 0.7	11.0 ± 0.2	18.0 ± 0.7	12.9 ± 0.4
	Na	310.5 ± 66.6	207.9 ± 5.3	118.4 ± 15.8	197.4 ± 7.3	119.7 ± 4.1
	P	3.7 ± 1.7	1.9 ± 0.1	0.88 ± 0.04	2.1 ± 0.1	1.1 ± 0.1
	S	42.0 ± 20.8	29.7 ± 0.6	14.2 ± 0.5	23.9 ± 0.6	16.5 ± 0.5
Ionic strength (mM)		23	15	10	13	8

DOC: dissolved organic carbon.
IC: ion chromatography.
ICP-OES: induced coupled plasma-optical emission spectrophotometer.
n = number of samples.

MS2 phage strain 15597-B1 (ATCC, Manassas, VA, USA) was cultured following the procedure ISO 10705-1 (ISO, 1995b). The feed concentration for MS2 phage was targeted at 10^8 $PFU \cdot mL^{-1}$.

The non-biological surrogates used were R-WT (Ortho Chemical Australia Pty. Ltd., Newmarket, Australia), salts (ions) measured by electrical conductivity (EC), sulfate and dissolved organic matter (DOM). R-WT is a non-hazardous chemical tracer and was selected because of its acceptance by the US Environmental Protection Agency for use in drinking water (USEPA, 2005a) and its use in numerous research studies (Kitis *et al.*, 2003a; Lozier *et al.*, 2003; Zornes *et al.*, 2010). The target feed concentration for R-WT was 100 $\mu g \cdot L^{-1}$. Salt, sulfate and DOM measurements were selected due to their natural presence in RO feed and their used as indirect integrity testings in previous studies (Lozier *et al.*, 2003; Zornes *et al.*, 2010; Pype, 2013a, 2013b).

3.2.2   Membrane filtration apparatus

Three commercially available high pressure membranes (ESPA2, BW30 and NF90) were tested and are presented in Table 8. ESPA2 membrane sheets (Hydranautics, Oceanside, CA, USA) used for the flat-sheet set-up were cut from a 4" spiral-wound element and were stored in Milli-Q water at 4ºC. BW30 and NF90 flat sheet membranes were supplied by Dow Filmtec (Minneapolis, MN, USA). The experiments studying the effect of temperature, cross-flow velocity, pH, permeate flux and feed composition were performed using a stainless-steel flat-sheet test unit consisting of a membrane element cell (effective membrane area: 140 cm²; Sterlitech Corporation, Kent, WA, USA), a Hydracell pump (Wanner Engineering Inc., Minneapolis, MN, USA) and a 15 L feed tank (Rota Moulding, Midvale, Australia). The feed pressure and the differential pressure between feed and concentrate lines were measured with two digital gauge transmitters (Endress + Hauser, North Ryde, Australia). The concentrate flow rate was controlled by adjusting the speed of the pump and by adjusting a needle valve (Swagelok, Brisbane, Australia) installed in the concentrate line. Permeate and concentrate flow rates were measured with a HPLC liquid flow meter (GJC Instruments Ltd, Cheshire, England) and a 1200 MPB flow meter (MPB industries Ltd, Kent, England), respectively prior to be returned to the feed tank. The temperature of the feed solution was measured in order to normalise the performance to 25°C. Sampling points (Swagelok, Brisbane, Australia) were located in the feed, permeate and concentrate lines. Figure 6 presents (a) a photo and (b) a drawing of the flat-sheet set-up.

One ESPA2 4040 spiral-wound membrane was used for the permeate recovery experiment. This system consisted of a CodeLine fiberglass pressure vessel model 40E30N (membrane shop, Australia), a Hydrovar CRN1-27 pump (Grundfos, Australia) and a 200 L feed tank. The feed pressure and the differential pressure between feed and concentrate lines were measured with two digital gauge transmitters. The concentrate flow rate was controlled by adjusting the speed of the pump and by adjusting a needle valve installed in the concentrate line. Permeate and concentrate flow rates were measured with a TX50 flow meter and a 1750 MPB flow meter (MPB industries Ltd, Kent, England), respectively prior to be returned to the feed tank. The temperature of the feed solution was controlled using a cooling thermostat (Lauda, Australia). Sampling points were located in feed, permeate and concentrate lines. Figure 7 presents (a) a photo and (b) a drawing of the 4" module set-up.

Prior each experiment, RO and NF membranes were compacted overnight at 8 bar and 5 bar, respectively. Each membrane was characterised by measuring the pure water permeability (K_w; $L \cdot h^{-1} \cdot m^{-2} \cdot bar^{-1}$) and solute rejection ($R_{salt\%}$, %) expressed as Equations (2) and (5), respectively.

Solute rejection was measured using a 1.5 $g \cdot L^{-1}$ NaCl solution for RO membranes and a 2 $g \cdot L^{-1}$ MgSO4 solution for NF membranes (Table 8). In order to compare the different membranes, permeate flux was hold at 20 $L \cdot m^{-2} \cdot h^{-1}$, cross-flow velocity was controlled at 0.1 $m \cdot s^{-1}$ and feed temperature was kept at 22.0 ± 0.5°C (normalised at 25°C). Unless otherwise stated, these operating conditions were used as baseline.

Table 8. Specifications for the three commercially available high pressure membranes used in this study.

Membrane	ESPA2	BW30	NF90
Manufacturer	Hydranautics	Dow	Dow
Material	Polyamide thin-film composite		
Membrane type	Reverse osmosis	Reverse osmosis	Nanofiltration
System	4" single module	Flat-sheet	Flat-sheet	Flat-sheet
J_w ($L \cdot h^{-1} \cdot m^{-2} \cdot bar^{-1}$)*	4.10 ± 0.02 (n = 1)	5.1 ± 0.2 (n = 5)	4.3 ± 0.2 (n = 5)	12.2 ± 0.3 (n = 4)
Solute (concentration)	NaCl (1.5 $g \cdot L^{-1}$)	NaCl (1.5 $g \cdot L^{-1}$)	NaCl (1.5 $g \cdot L^{-1}$)	MgSO4 (2 $g \cdot L^{-1}$)
Salt rejection (%)*	99.30 ± 0.02 (n = 1)	98.9 ± 0.3 (n = 5)	95.6± 0.6 (n = 5)	98.4 ± 0.3 (n = 5)

J_w and salt rejection = average ± standard deviation.
n = number of membrane.
Operating conditions: 20 $L \cdot m^{-2} \cdot h^{-1}$, 0.1 $m \cdot s^{-1}$, temperature normalised at 25°C.
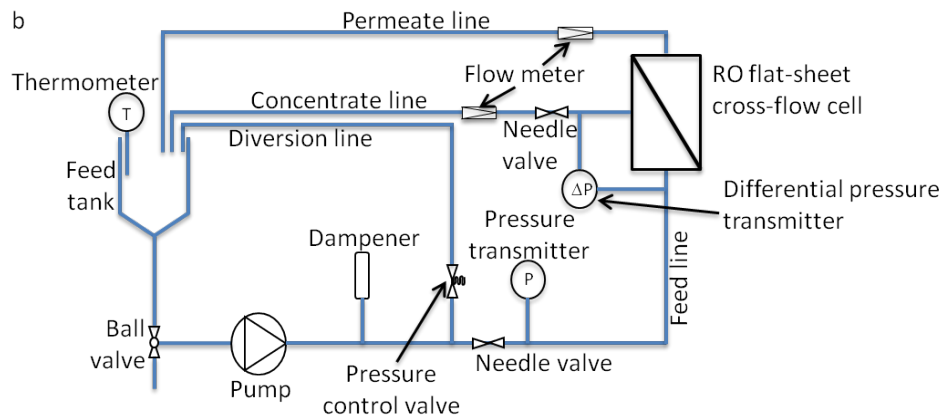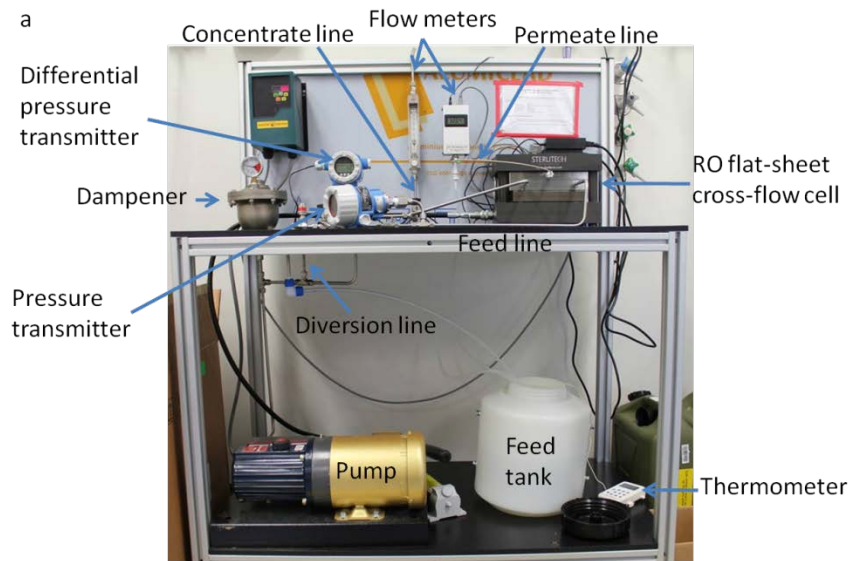
Figure 6. (a) photo and (b) drawing of the SS flat-sheet set-up.
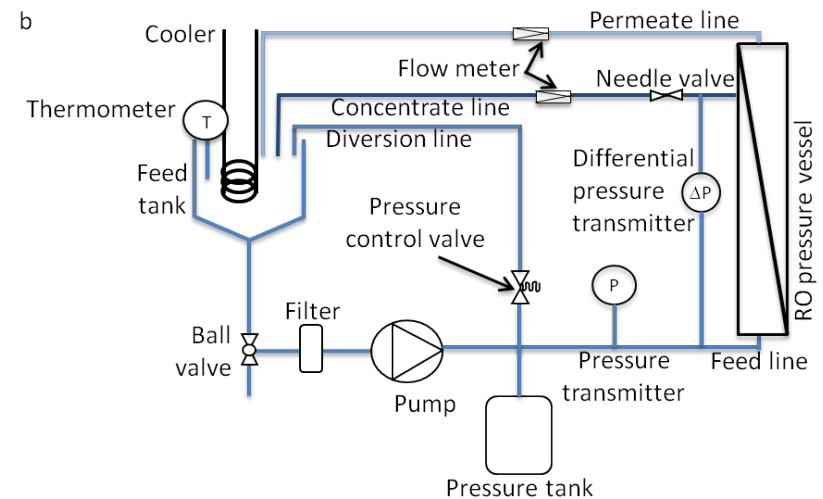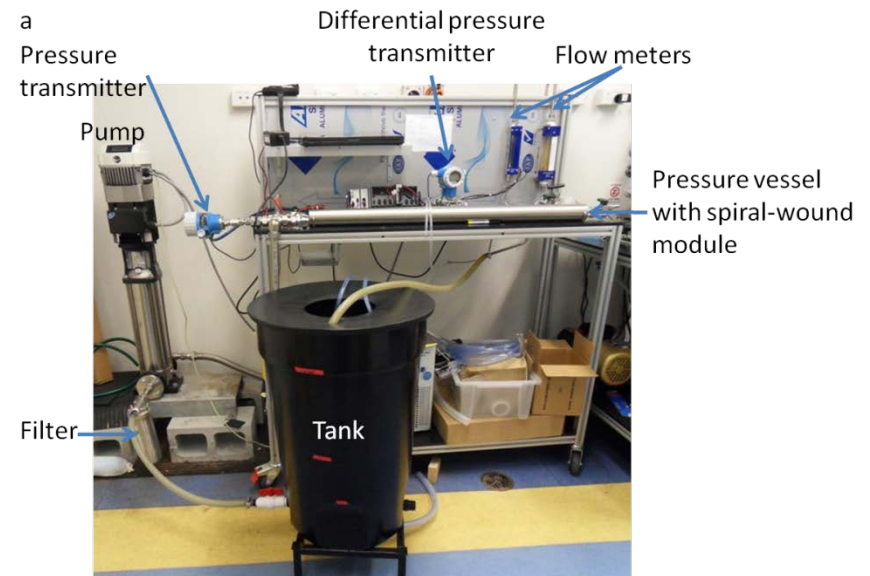
Figure 7. (a) photo and (b) drawing of the 4" module set-up.

3.2.3 Analysis of surrogates

Each surrogate has a specific detection method which is presented in Table 9 with its limit of quantification (LOQ).

Table 9. Summary of the different analytical techniques and their limit of quantification (LOQ) used to quantify the compounds.

Compound	Technique	LOQ
MS2 phage	Plaque-assay	0.2 PFU·mL^{-1}
R-WT	Fluorescence	25 ng·L^{-1}
DOM	Fluorescence EEM	N/A
Sulfate	Ion chromatograph	0.1 mg·L^{-1}
Salt	Electrical conductivity	1 µS·cm^{-1}

EEM: excitation-emission matrix.
N/A: not available.

3.2.3.1 MS2 quantification

The concentration of MS2 phage was determined by the plaque-assay method (ISO, 1995b). It is a simple technique which permits to enumerate viable MS2 phage (phage being able to infect its host) by its culture. It was applied to determine the concentrations of MS2 phage stock solution, feed and permeate samples inoculated with *E. coli* using the double agar layer procedure described previously (ISO, 1995b; Furiga *et al.*, 2011). When necessary, logarithmic dilutions of MS2 phage samples were performed obtaining a number of plaques below 300 (Figure 8). After incubation overnight at a set temperature of 37ºC, plates were examined to calculate the sample number of plaque forming units (N_{PFU}; PFU·mL^{-1}) as defined in Equation (6).

$$N_{PFU} = \frac{N \times D}{V} \tag{6}$$

where N is the number of plaque in one Petri dish, D the dilution factor and V (mL) the sample volume.
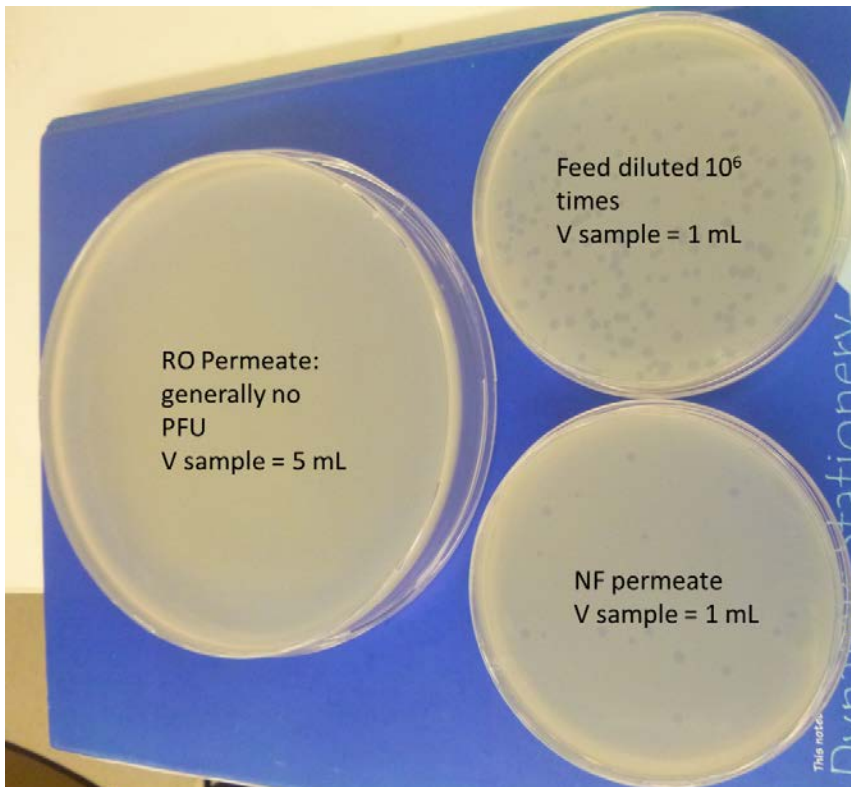
Figure 8. Petri dishes with presence or absence of plaque forming unit (PFU).

3.2.3.2 R-WT quantification

Fluorescence measurements of R-WT were performed using a PerkinElmer LS-55 luminescence spectrometer (PerkinElmer, Australia) in a 1 cm quartz cuvette operated with the Winlab® software provided by PerkinElmer. Fluorescence intensity was recorded using excitation and emission wavelengths of 550 and 580 nm, respectively. Excitation and emission scan slits were set to 3 nm for feed samples and to 10 nm for permeate samples in order to increase the sensibility of the instrument. The photomultiplier voltage was set to the automatic mode.

3.2.3.3 DOM analysis

This method has been previously described by Pype *et al.* (2013). Fluorescence measurements of DOM were performed using a PerkinElmer LS-55 luminescence spectrometer (PerkinElmer, Australia) in a 1 cm quartz cuvette operated with the Winlab® software provided by PerkinElmer. Fluorescence intensity was recorded by varying excitation wavelengths (λ_{ex}) from 200 nm to 400 nm at steps of 5 nm, and emission wavelengths (λ_{em}) from 280 nm to 500 nm at 0.5 nm steps generating a three-dimensional fluorescence EEM as previously described by Chen *et al.* (2003). A cut-off filter at 290 nm was used to limit the second-order Raleigh scattering. Excitation and emission scan slits were set to 10 nm, the scan speed was set to 1200 nm·min^{-1} and the photomultiplier voltage was set to the automatic mode. Samples were equilibrated at room temperature (air conditioned at 23ºC) prior analysis in order to minimise the temperature effect and all RO feeds were diluted 20 times to avoid the inner filter effect (absorption of photons of either incident or emitted light by the sample; $A_{230} < 0.05$) (Larsson, 2007; Lakowicz, 1999). This dilution allows measuring both types of samples (feed and permeate) in a similar chemical environment avoiding factors such as pH and salt concentration which could affect fluorescence. Regarding the pH experiment, permeate samples were adjusted to the same pH than their corresponding feed samples.

For all fluorescence spectra, Raman normalisation (λ_{ex} = 350 nm, λ_{em} = 371 - 428 nm) and a blank subtraction (Milli-Q water generated by Millipore Advantage fed by tap water previously filtered through activated carbon and RO) were applied as described previously (Lawaetz and Stedmon, 2009; Murphy *et al.*, 2010). A fluorescence regional integration (FRI) technique from fluorescence spectroscopy was used to quantify the contribution to the EEM spectra (Chen *et al.*, 2003; Singh *et al.*, 2009) of one delimited region (λ_{ex} / λ_{em} 320 - 350 / 405 - 440 nm defined as 'humic-like' by Coble *et al.* (1996)). Peak volumes and ratios between volumes of the selected EEM region were calculated following equations described by Chen *et al.* (2003) using R software (adapted from (Lapworth and Kinniburgh, 2009)). Briefly, the volume of fluorescence intensity (Φ_i) of region 'i' was calculated and normalised 'n' ($\Phi_{i,n}$) with a multiplication factor (MF_i) specific to region 'i' using Equations 7 and 8

$$MF_i = \left(\frac{(\Delta\lambda ex \Delta\lambda em)_i}{\sum(\Delta\lambda ex \Delta\lambda em)_i} \right)^{-1} \tag{7}$$

where $\Delta\lambda ex$ and $\Delta\lambda em$ are the interval of the excitation and emission wavelength, respectively.

$$\Phi_{i,n} = MF_i \Phi_i \tag{8}$$

The cumulative volume 'T' of the normalised fluorescence intensity ($\Phi_{T,n}$) was calculated by Equation (9).

$$\Phi_{T,n} = \sum_{i=1}^{3} \Phi_{i,n} \tag{9}$$

The percent fluorescence response of region 'i' ($P_{i,n}$) was calculated using (10).

$$P_{i,n} = \frac{\Phi_{i,n}}{\Phi_{T,n}} \times 100 \tag{10}$$

The rejection of the organics ($R_{DOM\%}$) which are responsible for the fluorescence of each region by the RO membranes, was determined by calculating the removal of fluorescence intensity using Equation (11).

$$R_{DOM\%} = \left(1 - \frac{\Phi_{p,n}}{\Phi_{f,n}} \right) \times 100 \tag{11}$$

where $\Phi_{p,n}$ and $\Phi_{f,n}$ are the normalised volume of permeate and feed fluorescence intensity, respectively.

3.2.3.4   Sulfate quantification

Sulfate ions from feed samples were measured as SO_4-S by a compact ICS-2000 ion chromatograph (IC; Dionex, Australia) with a DS6 heated conductivity detector (35°C). A potassium hydroxide gradient was applied with the Dionex automatic eluent generator using an EluGen cartridge (EGC II KOH). The gradient started at 12 mM KOH, was ramped up in 5 min to 34 mM where it was kept for 3 min, then in 1 min it was ramped up from 34 to 52 mM and kept at that concentration for another 11 min. The data acquisition time was 20 min and the total analysis time 25 min. The injection volume was 25 µL and the flow rate 1 mL·min^{-1}. The separation was achieved with a Dionex IonPac AG18 (4 x 50 mm) guard and an IonPac AS18 (4 x 250 mm) separating column. Both columns were heated to 35°C. The data processing was done with the Dionex Chromeleon software.

Sulfate ions from permeate samples were analysed with a compact Dionex ICS-2100 ion chromatograph equipped with a DS6 heated conductivity detector (35°C). A Dionex AERS 500 4mm suppressor (112mA) is used before the conductivity detector. The samples are injected with a Dionex AS-AP autosampler. The data processing is done with the Dionex Chromelon software. A potassium hydroxide eluent is applied with the Dionex automatic eluent generator using an EluGen cartridge (EGC III KOH). The KOH concentration is kept at 20mM KOH during the whole run. The data acquisition time is 17 minutes and the total analysis time 22 minutes. The eluent is degassed with a Dionex ICS-2100 degasser. The injection volume is 250µL and the flow rate 1mL/min. The separation is achieved with a Dionex IonPac AG19 (4x50mm) guard and an IonPac AS19 (4x250mm) separating column. Both columns are heated to 30°C.

3.2.3.5   Electrical conductivity

EC was measured using a Mettler Toledo SevenEasy. Salt rejection ($R_{salt\%}$) was calculated from conductivity measurements of each sample following Equation (5) above.

To calculate salt rejection, conductivity measurements (Λ_{meas}) were normalised as defined by Equations (12) and (13) below for the average feed salinity (f) and permeate salinity (p), respectively. Feed salinity is an average value of the feed water salinity that increases during filtration within a pressure vessel due to the passage of feedwater to the permeate channel.

$$\Lambda_f = \frac{\frac{\Lambda_{meas,f}}{TCF} \times \ln\frac{1}{1-R}}{R} \tag{12}$$

$$\Lambda_p = \frac{\Lambda_{meas,p}}{TCF} \tag{13}$$

where R is the stage recovery (%) and TCF is the temperature correction factor as expressed above in Equation 2.3 (Hydranautics, 2001).

3.2.4   Other chemical analysis

Dissolved organic carbon (DOC) was measured with a TOC-multi N/C 2100S (Analytik Jena, Australia) using the non-purgeable organic carbon (NPOC) method. Metals were measured using inductively coupled plasma-optical emission spectrometry (ICP-OES) from samples acidified at 10% with concentrated HNO_3. pH was measured using a Mettler Toledo SevenEasy.

3.2.5   Projection software

IMSdesign (Hydranautics) and ROSA (FilmTec) software were used to project water permeability and salt rejection with the different operating conditions used in this project. These values were then compared to the results obtained experimentally.

3.2.6   Statistical data analysis

Student's t-test was used to verify the statistical similarity between samples. If the p-value was below 0.05 (p-value < 0.05), the null hypothesis H_0 that two samples were significant was rejected with 5% of risk. Before running the t-test, Fisher's F-test was used in order to determine the homogeneity of the samples which allowed setting the parameters of the t-test.

3.3 Results and discussion

3.3.1 Permeate flux

Figure 9 presents the LRV of the surrogates as a function of permeate flux (Kw, $L \cdot m^{-2} \cdot h^{-1}$) at constant cross-flow velocity and temperature using the flat-sheet set-up. In such system, the transmembrane pressure, the permeate recovery and thus the solute increase along the cell are negligible.

MS2 phage was removed above 5 log by the three membranes (Figure 9a). MS2 rejection do not significantly change as a function of permeate flux.

For ESPA2 and NF90, R-WT rejections seemed to firstly reduce and then stabilise when increasing the permeate flux; whereas, R-WT rejections did not change with BW30. This decrease between 10 and 20 $L \cdot m^{-2} \cdot h^{-1}$ cannot be explained by the possible adsorption of R-WT into membrane at the beginning of the experiment, because the selection of the permeate flux was random during the experiments.
DOM rejections were not impacted by the change of permeate flux for the three membranes. The two RO membranes had a very similar efficiency to remove DOM and were higher than NF90.

According to Figure 9b, the rejection of solute increased when increasing the permeate flux. This increase was higher between 10 $L \cdot m^{-2} \cdot h^{-1}$ and 30 $L \cdot m^{-2} \cdot h^{-1}$ and then stabilised. At higher permeate flux, the diffusive flux of solute is lower that the water flux, which causes an increase of the water permeability and of the solutes rejection due to dilution effect in the permeate side (Spiegler and Kedem, 1966; Ochando-Pulido *et al.*, 2012). However, there is a limit to this phenomenon. At a certain feed pressure limit, the solutes rejection reaches a plateau due to the transport of salt with water (Filmtec, 1998).

3.3.2 Cross-flow velocity

Figure 10 shows the impact of cross-flow velocity on surrogates. According to this figure, MS2 is very well removed by both RO membranes and reach the LOD of the technique. ESPA2 presented a higher LRV than BW30 due to a higher MS2 feed concentration (10^9 PFU·mL^{-1} instead of 10^8 PFU·mL^{-1}). It can be concluded that if RO membranes are intact and show good MS2 rejection, no significant change will be made on virus LRV by modifying the cross-flow velocity of the system. Like MS2 phage, R-WT was not significantly (*t*-test *p-value* > 0.05) affected when changing the cross-flow velocity of the system.

DOM rejection presents two different patterns. With BW30, cross-flow velocity did not impact DOM rejection (*t*-test *p-value* > 0.05); whereas a reduction of 0.3 log in rejection was observed from 0.05 $m \cdot s^{-1}$ to 0.2 $m \cdot s^{-1}$ with ESPA2. At higher cross-flow velocity, concentration polarisation effect is reduced due to the flux turbulence at the membrane surface. Mattaraj *et al.* (2010) demonstrated a higher flux decline at low cross-flow velocity, whereas at high cross-flow velocity solute accumulation swept away from membrane surface. Thus, lower cross-flow velocity eases organic fouling, which blocks the membrane cavities and thus increases DOM rejection by blocking DOM passage through the membrane. The roughness of the membrane is measured by calculating the root-mean-square (RMS) from atomic force microscopy (AFM) micrograph. BW30 has a smoother surface than ESPA2 (Donose et al., 2013a) reducing the possible attachment of DOM on its surface and thus limiting fouling.

Sulfate and salt tend to be better rejected with higher cross-flow velocity with an increase of 0.1 log and 0.13 log with BW30 from 0.05 $m \cdot s^{-1}$ to 0.2 $m \cdot s^{-1}$, respectively. These trends can be explained using the concentration polarisation argument introduced previously.
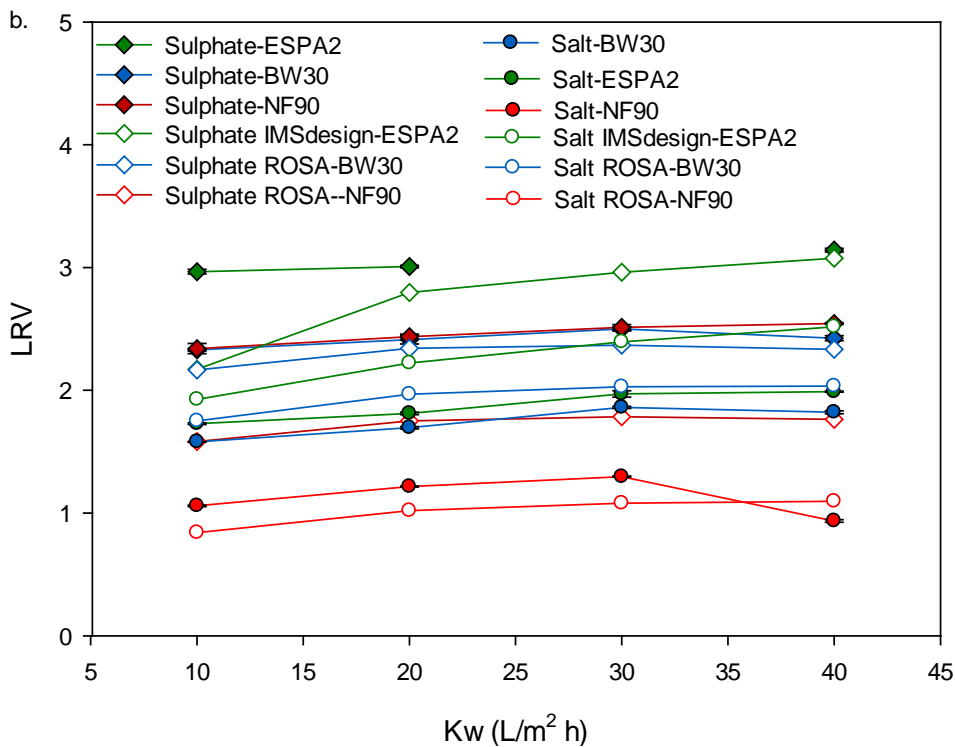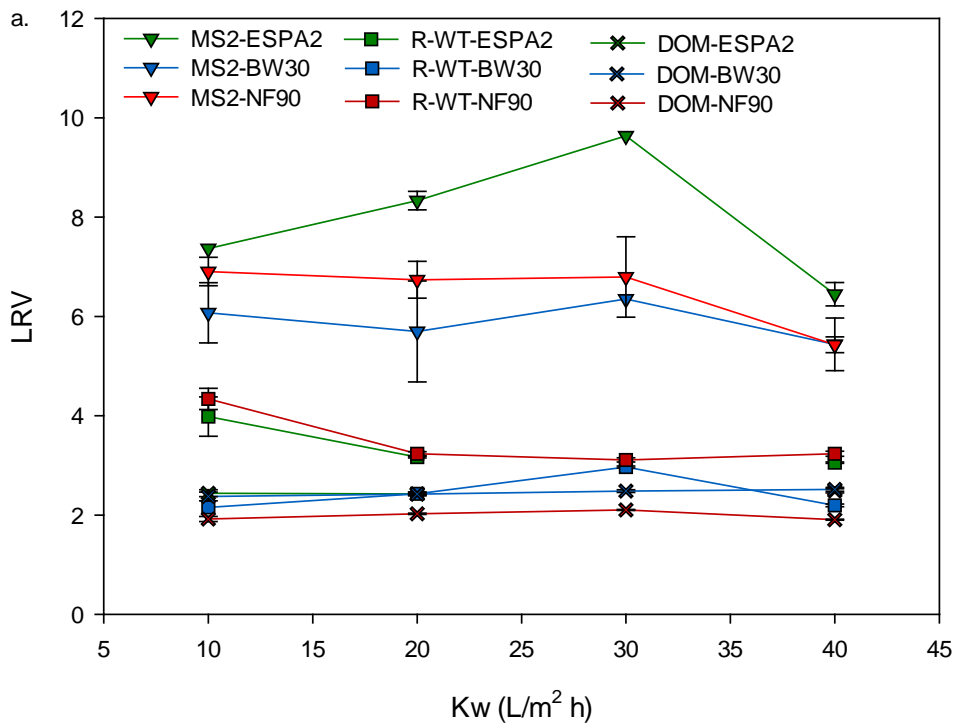
Figure 9. Impact of permeate flux on the LRV of (a) MS2 (▼), R-WT(■) and DOM (x), and (b) sulfate (♦), salt (●) and their projection using manufacturer software by ESPA2 (green), BW30 (blue) and NF90 (red). Operating condition: water A (pH = 7.2 − 7.6), cross-flow velocity = 0.1 m·s^{-1}, T = 22.0 ± 0.5 ℃ (normalised at 25 ℃). Error bars = standard deviation, n = 3.

Figure 10. Impact of cross-flow velocity on the LRV of (a) MS2 (▼), R-WT (■) and DOM (x), and (b) sulfate (♦), salt (●) and their projection using manufacturer software by ESPA2 (green), BW30 (blue) and NF90 (red). Operating condition: water A (pH = 7.2 – 7.6), permeate flux = 20 L·m^{-2}·h^{-1}, T = 22.0 ± 0.5 °C (normalised at 25 °C). Error bars = standard deviation, n = 3.

3.3.3 Temperature

Figure 11 presents the LRV of surrogates as a function of temperature with constant permeate flux and cross-flow velocity. Once again, the three membranes retained very well MS2 phage. Thus, the fluctuation between the different samples was more related to experimental errors than temperature effect.

Overall, the raise of temperature had a negative impact on the rejection of salt, R-WT and at a less extent DOM, except for R-WT with ESPA2 and DOM with BW30 which did not change. It has been previously shown (Sharma *et al.*, 2003; Sharma and Chellam, 2006; Ben Amar *et al.*, 2007) that high temperature increased the size of the cavities due to the relaxation of the polymer. Moreover, high temperature reduces water viscosity, which might contribute to the salt passage.

However, sulfate rejection had a tendency to significantly increase with the three membranes. When using the manufacturer software, the rejection of sulfate decreases as a function of temperature increase. One hypothesis could be that sulfate interacts with another compound present in the water such as DOM. The interaction between sulfate and DOM might also explain the lower impact of temperature on DOM rejection in comparison to salt and R-WT.

3.3.4 pH

Membrane surface charge of the PA layer depends on the feed water pH. At pH > pKa ($pKa_{COOH} \approx 4$), the PA layer is negatively charged. It has to be noted that manufacturers limit the use of their membranes in the pH range of 2 to 11 for cleaning purpose. Overall, it was observed an increase of membranes' performance from pH 3 to 8 and then a decrease at pH 10.

Table 10 presents the chemical properties of MS2 and R-WT.

Table 10. MS2 and R-WT chemical properties.

	MW	pKa/pI
MS2 phage[a]	$3.6 \, 10^6$ Dalton	3.2
R-WT[b]	$487 g \cdot mol^{-1}$	5.1

[a](Antony *et al.*, 2012)
[b](Vasudevan *et al.*, 2001)

At pH 10, MS2 phage is not viable causing an absence of plaque forming in the feed samples. MS2 phage is very well removed at all pH values. At pH 3, PA membrane is uncharged and MS2 is under its zwitterion form. Thus, there is no charge repulsion mechanism at this pH, only size exclusion mechanism. Size exclusion mechanism is sufficient to remove at least four log of MS2 with RO membranes, which can be the maximum log credit given by the regulators in Victoria (VDoH, 2013).

R-WT is negatively charged at pH > 5, allowing a higher removal due to a combination of size exclusion and charge repulsion mechanisms. At lower pH, R-WT rejection is reduced due to its removal by size exclusion mechanism only with RO/NF membranes.

The rejection of DOM as a function of pH is depending on its composition. In this study, no specific trend was observed.

The projection of the two RO membranes indicated an increase of the salt and sulfate rejections performance from pH 3 to 8 (Figure 12b). From pH 8, membrane performance stabilised or reduced. The projection of NF90 performance was not possible using the manufacturer software. According to the literature, higher electrostatic interaction at high pH causes pore shrinkage (López-Muñoz *et al.*, 2009). However, Donose *et al.* (2013a) proposed an increase of pore size at high pH. According to Figure 12b, salt removal increased from pH 3 to pH 8 by 0.12 log with BW30, but then decreased at pH 10. Regarding sulfate rejection, there was no much difference in rejection between pH 3 and pH 8; however there was again a reduction of its removal at pH 10. At pH 3, size exclusion is the only removal mechanism. As the pH increases, electrostatic interactions are becoming stronger which cause shrinkage of the membrane cavities. However, at high pH the size of the cavities increases reducing the size exclusion mechanism, which is the main one with RO membranes.
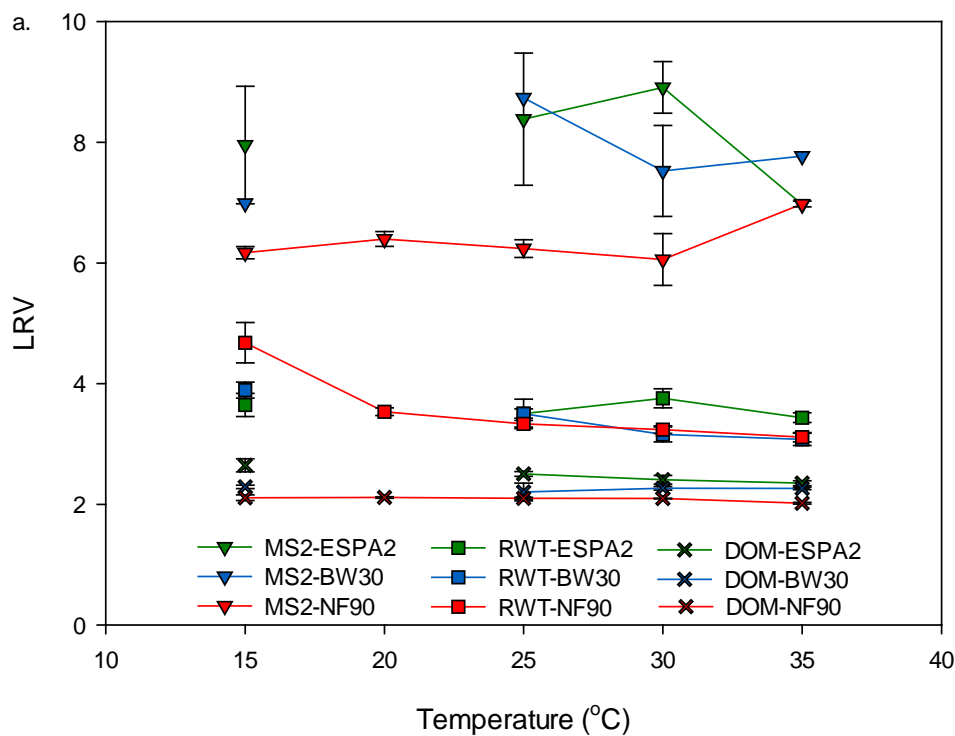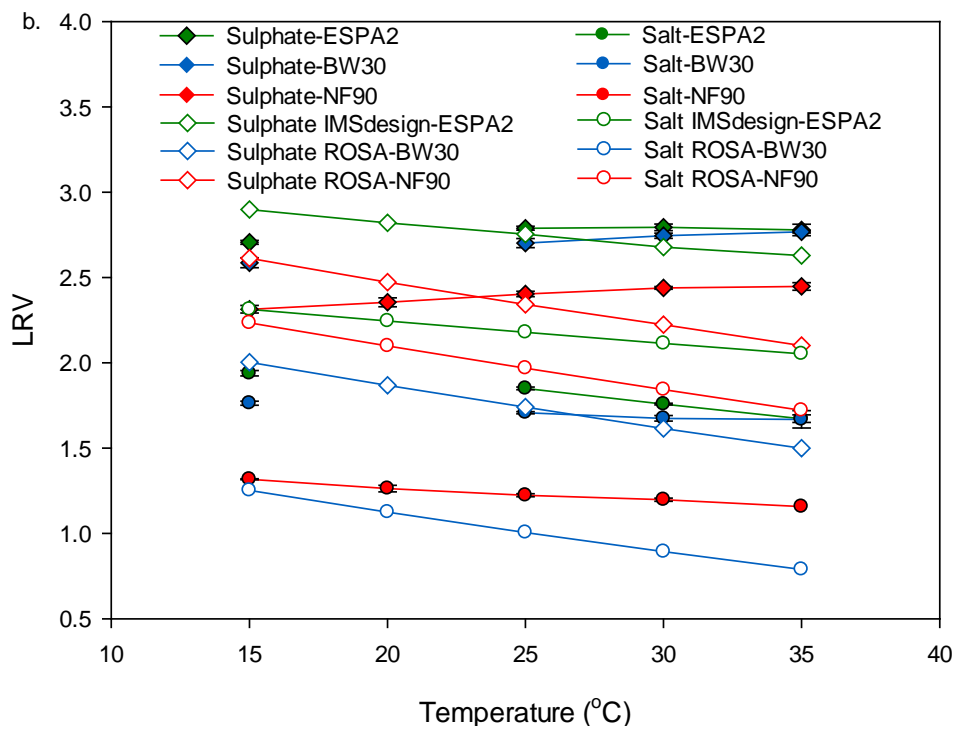
Figure 11. Impact of temperature on the LRV of (a) MS2 (▼), R-WT (■) and DOM (x), and (b) sulfate (♦), salt (●) and their projection using manufacturer software by ESPA2 (green), BW30 (blue) and NF90 (red). Operating condition: water A (pH = 7.2 − 7.6), permeate flux = 20 L·m^{-2}·h^{-1}, cross-flow velocity = 0.1 m·s^{-1}. Error bars = standard deviation, n = 3.
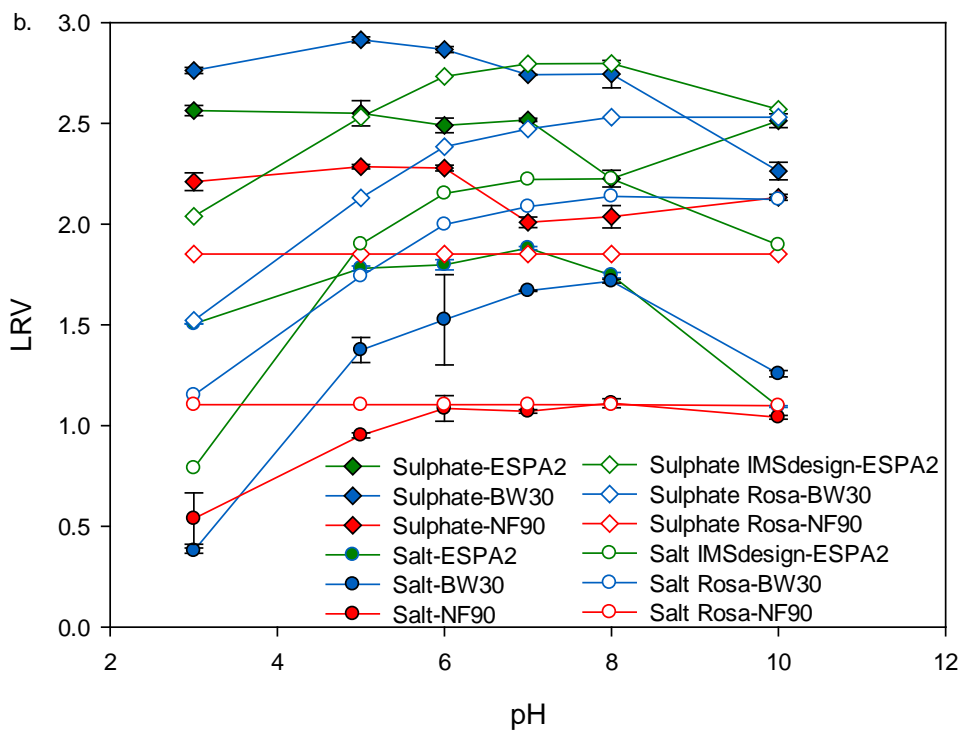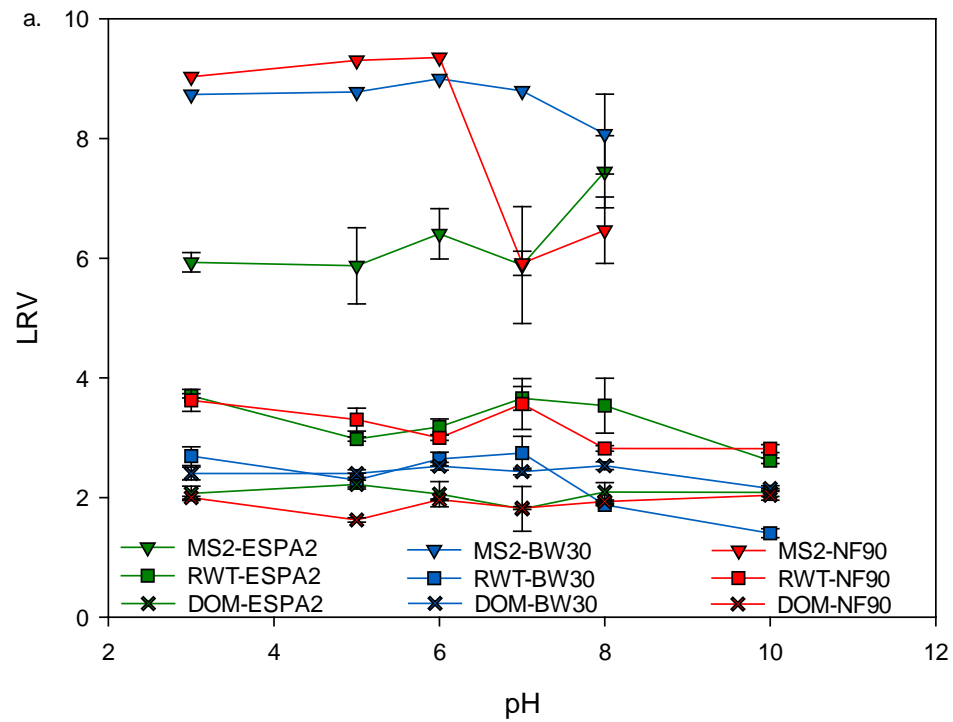
Figure 12. Impact of pH on the LRV of (a) MS2 (▼), R-WT (■) and DOM (x), and (b) sulfate (♦), salt (●) and their projection using manufacturer software by ESPA2 (green), BW30 (blue) and NF90 (red). Operating condition: water A, permeate flux = 20 L·m⁻²·h⁻¹, cross-flow velocity = 0.1 m·s⁻¹, T = 22.0 ± 0.5°C. Error bars = standard deviation, n = 3.

3.3.5 Feed composition

Table 7 presents the characteristics of the 5 waters used in this project.

Figure 13a presents the rejection of MS2, R-WT and DOM as a function of ionic strength. During the experiment with BW30, a problem occurred with MS2 solution. It was not possible to measure MS2 concentration in feed and permeate. However, it can be expected that BW30 will have a similar rejection than ESPA2. The rejection of MS2 with ESPA2 was higher than the LOD of the plaque-essay technique. The rejections of MS2 with NF90 were similar with the five types of waters. Thus, it can be concluded that MS2 phage is not influenced by organic matters and ions at pH 7. It has been previously demonstrated that viruses can aggregate with organic contaminants (1999). Virus rejection is more influenced at its zwitterion form (feed water pH close to Ip).

R-WT and DOM rejections were not influenced by the feed composition. We should mention that at low DOC, the concentration of DOM in permeate can be difficult to determine. Waters C and D (10 and 13 mM ionic strength) had low DOC (6 and 4.6 mg·L^{-1}, respectively). For this reason, their LRV were slightly below the 3 others waters.

Figure 13b presents the rejection of salt and sulfate with the three studied membranes as a function of ionic strength. The DOC concentration varied from 4.6 (water D) to 13.9 (water E). Feed composition tended not to have an impact on sulfate and salt rejections. It can be expected that in the presence of organic matter, salt rejection would increase due to salt-DOM affinity. An increase of salt concentration increases the concentration polarisation effect, which causes a decrease of salt rejection. Also, it has been previously shown that an increase of ionic strength can increase the size of the cavities.(Bargeman *et al.*, 2005). However, the ionic strengths used in this study were not strong enough to impact on the cavities size.
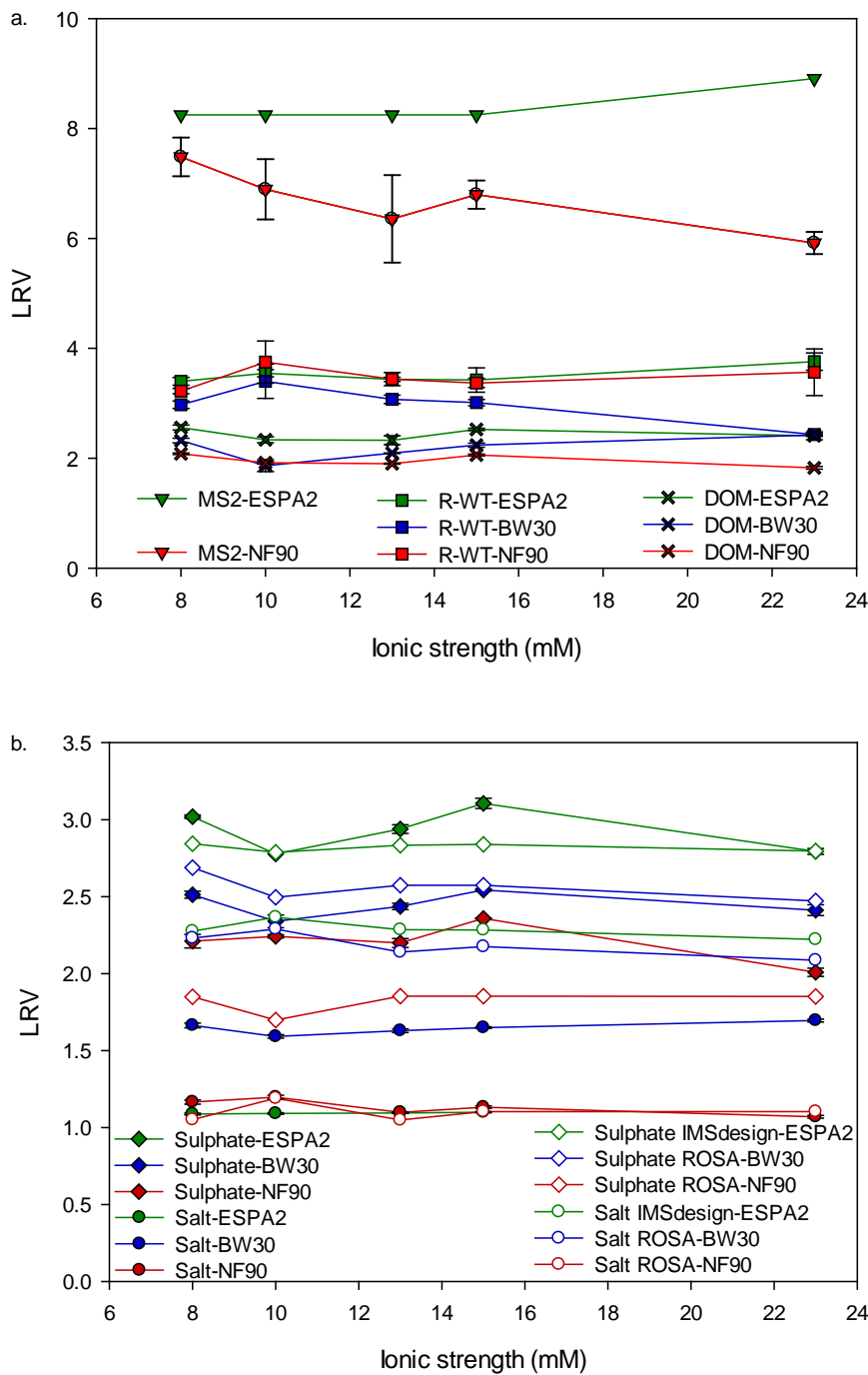
Figure 13. Impact of feed composition on the LRV of (a) MS2 (▼), R-WT(■) and DOM (x), and (b) sulfate (♦), salt (●) and their projection using manufacturer software by ESPA2 (green), BW30 (blue) and NF90 (red). Operating condition: permeate flux = 20 L·m⁻²·h⁻¹, cross-flow velocity = 0.1 m·s⁻¹, T = 22.0 ± 0.5°C, pH = 7.2 – 7.6. Error bars = standard deviation, n = 3.

3.3.6 Percentage permeate recovery

Figure 14 presents the LRV of surrogates as a function of the permeate recovery (%) at constant cross-flow velocity and temperature. It can be concluded that membrane recovery does not affect MS2 rejection. MS2 phage was very well removed by the 4" ESPA2 single wound spiral-module (above 7 LRV). It has to be noted that the permeate concentrations of MS2 were closed to the plaque-essay method LOQ. At this LRV, the fluctuation of MS2 concentrations between the different conditions was mainly caused by the experimental errors rather than the condition itself as it is very close to the LOQ.
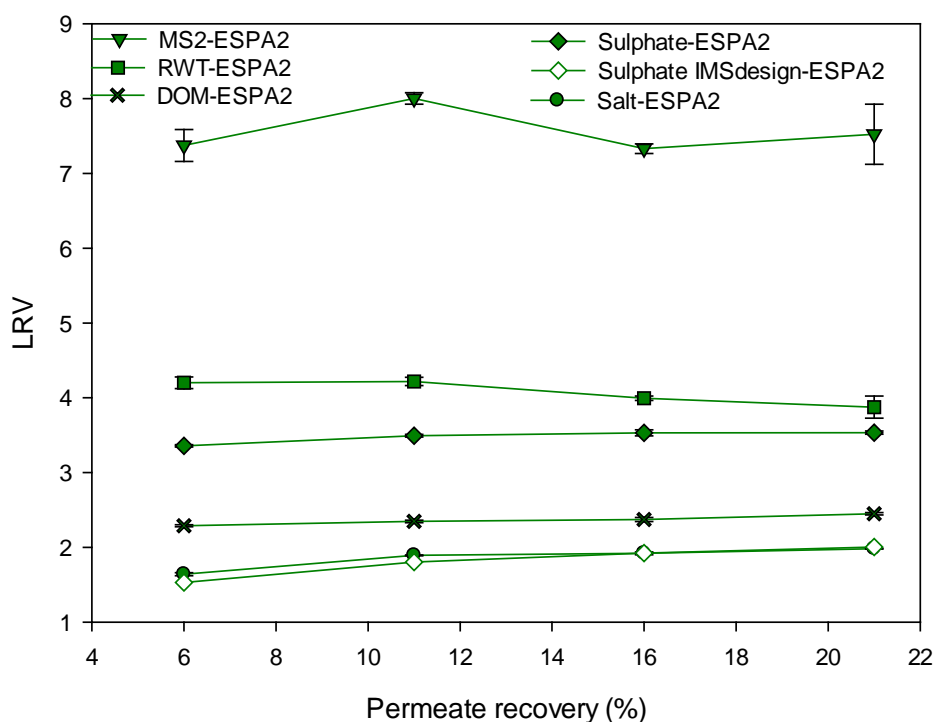
Figure 14. Effect of permeate recovery (%) on the LRV of surrogates. Operating condition: water A (pH = 7.2 – 7.6), cross-flow velocity = 0.1 m·s⁻¹, T = 22.0 ± 0.5°C. Error bars = standard deviation, n = 3.

Regarding the non-biological surrogates, R-WT tended to be less well removed when increasing the membrane permeate recovery. Whereas, the removal of the other surrogates slightly increased when increasing the permeate recovery. It can be noted that sulfate removal determined experimentally followed the same trend, but with a higher LRV, than sulfate projected using the IMSdesign software (Hydranautics). According to Figure 15, this module had a higher water permeability (J_w) and salt rejection (R_{salt}) than predicted. An increase of the permeate recovery, which means an increase of the permeate flux, increase the feed pressure. It has been proven that the percentage of recovery has an impact on the removal of contaminants (Chellam and Taylor, 2001) and that an increase of the net driving pressure (feed pressure) increases the solutes rejection by increasing RO process phenomenon (Filmtec, 1998). A long a pressure vessel (PV), the salt concentration of the feed water increases. An increase of the salt concentration increases the osmotic pressure and thus reduces the solute rejection by reducing the net driving pressure. In this experiment, a single 4" module has been used. The initial osmotic pressure of the system was 0.6 bar and slightly increased at the other end of the PV depending on the permeate flux. However, this increase of osmotic pressure does not significantly decrease the net driving pressure of the system (less than 0.1 bar at 20% permeate recovery), which could happen in a full-scale RO process with multi-modules in one PV.

R-WT is negatively charged at water pH. Hence, an increase of the salt concentration might create a complex R-WT-solute decreasing the charge repulsion mechanism and/or increasing the diffusion mechanism, which cause a reduction of its rejection. It has to be noted that the permeate samples of the 6% and 11% permeate recovery experiments were under the LOQ of the detection method. It can be expected that the LRV of the 6% permeate recovery is higher than the 11% one.

Finally, the rejection of DOM slightly increased by increasing the permeate recovery. An increase of solute concentration onto the membrane surface favourites the formation of a cake layer. Thus, the formation of an organic fouling layer onto the membrane surface appears quicker than at lower permeate recovery, which causes an increase of DOM rejection.
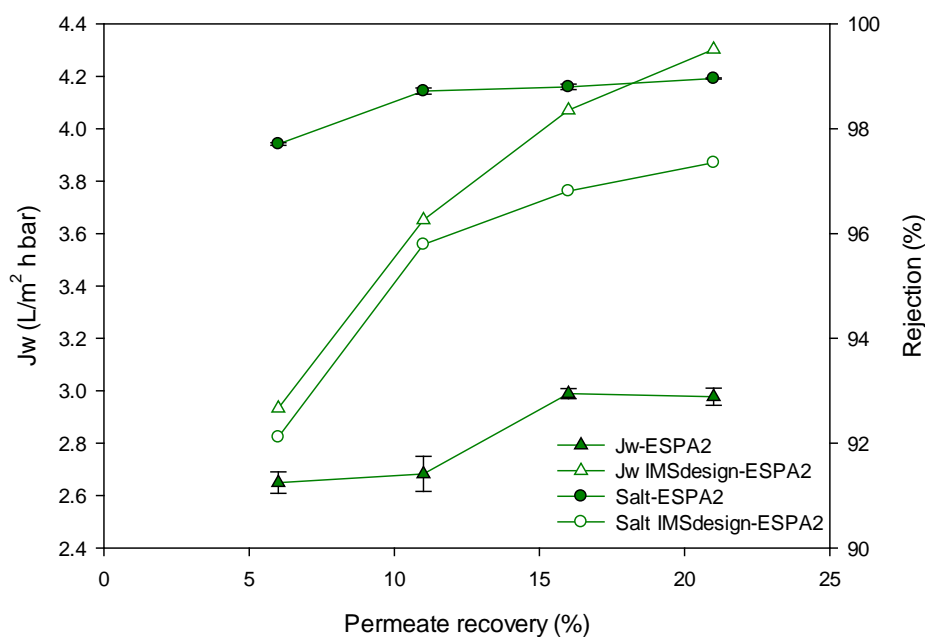
Figure 15. Water permeability (Jw, L·m^{-2}·h^{-1}·bar^{-1}) and salt rejection (%) of ESPA2 single RO module as a function of permeate recovery (%). Operating condition: water A (pH = 7.2 – 7.6), cross-flow velocity = 0.1 m·s^{-1}, T = 22.0 ± 0.5^{o}C. Error bars = standard deviation, n = 3.

3.4 Conclusions

In this study, permeate and concentrate were recirculate to the feed causing a stable surrogate concentration during the experiment. Overall, the three tested membranes were able to highly remove the virus surrogate MS2 phage. Thus, it is challenging to determine the impact of operating conditions on its removal. The operating conditions applied in this project, which respect manufacturer limitations, did not affect dramatically the rejection of MS2 phage. We can conclude that during normal operation (following manufacturer limits) with intact membrane and no compromised process such as O-ring leak, viruses should be removed for more than four log (limit determined by Victoria state to accredit one process) meaning that a RO process should not need to be revalidated if a change of operating conditions occurs such as an increase of permeate flux. This conclusion is only valid if MS2 phage is used as validation technique. Depending on the operating conditions, the LRV of other surrogates fluctuate. However, this statement does not take into account possible system impairment.

R-WT was removed for more than 3 LRV. Higher permeate flux and thus higher permeate recovery, higher cross-flow velocity, pH > 5 and lower temperature were slightly increasing its LRV.

Generally, DOM rejections were not influenced by operating conditions due to its heterogeneous composition. A higher removal was demonstrated at higher DOC feed composition and higher percentage of permeate recovery. Like MS2 phage and R-WT, DOM is not easily influenced by operating conditions. The advantages to monitor DOM in RO process are its natural presence in RO feed water and its ease to be measured by fluorescence. Therefore, DOM is a very good surrogate of MS2 phage and can be a good alternative to R-WT for lower removal credit.

Salt and sulfate were the two surrogates strongest influenced by the process conditions. The following operating conditions were reducing their removal:
- Low permeate flux
- Low cross-flow velocity
- High temperature
- pH < 4 or pH > 8
- Low permeate recovery

To validate a RO process, the previously mentioned conditions should be used to determine the lower limit of LRV that the process should be validated for.

4. Impact of Membrane Ageing on Reverse Osmosis Performance – Implication for Validation Protocols

While monitoring membrane treatment system performance is essential through appropriate validation and integrity monitoring protocols, it is important to note that there is no information available on the effect of membrane ageing on the membrane performance (Antony *et al.*, 2012). There is no monitoring protocol and recommended frequency of monitoring available to verify the membrane performance for pathogen rejection over long term operation. As a part of developing a national validation framework for reverse osmosis (RO), the impact of membrane ageing on the membrane performance is discussed in this section.

There is concern about the possibility that the membrane surface and sealing components could degrade or become damaged with time, allowing undetected increases in the passage of virus. In the case of composite membranes, where a thin, selective skin (supported by an underlying porous structural layer) is responsible for rejection of virus particles, any damage to this skin could allow increased virus passage, and therefore compromise public health. Some of the membrane system and process failures that can cause the virus passage include membrane ageing, membrane fouling, defects with the membrane module (abnormally big pores, compromised glue line, holes etc.) and associated filtration systems (compromised o-rings, broken mechanical seals etc.) (Sorber *et al.*, 1972; Urase *et al.*, 1994; Urase *et al.*, 1996; Adham *et al.*, 1998d; Lovins *et al.*, 2002; Hu *et al.*, 2003). Membrane ageing is the deterioration of the surface layer and sublayers of composite membranes due to irreversible deposition of foulants or by frequent exposure to chemical cleaning agents. Membrane ageing is inevitable in a filtration system and may result in gradual performance decline or complete membrane failure, both resulting in noncompliance and loss of process efficiency. In order to assist in risk management of RO systems used in water recycling, this study aims to develop quantitative information regarding the consequences of ageing on virus removal and assess the capability of current integrity monitoring practices in detecting potential process failures.

Generally, bench scale ageing studies involve exposure of a membrane to increased dosages of oxidizing chemicals, as they are expected to be the most likely source of damage to RO modules in an operational plant. However, it is suggested that exposure to oxidizing chemicals alone cannot accurately mimic actual membrane ageing. Therefore, in the present study, an accelerated ageing methodology involving cyclic fouling, cleaning and exposure to hypochlorite was performed in order to correspond more with field operation. For comparison, passively aged and industrially aged membranes were also tested to establish virus removal efficiency. A correlation of online electrical conductivity (LRV_{EC}), and spiked NaCl salt conductivity (LRV_{NaCl}) against the LRV_{MS2} was also established.

4.1 Methods, Materials and methodology

4.1.1 Filtration rig

Membrane performance testing and ageing through cycling fouling and cleaning was performed in a stainless steel crossflow filtration cell configured for flat sheet membranes, with an effective membrane area of 0.0139 m^2. The schematic representation of the filtration system is presented in Figure 16.

The feed and retentate pressure were controlled using a GE Fanuc Controller (GE automation Fanuc-Versa Max). The rig is equipped with flow meter, and online conductivity sensor coupled with transmitter. Experimental parameters such as flow rates, pressures, temperature, and conductivity were recorded and controlled using CIMPLYCITY software. All experiments were performed at constant retentate pressure. Flow and conductivity values of permeate and retentate were recorded every 20 seconds.
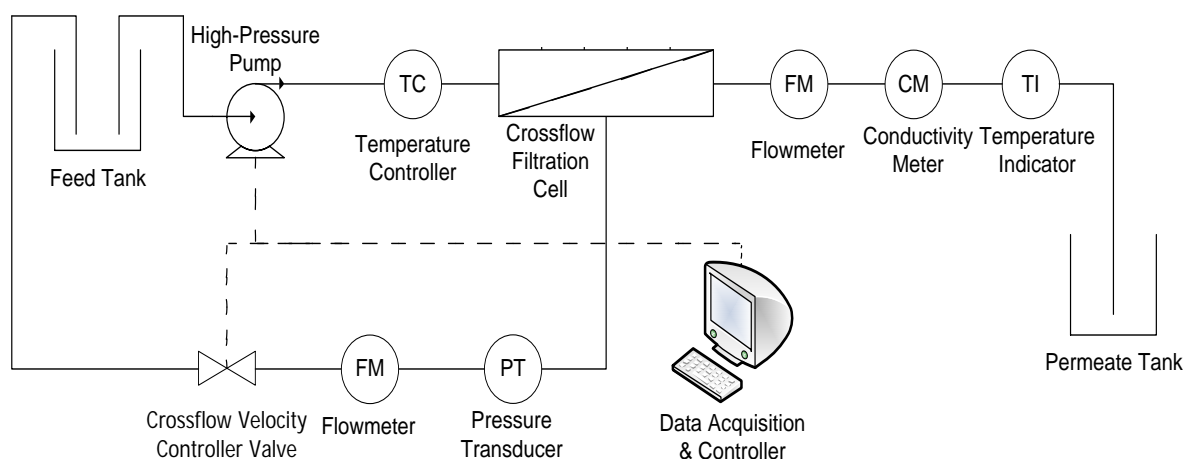
Figure 16. Schematic representation of RO cross-flow filtration system during filtration in batch, feed concentrating mode.

4.1.2 Membrane, fouling and cleaning solutions

All controlled ageing experiments were performed with commercially available BW-30 (Dow Filmtec) polyamide thin film composite (TFC) membrane. The manufacturer reported an operating pH range between 2 and 11 and a maximum temperature and free chlorine tolerance of 45°C and < 0.1 mg·L^{-1}, respectively.

For cycling ageing experiments, a model fouling solution was prepared with sodium sulfate (Na$_2$SO$_4$), potassium sulfate (K$_2$SO$_4$), magnesium chloride (MgCl$_2$.6H$_2$0), calcium chloride (CaCl$_2$), humic acid sodium salt, and sodium metasilicate pentahydrate (Na$_2$O$_3$Si.5H$_2$O). Each component was mixed in order to achieve a final solution concentration of 21 mg·L^{-1} of dissolved organic carbon (DOC), 80 mg·L^{-1} of calcium, 42 mg·L^{-1} of magnesium, 30 mg·L^{-1} of potassium, 24 mg·L^{-1} of Silica, and 274 mg·L^{-1} of sodium. Membrane cleaning was performed in two stages; stage 1 involved rinsing the feed side with 0.2 wt% HCl and 0.1 wt% NaOH for 30 min under no applied retentate pressure. Stage 2 followed, by circulation on the feed side with NaOCl (pH 10.5) for 30 min at concentrations of 200, 500 and 1000 ppm, (or 100, 250 and 500 ppm·h) dependent on desired exposure regime. The membrane was flushed with Milli-Q water before, after, and in between cleaning stages with different chemicals.

4.1.3 Cyclic ageing and performance testing methodology

At the beginning of the experiment, membranes were pre-conditioned by rinsing and soaking with Milli-Q water for 24 h and then compacted at 8 bar until a stable permeate flux was observed.
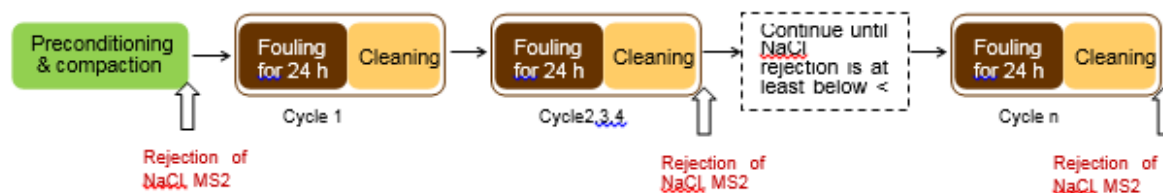
Figure 17. Cycling fouling, cleaning and intermittent check points in one experiment.

Fouling was performed in batch mode (concentrating the feed) at constant pressure of 8 bar transmembrane pressure, until a reduction in permeate flux of 1 L·m^{-2}·h^{-1}·bar^{-1} is reached; temperature was maintained at 25°C. During the fouling the membrane permeability and permeate conductivity were recorded. Upon every fourth cycle, the membrane rejection performance of spiked 2000 ppm NaCl salt (by measuring electrical conductivity) and MS2 were assessed. For 500 ppm·h experiment, membrane performance for NaCl and MS2 phage was tested after every cycle.

4.1.4 Passive ageing and industrially aged membranes

Deliberately ageing was achieved by passive soaking of membrane samples in either 20.8, 208, 1250, 1667 and 2550 ppm of hypochlorite for 24 h resulting in corresponding exposures of in 500, 5000, 30 000, 40 000 and 60 000 ppm·h. Free chlorine concentration in the hypochlorite solution (AR grade) was measured with a DPD calorimetric method (Clesceri *et al*., 1998). Details for four industrially aged membranes were tested and their details are given in Table 11.

Table 11. Details of the industrially aged membranes.

Sample	Manufacturer	Plant type	Age, approximate	Cleaning chemicals
IAM1	Toray TML 20-400	Advanced water treatment plant	5 years	NaOH/EDTA, Citric/HCl,
IAM2	Hydranautics ESPA2	Advanced water treatment plant	5 years	Not available
IAM3	Hydranautics ESPA2	Recycled water treatment plant	3 years	NaOH, citric acid,
IAM4	TORAY 20D-400	Brine concentrator	2 years	NaOH, Sodium lauryl sulfate, EDTA, HCl

4.1.5 Citrate capped silver nanoparticles (AgNP)

AgNP nanoparticles were prepared based on the method reported previously (Antony *et al*., 2014). Briefly, 1 mL of 1% solution of Sodium citrate was added to boiling solution of silver nitrate (9 mg dissolved in 50 mL of water) and mixed for 1 hour. Synthesized nanoparticles were dosed in Milli-Q water at 10 ppm concentration for challenging the membrane samples. Concentration of silver in the feed and permeate samples was determined using inductively coupled plasma – optical emission spectroscopy (ICP-OES) (Perkin Elmer Optima 3000 DV 3000, USA).

4.1.6 MS2 enumeration

MS2 was cultured and enumerated based on the International Organization for Standardization method (ISO, 1995a). *Escherichia coli F-amp* (ATCC 700891) was used as the host, inoculated and grown in tryptone soya broth at 37°C with shaking at 100 rpm for three hours. MS2 stock culture (ATCC 15597-B1) was then added to the *E. coli* culture as prepared above and incubated overnight 37°C. The next day, *E. coli* cells and other debris were eliminated by passing through a 0.45 µm cellulose acetate syringe filter. The final MS2 stock was enumerated via the double agar layer (DAL) method. In the DAL method, the bottom layer is prepared by dispensing 1.5% of tryptone soya agar (Oxoid CM0131) after autoclaving, cooling to less than 50°C and adding antibiotics ampicillin (Sigma Aldrich A9518) and streptomycin (Sigma Aldrich S6501) both to a final concentration of 15 mg/L of agar. The top layer was prepared by adding a mixture of 1 mL of sample, 5 mL of soft agar and 100 µL of host *E.Coli*. The soft agar layer was prepared by autoclaving a mixture of mixing 30 g·L^{-1} of tryptone soya broth (Oxoid CM0129) and 7 g·L^{-1} of bacteriological agar (Oxoid LP0011). Samples were serially diluted in tryptone water (Oxoid CM0087) in order to achieve final plaque counts in the range of 10 – 100 plaque forming units (PFU) per inoculated plate. The method limit of detection (LOD) was 100 PFU/100 mL. For challenge testing of membranes, MS2 phage was dosed at an approximate concentration of around 10^7 - 10^8 PFU/100 mL, according to the maximum target concentration of $10^{(6.5 + LOD)}$ specified in the USEPA membrane filtration guidance manual (USEPA, 2005b). After 30 minutes of filtration, feed and permeate samples were collected in triplicate for enumeration.

4.2 Results and discussion

4.2.1 Temporal changes in RO membranes during ageing

The performance of pristine BW-30 membranes after compaction is summarized in Table 12. The values presented were an average of five membrane samples, obtained from individual experiments.

Table 12. Characteristics of compacted BW30 membrane.

Parameter	Value (n=5)
Pure water permeability (Lm^{-2}·h^{-1}·bar^{-1})	2.8 ± 0.21
Salt rejection, 2000 ppm of NaCl (%)	96.9 ± 0.21
MS2 removal (LRV)	> 6.2*

* Not detected in permeate

Temporal changes to RO membrane performance during accelerated aging by cycling fouling, cleaning and exposure to hypochlorite solution was expected to accelerate the field degradation conditions. With intermittent exposure to 100, 250 and 500 ppm h concentrations, membranes were tested up to 72, 33 and 20 cycles respectively. For example, for 500 ppm·h, intermittent cleaning with 1000 ppm concentration of hypochlorite for 30 min for 20 cycles resulted in a total exposure of 10000 ppm, equivalent to continuous contact of the membrane with 0.1 ppm of free chlorine for 11.4 years. Similarly 100 and 250 ppm·h exposures were equivalent to constant 0.1 ppm exposure for 8.2 and 9.4 years.

With every ageing cycle, initial membrane permeability gradually increased. For example, representative change in permeability during the fouling step for one experiment (of ageing with 500 ppm·h) is presented in Figure 18. In this figure, only fouling cycles are shown and cleaning and performance checks were not presented. Membrane permeability, measured at the beginning of the fouling cycle, increased from 3.3 L·m^{-2}·h^{-1}·bar^{-1} at the first cycle to 17.7 L·m^{-2}·h^{-1}·bar^{-1} at the 20th cycle.
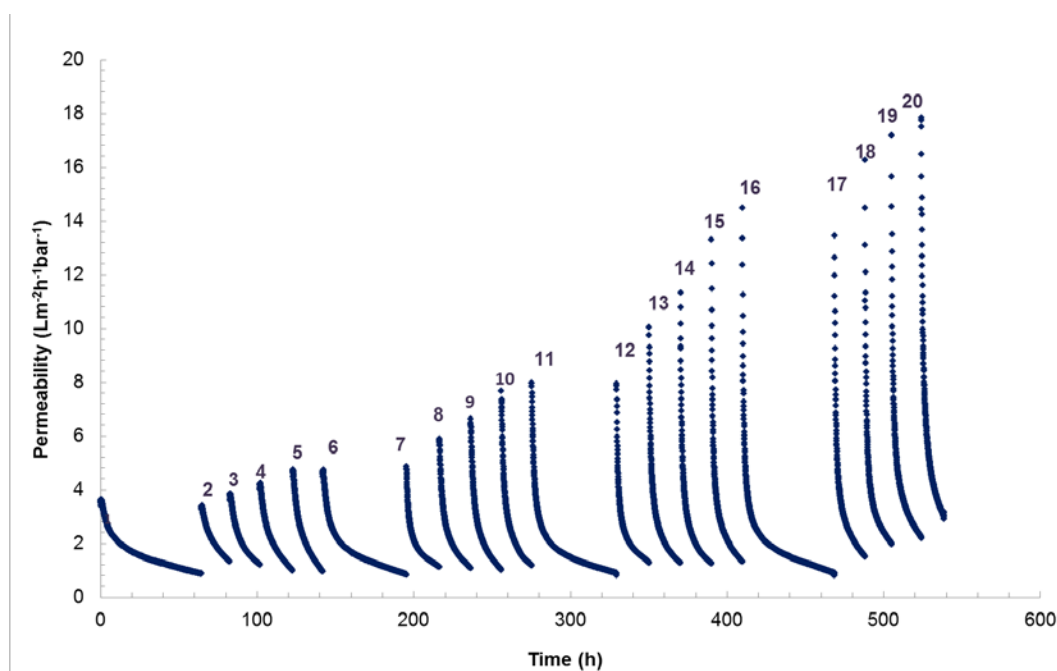
Figure 18. Membrane permeability during ageing with 500 ppm·h hypochlorite. Time (y-axis) scale indicates only the fouling time, does not include the cleaning schedules and testing with NaCl and MS2 phage.

Change in permeability and spiked NaCl salt rejection efficiency obtained during four experiments, at three different hypochlorite dosing concentrations 100, 250 and 500 ppm·h are presented in Figure 19. The number of cycles is presented in terms of equivalent hypochlorite concentration the membranes experienced. In all these experiments, membrane permeability decreased for the first few cycles. For example, during the exposure to 500 ppm·h, permeability slightly decreased from 3.3 to 3.2 in the second cycle, but increased to 3.7 for the third cycle. Correspondingly, spiked salt rejection increased from 97% at the first cycle to 98 % at the second cycle ad then decreasing to 96 for the third cycle. The reason for increasing salt rejection and decrease in permeability is referred as tightening effect of the polyamide membranes under mild chlorination conditions (Soice et al., 2003; Soice et al., 2004b; Do et al., 2012b). Exposure of a polyamide membrane to hypochlorite progresses through the transformation of N-H bond to N-Cl, followed by aromatic ring chlorination. Both of these chemical changes make the membrane more hydrophobic and the polymer chain more rigid due to conformation changes.
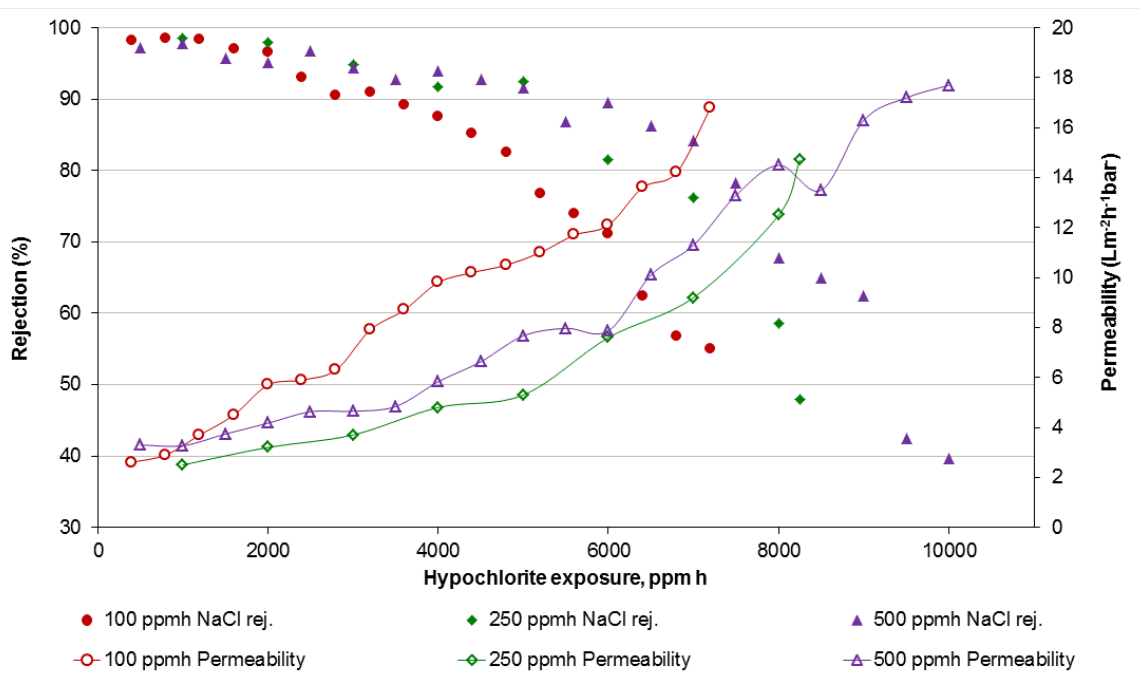
Figure 19. Permeability and salt rejection performance during the cycling ageing experiments with exposure to 100, 250 and 500 ppm·h during 72, 33 and 20 cycles. Performance was measured for every four cycles in the case of 100 and 500 ppm·h experiments and after every cycle for 500 ppm·h experiment.

For 100 ppm·h exposure, where the membrane was cleaned with 200 ppm of hypochlorite for 30 min at every cycle, spiked salt rejection decreased to 55% after 72 cycles, with total hypochlorite concentration of 7200 ppm·h. For 250 ppm·h, salt rejection reduced to 48% after 33 cycles (500 ppm of hypochlorite for 30 min after every cycle) equivalent to a total exposure of 8250 ppm·h. In the case of 500 ppm·h, 43% of salt rejection was observed only after 19th cycle, equivalent to 9500 ppm·h (1000 ppm of hypochlorite for 30 min after every cycle). With increasing hypochlorite exposure concentration, membrane damage seems getting delayed. In other words, for the available membrane area, low chlorine exposure for longer time is more deleterious than the exposure with high concentrations for short time.

LRV_{MS2} measured after each ageing cycle for three experiments, 100, 250, 500 ppm·h is presented in Figure 20. The standard deviation of the results varied between 0.01 to 1.2 LRV.
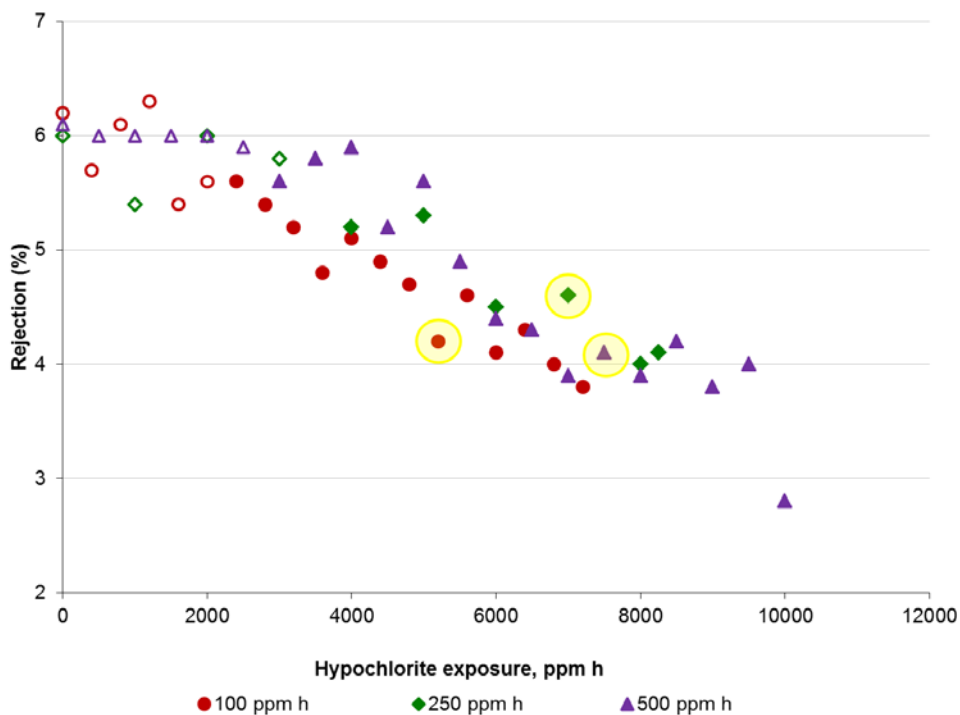
Figure 20. LRV$_{MS2}$ measured during the cycling ageing experiments with exposure to 100, 250 and 500 ppm·h). Open symbols denote that MS2 has not been detected in permeate. Yellow circles corresponds to the first point salt rejection was below 80%.

The LRV$_{MS2}$ decreased from 6.2 for a new membrane to 3.8 (corresponding NaCl rejection of 55%) for 100 ppm·h, 4.1 (corresponding NaCl rejection of 48%) for 250 ppm·h and 2.8 (corresponding NaCl rejection of 40%) for 500 ppm·. In all three experiments, when the salt rejection was closely below 80%, corresponding LRV$_{MS2}$ was above 4. In Figure 20, yellow circles indicate these three points, where LRV$_{MS2}$ values were 4.2, 4.6 and 4.1 corresponding to spiked NaCl rejection of 76.8%, 76.2% and 78.3% during 100, 250 and 500 ppm·h experiments respectively. This indicates that a RO membrane with 80% decline in the salt rejection performance can still be validated as a potential barrier for MS2 sized pathogens.

In Australia, a maximum LRV of 4 per unit operation in a water recycling scheme is mandated to encourage the use of multiple process barriers (Ottoson *et al.*, 2006). In this study, an RO membrane displaying a poor salt rejection of 80% was still capable of achieving an LRV$_{MS2}$ of 4. Furthermore, when the membranes were severely damaged, with unacceptable salt rejections, below 55%, LRV$_{MS2}$ was still appreciable, exceeding 3. Given that a maximum LRV$_{MS2}$ of 4 can be claimed and that conductivity was able to indicate significant removal deviations prior to reduction of LRV$_{MS2}$ below 4, the results of this study suggest that conductivity should be a conservative surrogate for virus removal.

There is an underlying assumption that LRV of salt is at a 1:1 ratio with LRV of much larger pathogens. This assumption may be flawed, as there is significant difference in the hydrated size of Na$^+$ (0.36 nm) and Cl$^-$ (0.33 nm) ions compared with the diameter MS2 (26 nm) (Israelachvili, 1985; Antony *et al.*, 2012). To investigate the assumption of a 1:1 LRV ratio, analysis of online conductivity and MS2 LRV were also assessed in this study.

4.2.2   Continuous conductivity measurements

The primary risks associated with water recycling schemes are pathogenic microorganisms, originating from sewage. Due to the expense, expertise and requirement for concentration of large samples (> 100 L) of treated water prior to analysis, it is impractical to use end point testing to assure treated water safety (Antony *et al.*, 2012). In order to control potential health impacts feasibly and efficiently, incorporation of hazard and critical control point (HACCP) risk management strategies for wastewater recycling schemes is often adopted (NRMMC *et al.*, 2006). In order to successfully implement HACCP, a critical control point (CCP) must be defined that has a significant action at reduction of pathogens and an online monitoring technique identified that can assure the nominal operation of the corresponding CCP (Dewettinck *et al.*, 2001). In this instance, RO is the CCP as through size exclusion with nominal membrane pathogens can

be significantly removed. Conductivity is chosen as the monitoring technique as a nominal reverse osmosis membrane should remove dissolved salts. Although application of conductivity is theoretically sound and widely employed, it is difficult to establish a quantitative and generic monitoring control limit specific to the application of virus removal (USEPA, 2005b). Cost of implementing conductivity monitoring is low (Kumar *et al.*, 2007) and the resolution of this method has been reported as 2 LRV, limited due to low feedwater conductivity and salt removal to below the meter limit of detection in the permeate (Adham *et al.*, 1998c; Kruithof *et al.*, 2001c; Lozier *et al.*, 2004; Kumar *et al.*, 2007).

During the 500 ppm·h experiments, online conductivity values were measured for feed and permeate streams, with rejection efficiency calculated for every fouling cycle. The upper reporting limits for the feed and permeate conductivity meters is 20000 and 200 µS respectively; the lower reporting limits was 100 and 10 µS respectively. Permeate conductivity online measurement during a typical fouling cycle is shown in Figure 21(a) and rejection efficiency calculated in Figure 21(b). Sufficient damage resulted in loss of salt rejection and a plateau of permeate conductivity at the upper reporting limit of 200 µS was observed between cycles 15 and 16. This in could result in LRV_{EC} calculations plateauing to a lower limit (i.e. < LRV).

(a)
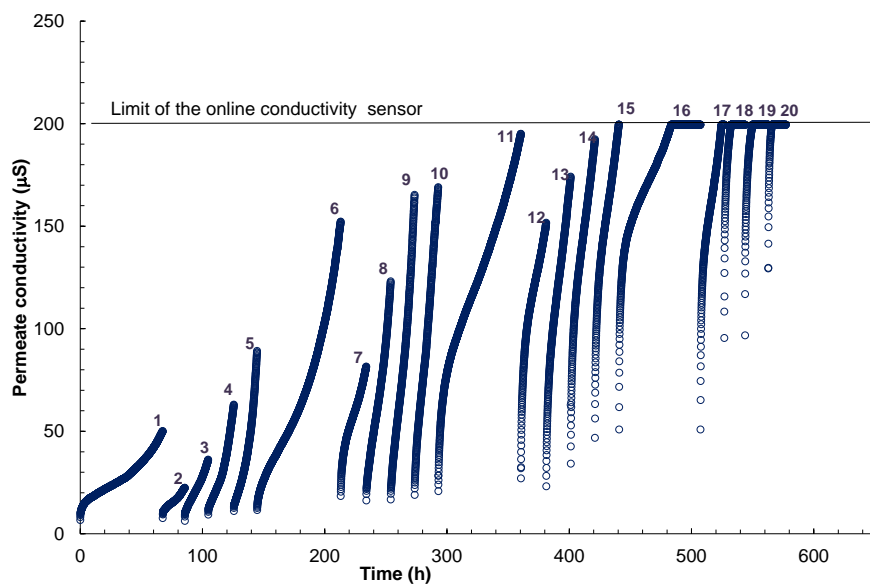
(b)
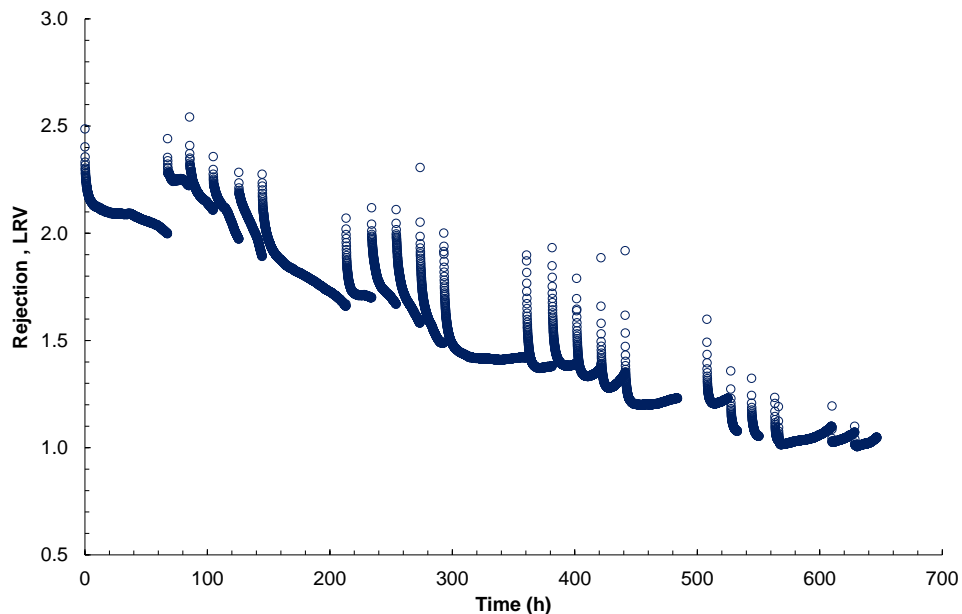
Figure 21. (a) Online electrical conductivity measured for the permeate stream during fouling and (b) rejection value calculated for the fouling cycles during the 500 ppm·h experiment.

For an undamaged membrane, with initial feed conductivity of 1870 ± 20 µS, a maximum of 2.5 LRV_{EC} could be obtained. The feed conductivity was contributed to by all feed solution components including, organics, high rejecting multi and divalent cations and anions and low rejecting monovalent cations and anions. In the current set of experiments, impact of cyclic ageing reduced the rejection efficiency close to 1 LRV_{EC} (90% rejection). With spiked 2000 ppm NaCl salt solution, rejection efficiency decreased from 1.6 LRV_{NaCl} for intact membrane to 0.2 LRV_{NaCl} for aged membrane after 20 cycles.

4.2.3 Correlation of MS2 rejection with spiked salt and online conductivity

Spiked salt conductivity is a simple test employed as quality assurance (QA) testing for RO membrane integrity, recommended by manufacturers. Commonly this test involves spiking 2000 ppm NaCl for a brackish water RO membrane or $MgSO_4$ for a NF membrane and challenge testing at an applied pressure of 7 – 15 bar. The type of salts, concentration and operating pressures may vary for different manufacturers. Performance of spiked salt testing on a regular basis during operation would enable the comparison of current against benchmarked initial performance.

Although the separation behaviour of salt is independent of MS2 or any other specific pathogen of concern, its rejection efficiency can be taken as a more conservative indication of the state of the membrane. Also, spiked salt rejection can be especially useful when the feedwater conductivity is low (i.e. the LRV_{EC} able to be demonstrated is limited by sensitivity of permeate conductivity meters). In addition, already installed online conductivity sensors can be used for membrane performance. In order to ascertain the level of reliability of online conductivity measurement (LRV_{EC}) and spiked salt (LRV_{NaCl}), values obtained in this study for 500 ppm·h experiments were correlated against corresponding LRV_{MS2} challenge test results (Figure 22).
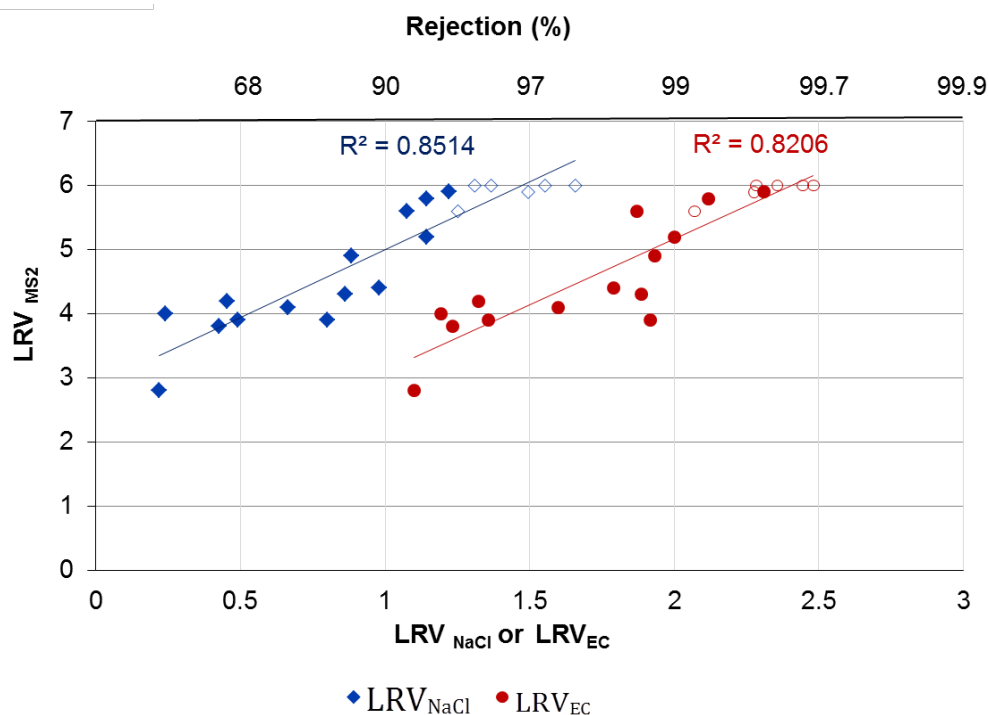
Figure 22. Correlation of LRV_{MS2} LRV against spiked NaCl rejection and online conductivity rejection. Open symbols indicate that MS2 phage was not detected in permeate.

LRV_{EC} is measured from the rejection behaviour for the model fouling solution, a mixture of organics, monovalent and multivalent salts. On the other hand, LRV_{NaCl} is measured form the rejection of 2000 ppm NaCl solution, prepared in Milli-Q water. Therefore, at all occasions during the accelerated ageing process, one would expect LRV_{EC} to be higher than the LRV_{NaCl}. The ratio of LRV_{MS2}:LRV_{Nacl} was roughly 4 - 5, but increased up to 12 as the membrane degradation is severe. The ratio of LRV_{MS2}: LRV_{EC} was generally between 3 and 4 throughout the ageing process. This further confirms that ageing and resulting degradation in the polyamide structure had greater impact to the passage monovalent salts when compared to virus sized particles and multivalent salts.

4.2.4 Ageing by passive exposure and industrially aged membranes

The virus removal performance was established for virgin, passively aged and industrially aged membranes by testing with MS2 phage, a non-microbial alternative nanoparticle, AgNP and spiked NaCl salt. Although MS2 challenge testing is currently believed to be the most appropriate surrogate for pathogenic virus removal by RO, there are significant practical and financial difficulties with implementation at full-scale facilities (Antony *et al.*, 2012; R Regel, 2012; Antony *et al.*, 2014; Irwin, September 2014). Recent challenge testing studies performed in Australia (R Regel, 2012; Irwin, September 2014) suggest that in spite of the rigorous precautions taken to avoid cross contamination, phage toxicity and maintaining the high concentration of phage in the feedwaters the detection was still extremely variable, proving it is not a conclusive and dependable method of LRV demonstration. The phage particles seem to readily aggregate and adhere to surfaces, which in turn influence the observed removal efficiency of the membrane. AgNP silver nanoparticles have been demonstrated as an alternative, non-microbial surrogate, suitable for UF membranes. Previously, AgNP challenge testing of intact UF hollow fibre membranes demonstrated rejection efficiency as high as 2.9 LRV, without affecting the hydraulic performance of the membranes (Antony *et al.*, 2014). Test results on virgin, passively aged and industrially aged membranes are presented in Table 13. Industrially aged membranes are samples from membrane modules of 2 to 5 years in service received from water treatment facilities and tested to provide a realistic baseline for comparison with the deliberate ageing methodology.

Table 13. Performance of virgin, passively aged and industrially aged membranes.

Membrane	Indicative service life in years, 0.1 ppm exposure	Permeability ($Lm^{-2}\cdot h^{-1}\cdot bar^{-1}$)	LRV_{NaCl}	LRV_{AgNP}	LRV_{MS2}	$\dfrac{LRV_{MS2}}{LRV_{NaCl}}$	$\dfrac{LRV_{AgNP}}{LRV_{NaCl}}$
Virgin		2.8	96.9	3.1	> 6.2	4.1	2.1
500 ppm·h	0.6	2.6	1.6	3.4	> 6.0	3.9	2.2
1000 ppm·h	1.1	4.4	1.2	3.0	> 5.9	4.9	2.5
5000 ppm·h	5.7	4.6	1.1	3.0	> 5.9	5.6	2.8
10000 ppm·h	11.4	7.3	0.9	2.9	> 5.6	6.2	3.2
20000 ppm·h	2.3	9.2	0.8	2.9	> 5.6	7.1	3.7
30 000 ppm·h	34.2	10.5	0.7	2.9	> 5.7	8.1	4.1
40 000 ppm·h	45.7	13.1	0.5	2.6	5.3	10.6	5.2
60 000 ppm·h	68.5	24.1	0.2	1.4	4.8	24.4	7.1
Membrane age in years							
IAM1	5	5.2	1.5	2.6	> 5.5	3.7	1.7
IAM2	5	3.2	1.8	2.8	> 5.7	3.3	1.6
IAM3	3	2.3	1.9	3.0	> 6.1	3.2	1.6
IAM4	2	4.9	0.5	1.9	4.6	9.1	3.7

Deliberate ageing with passive single dosages of hypochlorite resulted in significantly less membrane damage when compared to equivalent exposure of the cyclic ageing method. For example, during the cycling ageing of exposing the membrane to 500 ppm of hypochlorite for 20 cycles (total chlorine exposure after 20 cycles equivalent to 10000 ppm·h), membrane permeability increased to 17.7 $L\cdot m^{-2}\cdot h^{-1}\cdot bar^{-1}$ and corresponding spiked salt rejection decreased to 40%. With passive, single exposure to the same concentration of 10000 ppm·h, membrane permeability was 7.3 $L\ m^{-2}\cdot h^{-1}\cdot bar^{-1}$ and corresponding salt rejection was 87%. A similar trend was observed for LRV_{MS2}, 5.6 for membranes passively exposed to 10000 ppm·h compared to 2.8 for the membrane aged via the cyclic method. The effect of cyclic ageing is believed to be exacerbated, when compared to passive ageing, by a combination of factors including, fouling, cleaning and exposure to chlorine.

The three membranes originating from municipal wastewater recycling schemes (IAM1, IAM 2 and IAM3) demonstrated LRV_{MS2} greater than 5.5 LRV and salt rejection as high as 97%. Membrane sample IAM4 sample is from an industrial brine concentrator plant, was determined to have seen significant exposure to oxidising chemicals, as confirmed by a positive result for the Fujiwara test (a dye test performed during standard RO autopsies to detect the membrane damage due to oxidative damage by halides). As expected, IAM4 showed lower salt rejection 69% when compared to IAM1, 2 and 3. However, LRV_{MS2} for IAM4 was still appreciable at 4.6. During the controlled cycling ageing of membranes, LRV_{MS2} was close to 4 only when corresponding salt removal was 80% (Figure 20) and when salt rejection started to decline further, LRV_{MS2} was always less than 4.

For passively aged membranes exposed to 40 000 ppm·h, permeability was 13.1 $Lm^{-2}·h^{-1}·bar^{-1}$, spiked NaCl rejection was 68% and LRV_{MS2} was 5.3. For the membranes aged during cyclic fouling and cleaning experiments, at 70% spiked salt rejection (LRV_{NaCl} 0.5), permeability was close to the above value, 11 - 12 $L·m^{-2}·h^{-1}·bar^{-1}$ (Table 13) and LRV_{MS2} was approximately 4 (Figure 22). These results for cyclic and passively aged membranes tested during this study showed higher permeability than the industrially aged samples, which resulted in 2-5 $L·m^{-2}·h^{-1}·bar^{-1}$. The LRV_{MS2} and LRV_{EC} for the industrial aged membranes are close to that of virgin membranes, but with lower permeability. This could be due to the formation of irreversible fouling layer, assisting the preservation of MS2 rejection, but minimising the membrane permeability.

Challenge tests with the non-microbial surrogate, AgNP, were capable of demonstrating an LRV as high as 3.1. LRV_{AgNP} correlated well with the LRV_{MS2} values (R^2 = 0.8998) for the membrane samples tested.

4.2.5   TFC structure and implications for virus rejection

Typically, TFC membranes consist of three parts as represented in Figure 23. The top layer is the active surface layer of approximately 100 nm thickness. This is the PA layer (A), formed on the substrate after interfacial polycondensation reaction. The middle layer is the Poly sulphone microporous substrate of approximately 50 µm thickness Poly sulfone material is mostly used. The bottom layer is the reinforcing fabric support for additional mechanical strength, usually woven or nonwoven polyester materials of approximately 120 – 150 µm thickness is used. The TEM cross section of RO membrane given in Figure 23(b) shows the active surface layer and PS support layer.
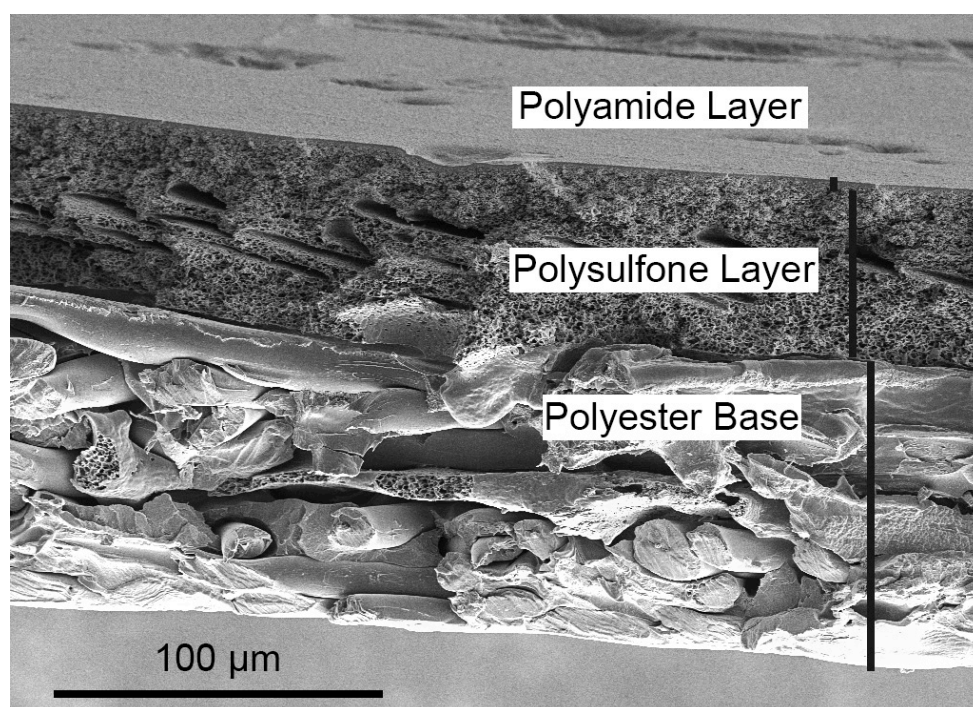
Figure 23. Cross section view of RO membrane showing the composite structure.

Exposure of RO membrane to high concentration (300,000 ppm·h) hypochlorite solution resulted in the removal of polyamide active layer, resulting in a product performing close to 10 kDa ultrafiltration (UF) membrane (Lawler *et al.*, 2013); Such damaged membranes demonstrated 2.4 LRV when challenged with non-microbial AgNP indicators compared to 2.6 LRV for a 10 kDa UF membrane. Previous studies report removal efficiencies of 3 to > 7 LRV for UF membranes with various model and native viruses (Jacangelo et al., 1991; Adham and Jacangelo, 1994; Jacangelo *et al.*, 1995; Madireddi *et al.*, 1997a; Kruithof *et al.*, 2001c; Jacangelo *et al.*, 2005). Also, UF, as a standalone process, was granted 4 log removal credit in four states of the USA (USEPA, 2005b).

Exposure to severe doses of free chlorine that removes the polyamide layer or any similar incidents damages the active will result in a poor removal of salts, however the underlying UF membrane or support layer is expected to warrant the removal of virus sized particles.

4.3   Conclusion

- Membrane ageing through cyclic, fouling, cleaning and resulted in a higher level of degradation than for a membrane aged passively, with a single equivalent exposure to hypochlorite.
- Online conductivity removal, LRV_{EC} was 2 to 3 times lower (i.e. more conservative) but displayed a good correlation with LRV_{MS2} for the samples tested in this study.
- LRV_{NaCl} was up to 4 times lower than the corresponding LRV_{MS2} and also correlated well. Given the significantly smaller size of NaCl and the correlation observed in this study, spiked salt rejection can be considered as a highly conservative procedure for confirmation of LRV_{MS2}, even if a 1:1 ratio is assumed. Given the factor of 4 difference observed in this study, a safety factor of at least 1 log could be adopted and LRV_{NaCl} to LRV_{MS2} could be considered appropriate as a 1:2 or even 1:3 ratio (i.e. LRV_{MS2} = 2 or 3 x LRV_{NaCl}). Adoption and acceptance of NaCl challenge testing in place of MS2, as described, would result in significant financial savings for full-scale RO processes employed in water recycling schemes or permit much more frequent testing at the same cost.
- Industrially aged membranes of 2 - 5 years, tested in this study, were still a resilient barrier for MS2 sized particles. For the industrially aged membranes tested, when compared with aged virgin membranes, a higher LRV_{MS2} was observed at equivalent conductivity removal, but permeability was lower, suggesting development of an irreversible fouling layer. The irreversible fouling layer may assist with preservation of virus rejection, however, the reduction in conductivity removal and permeability decline would likely trigger membrane replacement, prior to dangerous reductions in LRV.
- Silver nanoparticles are potential alternatives for microbial challenge testing and were capable of demonstrating LRV as high as 3.

5. Impact of RO membrane ageing on adsorption of MS2 phage

Membranes are a mechanical form of disinfection that works by physical separation of the target pathogen. Theoretically, an intact membrane is a barrier to pathogens that are larger in size than the pore size of the membrane. However, in practice the pore size distribution or molecular weight cut off only provide an indication of the separation efficiency. The general mechanism of pathogen removal by membrane processes is predominantly achieved by size exclusion, but influenced by the physicochemical properties of the membrane, surface properties of the pathogens and the solution environment (Antony *et al.*, 2012). High pressure membranes function by three primary removal mechanisms: size exclusion, electrostatic repulsion, hydrophobic interaction and adsorption.

The development of a fouling layer on the membrane surface was observed to increase the virus removal efficiency. Membrane fouling was found to heal membrane imperfections, which is also a function of the membrane type and the nature of the feed water foulants. If the fouling is reversible, then the membrane healing will get reverted with chemical cleaning (Kitis *et al.*, 2003b; Lozier *et al.*, 2004). However, literature is silent on the effects of long term membrane operation on virus removal. Consequently, while the development of increased irreversible fouling may enhance virus removal, it is not known if general decay or decomposition of the membrane may result in decreased rejection over the long term operation. There is not enough information available on the changes in the physicochemical nature of the membrane as a function of ageing. The present study aims at assessing the changes in the physicochemical nature of the membrane surface and virus adhesion capacity as a function of ageing.

Challenge testing with MS2 bacteriophage seeding is currently considered to be the best process indicator for validation RO membrane systems for enteric virus removal. As a surrogate for membrane processes in water treatment, in addition to the morphological and structural resemblance of MS2 phage to enteric viruses and ability culture at high concentrations it has two more advantages including (a) MS2 phage has a low isoelectric point (pI) of 3.5 - 3.9.; below this pH they carry a net positive charge while at this pH and above, they carry a net negative charge (Antony *et al.*, 2012). Therefore they are not expected to be adsorbed by negatively charged membranes (Overby *et al.*, 1966; Penrod *et al.*, 1995; Langlet *et al.*, 2008a; Langlet *et al.*, 2008b) (b) MS2 phage also possesses a certain degree of hydrophobicity, thus reducing the possibility of significant adsorption by hydrophilic membranes (Gerba, 1984; Shields and Farrah, 1987; Lytle and Routson, 1995).

5.1 Methods and materials

5.1.1 Membrane samples

All experiments was performed with BW-30 (Dow Filmtec) membrane; manufacturer reports an operating pH range between 2 and 11 and a maximum temperature and free chlorine tolerance of 45 °C and < 0.1 $mg \cdot L^{-1}$ respectively. Membrane samples of 0.0139 m^2 area was cut and exposed to nine different concentration of sodium hypochlorite solution for 24 h to obtain the exposure concentrations of 500, 1000, 2000, 5000, 10000, 20000, 30000, 40000 and 60000 ppm·h; their equivalent years of chlorine exposure concentrations in field application at 0.1, 0.5 and 1 ppm is given in Table 14. The samples were then rinsed thoroughly with Milli-Q water and tested.

5.1.2 Membrane characterisation

Membrane surface charge was calculated from the zeta potential measure as a function of pH over the range 2 to 8 against a 1 mM KCl background using an electrokinetic analyser (SurPass, Anton Paar GmbH, Graz, Austria). The operating pressure range varied between 0 to 500 mbar and the zeta potential values were obtained based on the Fairbrother and Mastin equation. The membrane contact angle was measured by sessile drop technique using a goniometer (KSV Cam 200 contact angle goniometer, Rame-Hart, USA) equipped with contact angle software. Presence of inorganic constituents present in the fouling layer and their elemental composition were examined by energy dispersive X-ray analysis (EDX) using a Hitachi S3400-N scanning electron microscope (SEM) coupled with Thermo Scientific EDX spectrometer. Functional group analysis was performed with ATR - FTIR characterisation using Spectrum 100 FT-IR spectrometer (PerkinElmer, USA) equipped with diamond crystal ATR unit. All spectra were collected with 32 scans at 1 cm^{-1} resolution and analysed with Omnic 7.3 software.

Table 14. Membrane ageing concentrations and their equivalent chlorine concentrations in field.

ppm·h	Equivalent years of chlorine exposure concentrations		
	0.1 ppm	0.5 ppm	1 ppm
Virgin Membrane	0	0.00	0.00
500	0.6	0.11	0.06
1000	1.1	0.23	0.11
2000	2.3	0.46	0.23
5000	5.7	1.14	0.57
10000	11.4	2.28	1.14
20000	22.8	4.57	2.28
30000	34.2	6.85	3.42
40000	45.7	9.13	4.57
60000	68.5	13.70	6.85

5.1.3   Membrane performance testing

Pure water permeability and salt rejection of the membrane samples were tested in stainless steel cell configured for flat sheet membranes with an effective membrane area of 0.0139 m^2. The schematic and details of this rig is presented in Figure 16 and section 3.1.1. At the beginning of the experiment, the membrane samples were soaked in Milli-Q water for 24 h and then operated at 8 bar to measure the stable clean water flux followed by testing the rejection of 2000 ppm of NaCl salt solution and 10^8 PFU/mL of MS2 phage seeded in Milli-Q water.

5.1.4   MS2 enumeration and adhesion test

MS2 bacteriophage is cultured and enumerated based on the International Organization for Standardization method (ISO, 1995a). Escherichia coli (ATCC 700891) is used as the host, inoculated and grown in tryptone soya broth at 37°C with shaking at 150 rpm for six hours. MS2 stock culture is then added to the *E.Coli* culture as prepared above and incubated overnight 37°C. Then the *E.Coli* cells and other debris are eliminated by passing through a 0.22 μm polysulfone filter. The final MS2 stock is enumerated through enumeration by double agar layer method. In the DAL method, the bottom/first layer is prepared by dispensing 1.5% of tryptone soya agar after autoclaving and adding antibiotic (ampicilin and streptomycin). The top layer is prepared by adding a mixture of 1 mL of sample, 5 mL of soft agar and 100 μL of host *E.Coli*. The soft agar layer is prepared by autoclaving a mixture of mixing 30g·L^{-1} of tryptone soya broth and 7 g·L^{-1} of bacteriological agar. For the challenge testing of membranes, MS2 phage is dosed at an approximate concentration of around 10^8 PFU/100 mL. After 30 minutes of filtration, feed and permeate samples were collected in triplicates for enumeration.

The analysis of MS2 adhesion on pristine and aged membranes was performed under passive mode. The membrane samples were held in a hook and soaked in beakers containing 1L of Milli-Q water seeded with 10^8 PFU/mL of MS2 phage. All membranes samples were taken out after 30 minutes of soaking. They were then placed in centrifuge tubes filled with Milli-Q water and sonicated for 10 min, to discharge the phage particles. MS2 phage in the collected water was then enumerated.

5.2   Results and discussion

5.2.1   Performance of RO membranes as a function ageing

The performance of the RO membranes as a function of ageing are based on the water permeability and salt rejection tests performed. The results are summarized in Table 15.

Table 15. Membranes water permeability and Salt rejection.

Membrane	Permeability (L·m^{-2}·bar^{-1})	NaCl Salt Rejection (%)
Virgin Membrane	1.18	95.03
500 ppm·h	4.30	91.92
1000 ppm·h	4.41	91.87
2000 ppm·h	4.59	91.17
5000 ppm·h	5.95	89.13
10000 ppm·h	7.30	87.29
20000 ppm·h	10.28	83.88
30000 ppm·h	13.93	80.21
40000 ppm·h	15.43	68.38
60000 ppm·h	19.71	36.36

5.2.2 ATR-FTIR

FTIR spectrum obtained from the ageing of BW30 membranes is shown in Figure 24. FTIR spectroscopy analysis was used to distinguish the changes on the polyamide (PA) active layer on the RO membranes.
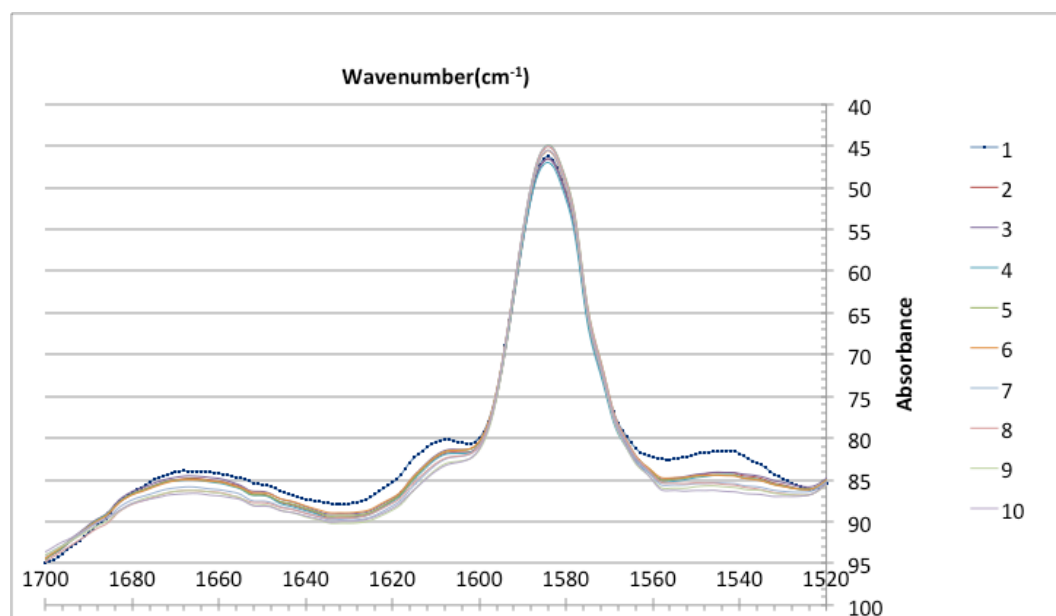
Figure 24. ATR-FTIR Spectrum of membranes as a function of ageing.

Significant changes on the polyamide (PA) layer of the RO membranes can be observed at characteristic wavenumbers 1542 cm^{-1}, 1609 cm^{-1}, and 1664 cm^{-1} representing zones amide II, C=C and amide I respectively. A close up around these characteristic wavenumbers can be shown in Figure 25a-c. Studies have shown similar set of results that showed significant changes on the polyamide (PA) layer were seen at wavenumbers stated above(Antony *et al.*, 2010; Ettori *et al.*, 2011; Lee *et al.*, 2013). The characteristic peak at 1664 cm^{-1} (amide I band) is contributed majorly by the stretching of C=O, C-N stretching and C-C-N deformation vibration (Antony *et al.*, 2010; Ettori *et al.*, 2011; Lee *et al.*, 2013). Whereas at characteristic peak 1609 cm^{-1}, it is the representative of the C=C stretching vibration (Antony *et al.*, 2010; Ettori *et al.*, 2011; Lee *et al.*, 2013). Lastly at characteristic peak of 1542 cm^{-1}, this represents the N-H in plane bending (Antony *et al.*, 2010; Ettori *et al.*, 2011; Lee *et al.*, 2013). The changes observed at the mentioned wavenumbers are tabulated in Table 16.
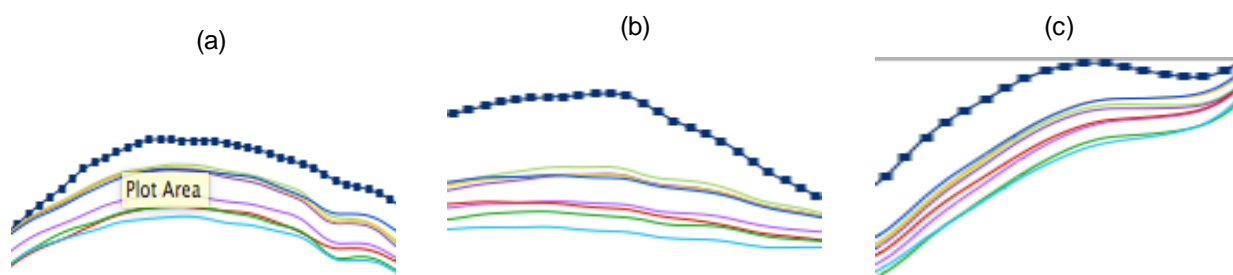
Figure 25. Close up of individual characteristic peaks (a) Amide I peak at characteristic wavenumber 1664 cm^{-1} (b) Amide II Peak at characteristic wavenumber 1542 cm^{-1} (c) C=C Peak at characteristic wavenumber 1609 cm^{-1}.

Table 16. Absorbance at Characteristic peaks of 1540 cm^{-1}, 1609 cm^{-1}, and 1664 cm^{-1} for FTIR analysis.

	Membrane	Absorbance (%) at Characteristic Peaks		
		1542 cm^{-1}	1609 cm^{-1}	1664 cm^{-1}
1	Virgin Membrane	81.83	80.25	86.71
2	500 ppm·h	84.39	82.05	87.9
3	1000 ppm·h	84.24	81.74	87.52
4	2000 ppm·h	84.61	82.20	88.09
5	5000 ppm·h	84.63	81.89	87.79
6	10000 ppm·h	84.68	81.89	87.47
7	20000 ppm·h	85.58	82.84	88.40
8	30000 ppm·h	85.74	82.71	88.47
9	40000 ppm·h	86.00	83.41	88.84
10	60000 ppm·h	86.52	83.61	88.84

The structural changes of RO membranes during the ageing takes place in two mechanisms, the N-chlorination mechanism followed by the rearrangement reaction which is known as the Orton rearrangement. This brings about the changes in hydrogen bonding and ring chlorination, which in turn affects the stretching and bending vibrations of the amide and carbonyl group. The hydrogen bonding of a virgin RO membrane is formed between two groups namely proton donor group (amide) and proton acceptor group (carbonyl). These groups get destroyed when exposed to hypochlorite solution. From the results of the spectra obtained, obvious changes at certain wavenumbers were seen when compared to a virgin RO membrane. According to the studies made by Anthony *et al.* (2010), disruption in the hydrogen bonding will result in the shifting of frequencies for N-H bending, C=O and N-H stretching(Antony *et al.*, 2010). This is can be further proven by the changes seen in the absorbance values at 1542 cm^{-1}, 1609 cm^{-1} and 1664 cm^{-1}. Peak 1542 cm^{-1} corresponds to zone of amide II representing N-H bending (Kwon and Leckie, 2006; Antony *et al.*, 2010; Ettori *et al.*, 2011). Peak 1664 cm^{-1}, corresponds to amide I band, contributed mostly by the stretching of C=O, but also C-N stretching and C-C-N deformation vibration (Kwon and Leckie, 2006; Antony *et al.*, 2010; Ettori *et al.*, 2011). Whereas at peak 1609 cm^{-1}, it is the representative of the C=C ring stretching vibration (Kwon and Leckie, 2006; Antony *et al.*, 2010; Ettori *et al.*, 2011).

During chlorination, amide I band at peak 1664 cm^{-1} was found to shift to a higher frequency and this is due to the replacement of hydrogen on the amide nitrogen with chlorine (Antony *et al.*, 2010). Antony *et al.*, also stated that as the chlorine concentration increases, bond strength weakens causing changes in the carbonyl group from hydrogen bound to free carbonyl (Antony *et al.*, 2010). Before the RO membranes went through chlorination, at peak 1542 cm^{-1}, amide II band that represents the N-H plane bending is restricted due to the hydrogen bonding with neighboring groups. After chlorination occurs, N-H gets converted to N-Cl, which weakened and destroyed the hydrogen bond causing the suppression and the shifting of the characteristic peak at 1542 cm^{-1} to a lower frequency. The disappearance of the peak at 1542 cm^{-1} also indicates that the chlorines were bounded to the membrane surface by replacing the hydrogen attached to the amide nitrogen and that the number of hydrogen binding sites decreased in the membrane (Kwon and Leckie, 2006).

As for peak 1609 cm^{-1}, the absorbance intensity decreases progressively, as the chlorine concentration exposure increases due the suppression of the C=C ring stretching vibration and the occurrence of ring chlorination. Referring to the research performed by Avlonitis *et al.*, the chlorination could lead to the change in the polymer morphology transforming them from crystalline to amorphous state, which changes the membrane performance. The high permeability and salt passage under pressurized conditions could be owing to the increase in the chain flexibility and the transformation of crystalline to more amorphous state. This can be proven from the high permeability and low salt rejection obtained at high chlorine concentration.

5.2.3   Contact angle

The hydrophobicity of the aged membranes measured through contact angle is presented in Figure 26. Contact angle increases until 2000 ppm and started to slightly decrease thereafter. Until 2000 ppm·h, the membrane hydrophobicity increases since there is a reduction in the number of hydrophilic N-H groups (Soice *et al.*, 2004a). Beyond this point, the hydrophobicity starts to decrease, however, more hydrophobic than the pristine membrane. A hydrophilic surface at high chlorine exposure concentration was reported earlier (Donose *et al.*, 2013b).
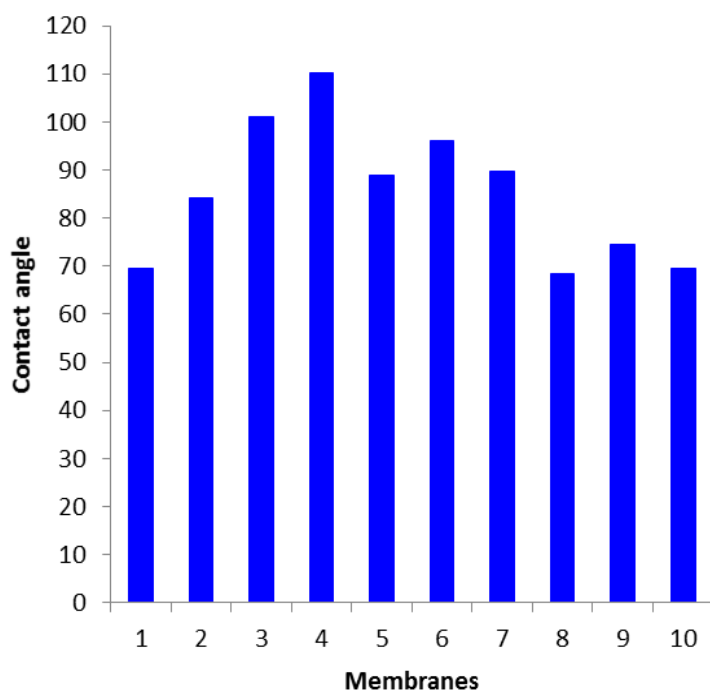
Figure 26. Average contact angle of RO membranes as a function of ageing.

Any chemical coming in contact with the RO membranes may alter the surface by attaching or detaching some functional moieties, possibly changing the hydrophobicity and surface charge of the membrane (Antony and Leslie, 2011). The hydrophobicity/hydrophilicity of the membranes were measured by contact angle analysis where lower contact angle suggests more hydrophilic traits making the surface more wettable. Results from the experiments showed the difference in hydrophobicity at different stages of the chlorine exposure concentration. At mild concentrations of 500 ppm·, 1000 ppm·h and 2000 ppm·h, hydrophobicity increases, showing a linear trend. The increase in hydrophobicity at mild chlorine exposure concentrations is caused by the incorporation of chlorine on the surface through chlorination (Do *et al.*, 2012a). As membranes get further damaged at severe conditions, a trend can be seen indicating that membranes became more hydrophillic. Studies have also shown that the increase in hydrophilicity after chlorination is possibly due to the introduction of unbalanced dipole moments on the membrane surface (Kwon and Leckie, 2006). Do *et al.*, 2012 have also reported that N-chlorination can promote hydrolysis of the amide C-N bond to form more hydrophillic carboxyl –COOH groups, therefore increasing membrane hydrophilicity (Do *et al.*, 2012a). Other studies have also reported that chlorine-exposed membranes become more hydrophillic probably owing to bigger pore size and charged species by chain scission (Arkhangelsky *et al.*, 2007; Antony and Leslie, 2011). Increase porosity could be responsible of the spreading out of the drop of the capillary. This is supported by the increase in the

permeability outcomes at severe exposure condition as explained earlier. However at concentrations 5000 ppm·h and 30000 ppm·h, the contact angles decreased more than what are expected making the trend at severe chlorine concentrations less linear. This can be explained by the minor yet significant variations in standard deviation among contact angle measurements which probably resulted from local variations that includes, surface roughness, dents, scratches and cracking on the surface (Kwon and Leckie, 2006).

5.2.4   Zeta potential

The surface charges of the aged membranes were analyzed based on their zeta potential values, presented in Figure 27. Zeta potential analysis on RO membranes as a function of ageing. Figure 27. Surface potential at pH 6.5 (operating pH) and isoelectric point derived in Figure 27 is presented in Table 17. For some of the aged membranes, isoelectric point could not reached, therefore no value available for these conditions. Nevertheless, a general trend could be seen, the isoelectric point changes from pH 3.9 to lower pH values as membrane ages. At pH 6.5, the surface charge of the membrane becomes more negative in the sequence of membranes 1, 9, 3, 5, 7, 6, 8, 10, 2, and 4. Temporarily disregarding the odd sequencing of the increasing negative surface charge, it is obvious that the surface charge becomes more negative when membranes are exposed to sodium hypochlorite solution especially when being compared to a virgin RO membrane.
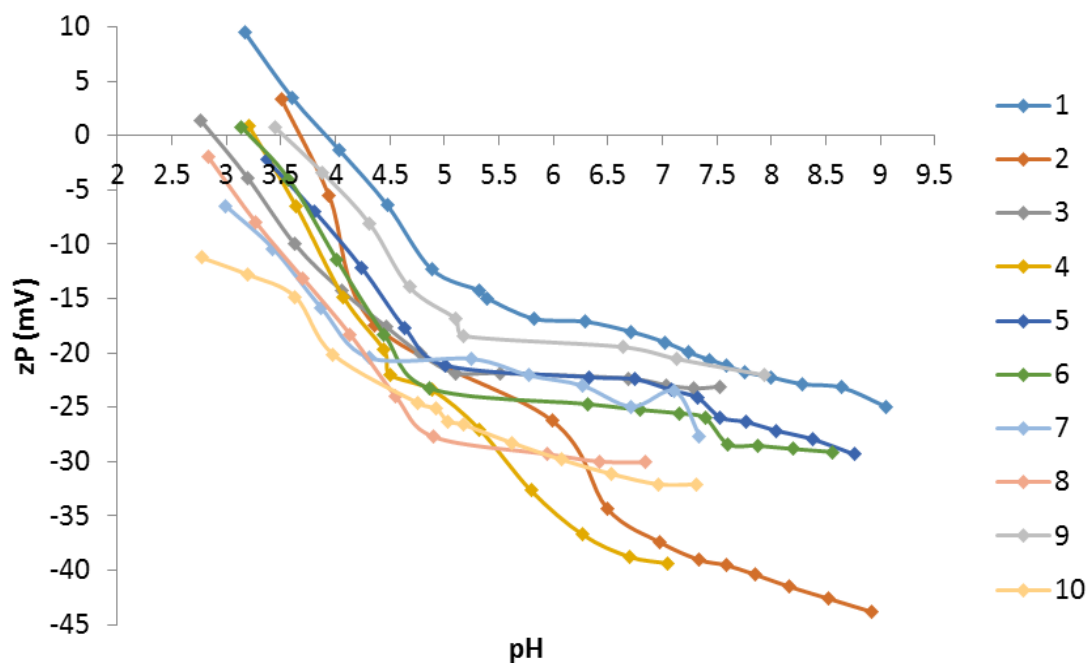
Figure 27. Zeta potential analysis on RO membranes as a function of ageing.

Table 17. Zeta potential analysis on RO membranes at isoelectric point and typical RO water pH.

	Membranes	Isoelectric point (mV=0)	At pH=6.5
1	Virgin Membrane	pH 3.9	-17.5 mV
2	500 ppm·h	pH 3.7	-35.5 mV
3	1000 ppm·h	pH 2.9	-22 mV
4	2000 ppm·h	pH 3.25	-38 mV
5	5000 ppm·h	-	-22 mV
6	10000 ppm·h	pH 3.20	-25 mV
7	20000 ppm·h	-	-24.5 mV
8	30000 ppm·h	-	-30 mV
9	40000 ppm·h	pH 3.5	-20 mV
10	60000 ppm·h	-	-31 mV

As the pH becomes more alkaline, the streaming potential measured in the background solution showed an increase in the negativity of the charge. This indicates that as membrane ages, the surface charge was shown to be more negative in comparison to the virgin membrane. This is supported by studies that have reported that chlorination promotes the hydrolysis of C-N bond incorporates more –COOH groups on the surface which lowers the surface charge of the RO membranes which can be proven from the zeta potential analysis performed (Do *et al.*, 2012a). According to the results obtained, it can be concluded that the surface charge properties of the RO membranes are very sensitive to the pH of the KCl electrolyte solution or the background solution. This statement is further supported by a study indicating that the surface charges of the membranes to the pH values should be closely related to the strong static interactions between the charged carboxyl groups and H^+ and/or OH^- ions (Li *et al.*, 2014). As a result their surface charge can be promptly changed with varying pH values. Xu *et al.* (2013) have also reported that hydrophobic chlorine atom bound to the membrane surface can cause a decrease in hydrophilicity and slight decrease zeta potential after chlorination at pH 4 and 7 (Xu *et al.*, 2013). This can be used as an explanation as to why the contact angle values at mild chlorine exposure concentrations show more hydrophobicity traits. However, at higher pH values, the complete conversion of the –COOH groups to –COO- groups in the linear part of the cross-linked aromatic polyamide lead to an increase in hydrophilicity and a relatively larger decrease in zeta potential (Xu *et al.*, 2013). This again can be used to explain the decrease in contact angle values at high chlorine exposure, which correlates to the larger decrease in zeta potential. Xu *et al.* (2013) have also reported that at harsh conditions, chlorination results in the cleavage of cross-linked aromatic polyamide chains leading to the local collapse on the membrane surface followed by the separation between the active layer and support layer (Xu *et al.*, 2013). This relates to the smooth membrane surfaces at high chlorine exposure concentrations obtained from the AFM images.

5.2.5 Surface roughness

Membrane surface roughness calculated as Root mean square (RMS) roughness for the membranes is presented in Table 18 and images are presented in Figure 28.

Table 18. Membrane surface calculated from AFM.

	Membranes	Average RMS value
1	Virgin Membrane	41.8
2	500 ppm·h	62.8
3	1000 ppm·h	88
4	2000 ppm·h	161
5	5000 ppm·h	91.7
6	10000 ppm·h	175
7	20000 ppm·h	163.8
8	30000 ppm·h	55.3
9	40000 ppm·h	57.2
10	60000 ppm·h	32.8

At mild concentrations, the roughness was shown to vary but an increasing trend can be seen. It has also been reported that the decrease in surface roughness was also observed after hypochlorite treatment (Simon, 2014). According to Kwon *et al.*, 2008, the degradation mechanisms, N-chlorination and Orton rearrangement could result in either a decrease of an increase in membrane surface roughness depending on the actual chemical composition and initial surface morphology of the membranes (Simon, 2014). Despite the variations in RMS values, it is noticeable that virgin RO membrane shows the roughest surface whereas the most damaged membrane at 60000 ppm·h shows a smooth surface. It is obvious that chlorine attack on the membrane surface disrupts the PA layer affecting the performance and other state conditions of the membrane such as the surface charge and hydrophobicity.

Virgin Membrane

500 ppm·h

1000 ppm·hr

2000 ppm·h

5000 ppm·h

10000 ppm·h

20000 ppm·h

30000 ppm·h

40000 ppm·h

60000 ppm·h
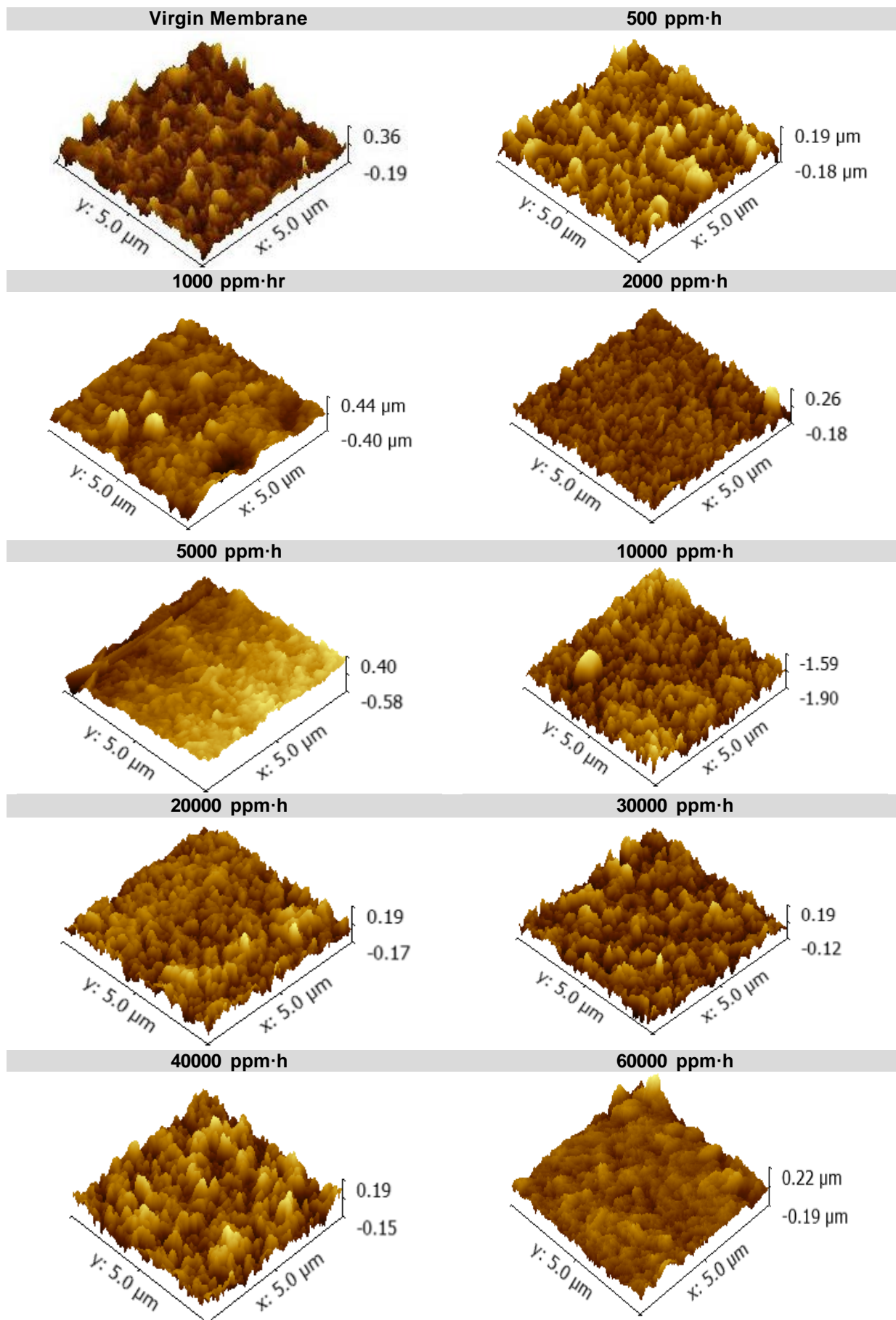
Figure 28. AFM images of pristine and aged membranes.

5.2.6   Impact of membrane ageing on performance of membrane performance

As a function of ageing due to exposure to increasing hypochlorite concentrations, water permeability increased salt rejection decreased correspondingly. Studies have shown that the increase in water permeability after chlorination can cause cross linkages decrease which may attribute to induced membrane hydrolysis due to the hypochlorite attack of the amide nitrogen (Do *et al.*, 2012a). The decrease in cross linkages on the polyamide (PA) layer of the RO membrane may lead to pore loosening effect caused by the oxidation of the active layer, modifying the structure hence increasing the water passage (Maruf *et al.*, 2012). However, at mild chlorine concentration conditions, which include 500 ppm·h, 1000 ppm·h and 2000 ppm·h, water permeability remained similar to one another due to the tightening effect that occurred at these chlorine exposure concentrations (Cran *et al.*, 2011; Do *et al.*, 2012a). Tightening effect occurs because of the formation of additional linkage via azo compounds on the surface causing the membranes to be less permeable at these conditions (Do *et al.*, 2012a).

Salt rejection performance can be associated with the increase in water permeability in which the oxidation of the active layer leads to the pore loosening effect hence the decrease in salt rejection. Some studies have reported that chlorination promotes the hydrolysis of C-N bond incorporates more –COOH groups on the surface which lowers the surface charge of the RO membranes which can be proven from the zeta potential analysis performed (Do *et al.*, 2012a). It is also stated that, enhanced surface negativity, together with the tightening effect, supposedly increases the rejection at mild chlorine concentration exposure. This statement is then again supported by the salt rejection results obtained at mild chlorine concentration conditions. At 500 ppm·h, 1000 ppm·h and 2000 ppm·h, it was found that the salt rejection for NaCl remained 91%. No decrease in NaCl salt rejection was observed during these conditions even though chlorine concentration exposure increased. One possible reason is due to the tightening effect, which was further elaborated earlier. Membranes which were exposed to severe chlorine conditions showed no signs of tightening effect which then again proves that the statement indicating enhanced surface negativity supposedly increases the rejection is only applicable to conditions experiencing the tightening effect. The drastic decrease in salt rejection performance at severe chlorine conditions could be most likely due to the polymer chain degradation and the creation of more open PA structure in the rejection layer.

5.2.7   MS2 Adhesion analysis

The number of MS2 phage adhered on to the membranes is presented in Table 19. MS2 adhesion generally increased on as a function of ageing, highest for membrane aged in the range of 1000 to 10000 ppm during which the surface roughness was high. At higher exposure concentrations, MS2 adhesion decreased.

Table 19. MS2 adhered on the pristine and aged membrane samples.

Sl.No	ppm·h (time 24 h)	Number of MS2 plaques adhered	
		Batch 1	Batch 2
1	0 (pristine)	9	26
2	500	29	223
3	1000	14	497
4	2000	25	503
5	5000	53	440
6	10000	110	453
7	20000	48	240
8	30000	92	473
9	40000	12	187
10	60000	27	242

5.2.8   Mechanisms of Virus Rejection

MS2 bacteriophages have an isoelectric point at pH 3.9, suggesting that the charge will be negative above this pH. Therefore, when the membrane and the virus particles hold a negative charge, these repulsive forces could assist with the rejection of viruses (Antony *et al.*, 2012). Hence, as MS2 carries a net negative charge above the isoelectric point, improved rejection should be expected due to charge repulsion between the negatively charged membrane and MS2. MS2 adhesion analysis in passive mode was evaluated against factors, surface charge at pH 6.5, contact angle, and zeta potential and surface

roughness. Among the three factors correlated, surface roughness of the membrane gave the maximum correlation. Representative correlation graphs for one batch of adhesion experiment are plotted in Figure 29. Increase in surface are with increasing roughness seems to enhance provide additional space for MS2 to adhere, overcoming the charge and hydrophobic repulsions.
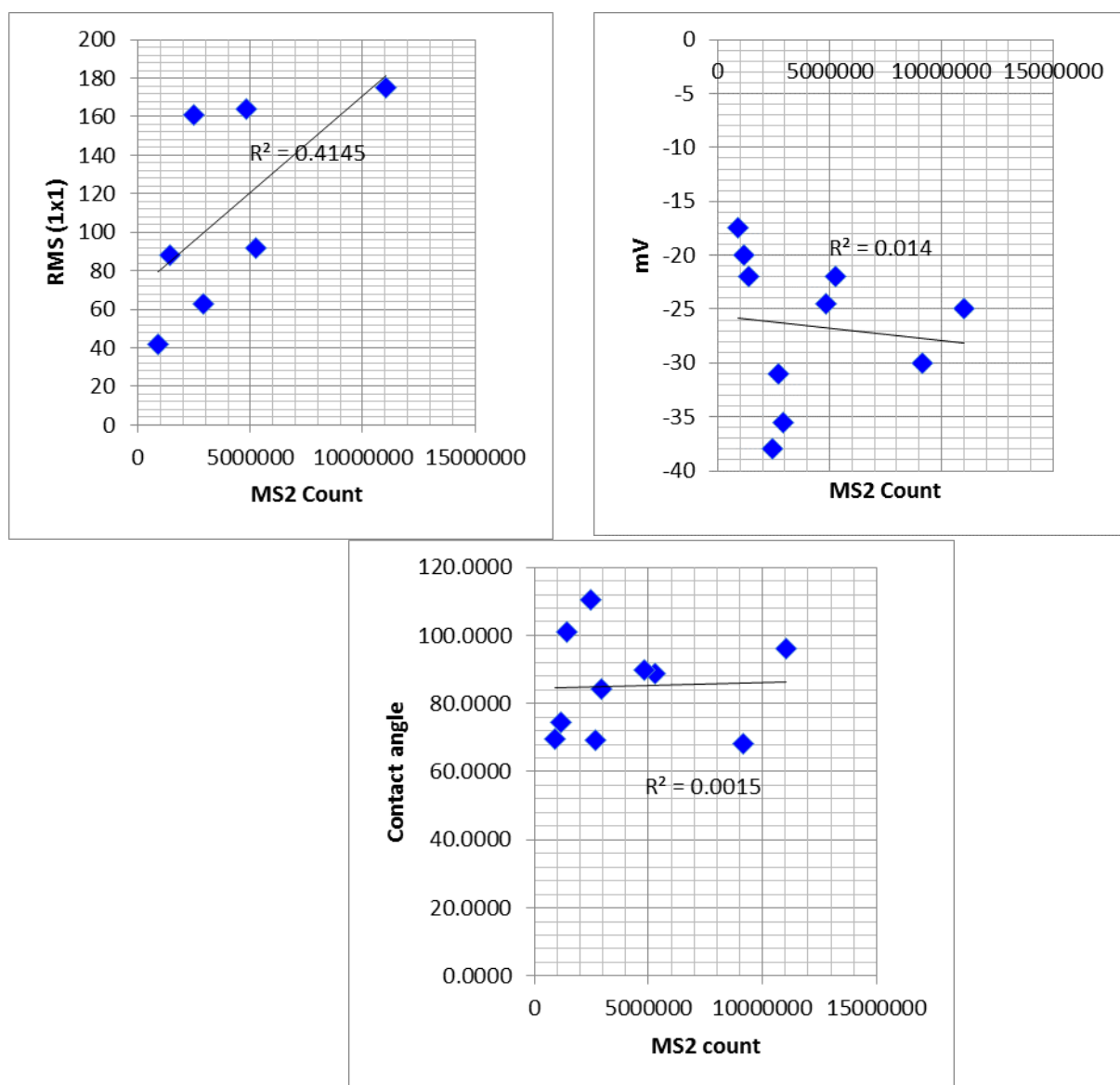
Figure 29. Correlation graphs for MS2 adhesion of ageing RO membranes.

5.3   Conclusion

There are three mechanisms that could affect virus removal efficiency: size exclusion; charge repulsion; and adsorption. This study has focused more in determining the impact of charge repulsion and adsorption mechanisms as a function of ageing RO membranes, using MS2 phage as the indicator organism for virus. It was found that membranes became more negative as they age which causes greater repulsion between the MS2 and membrane surface. This contradicts with the decrease in MS2 removal efficiency.

The outcomes of the MS2 adhesion analysis were then associated with other changing membrane properties such as surface roughness, hydrophobicity and charge to check for any correlations between MS2 adhesion and other membrane parameters. It can be concluded that the greatest correlation to the MS2 adhesion was found to be the surface roughness of the membrane. As a function of ageing, membranes became smoother towards severe chlorine concentration indicating the deterioration of polyamide layer.

Appendix A. Sulfate sensor development

A.1. Background/Introduction

The objective of this work is to develop and assess the viability of an ion sensor for the detection of sulfate ions. This ion sensor is to be examined for the measurement of LRVs of RO membranes in which sulfate serves as a surrogate. Studies reported here were focused on identifying suitable reagents for the experimental studies and assessing the experimental performance of the prototype sensors.

A.1.1. Sensor principle

The principle of the sensor to be developed is that the transfer of an ion species from a water phase to an immiscible liquid phase can be assessed by electrochemical parameters, such as the potential of ion transfer (different ions will transfer at pdifferent applied potentials, dependent on their characteristics and the nature of the two immiscible liquid phases, as reflected by the ions' Gibbs energy of transfer) and the ion-transfer current (which will depend on the concentration of ion species transferring). In an interface system formed between water (W) and an organic solvent (O), in which both liquids contain dissolved electrolytes, the interface is referred to as the interface between two immiscible electrolyte solutions (ITIES). In such a system, it can be envisaged that the W phase is a water sample containing the ion species to be sensed. If the target ions are very hydrophilic, their transfer potentials will not be easily amenable and an ionophore (Greek: ion-loving) is added to the O phase. The function of the ionophore is to lower the energy required to transfer the target ion species across the interface, by forming a complex between the ion and the ionophore. The lowered transfer energy is seen in a transfer potential for the ion that is experimentally amenable.

For the present sensor, the target ion, sulfate, is highly hydrophilic, and a commercially available ionophore is examined for the purposes of facilitated ion transfer (FIT), as depicted in Figure 30.
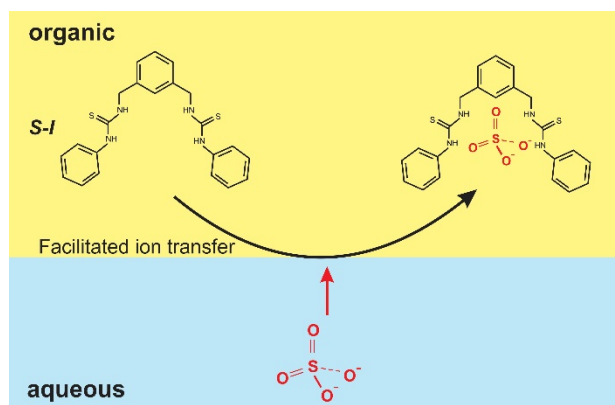
Figure 30. Cartoon of facilitated ion transfer of sulfate across the interface between water and organic phases. S-I = sulfate ionophore.

The essential nature of the new sensor prototype will be the reaction of sulfate anion with the ionophore (L) at the liquid-liquid interface (Equation *14*).

$$SO_4^{2-}{}_{(aq)} + xL_{(org)} \rightarrow L_x SO_4^{2-}{}_{(org)} \ (x = 1 \ or \ 2)$$ (14)

This reaction causes sulfate to move into the organic phase; the movement of anions across the interface is measured as an electrical current whose magnitude is dependent on the concentration of the sulfate anion. The potential at which this reaction occurs under electrochemical control is indicative of the ease with which the reaction can be driven.

A.1.2. Materials and Methods

A.1.2.1. Reagents

All the reagents were purchased from Sigma-Aldrich Australia Ltd. The hydrophobic organic electrolyte (BTPPA$^+$TPBCl$^-$) was prepared by metathesis of bis(triphenylphosphoranylidene)ammonium chloride (BTPPA$^+$Cl$^-$) and potassium tetrakis(4-chlorophenyl)borate (K$^+$TPBCl$^-$). 10 mM BTPPA$^+$TPBCl$^-$ solutions were prepared in different organic solvents: nitrobenzene (NB), 1,2-dichloroethane (DCE), 1,6-

dichlorohexane (DCH) and o-nitrophenyl octyl ether (NPOE) in the presence or absence of the commercial sulfate-ionophore I (S-I) (Figure 31). All aqueous solutions (Na_2SO_4, H_2SO_4 and LiCl) were prepared in purified water, from a USF Purelab plus UV, with a resistivity of 18.2 MΩ·cm.
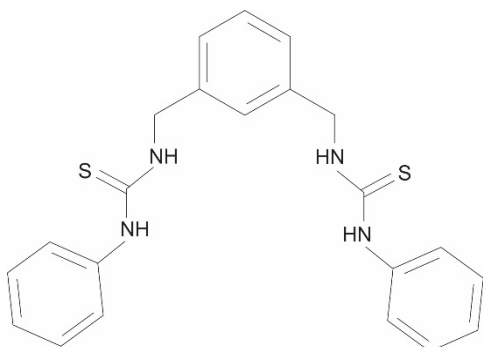
Figure 31. Chemical structure of Sulfate-Ionophore I (S-I), 1,3-[Bis(3-phenylthioureidomethyl)]benzene. This is commercially available from Sigma-Aldrich.

To aid the dissolution of other ionophores tested, THF was added to the organic mixture and left to evaporate for 24 h prior to use. This is a common strategy in the preparation of polyvinyl chloride-ion selective electrodes (PVC-ISE) based membranes.

A.1.2.2. Electrochemical cell.

The liquid-liquid microinterfaces were formed using a silicon membrane consisted of 30 micropores of 22.4 μm diameter (Zazpe *et al.*, 2007). These microporous silicon membranes were sealed onto the lower orifice of a glass cylinder using a silicone rubber (Acetic acid curing Selleys glass silicone (Selleys Australia & New Zealand)). The organic phase solution (yellow solution in Figure 32) was introduced into the silicon micropore array via the glass cylinder and the organic reference solution was placed on top of the organic phase. The silicon membrane was then immersed into the aqueous phase (Figure 32a). A two-electrode electrochemical cell was employed, whereby, the micro-interface array was polarised by applying a potential difference between two electrodes (Ag in the aqueous solution and Ag/AgCl in the organic reference solution).

The electrochemical cell employed is summarised in Figure 32b-c. All electrochemical measurements were performed using an Autolab PGSTAT302N electrochemical analyser (Metrohm Autolab, Utrecht, The Netherlands). Cyclic voltammetry (CV), differential pulse voltammetry (DPV) and differential stripping voltammetry (DPSV) experiments were carried out at 10 mV·s^{-1}. The pulse parameters for DPV and DPSV were 5 mV step potential, 75 mV amplitude, 0.2 s pulse time and 0.5 s interval time (see Section A.2.3 for more detail).
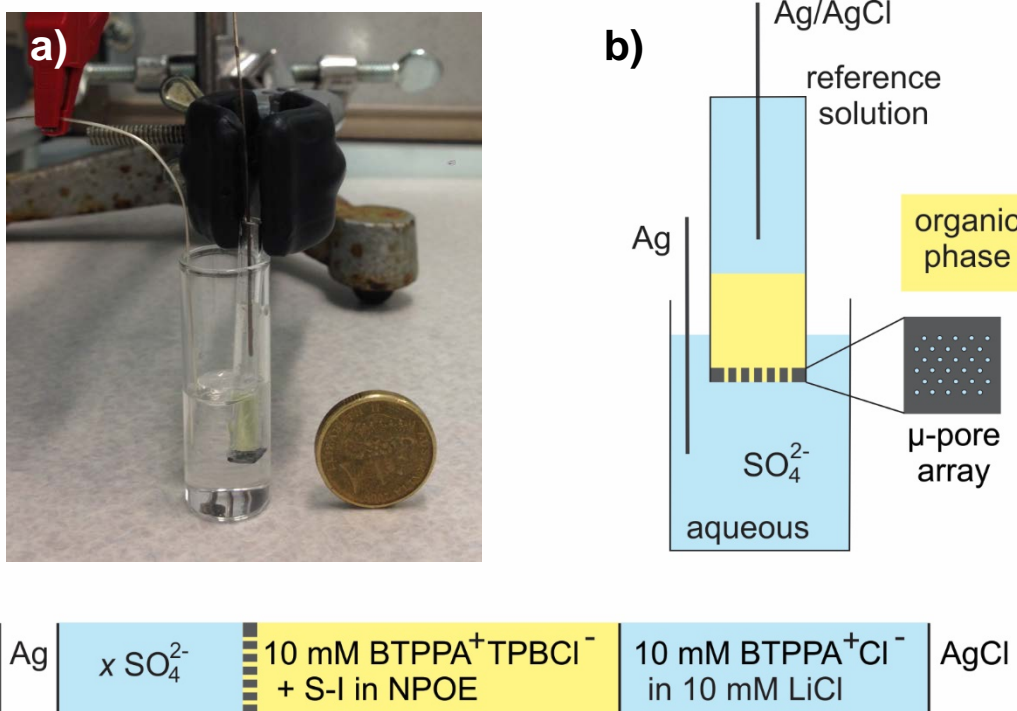
Figure 32. a) Photograph of the two-electrode set-up of the liquid-liquid electrochemical cell beside an Australian $2 coin; b) schematic diagram of the electrochemical cell set-up showing all of the components; c) Schematic of the electrochemical cell with aqueous and organic phase compositions; NPOE is the organic solvent, S-I is the sulfate-ionophore, x is the sulfate (SO_4^{2-}) concentration, BTPPA$^+$TPBCl$^-$ is the organic electrolyte present in the organic phase.

A.1.2.3. Conductivity

HQ40d Portable Conductivity probe was used for conductivity measurements of the pre- and post-RO samples. The probe was calibrated to a 1413 $\mu S \cdot cm^{-1}$ standard solution prior analysis.

A.1.2.4. Ion chromatography (IC)

Ion chromatography analysis was performed to determine the possible interferences present in the post-RO samples using a Dionex ICS-90 ion chromatography system. A column chemically modified with alkanol quaternary ammonium salts (Dionex Ion Pac AS23 4x250 mm) was employed for anion separation prior to ion detection via conductivity measurements. The samples were prepared in 0.5 mL Polyvials which contained a 0.45 μm filter. The eluent was 18 mM carbonate/ 3.2 mM bicarbonate, reagent 50 mM sulphuric acid, the flow rate 1 $mL \cdot min^{-1}$ and the injection volume was 20 μL. The system also contained a guard column and a suppressor (ARS 300 4 mm) to reduce the background conductivity from the eluent.

A.1.2.5. Electro spray ionisation – high resolution mass spectrometry (ESI-HRMS)

A Thermo Scientific LTQ XL Orbitrap mass spectrometer (Thermo Fisher Scientific Corporation, Waltham, USA) was employed for high accuracy mass determination of ionophores and complexes. Emulsions of NPOE in aqueous phase (1:1 in volume) were formed by sonication and then diluted (c.a. 1:4 in volume) with methanol. Solutions were infused at 3 - 8 $\mu L \cdot min^{-1}$ into the mass spectrometer using a syringe pump. ESI and MS parameters are summarised in Table 20. The emulsions of NPOE contained the ionophore (2.5 mM) and organic electrolyte (10 mM BTPPA$^+$ TPBCl$^-$) to mimic the ITIES conditions. Full calibration of the LTQ Orbitrap XL in the 70-2000 m/z range was conducted prior to each measurement with the positive and negative ion calibration solutions provided by Thermo Scientific. Optical lenses were optimised with a standard solution of caffeine prior to each measurement. For increased mass accuracy on the LTQ Orbitrap XL, a plasticizer interfering peak present in the background (n-butyl benzenesulfonamide, $C_6H_5SO_2NH(CH_2)_3CH_3$, [M+H]$^+$ = 214.0896 m/z), was used for the lock mass function. The screening analysis was conducted by operating the LTQ Orbitrap XL mass spectrometer in full-scan mode from 70 - 1000 m/z with a mass resolution of 30.000 (@ 400 m/z). Where necessary, samples were analysed by operating the LTQ Orbitrap XL in HRMS^2 mode, where the

mass spectrometer is forced to isolate the parent compound, fragment it in the LTQ ion trap and then scan for the product ions in the Orbitrap mass analyser. A mass resolution of 30000 (@ 400 m/z) was used for the fragmentation experiments. For substance identification the deviation of the measured mass (i.e. parent compound and fragments) was compared against the theoretical mass (< 5 ppm, relative error). The measured isotope pattern was also compared with that obtained from isotopic simulation. Data was processed using Xcalibur QualBrowser 2.0.7 SP1.

Table 20. Summary of ESI and HRMS^n parameters used analysis of ionophores and complexes.

Parameters	Settings (+ eV)	Settings (- eV)
Spray voltage (kV)	4.0	-3.5
Capillary voltage (V)	-35	+25
Capillary temperature (°C)	275	275
Sheath gas flow rate (Arb)	10	10
Aux gas flow rate (Arb)	0	0
Sweep gas flow rate (Arb)	0	0
Tube Lens (V)	-110	+70
Scan range (m/z)	70-2000	70-2000
IT full MS AGC target	3E4	3E4
IT MS^n AGC target	1E4	1E4
FT full MS AGC target	2E5	2E5
FT MS^n AGC target	1E5	1E5
Ion trap and FT micro scans	3	3
IT full MS Max ion time (ms)	10	10
FT MS^n Max ion time (ms)	200	200
MS^2 isolation window (m/z)	1	1

AGC: Automatic Gain Control.
Arb: arbitrary units.
FT: Fourier Transform (Orbitrap mass spectrometer).
IT: Ion trap.
ms: milliseconds.

A.2. Results and Discussion

Initial studies were aimed at identifying suitable reagents to employ in the prototype sensor construction. These are primarily the organic solvent to be used in formation of the organic electrolyte phase, and the ionophore used to facilitate the transfer of the target ion, sulfate. A variety of commercially-available polar solvents are available for the former, while for the latter, a single commercially-available ionophore (S-I, Figure 31) is available.

The solubility of S-I in organic solvents is important, since its presence in the organic phase is needed to enable the reaction depicted in Figure 30 to occur. The solubility of S-I in a variety of organic solvents (NB, NPOE, DCE and DCH) was investigated by visual inspection for a range of S-I concentrations (0.025 – 10 mM) in order to optimise the electrochemical behaviour of the sensor. This is an important step as the nature of the organic phase composition can limit the sensing capabilities of the system. The order of decreasing solubility of S-I in these solvents was found to be: NB > NPOE > DCE > DCH.

A.2.1. Cyclic voltammetry

In addition, the electrochemical response of these organic phases (containing dissolved electrolyte, as shown in the cell composition, Figure 32) was studied both in the absence (Figure 33a) and in the presence of S-I Figure 33b) by recording of current-potential curves, called voltammograms, obtained by measuring the electrical current as a function of the applied potential difference at the polarised interface (W-NB, W-DCE, W-DCH, W-NPOE; Figure 33). In these experiments, the aqueous phase contained 10 mM LiCl. The data presented provide the available electrochemical window (range of potentials within which a charge transfer processes can be measured without the interference from background electrolyte transfers) for each organic phase. Figure 33a illustrates the available potential window at the various

polarised interfaces, depending on the organic solvent used: *i.e.* 0.54 V (NB) and 0.68 V (DCH). In addition, Figure 33b shows the effect of S-I added to the organic phase: it does not affect significantly the available potential window.
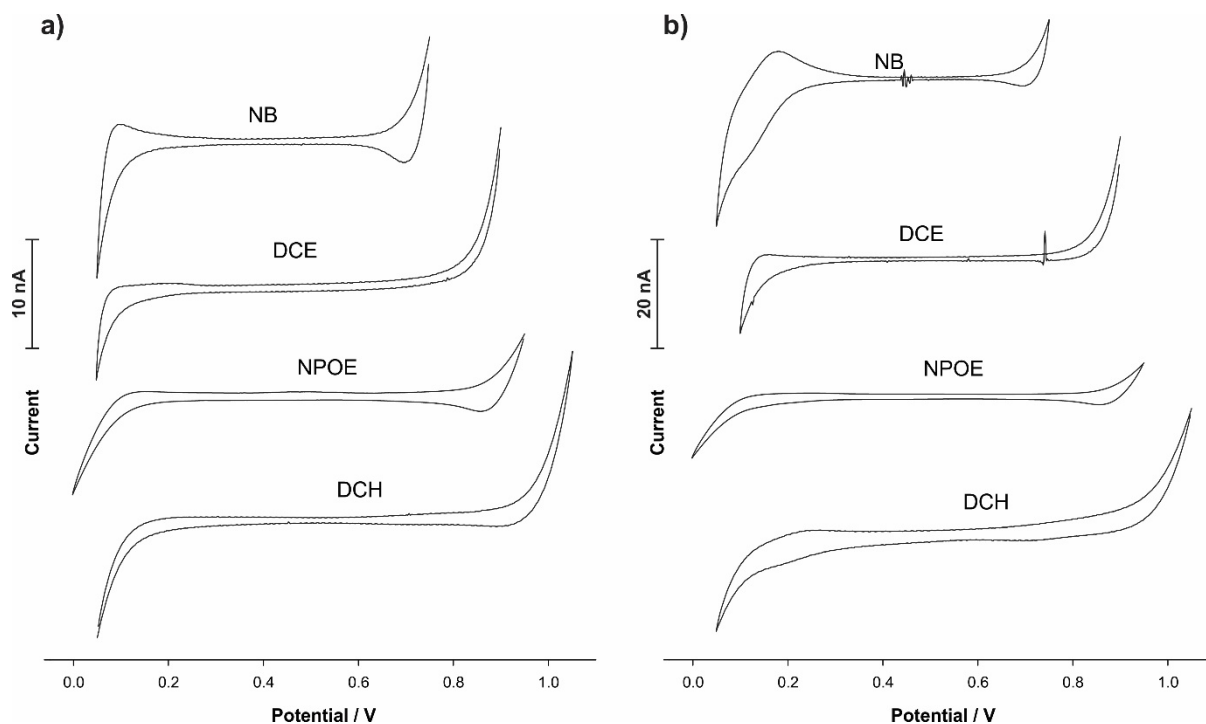
Figure 33. *CV at W-NB, W-DCE, W-NPOE, W-DCH interfaces (a) in the absence of S-I and (b) in the presence of 2.5 mM S-I in the organic phase.*

Moreover, in the case of organic phases formed from NB and DCH, the shape of the voltammogram changed significantly at *ca.* 0.2-0.3 V region (Figure 33b). This is attributed to the interaction between chloride ions (Cl$^-$) and the ionophore (S-I). To study the influence of Cl$^-$, different concentrations of LiCl were characterised (data not shown here). The results showed that the peak current varied with concentration of LiCl and suggests that S-I can form a complex with chloride in both NB and DCH media and may lead to selectivity issues in sensor performance.

Based on these data, NPOE was chosen as the optimum organic solvent because the potential window is large enough (*ca.* 0.68 V), S-I is more soluble in NPOE than in DCH (0.68 V potential window), and there is an absence of an apparent chloride transfer peak within the organic phase solvent is NPOE.

Nevertheless, it was considered prudent to carry out further studies of the sulfate – S-I system in the absence of chloride. For this reason the reference electrode used in the aqueous solution was switched to a pseudo-reference (Ag wire) instead of the classical Ag/AgCl, as the latter may be a source of interference (Cl$^-$).

Different concentrations of ionophore (0.025, 0.050, 0.25, 0.50, 1.25 and 2.5 mM) in NPOE organic phase were investigated (Figure 34) with the aqueous phase always being 0.1 M Na$_2$SO$_4$. The increased currents at *ca.* 0.2-0.3 V are attributed to the facilitated transfer of sulfate ions across the interface. Figure 34 (inset) shows the control voltammogram when S-I is not present in the experiment and transfer currents in this potential region are observed.
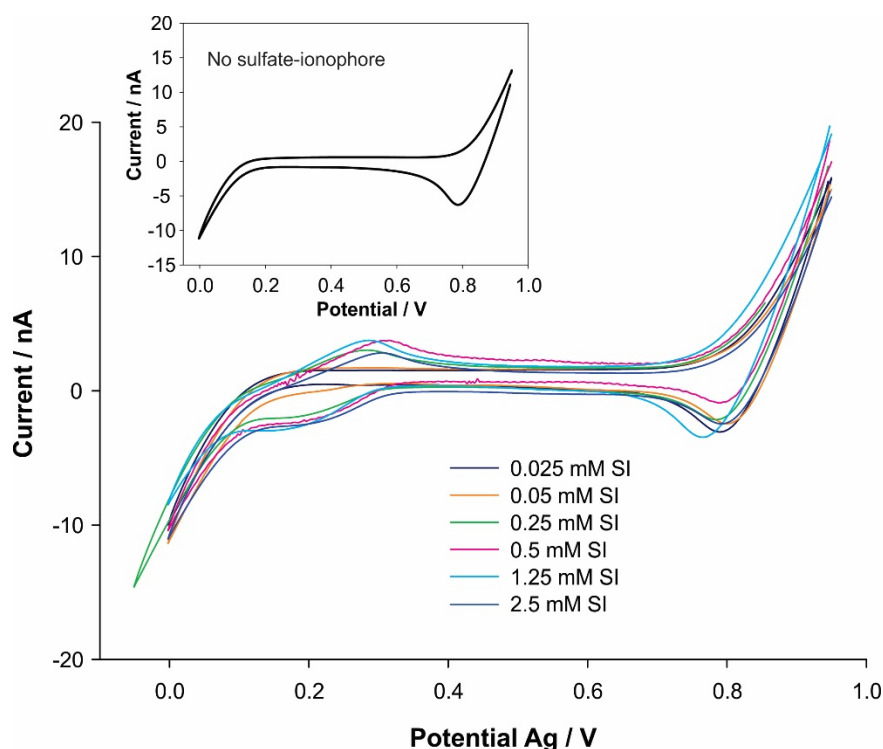
Figure 34. CV of 0.1 M Na₂SO₄ at W/NPOE interface in the presence of different concentrations of sulfate-ionophore I (0.025 – 2.5 mM). Inset shows the response without S-I in the organic phase.

Moreover, a wide range of Na_2SO_4 concentrations (10^{-7} to 10^{-1} M) were evaluated in order to investigate the sensitivity of the system Figure 6 shows how the transfer potential and the transfer current in the region of 0.2 - 0.3 V varies with the aqueous phase sulfate concentration. The peak at ~ 0.2 V on the forward scan (negative current) shifts to more negative potentials at lower sulfate concentrations. A similar influence is observed in the reverse peak (positive currents at ~ 0.3 V, Figure 35).
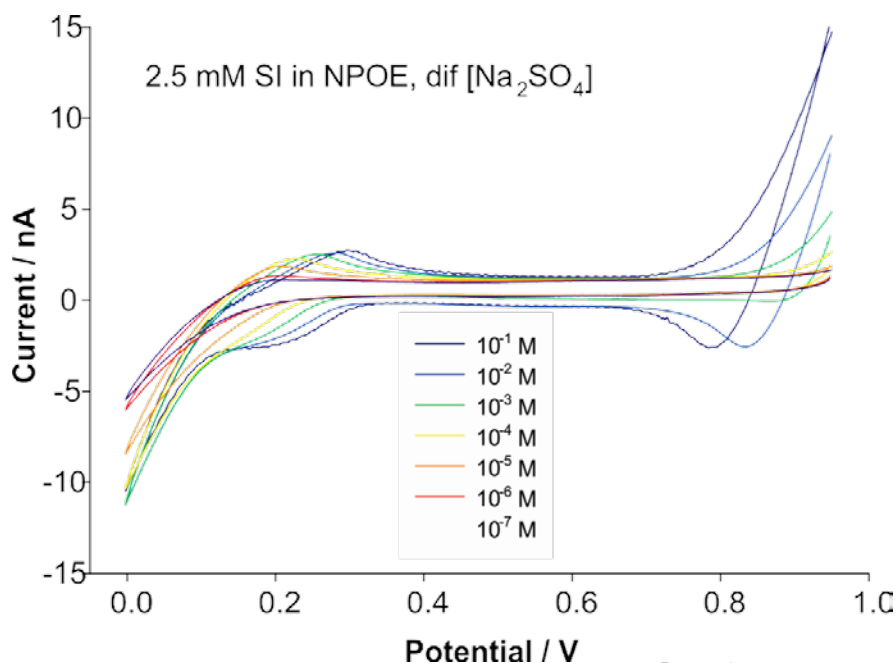
Figure 35. CV of different Na₂SO₄ concentrations (10^{-7} - 10^{-1} M) at W/NPOE interface in the presence of 2.5 mM sulfate-ionophore I in the organic phase.

H_2SO_4 was also investigated in similar conditions (10^{-7} to 10^{-1} M) to evaluate the sensor's behaviour in the presence of protons (H^+) which alter the sample's pH. Figure 36 shows the voltammograms obtained for different concentration of H_2SO_4 (10^{-7} to 10^{-1} M) which show the sulfate transfer current variation with the H_2SO_4 concentration.
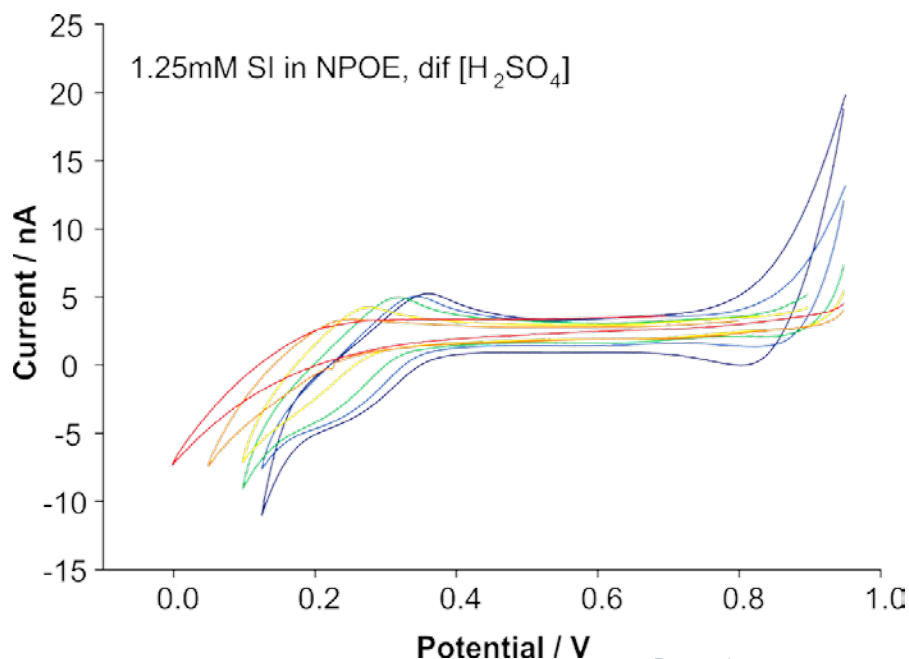
Figure 36. CV of different H_2SO_4 concentrations (10^{-7} - 10^{-1} M) at W/NPOE interface in the presence of 1.25 mM sulfate-ionophore I in the organic phase.

The limit of detection (LOD) calculated for SO_4^{2-} by CV is *1.3 µM*. The concentration range studied varied from *10^{-1} M to 10^{-8} M SO_4^{2-}*. The studies have also shown a potentiometric response similar to ion selective electrodes (ISE), with a shift in the half-wave potential of 28.4 mV·dec^{-1} corresponding to a two negative charge ion transfer. Table 21 summarises the analytical performance of the sulfate detection via CV for the forward and reverse voltammogram for 10^{-1} M - 10^{-8} M SO_4^{2-}.

Table 21. Summary of information obtained from the forward and reverse voltammograms (linear range, sensitivity, limit of detection - LOD -) when testing different concentrations of Na2SO4 in the water phase. The organic electrolyte was 10 mM BTPPA+TPBCl- in NPOE.

[S-I] / mM	Forward				
	Linear range / M	sensitivity/ mV·dec^{-1}	Int-$\Delta\phi_{1/2}$ (vs TEA transfer) / mV	r	LOD / M
2.50	10^{-1} - 10^{-6}	36	-384	0.966	3×10^{-6}
	10^{-1} - 10^{-6}	41.3	-352	0.995	7×10^{-7}
	10^{-2} - 10^{-6}	28.3	-460	0.999	1×10^{-6}
1.25	10^{-2} - 10^{-6}	32.6	-353	0.982	2×10^{-7}
	10^{-2} - 10^{-6}	38	-367	0.988	3×10^{-7}
	10^{-1} - 10^{-6}	24.1	-429	0.979	1×10^{-6}
	10^{-1} - 10^{-6}	26.9	-333	0.952	1×10^{-6}
	10^{-2} - 10^{-6}	27.8	-329	0.972	2×10^{-6}
	$\neq 10^{-1}$ - $10^{-5.5}$	25.2	-359	0.983	2×10^{-7}
[S-I] / mM	Reverse				
	Linear range / M	sensitivity / mV·dec^{-1}	Int-$\Delta\phi_{1/2}$ (vs TEA transfer) / mV	r	LOD / M
2.50	10^{-1} - 10^{-6}	12.3	-349	0.956	6×10^{-7}
	10^{-1} - 10^{-6}	16.5	-346	0.978	1×10^{-6}
	10^{-2} - 10^{-7}	26.2	-406	0.991	3×10^{-7}
1.25	10^{-1} - 10^{-6}	22.4	-340	0.988	1×10^{-6}
	10^{-1} - 10^{-5}	23.0	-444	0.990	1×10^{-5}
	10^{-2} - 10^{-6}	24.4	-332	0.991	2×10^{-6}
	10^{-1} - 10^{-6}	25.0	-371	0.982	2×10^{-6}
	10^{-2} - 10^{-6}	27.8	-298	0.987	1×10^{-6}
	$\neq 10^{-1}$ - 10^{-6}	28.6	-327	0.962	3×10^{-7}

$\neq$ 5 mM TDA$^+$TPBCl$^-$ organic electrolyte

The mean value for the limit of detection without any manipulation is 1.3×10^{-6} M (*ca.* 1.3 μM) which is one order of magnitude higher than our target (10^{-7} M). This also presented a sensitivity of 28.4 mV dec^{-1} which is in agreement with the potential shift for an ion with two charges, suggesting the formation of 1:1 sulfate-ionophore complexes.

CALIBRATION:

For a full and accurate characterisation of the capabilities of this sensor prototype, an internal reference for the potential axis is required, as the pseudo-reference electrode used in the aqueous phase is not as stable as classical Ag/AgCl electrodes. This can lead to inaccurate results. Tetraalkyl ammonium cations are commonly used as model ions with a known energy of transfer at liquid-liquid interfaces, e.*g.* tetraethylammonium chloride (TEA$^+$Cl$^-$) with a Galvani potential of transfer from water to NPOE ($\Delta_G^W \phi_{NPOE}^{w\frac{1}{2}}(TEA^+)$) of -3 mV (Valent *et al.*, 1987) based on the tetraphenylarsonium tetraphenylborate (TATB) assumption.

However, the possible chloride interference prevents the use of this salt in the aqueous phase. Thus, a more hydrophobic salt such as TEA$^+$TPBCl$^-$ which can be incorporated in the organic phase to provide the TEA$^+$ potential transfer so that the potential axis can be calibrated, must be employed. Tetraethylammonium tetrakis(4-chlorophenyl)borate (TEA$^+$TPBCl$^-$) was prepared by metathesis of TEA$^+$Cl$^-$ and K$^+$TPBCl$^-$ in H$_2$O:methanol (1:2). Then 10 μM of TEA$^+$TPBCl$^-$ was added to the organic phase (NPOE) so that the TEA$^+$ potential of transfer from NPOE to the aqueous phase can be assessed

for any measurement performed. Figure 37 shows the cyclic voltammograms of TEA^+ transferring from the NPOE to the aqueous solution in the presence ($-$) and absence of Na_2SO_4 ($-$). Thus the SO_4^{2-} potential transfer can be calibrated to the TEA^+ potential transfer (internal reference potential).
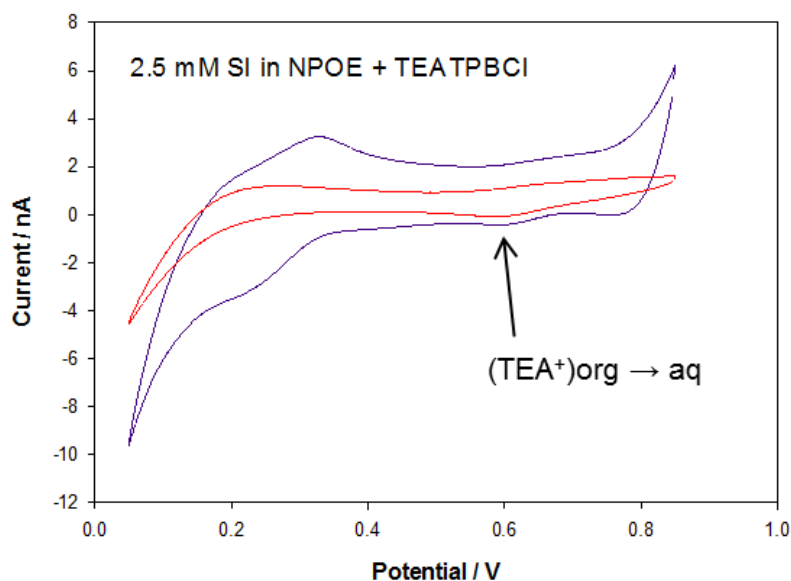
Figure 37. CV of 0.1 M Na_2SO_4 at W/NPOE interface in the presence of 2.5 mM sulfate-ionophore I + 10 µM TEA^+TPBCl^- in the organic phase.

A.2.2.   Sulfate-ionophore complexation

For the characterisation of the sulfate-ionophore complex formation, the ionophore (ligand) was prepared in water:methanol (50:50) mixture and sprayed to study its mass via ESI-MS. Its anionic form (loss of one proton) showed a mass (m) of 407.1353 g·mol^{-1} (z = -1) and the protonated form (positive mode) presented a peak at 405.1202 m/z (z = +1). These values agree with the molecular formula of the ionophore ($C_{22}H_{22}N_4S_2$). The same procedure was followed to mimic the ionophore media in the electrochemical set-up (ionophore + organic electrolyte + NPOE). For this study, the mixture of 2.5 mM ionophore +10 mM organic electrolyte + NPOE was diluted (1/4) in methanol to facilitate the sample electro-spray ionisation. As shown in Figure 38, the ionophore and the anionic component (TPBCl$^-$) of the organic electrolyte were identified at m/z values of 405.1202 and 457.0089.
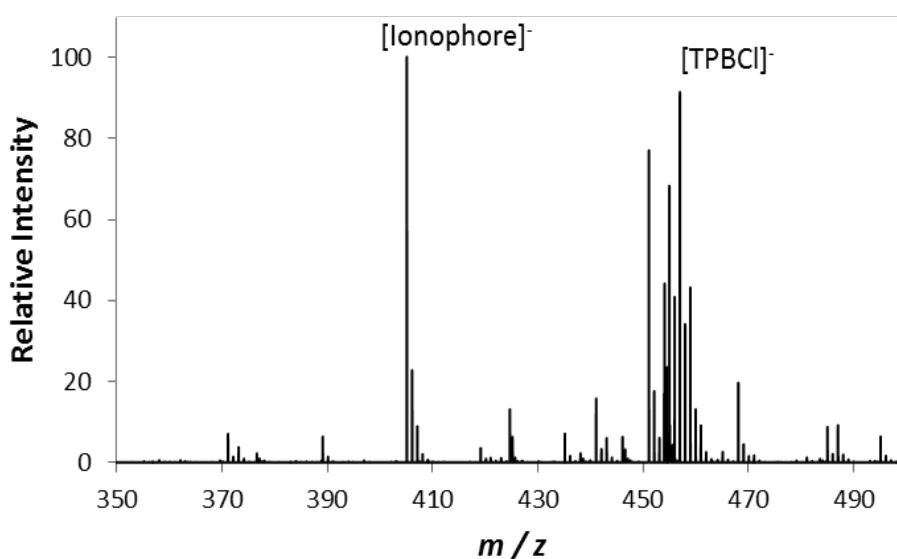
Figure 38. Spectrum of 2.5 mM Ligand (ionophore) + 10 mM BTPPA$^+$TPBCl$^-$ in NPOE after emulsification with water:methanol (50:50).

Then the same approach was undertaken to identify the ligand-sulfate complexation in both media, methanol:water and methanol:water/NPOE (Figure 32a-b). The emulsion corresponds to 0.1 M sulfate in the aqueous phase and 0.0025 M ionophore in NPOE phase (1:1), which was diluted in methanol (1/4) for ionisation. The excess of sulfate allows complexation and determination via ESI-MS. In the spectra represented in Figure 39, a new peak not observed in the absence of sulfate appeared at *ca.* 503 *m/z*. This value corresponds to the mass of a 1:1 ionophore:sulfate complex formed in both media, which confirms the strong interaction between the neutral ionophore and sulfate ions.

a) MeOH:H$_2$O (50:50)

b) MeOH:H$_2$O / NPOE emulsion
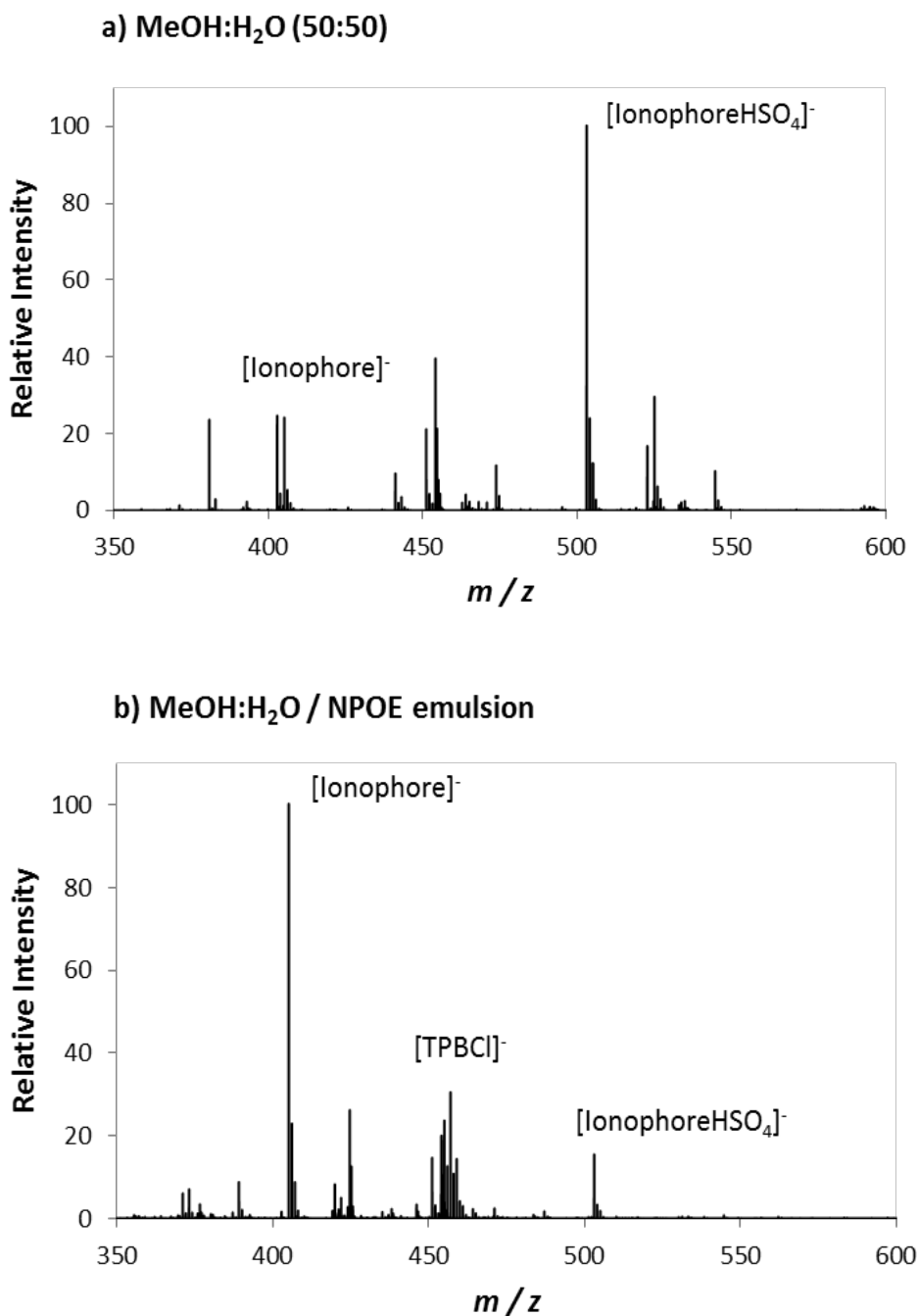
Figure 39. Spectra of a) ionophore with an excess of sulfate (0.1 M) in water:methanol (50:50) and b) of 2.5 mM ligand (ionophore) + 10 mM BTPPA$^+$TPBCl$^-$ in NPOE with an excess of sulfate (0.1 M) in water:methanol (50:50).

The theoretical and experimental ionophore:sulfate (1:1) complex mass (*m*) values from Figure 39a-b are summarised in Table 22 together with the deviation (*Δm*) between both mass values. These correspond to [C$_{22}$H$_{23}$N$_4$S$_3$O$_4$]$^-$, ionophore-HSO$_4^-$, a 1:1 complex with only one negative charge as small molecules tend to present low charge states in MS spectra.

Table 22. Summary of the theoretical (mthe) and experimental mass (mexp) determined by ESI-MS for the sulfate ionophore-sulfate complex (ionophore:HSO4⁻) in aqueous media and W/NPOE emulsions.

Sample description	Molecular formula	m_{the} / $g \cdot mol^{-1}$	m_{exp} / $g \cdot mol^{-1}$	Δm / ppm
S-I-HSO₄¹⁻ complex in MeOH:H₂O (Aqueous)	$[C_{22}H_{23}N_4S_3O_4]^-$	503.0920	503.0870	-1.121
S-I-HSO₄¹⁻ complex in MeOH:H₂O/NPOE (Emulsion)	$[C_{22}H_{23}N_4S_3O_4]^-$	503.0920	503.0872	-0.374

A.2.3. Differential pulse voltammetry

Another approach to detect low concentration of sulfate is using more sensitive electrochemical techniques such as differential pulse voltammetry. These voltammetric techniques can reduce the charging current which translate in an enhancement of the Faradaic current measured.

A.2.3.1. Optimisation of DPV and DPSV parameters

For a full characterisation of differential pulse voltammetry (DPV) at liquid-liquid interfaces, a model analyte (tetraethylammonium chloride, TEACl) was studied. Control experiments by CV were also performed in order to compare the capabilities of this pulsing technique. Figure 40 shows an example of the cyclic voltammetric response (red line), when 10 µM TEACl is added to the aqueous phase, and the DPV voltammogram obtained for the same conditions (10 µM TEACl in 10 mM LiCl) is illustrated in the inset.
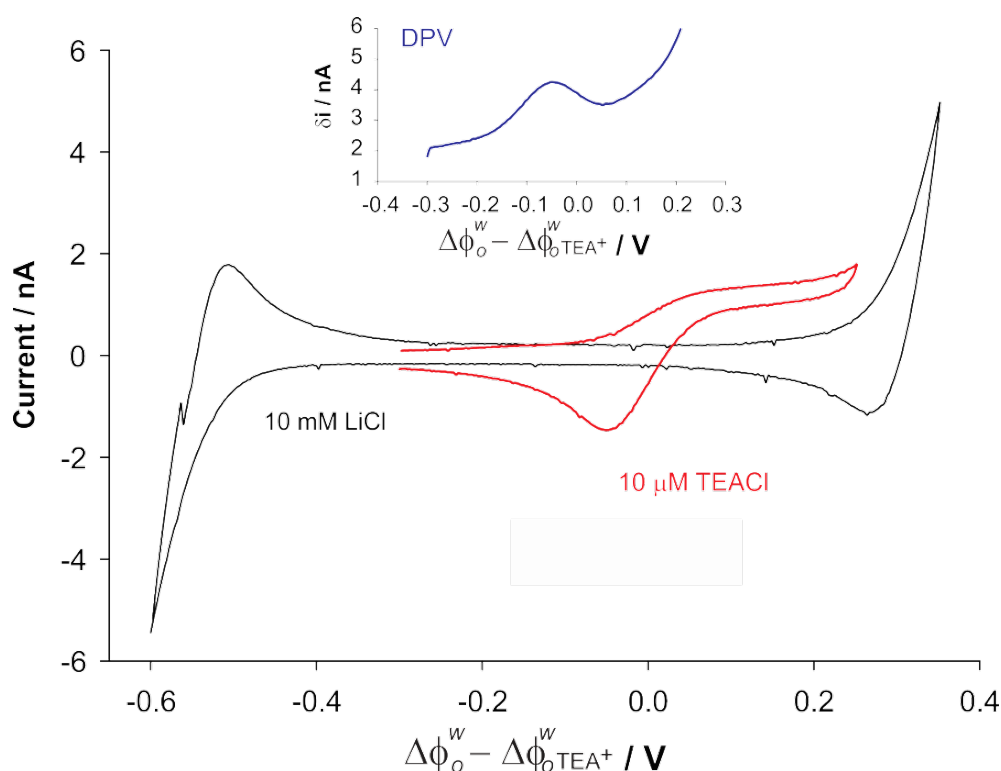
Figure 40. CV of 10 mM LiCl at W/NPOE micro-interfaces in the absence (black line) and presence of 10 µM TEACl (red line) in the aqueous phase. Org: 10 mM TDA+TPBCl⁻ in NPOE and Aq: 10 mM LiCl. Inset: DPV of 10 µM in 10 mM LiCl at W/NPOE micro-interfaces. DPV parameter: 5 mV step potential, 75 mV amplitude, 0.2 s pulse time and 0.5 s interval time.

DPV consists of the superposition of pulses on a staircase increment of potential. In this technique, the current is measured twice: 1) at the base of the pulse and 2) at the end of the pulse. Then the current difference is plotted against the potential applied. This process enables the elimination of the charging current as it decays exponentially whilst the Faradaic current decays as $1/t^{1/2}$ (Bard and Faulkner, 2001). Figure 41 illustrates the nature of the pulses applied and describes the parameters which can be tuned by the electrochemical instrumentation.
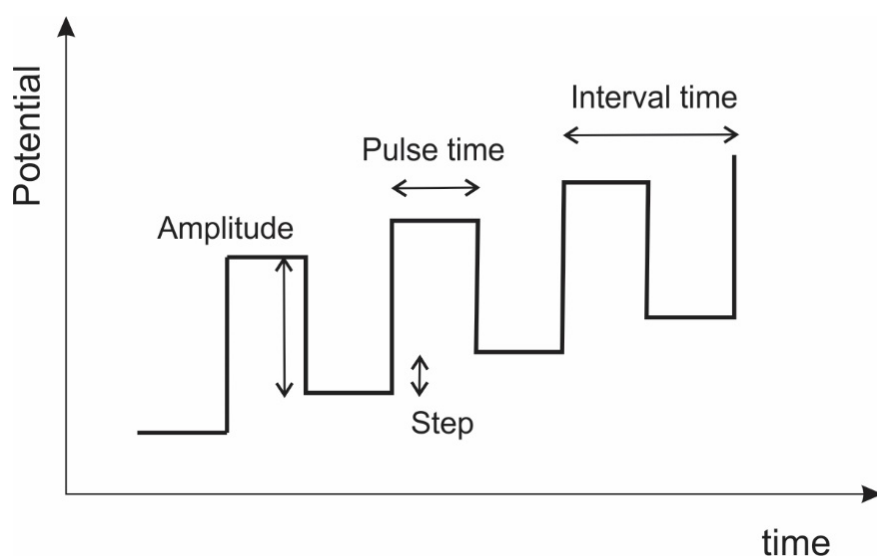
Figure 41. DPV waveform (potential applied versus time).

Step potential, amplitude, pulse and interval times have been studied independently to optimise the ideal conditions for a well resolved TEA transfer peak (Table 23).

Table 23. DPV variables studied at W/NPOE micro-interfaces. 10 μM TEACl was present in the aqueous phase (10 mM LiCl) and 10 mM TDA$^+$TPBCl$^-$ in NPOE.

Step potential mV	Amplitude mV	Pulse time s	Interval time s	Scan rate mV·s^{-1}
5	25	0.01	0.1	5
		0.02	0.2	6.7
10	50	0.05	0.5	10
		0.1	0.75	12.5
20	75	0.2	1.00	25
		0.3		

Increasing amplitudes translate into higher current and the same effect was observed for short pulse times (< 0.1 s; Figure 42a-b). Larger step potentials reduced significantly the number of data points acquired and introducing noise into the voltammetric signal. The optimum parameter for TEA transfer at W/NPOE interfaces were: 5 mV step potential, 75 mV amplitude, 0.2 s pulse time and 0.5 s interval time which corresponded to 10 mV·s^{-1} scan rate (optimum conditions are bold and in grey in Table 23).
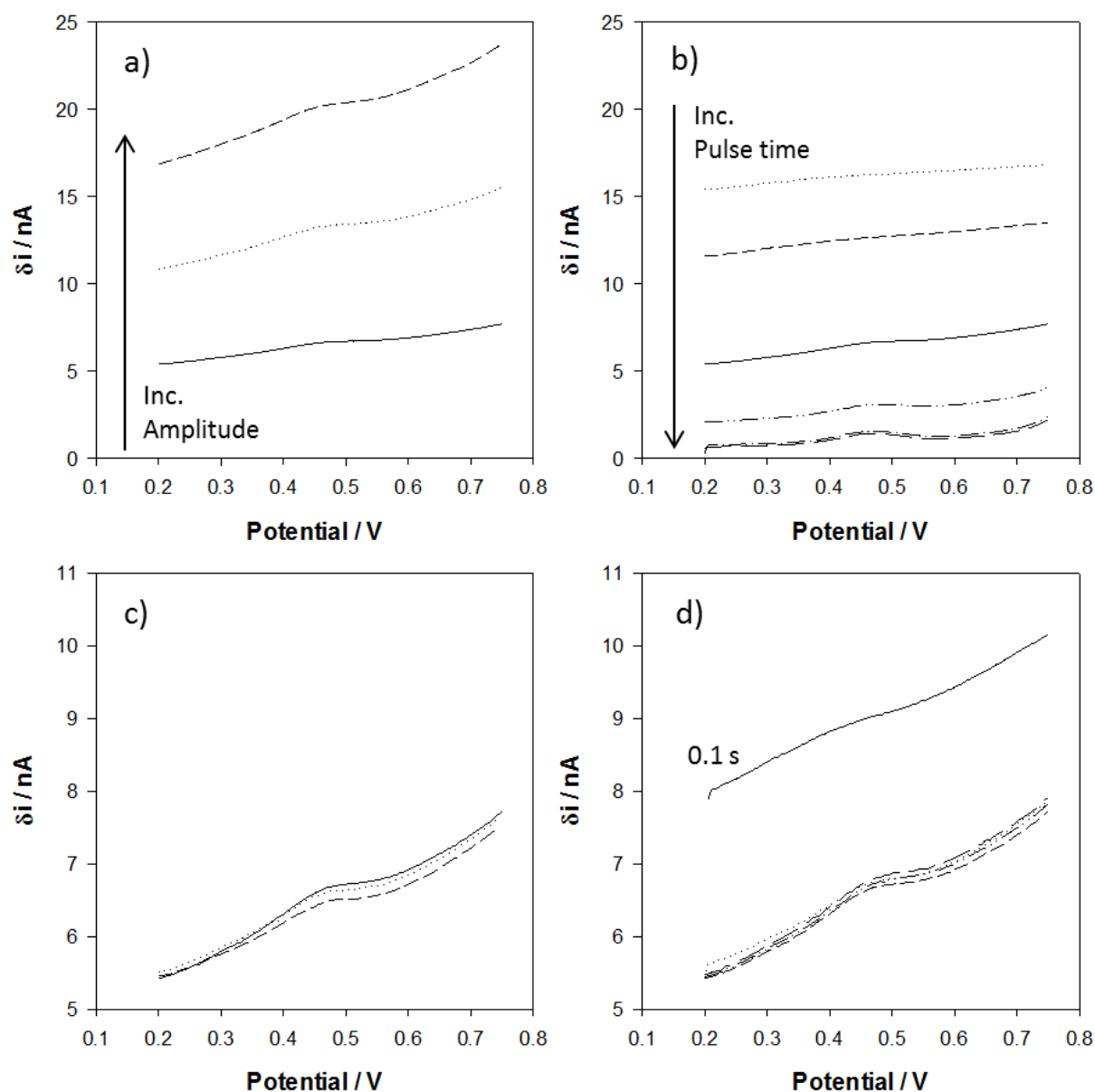
Figure 42. Voltammetric effect of varying the pulse parameters in a) amplitude, b) pulse time, c) step potential and d) interval time.

Also, the effect of the solvent in DPV was evaluated for DCE, DCH and NPOE. Table 24 shows the different sensitivity of DPV with different organic phases in various TEACl concentrations.

Table 24. Comparison DPV of TEA transfer at W/DCE, DCH and NPOE 60 s pre-conditioning time.

	Slope10^{10} A μM^{-2}	int-I 10^{11} A	R^2	Linear range μM	N	LOD μM
DCE	0.96	0.21	0.996	0.8 - 17	14	1.1
DCH	1.36	9.56	0.985	2.0 – 17	10	2.3
NPOE	1.25	1.24	0.995	0.2 – 16	14	0.9

NPOE presented lower detection limits than DCE and DCH with a LOD of 0.9 µM.

The combination of pre-concentration and DPV leads to the technique of differential pulse stripping voltammetry (DPSV). In Figure 43, DPV (black line, scan to more positive potentials), DPSV with no pre-concentration (dashed line, scanned to negative potentials) and DPSV with 60 s pre-concentration at 0.15 V (red line, scanned to negative potentials) are illustrated.
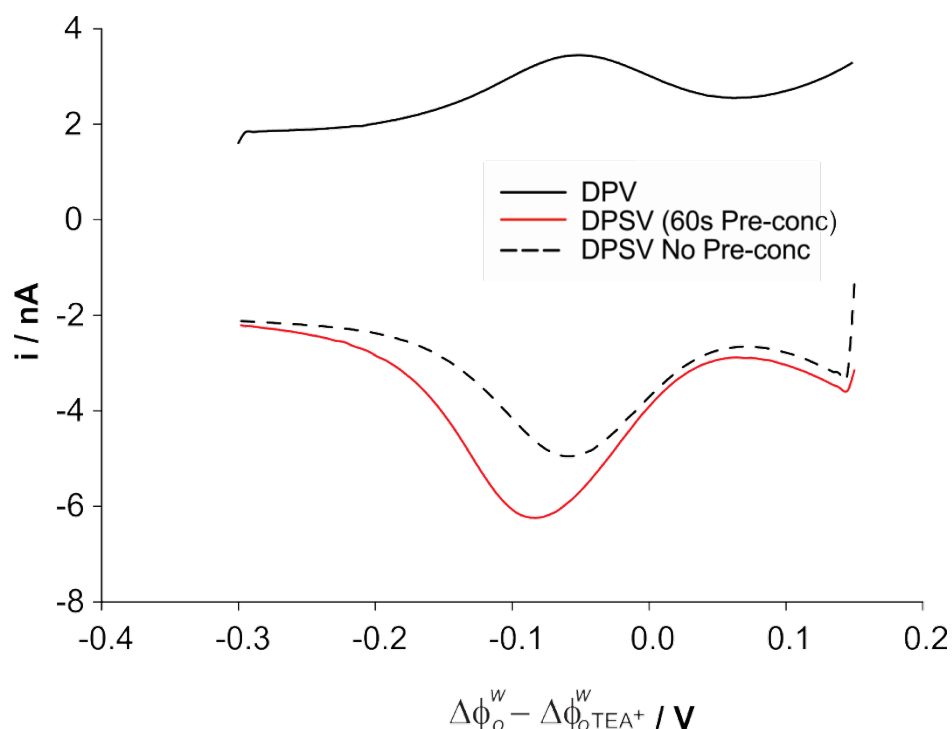
Figure 43. Differential Pulse voltammetry signal of 10 µM TEACl in 10 mM LiCl at W/NPOE micro-interfaces when the potential applied was scanned from 0.1 to 0.55 V (solid line), the scan was reversed (0.55 to 0.1 V, dashed line) and with a pre-concentration step of 60 s at 0.55 V prior voltammetry. Org: 10 mM TDA⁺TPBCl⁻ in NPOE and Aq: 10 mM LiCl. Step potential: 5 mV, Amplitude: 75 mV, Pulse time: 0.2 s and Interval time: 0.5 s.

The influence of pre-concentration time was further evaluated to optimise the DPSV conditions. Figure 44 illustrates the increase of current with the accumulation time over 20 min (1200 s) which plateaus from 300 s onwards for *ca.* 10 µM TEACl.
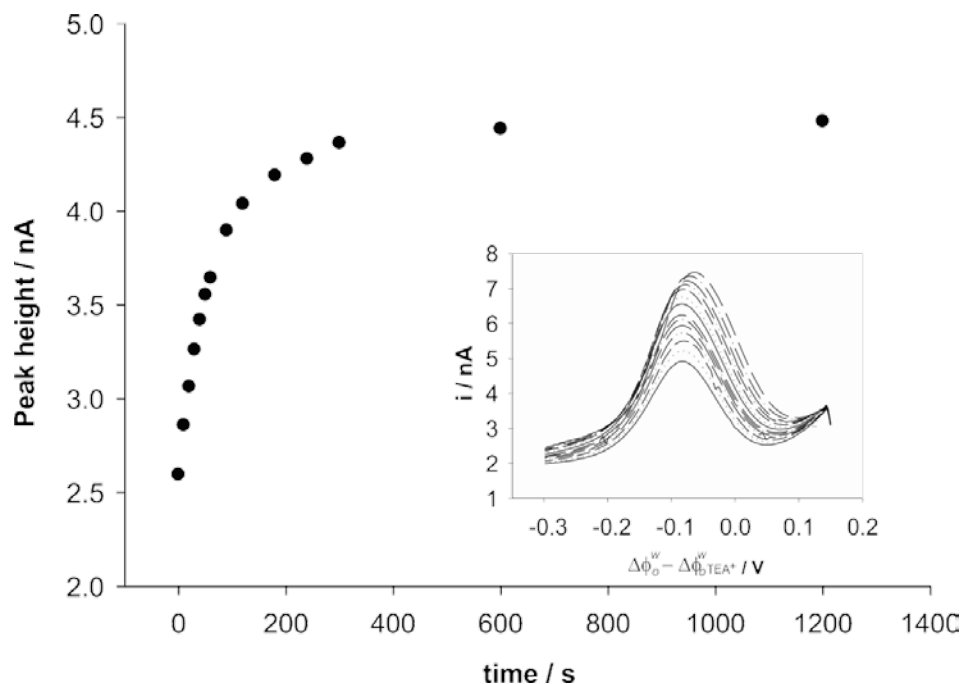
Figure 44. Peak height current measured from the DPSV voltammograms when different pre-concentration times were applied for a fixed potential (0.55 V). Inset shows the raw data from the DPSV for 10 µM TEACl in 10 mM LiCl at W/NPOE. A Pre-conditioning step at 0.1 V for 60 s was applied prior to any measurement. Step potential: 5 mV, Amplitude: 75 mV, Pulse time: 0.2 s and Interval time: 0.5 s.

Thus, fixed accumulation times (0, 60 and 600 s) were investigated at W/NPOE interfaces, as is shown in Figure 45. When increasing the pre-concentration time, the linearity of the current response shortens significantly, from 20 µM to < 5 µM TEACl.
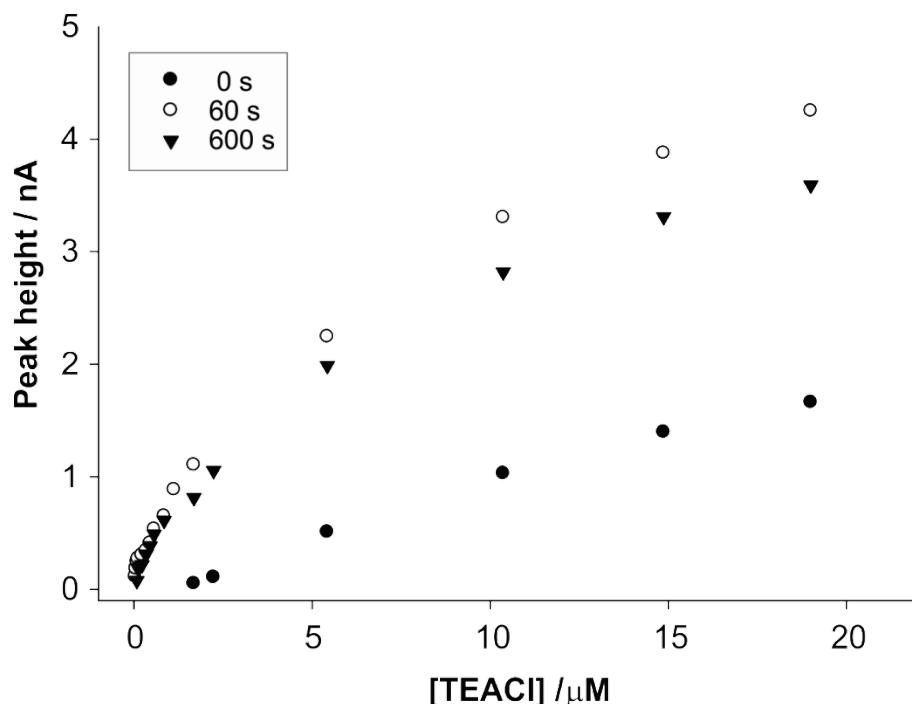
Figure 45. Calibration curves obtained for the detection of TEACl at W/NPOE interfaces via DPSV after 0 s pre-concentration time (●), 60 s (○) and 600 s (▼). Org: 10 mM TDA⁺TPBCl⁻ in NPOE and Aq: 10 mM LiCl. Step potential: 5 mV, Amplitude: 75 mV, Pulse time: 0.2 s and Interval time: 0.5 s.

Following this, CV, DPV and DPSV for 0, 60 and 600 s were studied for a range of concentrations (0.1 – 20 µM TEACl) at W/DCE and W/NPOE interfaces in an attempt to assess these pulsed voltammetric techniques when employing different organic phases. Different analytes (*i.e.* TEA⁺) present different solubilities and diffusion rates in the organic phase. The diffusion coefficient ratio ($\gamma = \frac{D_o}{D_w}$) becomes smaller when the diffusion of the analyte in the organic phase (D_o) is significantly slower. This effect has been reported previously for DCH (Strutwolf and Arrigan, 2010) with finite element computational simulations and explains the larger reverse peak for NPOE in comparison to DCE. NPOE possesses a larger viscosity whilst DCE possesses similar diffusion coefficients in water and DCE ($D_{TEA^+}^w \approx D_{TEA^+}^{DCE}$). A summary of all the data obtained when performing cyclic voltammetry (CV), differential pulse (DPV) and differential pulse stripping voltammetry (DPSV) at two different organic phases (DCE and NPOE) is presented in Table 25.

0.2 µM TEA concentrations were achieved implementing DPSV at W/NPOE after pre-concentration times of 60 and 600 s improving at least 10-fold the detection limit obtained via CV and DPV (Table 25).

Table 25. Comparison of TEA transfer calibration curve parameters by various techniques (CV, DPV, DPSV 60s and DPSV 600s) at W/DCE and W/NPOE 60 s pre-conditioning time.

	Technique	Pre-Cond time s	Pre-Conc time s	Slope 10^{10} A µM^{-2}	int-I 10^{11} A	R^2	Linear range µM	N	LOD µM
DCE	CV (forward peak)	0	0	0.71	11.0	0.974	1 - 19	14	2.9
	DPV	60	0	0.96	0.21	0.996		14	1.1
	DPSV 0s	60	0	1.74	29.1	0.997	0.9 - 19	14	1.0
	DPSV 60s	60	60	1.90	11.8	0.998	0.4 – 19	14	0.9
	DPSV 600s	60	600	1.53	32.1	0.991	0.2 – 19	14	1.9
NPOE	CV (forward peak)	0	0	0.90	4.15	0.997	1 – 19	6	1.3
	CV (reverse peak)	0	0	1.35	1.49	0.992	0.4 - 19	10	2.0
	DPV	60	0	1.25	1.24	0.995	0.3 - 16	14	0.9
	DPSV 0s	60	0	1.04	-9.57	0.994	1 - 15	5	1.5
	DPSV 60s	60	60	5.84	16.7	0.983	0.1 - 2	11	0.2
	DPSV 600s	60	600	6.68	7.36	0.970	0.1 – 1.5	7	0.2

N: number of points employed for the calibration curve (LOD calculations).
Int-I: intercept in y-axis.

A.2.3.2. DPV of sulfate

In the case of DPV, the current measured is the difference between the pulsed current and the background current. The calculated LOD is *1.3 µM* when concentrations were run experimentally between *0.05 and 12 µM SO$_4^{2-}$* (Figure 46).
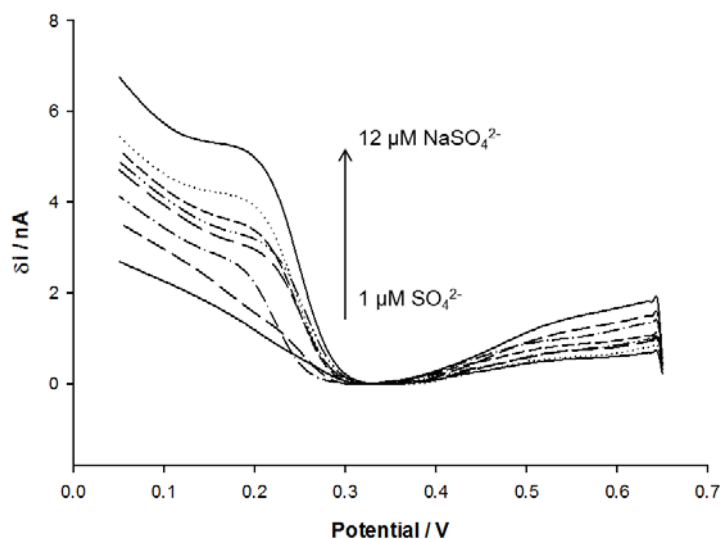
Figure 46. DPV of different concentrations of Na$_2$SO$_4$ in Milli-Q water. Scanned from 0.65 to 0.05 V at 10 mV·s^{-1} with 75 mV amplitude and 5 mV step potential.

A.2.3.3. DPSV of sulfate

The implementation of a pre-concentration strategy has shown an improvement in the LOD for TEA (previous section Table 24). For a pre-concentration time of 30 s at 0.1 V, the LOD is *1 µM* and for 60 s LOD = *0.7 µM* (Figure 47). In the case of 120 s, LOD is *1 µM* SO$_4^{2-}$. For larger pre-concentration times than 120 s, the LOD could be compromised by the organic electrolyte concentration and the conditioning step and it shown no improvement.
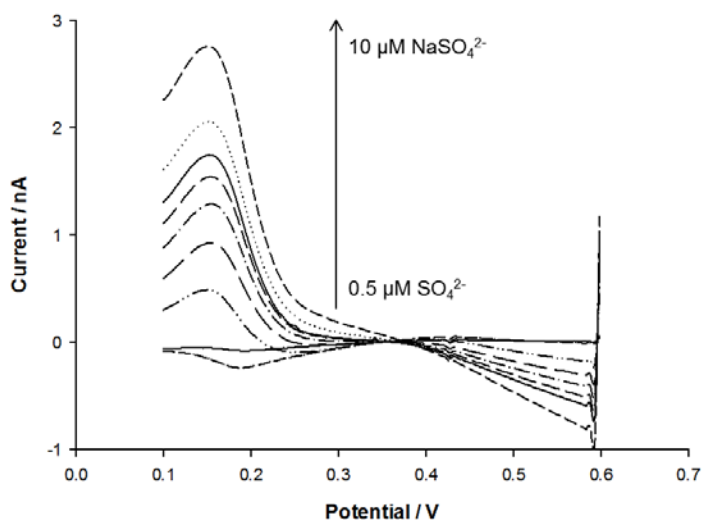
Figure 47. DPSV of different concentrations of Na$_2$SO$_4$ in Milli-Q water after 60 s pre-conditioning at 0.6 V and 60 s pre-concentration at 0.1 V. The voltammograms illustrated are normalised and background (Milli-Q) subtracted. Scanned from 0.1 to 0.6 V at 10 mV·s^{-1} with 75 mV amplitude and 5 mV step potential.

Data treatment was carried out to enhance the sulfate signal at low concentrations. A diagram illustrating the data processing is shown below for clarity (Figure 48). Firstly, the voltammograms were normalised to the lowest current value. Secondly, the background signal (measured in Milli-Q water aqueous phase) is subtracted from the sulfate signal.
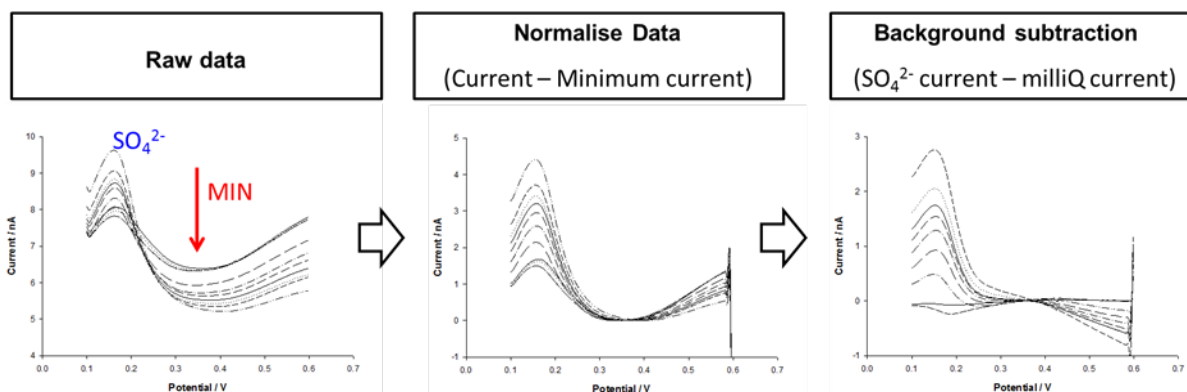
Figure 48. Summary of data processing implemented on the voltammetric data.

Finally, preliminary data analyses consisting of background subtraction have been performed in order to assess whether an improved platform to measure the sulfate response at low concentrations can be achieved (Figure 48). Note that background signal corresponds to measurement performed with an aqueous phase of ultrapure water, 18.2 MΩ·cm conductivity.

Various studies at 60 s DPSV are shown in Figure 49a-b. The LOD range for DPSV is 0.5 to 0.8 µM for a pre-concentration time of 60 s (Figure 49a). The mean value is 0.6 µM (Figure 49b), equivalent to *ca.* 0.06 ppm, which is lower than the ion chromatography method routinely employed previously (0.1 ppm). Table 26 shows the calibration curve results for four separate DPSV experiments.
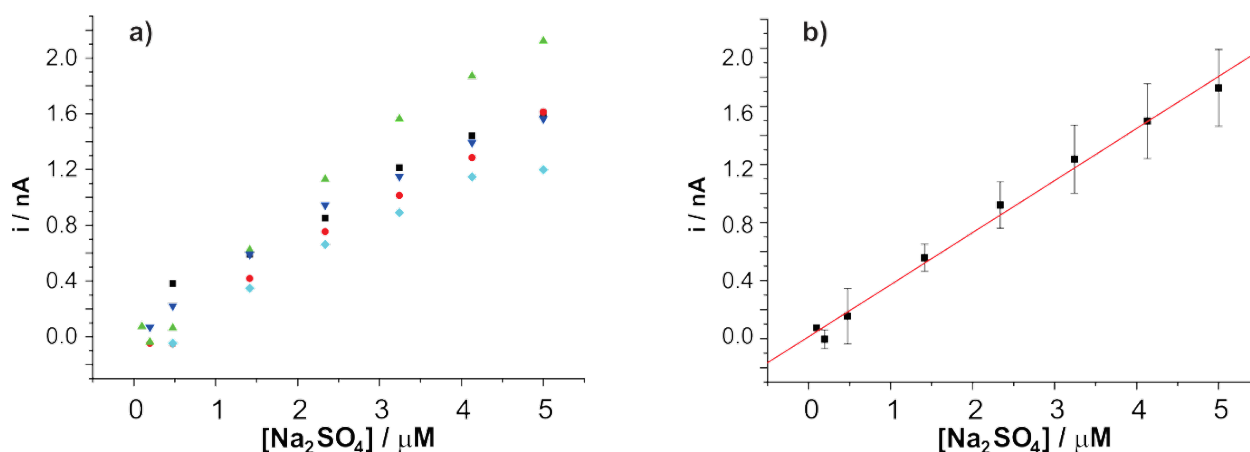
Figure 49. Calibration curves for 0.05-5 µM Na_2SO_4 at W/NPOE micro-interfaces in the presence different ionophores.

Table 26. Summary of sensitivity measurements for DPSV for 60 s pre-concentration time.

Concentration Range µM	Slope nA·µM^{-1}	Intercept nA	n	SD	LOD µM	r	P
0.05 - 5	0.285	0.225	6	0.053	0.55	0.9953	<0.0001
	0.351	-0.129	7	0.057	0.49	0.9967	
	0.459	-0.044	8	0.106	0.69	0.9936	
	0.311	0.101	7	0.085	0.82	0.9908	

Another signal treatment strategy consisted of subtracting the current signal of the same sulfate concentrations (0.1 to 5 µM) recorded in the <u>absence of the ionophore</u> (Cuartero *et al.*, 2013). For 60 s pre-concentration followed by DPSV, the sensitivity achieved was 0.379 nA·µM^{-1}, the intercept -0.179 nA, r = 0.9799 with an estimated LOD of *1.2 µM*, which did not improve the detection capabilities of the sensor.

A.2.4.   Sensitivity

In summary, the sensitivity was improved by implementing a stripping voltammetry technique.

- The limit of detection (LOD) for cyclic voltammetry (CV) was determined to be **1.3 µM**.
- Differential pulse voltammetry (DPV) produced a similar behaviour as CV, with a LOD of **1.3 µM**. In parts per million values, these are *ca*. 0.13 ppm. [Our target for sulfate detection was 0.01 ppm (0.1 µM)].
- By implementation of a pre-concentration step, called stripping voltammetry, a decrease in the LOD was achieved:
   - Differential pulse stripping voltammetry (<u>DPSV</u>) produced LODs of **1.0, 0.6** and **1** µM SO_4^{2-} when implemented with pre-concentration times of 30, 60 and 120 s, respectively.
   - The LOD of 0.6 µM is equivalent to *ca*. <u>0.06 ppm</u>, which is lower than the present standard method (ion chromatography) LOD of 0.1 ppm.
   - Further improvement in the LOD has not yet been possible, and may be limited by background electrolyte concentrations in our experimental arrangement.
- Data processing and normalisation were implemented (as outlined in Section 4.5) in order to reach the above achievements.

LOD range for DPSV is 0.5 to 0.8 µM for a pre-concentration time of 60 s. The mean value is **0.6 µM**, the equivalent to *ca.* 0.06 ppm, which is lower than the ion chromatography (0.1 ppm).

Another strategy consisted of subtraction the current signal of the sulfate concentrations in the absence of the ionophore   which did not improve the sensitivity presented an estimated LOD of 1.2 µM (Cuartero *et al*., 2013).

A.2.5.   Selectivity

A series of anions were examined via cyclic voltammetry (CV): PO_4^{3-}, $H_2PO_4^-$, SO_3^{2-}, NO_3^-, CH_3COO^-, OH^- Cl^- and SCN^-.

- PO_4^{3-} showed a similar response to sulfate at higher concentrations, and may be a major interference, although the presence of this anion in water is pH-dependent.
- <u>Cl</u>$^-$ and OH$^-$ showed a significant increase in current at high concentrations (10^{-3} to 10^{-1} M), indicating Cl$^-$ might be a problem for selective detection, while the presence of OH$^-$ is pH-dependent.
- NO_3^- showed lower potential of transfer, in particular at high concentrations (10^{-1} – 10^{-2} M concentration, Figure 50). However, extremely high concentration is unlikely to be present in RO water samples.
- $H_2PO_4^-$, SO_3^{2-}, SCN$^-$ and CH$_3$COO$^-$ did not show interaction with the ionophore in our experimental conditions, indicating selectivity over these.

Figure 50 shows some of the cyclic voltammetry of various anions investigated at concentrations varying from 10^{-8} M to 10^{-1}M.
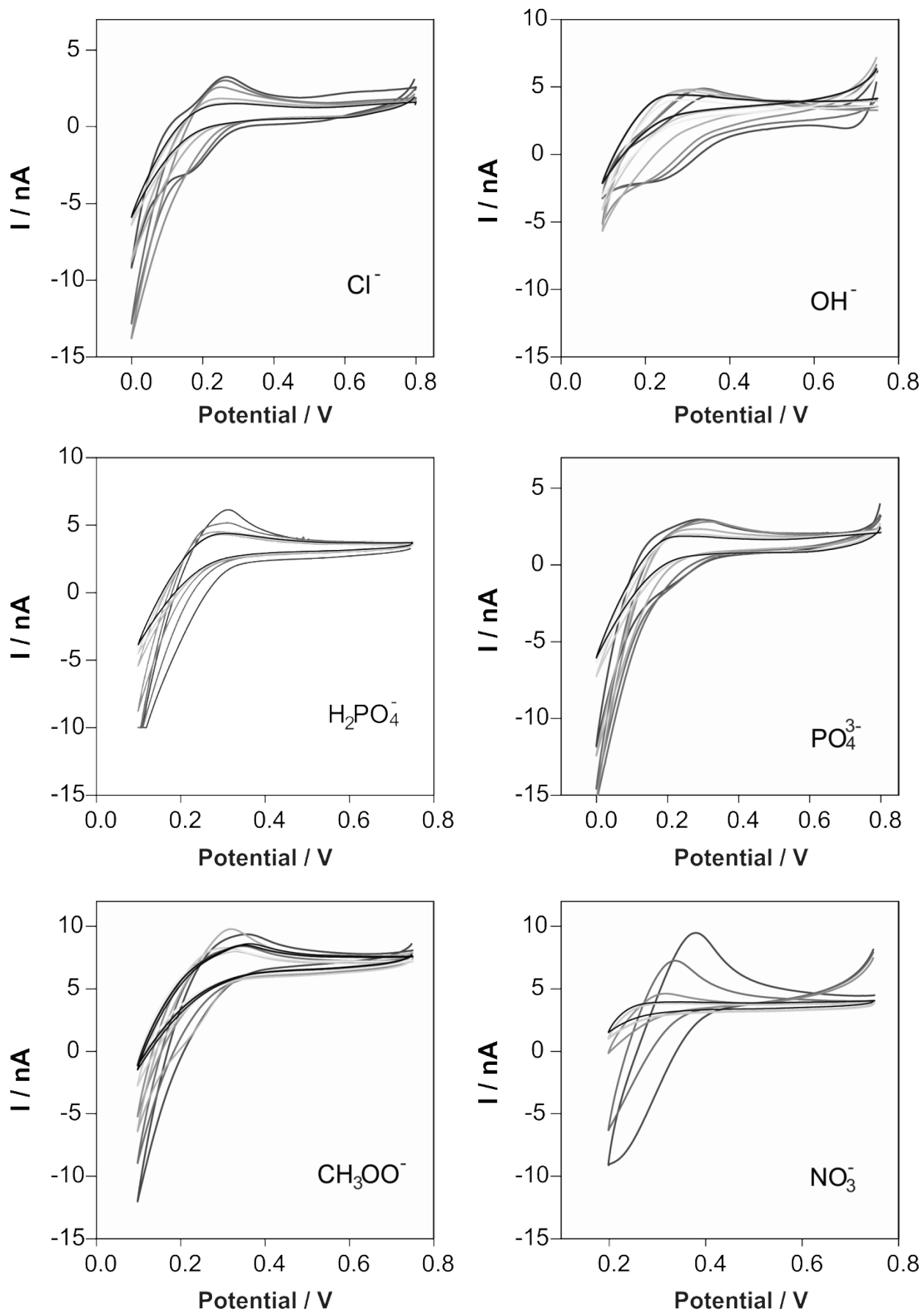
Figure 50. CV of Cl⁻, OH⁻, H₂PO₄⁻, PO₄³⁻, CH₃COO⁻, and NO₃⁻ at concentrations ranging from 10^{-8} to 10^{-1} M.

After this, the selectivity was investigated at lower concentrations (0.1 mM sulfate) in the presence of 0.1 or 1 mM interference. The amperometric signal obtained via DPV and DPSV was evaluated with the fixed analyte concentration method (Macca and Wang, 1995). In this methodology, the selectivity coefficient ($k_{i,j}^{amp}$) is measured by determining the peak current of the analyte of interest in the absence and presence of a fixed interferent concentration, as shown in Equation *(15*.

$$k_{i,j}^{amp} = \frac{(i_t - i_i)C_i}{i_i C_j}$$ (15)

where i_t is the current for analyte and interference, i_i the current for analyte of interest 'i', C_i is the concentration of I and C_j is the concentration of the interference 'j'.

Figure 51 shows an example of the current measured to calculate the selectivity coefficient when implementing the fixed analyte method. In this figure, the current measured (i_t) is represented with an arrow whilst the equivalent for i_i would correspond to the similar current measurement for only the analyte of interest (sulfate, red line).
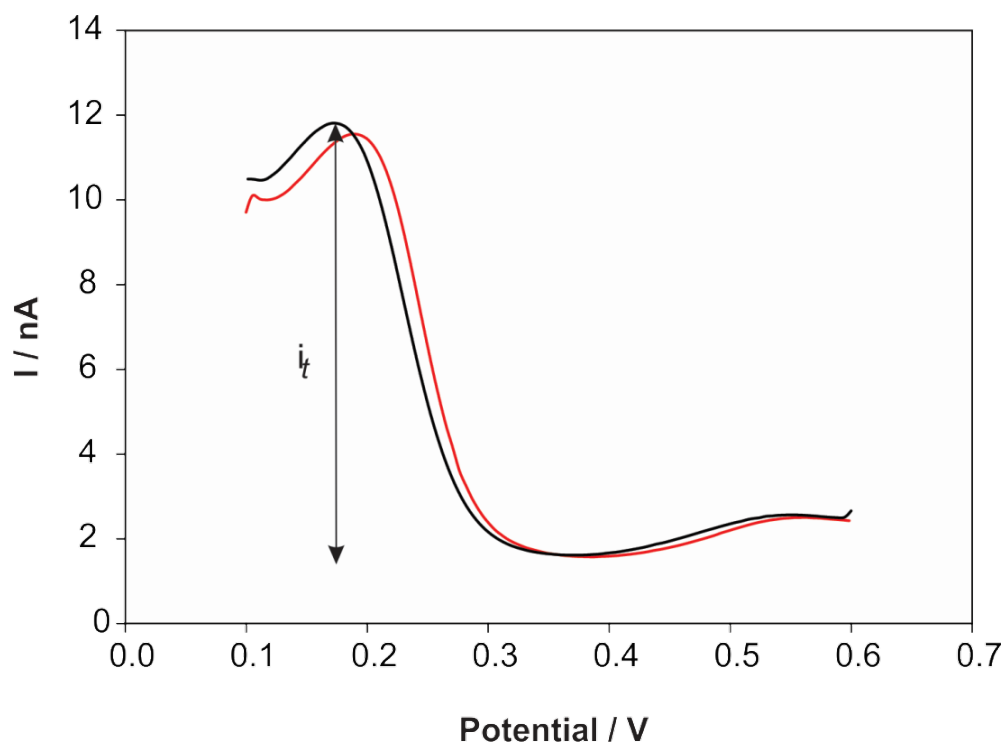
Figure 51. DPSV of 1 mM Na$_2$SO$_4$ (red line) and 1 mM Na$_2$SO$_4$ + 1 mM NaCl (black line). 60 s pre-concentration at 0.1 V with 75 mV amplitude and 5mV step potential.

Table 27 and Table 28 show the current variation ($i_t - i_i$) in the presence and absence of another anion at a 1:1 ratio (Table 27) and 1:10 (Table 28). The values for $log\,k_{i,j}^{amp}$ ranged from -0.5 to -3 which showed reasonable values in comparison to ISE probes.

Table 27. Selectivity coefficient for a 1:1 sulfate:interference ratio, 0.1 mM and 0.1mM interference (equivalent to 150 mg·L^{-1} SO$_4{}^{2-}$).

Anion	$(i_t - i_i)$ DPV nA	$(i_t - i_i)$ DPSV nA	$logk_{i,f}{}^{amp}$ for DPV	$logk_{i,f}{}^{amp}$ for DPSV (60 s)
Cl$^-$	0.21	0.19	-1.1	-1.4
OH$^-$	0.88	0.58	-0.5	-1.4 (lose peak shape)
CH$_3$COO$^-$	0.01	0.14	-2.1	-1.4
SCN$^-$	-	-	- (transfer at ↓potential)	-
NO$_3{}^-$	0.17	0.12	-0.6	-1.1
HCO$_3{}^-$	-	-	-	double peak
H$_2$PO$_4{}^-$	0.15	0.01	-1.3	-3.0
KHSO$_4{}^-$	0.09	0.11	-1.5	-1.5
SO$_3{}^{2-}$	0.32	0.19	-0.9	-1.4
PO$_4{}^{3-}$	0.56	1.4?	-0.7	-0.6

Table 28. Selectivity coefficient for a 1:10 sulfate:interference ratio, 0.1 mM and 1 mM interference (equivalent to 150 mg·L^{-1} Na$_2$SO$_4$).

Anion	$(i_t - i_i)$ DPV nA	$(i_t - i_i)$ DPSV nA	$logk_{i,f}{}^{amp}$ for DPV	$logk_{i,f}{}^{amp}$ for DPSV (60 s)
Cl$^-$	0.21	0.01	-2.1	-3.6
OH$^-$	0.62	1.04	-1.5	-1.3 (lose peak shape)
CH$_3$COO$^-$	0.18		-2.1	-2.3
SCN$^-$	-	-	-	-
NO$_3{}^-$	0.23	0.86	-2.0	-1.2
HCO$_3{}^-$	-	-	-	double peak
H$_2$PO$_4{}^-$	0.15	0.18	-2.1	-2.4
KHSO$_4{}^-$	0.34		-2.0	-1.8
SO$_3{}^{2-}$	0.02	1.5	-3.3	-1.7
PO$_4{}^{3-}$	0.33		-1.9	-1.3

A.2.6. Reproducibility and robustness

In terms of reproducibility, the cyclic voltammetry (CV) experiments for the range of 10^{-1} M to 10^{-7} M SO$_4{}^{2-}$ were repeated 10 times: the current values were within the 10% relative standard deviation (RSD).

In terms of robustness, a single sensor was assessed during 11 days stored in high purity (de-ionised, Milli-Q) water and its response to 10^{-2} M Na$_2$SO$_4$ measured every 24h. The current data showed a 15% RSD over this period of time.

Polyvinylchloride (PVC) has also been studied to gel the organic phase, leading to better mechanical stability. This has been shown to decrease the forward current response due to a lower diffusion coefficient of the ions in the gel, Figure 52. The current associated to the facilitated transfer of sulfate decreased significantly in magnitude when the organic phase is gelled with 10% PVC (w/v).
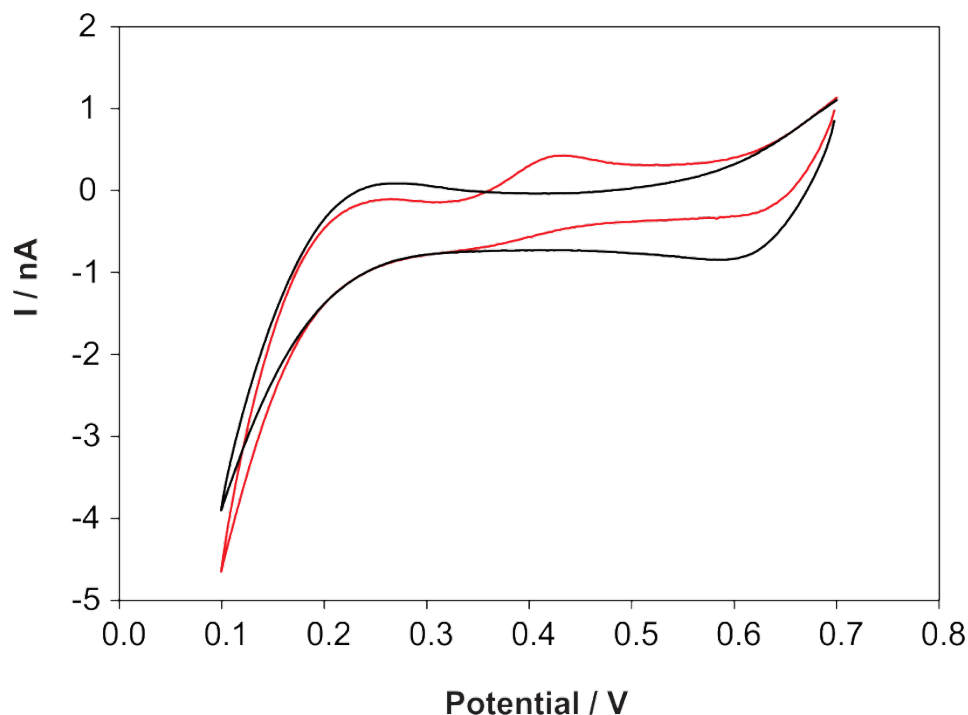
Figure 52. CV of *Milli-Q* (black line) and 0.1 M Na_2SO_4 at 10% PVC-NPOE/water interfaces. Scan rate: 5 mV s^{-1}.

A prototype in plastic (micropipette tips) was also tested (Figure 53) for the transfer of 10 µM tetrapropylammonium chloride at different size pipettes (1, 2 and 3; Figure 53b). A single hole contains the 10% PVC-organic phase (red line). Figure 53a shows a diagram of the 2 electrode set-up for these micro-pipettes. An image taken of the 10% PVC-DCH within the plastic tips is shown in Figure 53b. The corresponding CVs for 10 µM tetrapropyl ammonium transfer are represented in Figure 53c which reveals an increase in the charging current for greater tips (3). Nonetheless, these results suggested that single micro-holes fabricated in polymer could also be implemented for the sulfate detector.
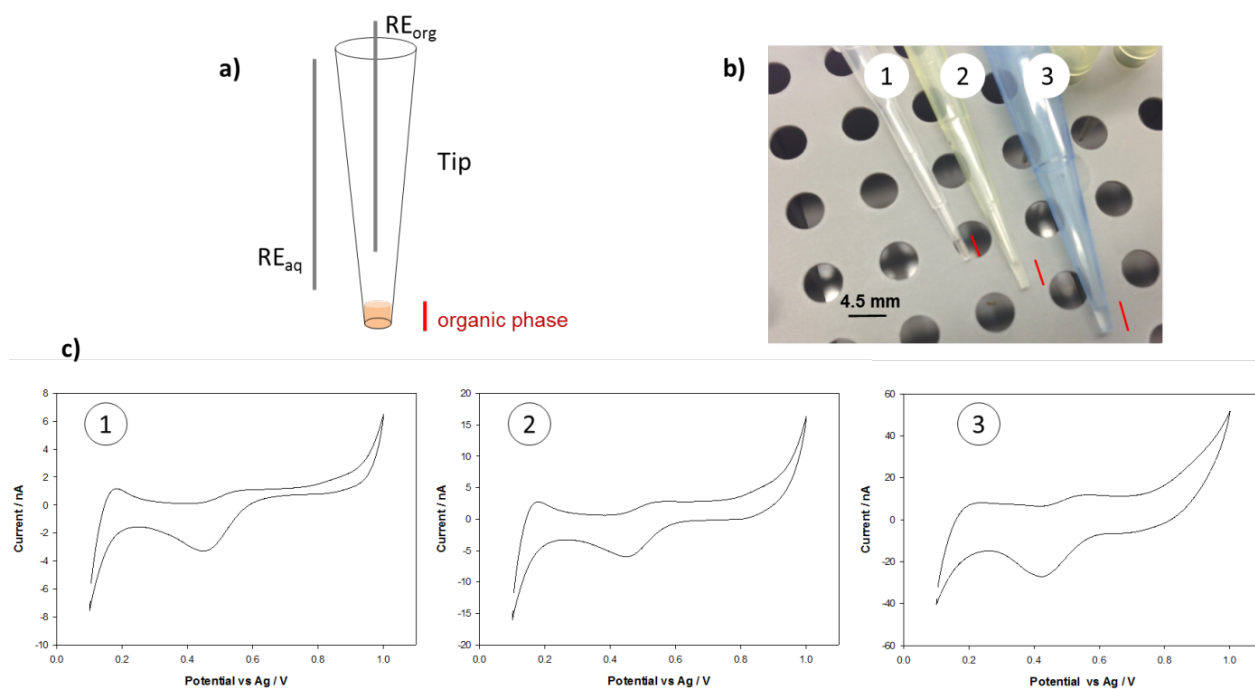
Figure 53. a) Scheme of the 2-electrode tip set-up, b) image of the different tips filled with 10% PVC-DCH + 10 mM BTPPA$^+$TPBCl$^-$ and c) CV's for 10 µM tetrapropyl ammonium transfer at these interfaces with a scan rate of 5 mV s^{-1}.

A.2.7.   Real samples

Pre- and post-RO samples have been analysed via cyclic voltammetry (CV) and differential pulse stripping voltammetry (DPSV).

The samples studied are the following:

- 6 pre- and post-RO samples collected in the Beenyup groundwater replenishment trial plant (20th August 2014).
- Sample S1006682 (pre-RO) and S1006684 (post-RO) collected in July 2014 (at the Beenyup groundwater replenishment trial plant) and analysed via ion exchange chromatography by Chem Centre.

A.2.7.1. Electrochemical analysis

Pre-RO samples were investigated via cyclic voltammetry (Figure 54) and the estimated concentration was within the millimolar range as expected for high concentrations of sulfate pre-RO.
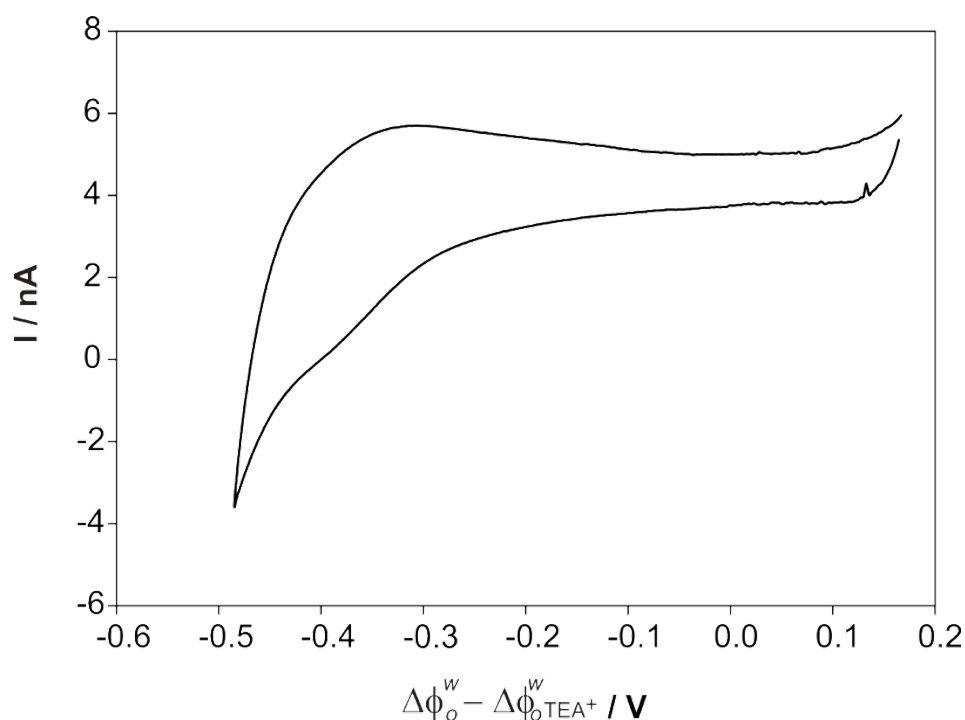
Figure 54. CV of a pre-RO sample collected the 11th June 2014. Org: NPOE (2.5mM S-I + 10 mM BTPPA⁺TPBCl⁻).

Thus, the Beenyup samples collected in August 2014 were also analysed via cyclic voltammetry with the optimised conditions. CVs corresponding to water at different stages in the plant such as post-RO, permeate combined, RO stage 1 permeate combined, post-MF, RO stage 2 feed and concentrate stage 2 are represented in Figure 54. It is clear that the increase in current at more negative potentials correspond to the association and transfer of anions by the ionophore present in NPOE. For post-MF, RO stage 2 feed and concentrate stage 2, this trend was expected. However, for post-RO, permeate combined and stage 1 permeate combined, the signal was greater than what it was anticipated for ~ 1ppm sulfate. For this reason, conductivity measurements were conducted to evaluate the ionic concentration of these samples. The values indicated conductivity values between *ca.* 40 and 3000 µS·cm⁻¹ (Table 29). The post-RO samples obtained from ChemCentre were also characterised via CV. Similar response was recorded (Figure 56) and corresponding conductivity analyses were carried out.
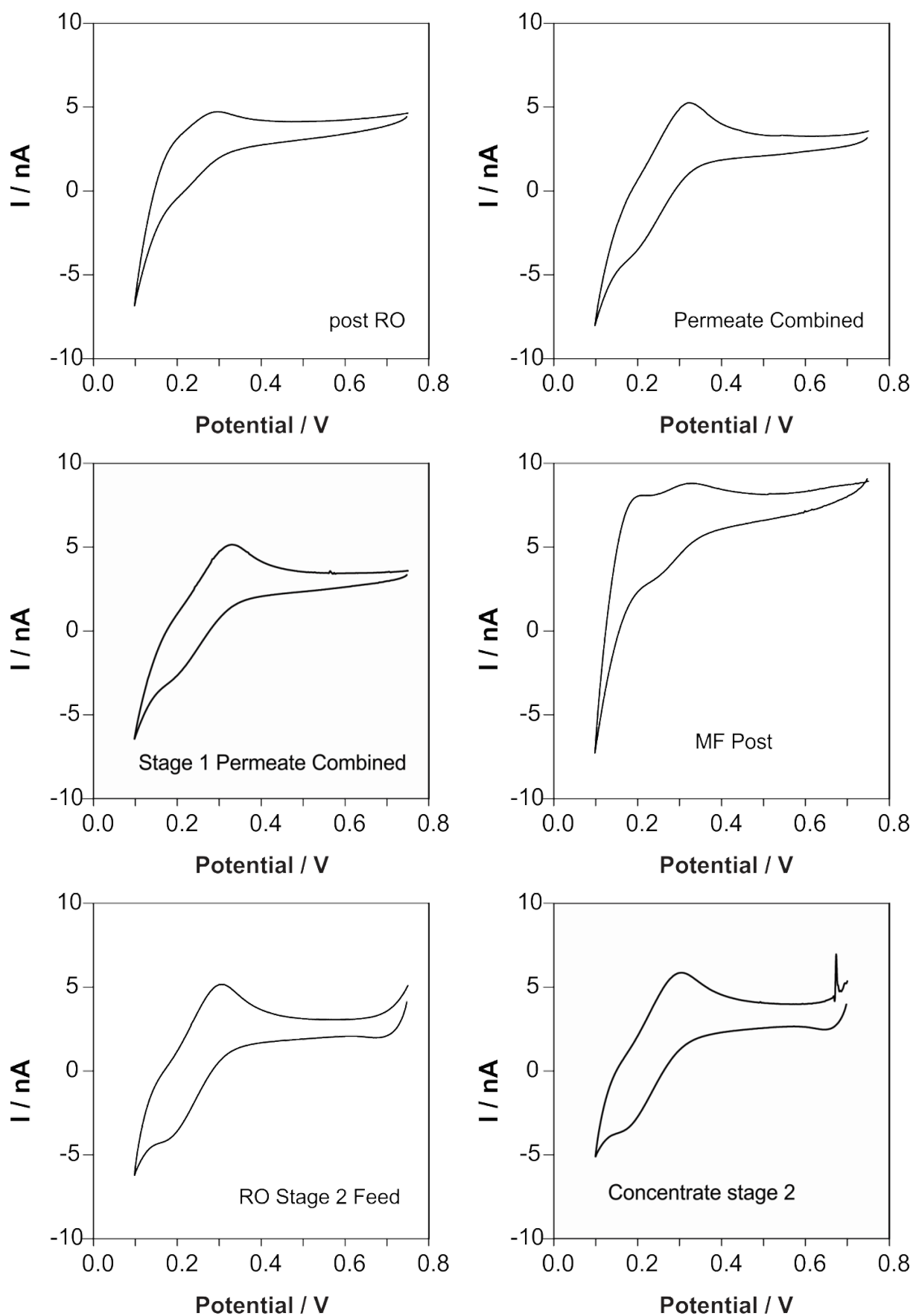
Figure 55. CV of samples collected the 20th August 2014. Org: NPOE (2.5 mM S-I + 10 mM BTPPA$^+$TPBCl$^-$).
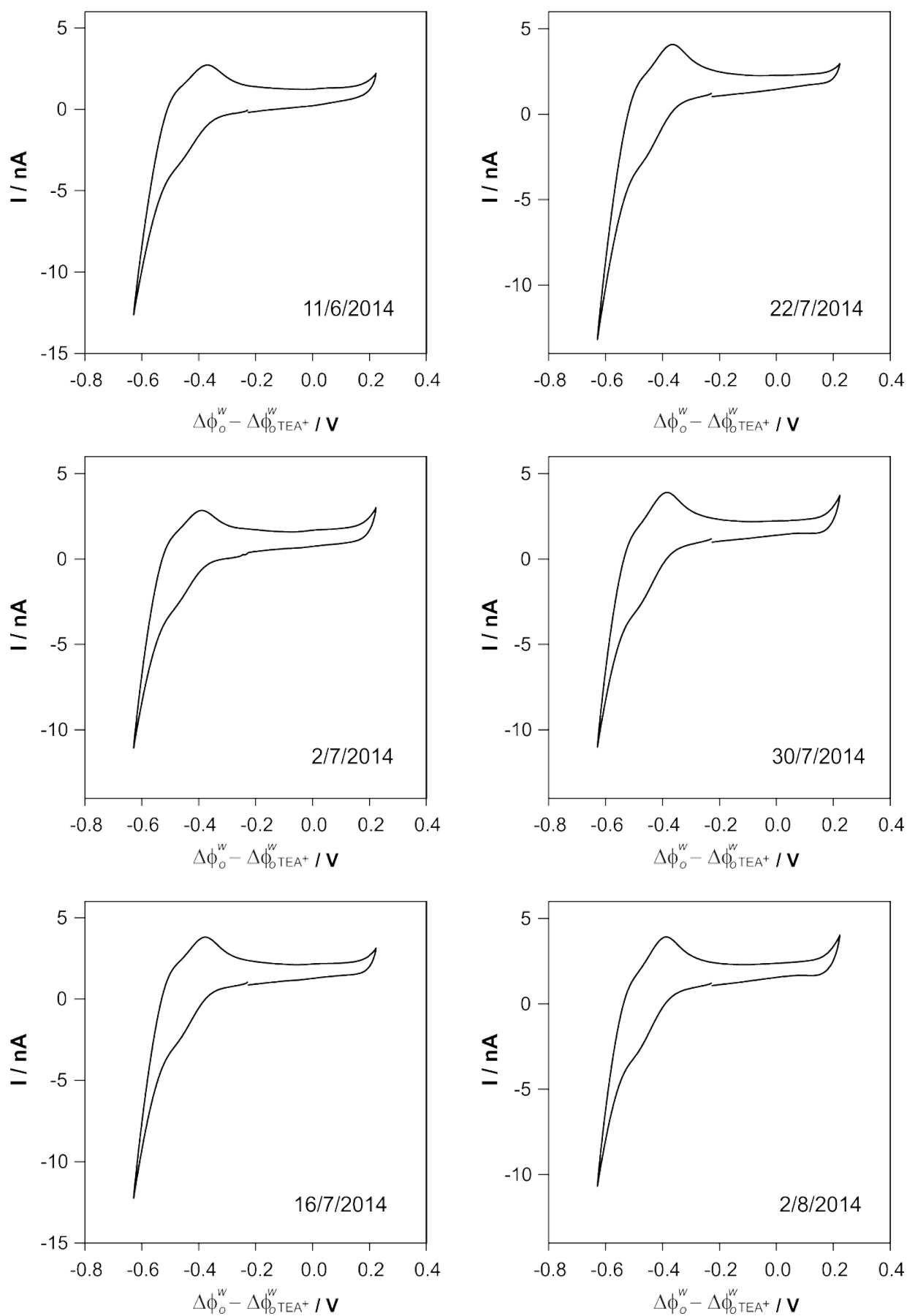
Figure 56. CV of post-RO samples collected different days W/NPOE (2.5 mM ionophore) micro-interfaces.

The electrochemical analysis of post-RO samples (Figure 56) revealed that the ion content is also significantly higher than expected (Table 29). For this reason, ion chromatography measurements were carried out to determine the interfering ions and their concentration in solution.

In addition, with the half-wave potential ($\Delta_o^w\phi^{1/2}$) measured in the cyclic voltammograms in Figure 54 - Figure 56. From the intercept and slope calculated for the linear regression curve for various concentrations of sulfate (int-$\Delta_o^w\phi^{1/2}$ = - 0.328 V and slope = 0.0284 V·dec^{-1}), we can estimate the sulfate concentration in the real samples. These values are summarised in Table 29 under C_{Na2SO4} (CV). For post-RO samples, the concentration was above 1 ppm, *ca.* 4 x 10^{-4} M.

Table 29. Conductivity measurements, approximate sulfate concentration reported by ion-exchange-chromatography (IEC) and cyclic voltammetry (CV) in water samples collected in the Beenyup groundwater replenishment trial plant.

Sample ID	Date of collection	Conductivity µS·cm^{-1}	C_{Na2SO4} (IEC)* ppm	C_{Na2SO4} (CV) ppm
Milli-Q water	18 August 2015	0.96	NA	NA
S1006684	11 June 2014	57.3	< 1	> 1
S1006684	2 July 2014	51.6	< 1	> 1
S1006684	16 July 2014	47.7	< 1	> 1
S1006684	22 July 2014	49.3	< 1	> 1
S1006684	24 July 2014	40.3	< 1	> 1
S1006684	30 July 2014	47.8	< 1	> 1
S1006684	3 August 2014	45.6	< 1	> 1
Post-RO	20 August 2014	40	-	> 1
Permeate Combined	20 August 2014	38.3	-	> 1
RO Stage 1 Permeate	20 August 2014	35.7	-	> 1
Post-MF	20 August 2014	980	-	
RO Stage 2 Feed	20 August 2014	1811	-	
Concentrate Stage 2	20 August 2014	3340	-	*80400*
S1006682	11 June 2014	1029	~150	*35200*
S1006682	2 July 2014	1075	~150	NA
S1006682	16 July 2014	1155	~150	NA
S1006682	22 July 2014	1135	~150	NA
S1006682	24 July 2014	1203	~150	NA
S1006682	6 August 2014	952	~150	NA

*Approximate values provided by ChemCentre (Hanna May).

A.2.7.2. Ion chromatography (IC)

Ion chromatography was performed in order to confirm the presence of interfering species in post-RO water samples as revealed by the electrochemical and conductivity measurements. A Dionex ICS-90 ion chromatography system with an alkanol quaternary ammonium column was employed for anion separation and the individual ion concentrations were detected via conductivity. For identification (retention time) and quantification (area of the peak chromatogram), five anion (Cl$^-$, NO$_2^-$, NO$_3^-$, PO$_4^{2-}$ and SO$_4^{2-}$) standard solutions were prepared from 0.1 to 100 ppm (Figure 57).
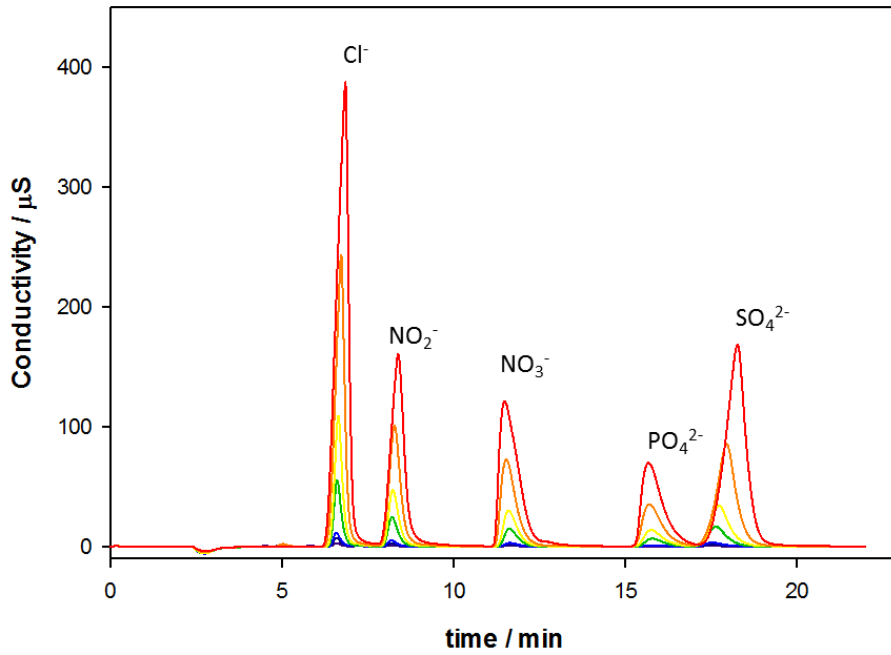
Figure 57. Ion chromatogram of various concentrations (0.1, 0.5, 1, 5, 10, 25 and 100 ppm) of five anions (NH_4Cl, $NaNO_2$, KNO_3, KH_2PO4 and $(NH_4)_2SO_4$).

The corresponding calibration curves for these anions are represented in Figure 57. For all the ions under study, a good linearity was observed between 0.1 and 100 ppm (N = 7) and 0.1 to 25 ppm (N = 6). However, as the post-RO samples analysed presented ion concentrations with maximum conductivity of 140 µS, the ion determination was carried out in a shorter linear range (0.1 - 25 ppm). Chloride presents the largest peak area for 100 ppm which corresponds to a greater concentration in molarity terms. All the parameters obtained from the linear relationship observed in Figure 58 between peak area and concentration are summarised in Table 30.
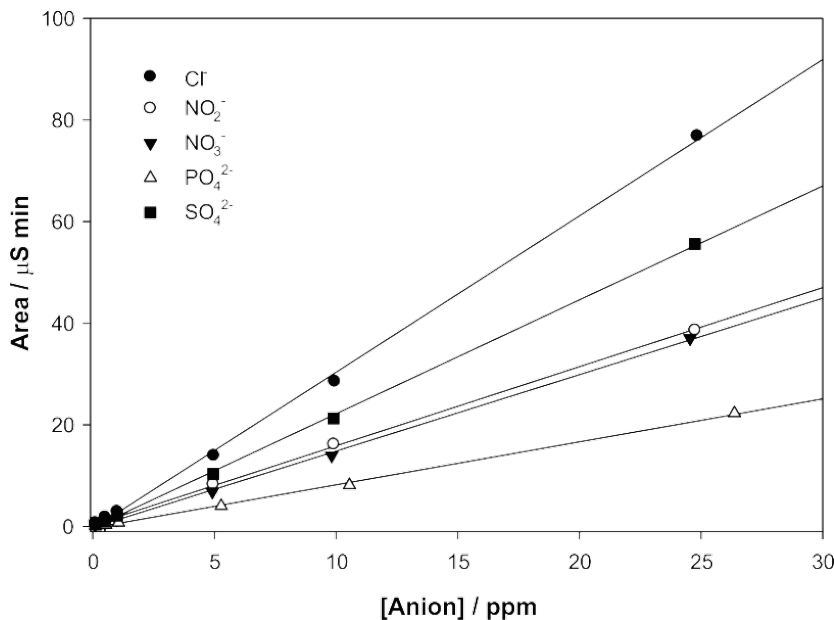
Figure 58. Calibration curves obtained for the standards prepared for chloride, nitrite, nitrate, phosphate and sulfate.

Table 30. Summary of calibrations curves obtained via IC for chloride, nitrite, nitrate, phosphate and sulfate.

Anion	t min	Linearity ppm	Sensitivity µS·min·ppm^{-1}	int-y	SD	R	R^2	LOD ppm	N	P
Cl$^-$	6.58	0.1 - 25	3.077	-0.420	1.155	0.9994	0.9988	1.1	6	<0.0001
NO2-	8.19	0.1 - 25	1.557	-0.290	0.322	0.9998	0.9996	0.6	6	<0.0001
NO3-	11.654	0.1 - 25	1.504	-0.211	0.452	0.9996	0.9992	0.9	6	<0.0001
PO42-	15.804	0.1 - 25	0.845	-0.255	0.344	0.9994	0.9987	1.2	6	<0.0001
SO$_4$$^{2-}$	17.537	0.1 - 25	2.241	-0.234	0.532	0.9998	0.9995	0.7	6	<0.0001

Thus 7 post-RO samples (Figure 59a) and a diluted pre-RO (pre-RO/ Milli-Q, 1/20) (Figure 59b) were run after the standards, allowing the identification and quantification of the anions present in these solutions.

Figure 59. Ion chromatograms of 7 post-RO water samples collected between June and August 2014 (a) and a diluted (1/20) pre-RO water sample collected the 6th August 2014 (b).

Figure 59a shows 4 peaks in the chromatograms, which correspond to chloride (6.66 min), nitrate (11.63 min), sulfate (17.55 min), and possibly fluoride at 4.17 min, based on the retention time reported by the anion IC column manufacturer for the conditions employed (flow rate, eluent and reagent). An additional peak is observed in the diluted pre-RO sample at 15.81 min, which corresponds to phosphate (Figure 59b).

Hence, chloride and nitrate anions contribute to the large conductivity values measured in post-RO water samples ($\sim$ 50 µS·cm^{-1}; Table 29) and the significant current signal in the cyclic voltammograms (Figure 54) observed for these samples.

The estimated concentration of chloride, nitrate, phosphate and sulfate in post-RO samples and pre-RO based on the calibration curves obtained for 6 standard concentrations (0.1, 0.5, 1, 5, 10 and 25 ppm) are presented in Table 31. The mean concentration of chloride is 10.9 ppm (*ca.* 0.2 mM) and nitrate is 8.7 ppm (0.1 mM) in post-RO water, which is quite significant. The estimated concentration of sulfate via CV is greater than 1 ppm as the signal recorded provided an electrochemical signal that fits within 10^{-4} - 10^{-3} M range for sulfate.

Table 31. Concentration of anions present (Cl⁻, NO₃⁻, PO₄²⁻ and SO₄²⁻) in post-RO water (S1006684) and pre-RO (S1006682) measured via IC and estimated sulfate concentration determined via voltammetry at W/NPOE with 2.5 mM S-I ([SO4²⁻] (CV)).

Sample ID	Date of collection	[Cl⁻] ppm	[NO₃⁻] ppm	[PO₄²⁻] ppm	[SO₄²⁻] ppm	[SO₄²⁻] (CV) ppm
S1006684	11 June 2014	12.4	8.9	-	0.7	> 1
S1006684	2 July 2014	11.4	9.0	-	0.2	> 1
S1006684	16 July 2014	11.4	9.0	0.3	0.2	> 1
S1006684	22 July 2014	9.5	7.1	-	0.2	> 1
S1006684	24 July 2014	11.4	8.5	-	0.4	> 1
S1006684	30 July 2014	10.4	9.3	-	0.2	> 1
S1006684	6 August 2014	9.9	8.8	-	0.2	> 1
S1006682	6 August 2014	233.6	49.9	33.4	184.9	352 mM

A.2.7.3. Mass Spectrometry (MS)

The pre-RO and post-RO samples were also investigated via MS, after the formation of an emulsion with the organic phase containing the ionophore (2.5 mM S-I), organic electrolyte (10 mM BTPPA⁺TPBCl⁻) and the solvent (NPOE) in a one to one volume ratio.

The same approach as explained in Section A.2.2. was carried out. In the case of pre-RO water, complexes of S-I with HSO_4^-, NO_3^- and Cl^- were identified with m/z values of 441.09705 (Δm = 0.357 ppm), 468.11523 (Δm = -1.340 ppm) and 503.08699 (Δm = -1.200 ppm), respectively. However, for post-RO samples, only Ionophore-Cl⁻ was observed at *m/z* ~ 441.097, which indicates that these complexes are harder to analyse with this emulsion approach at low concentrations. Note that chloride is the most abundant anion (0.2 mM) in post-RO samples.

Based on the above analyses of real water samples, it is clear that selectivity for sulfate over chloride is not ideal with the commercially available sulfate ionophore (S-I). To overcome this issue, several strategies might be implemented:

Chloride removal could be performed via Cl⁻ electrochemical deposition on a silver wire, as a sample pre-treatment step (Section A.2.9.).

The use of better ionophores which bind more selectively to sulfate over chloride could be used (Section A.2.9.).

Incorporation of an ion-exchange membrane at the ITIES before sulfate detection might be beneficial, as reported by Hu *et al.* (2014).
Nitrate (NO_3^-) could be also removed by electrolysis, as reported in other studies (Polatides *et al.*, 2005).

A.2.8. Cl- removal via formation of AgCl(s)

Chloride removal via electrolysis (oxidation of silver in the presence of chloride to form AgCl solid) has been previously reported as a pre-treatment step for seawater analysis via ion chromatography (Grygolowicz-Pawlak *et al.*, 2012) and could be implemented in the sensor device suggested here prior to sulfate measurements at liquid-liquid interfaces. Figure 60a shows the oxidation (0.2 V) of Ag₍ₛ₎ to AgCl in the presence of chloride ions and the reverse reaction at -0.2 V in a 2-electrode set-up (Ag wire as working electrode and Pt as counter/reference electrode). Figure 60b represents a chronoamperometric curve for Ag oxidation at 0.25 V for a short period of time (60 s).

Figure 60. a) Cyclic voltammetry and b) chronoamperometry at 0.25 V vs Pt of 0.2 mM NaCl in a Ag (WE) and Pt (CE/RE) electrode system.

From the area under the curve in Figure 60b (*I vs t*), the charge (*Q*) for chloride deposition on a 0.79 cm^2 Ag wire was determined to be 1.3 x 10^{-4} C for 60 s electrolysis at 0.25 V. The surface area of the Ag wire was calculated using the formula for a cylinder with only one of the circular edges exposed ($A = 2\pi rh + \pi r^2$) where *r* is the radius of the wire (0.025 cm) and *h* the length (5 cm). Then the electrolysis (constant oxidation of Ag to form AgCl$_{(s)}$) was performed for the required time according to the volume of sample. With the volume of sample (aqueous phase) and chloride concentration, the number of moles can be determined thus the charge (*Q*) can be calculated using Equation *(16*.

$$Q = nNF$$ (16)
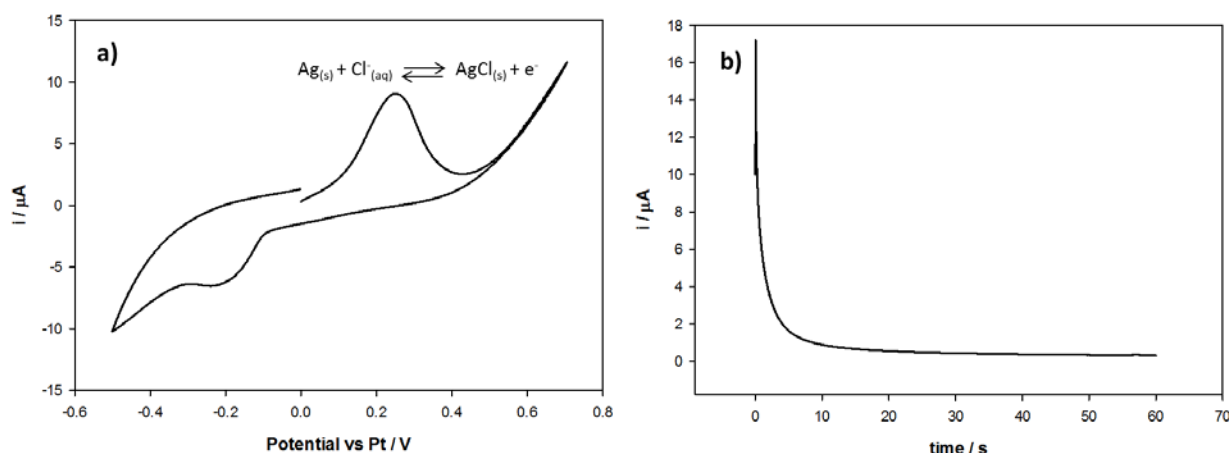
where *Q* is the charge, *n* the number of electrons, *N* number of moles and *F* the Faraday constant.

For instance, Grygolowicz-Pawlak *et al.* (2012) reported that 20 µL of 0.6 M NaCl, required only 90 s of electrolysis for a 90% chloride removal and this was further improved to 99.5% with four times the electrolysis time.

Figure 61 shows the removal of 73% chloride in a post-RO sample with a removal rate of 2 x 10^{-6} mol·s^{-1} for a silver wire surface area of 0.79 cm^2. This demonstrates the potential of this pre-treatment step, which can be further optimised for an efficient chloride removal form RO water samples.
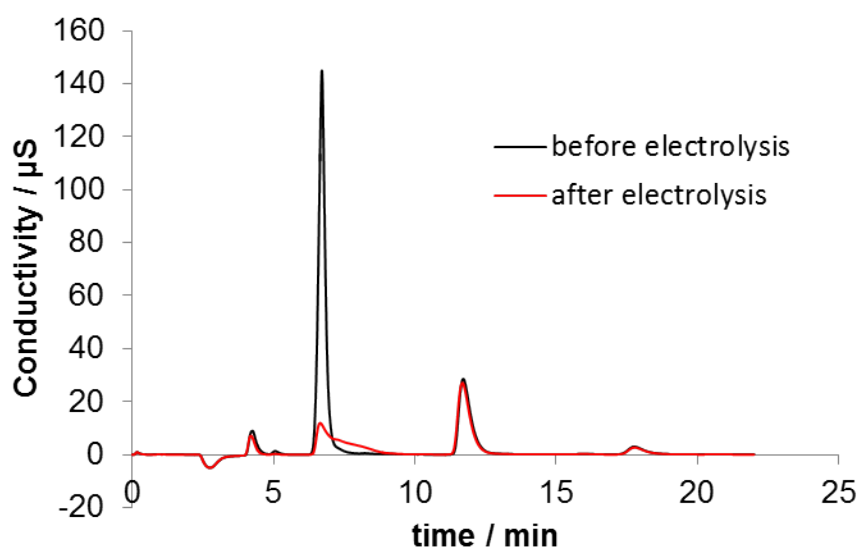
Figure 61. Ion chromatogram of post-RO sample before (black line) and after 73% removal of chloride via electrolysis at 0.9 V vs Pt electrode (red line).

A.2.9. Different ionophores

A total of nine ionophores synthetised by two external laboratories (University of Sydney; (Elmes *et al.*, 2014) and University of Murcia; (Mas-Montoya *et al.*, 2015)) have been tested under the conditions previously optimised for the commercial sulfate ionophore: 2.5 mM ionophore in the NPOE organic phase and excess of Na_2SO_4 in the aqueous (10 mM; Figure 62 and Figure 63). Figure 62 illustrates the cyclic voltammograms obtained for the dipeptide based receptor structures with thiourea: a) di-Lys TU; b) mono-Lys TU and squaramides; c) T-2; d) T-4; e) T-5; and finally f) the commercial sulfate ionophore (S-I). These ionophores (a-e) have been synthetised by Elmes *et al.* (2014) as previously reported. A first inspection of the CVs reveals a lack of response for the thiourea di- and mono-Lys TU ligands. Then T-2, T-4 and T-5 showed similar increases of current on the forward wave (towards more negative potentials, *ca.* -0.4 V) as the commercial sulfate ionophore (S-I).

When the thiourea groups (mono- and di-Lys TU) were replaced by squaramides (T-2, T-4 and T-5), the hydrogen bond-donor strength is enhanced, inducing stronger binding to sulfate, as observed in the voltammograms (Figure 62c-e). However, all these three neutral squaramide ionophores showed very similar sulfate transfer potentials as the commercially-available S-I, *ca.* 17 mV more negative in potential.
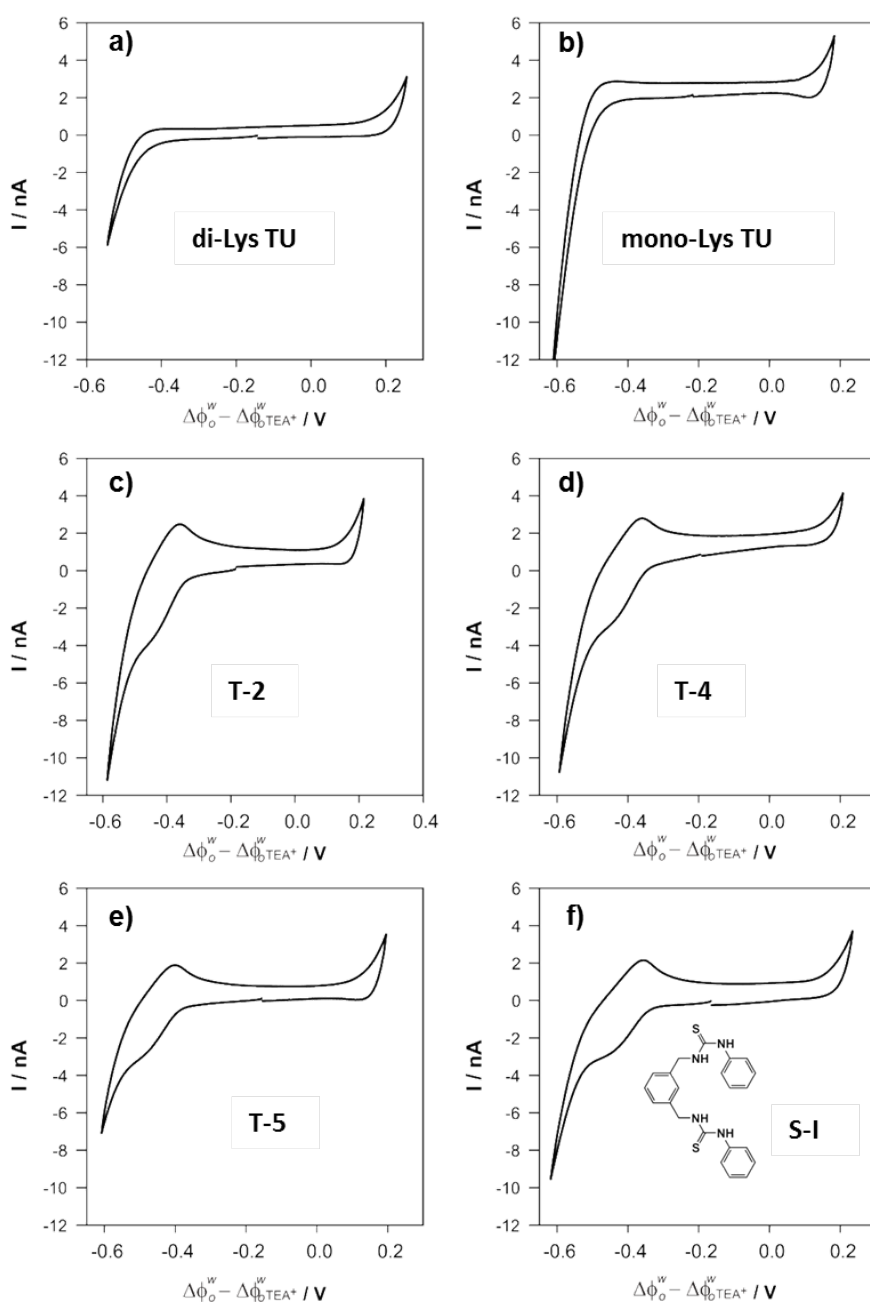
Figure 62. CV of 10 mM Na_2SO_4 at W/NPOE micro-interfaces in the presence different ionophores (2.5 mM) in the organic phase; a) di-Lys TU, b) mono-Lys TU, c) T-2, d) T-4, e) T-5 and f) S-I.

Figure 63 represents the cyclic voltammetric behaviour of 2.5 mM of four acyclic isophthalamide based ionophores donated by the University of Murcia (David Curiel's group). Only compounds BIA-1 and PIA-1 have been previously reported by their group (Mas-Montoya *et al.*, 2015). The attachment of aminomethylpyrrole groups (PIA-1 and PIA-2) improves the anion-binding as shown in Figure 63c-d. In the absence of the aminomethylpyrrole group (Figure 63a-b) the ligand is not capable of assisting the transfer of sulfate. However as illustrated in Figure 63c-d, a significant current wave is detected at *ca.* -0.43 and -0.38 V, respectively.
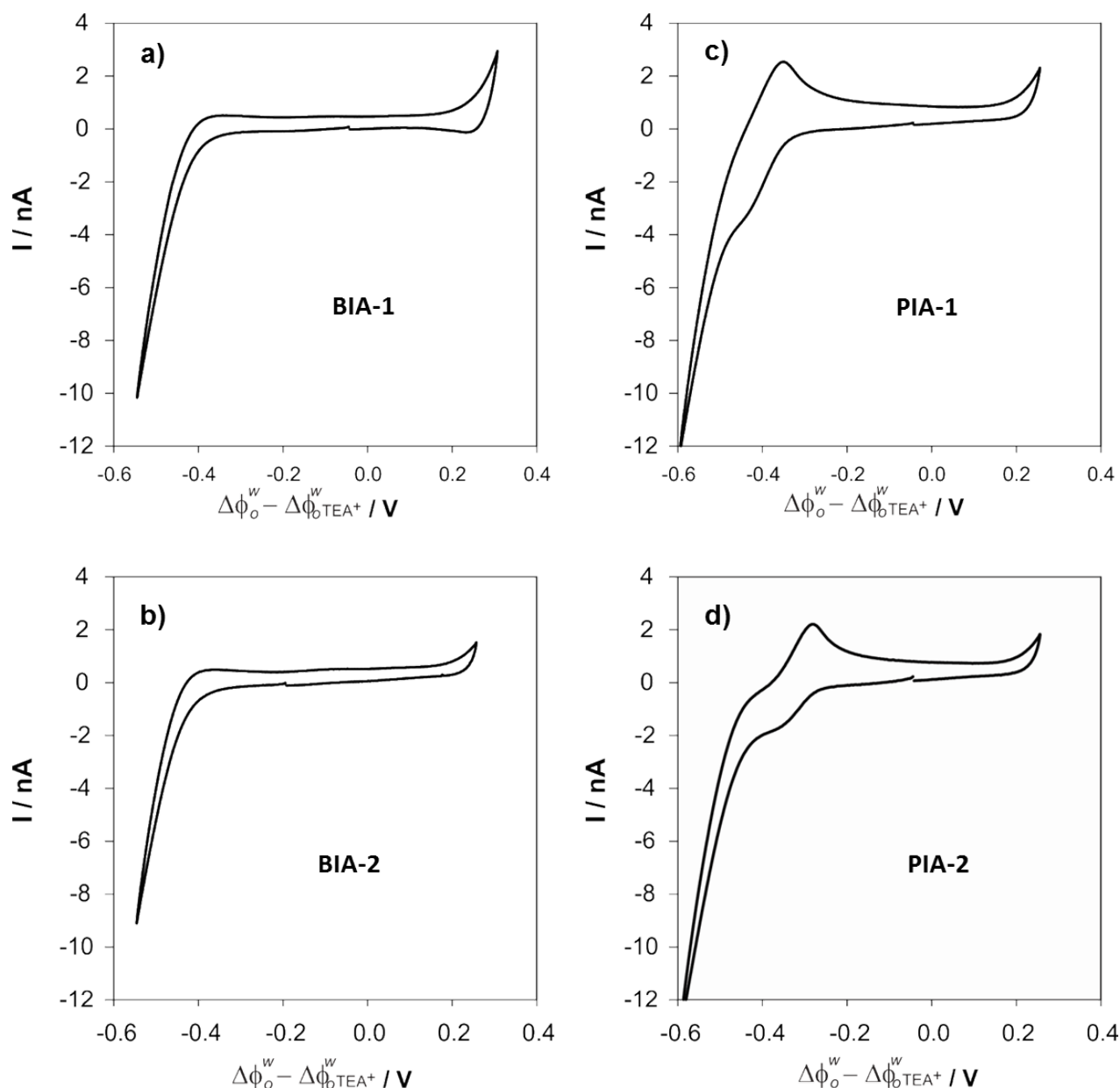
Figure 63. CV of 10 mM Na_2SO_4 at W/NPOE micro-interfaces in the presence different ionophores (2.5 mM) in the organic phase; a) BIA-1, b) BIA-2, c) PIA-1 and d) PIA-2.

In addition, the attachment of a nitro (NO_2) group (strong electron withdrawing group) in position meta- of the benzene ring induces a more basic H-bond to bind sulfate, which further enhanced the binding effect of the aminomethylpyrrole moiety. This stronger binding effect influences the sulfate transfer potential by a 48 mV decrease of the $\Delta\phi_o^w(SO_4^{2-})$ compared to the voltammetric performance of PIA-1.

In Figure 64, the forward voltammetric wave is presented with respect to tetraethylammonium transfer after background (voltammogram in the absence of ionophore) subtraction. Along with this figure, Table 32 summarises the potential of transfer for the ten new ionophores studied.
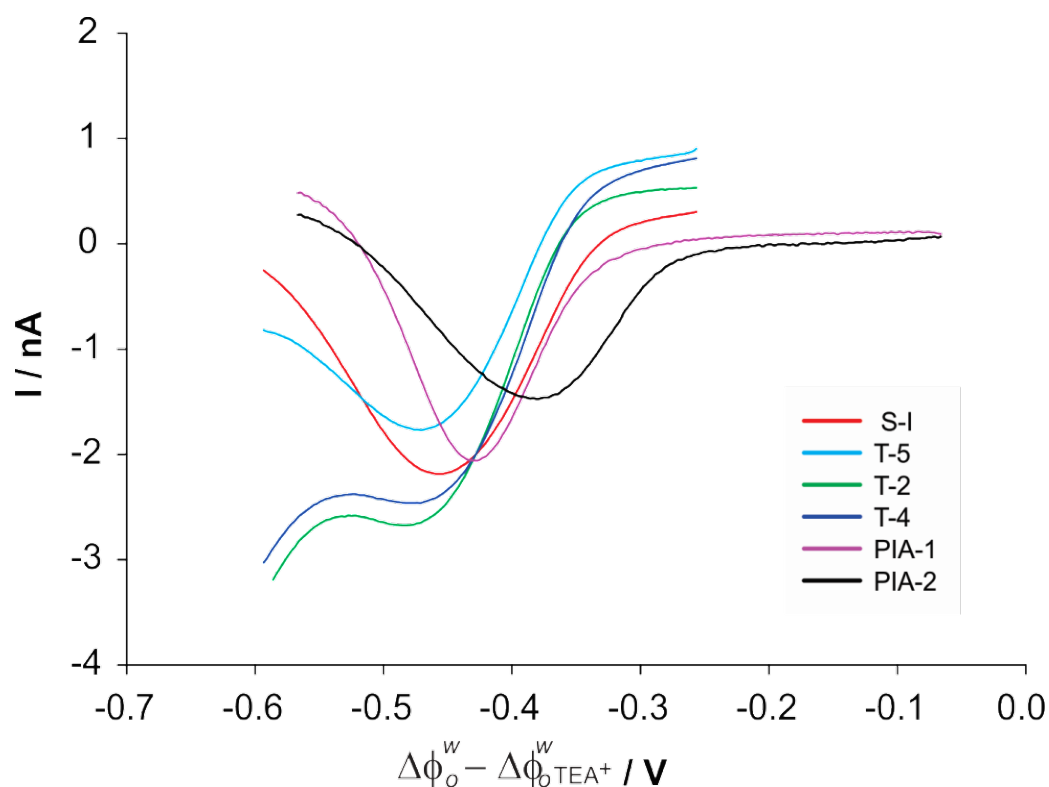
Figure 64. Forward voltammogram of 10 mM Na$_2$SO$_4$ at W/NPOE micro-interfaces in the presence of 2.5 mM ionophores (see legend) in the NPOE phase after subtraction of the voltammogram in the absence of ionophore.

Only two ionophores reduced significantly the potential of transfer of sulfate, PIA-1 and PIA-2, both with an aminomethylpyrrole attached to the acyclic isophthalamide; these decreased the potential of transfer by 27 and 75 mV, respectively, with respect to the commercial ionophore (S-I; Table 32). The greater reduction of PIA-2 is attributed to the presence of a strong electron withdrawing group (nitro group) in position 5 of the isophthalamide.

Table 32. Potential of transfer of sulfate at W/NPOE by FIT mechanism and peak current for different ionophores present in NPOE, in increasing order.

Ionophore	$\Delta\phi_o^w - \Delta\phi_{o,TEA^+}^w$ (10mM Na$_2$SO$_4$) mV	I (FIT) nA
PIA-2	-379	1.473
PIA-1	-427	2.059
S-I	-454	2.186
T-2	-471	2.674
T-5	-471	1.769
T-4	-483	2.463
Mono-Lys TU*	-	-
Di-Lys TU*	-	-
BIA-1*	-	-
BIA-2*	-	-

- No FIT observed.

Ionophore PIA-2 was evaluated under various scan rates and it was noted that the process observed is diffusion controlled, limited by the diffusion of the ionophore within the organic phase located in the micropores. In other words, there is a linear dependence between the peak current and the square root of the scan rate ($i \propto v^{1/2}$). For the forward scan, i (nA) = -12.795 v$^{1/2}$ (V·s^{-1})$^{1/2}$ - 0.7126, R² = 0.9998. Based on these values, the diffusion of the ionophore is estimated to be significantly slow in the organic phase. Assuming a charge of 1 or 2, the diffusion coefficients vary from 2.6 x 10^{-10} cm^2·s^{-1} to 3.3 x 10^{-11} cm^2·s^{-1}.

Ionophore characterisation via Mass Spectrometry:

Moreover, mass spectra of the ionophores in the NPOE phase were determined via ESI-MS. The ionophores were dissolved in NPOE (2.5 mM) and diluted in methanol (1/4) to electro-spray the sample before MS analysis. The protonated molecules were identified in the positive mode for the structures received from University of Murcia and also the commercial sulfate ionophore (S-I; Table 33). The experimental mass for the positively charged ($z = +1$, protonated structure) molecules matched perfectly the expected mass (Δm < 5ppm).

Table 33. Summary of the theoretical and experimental mass determined by ESI-MS for various ionophores in NPOE/methanol (1/4).

Ionophore	Molecular formula	Theoretical g·mol⁻¹	Experimental g·mol⁻¹	Δm ppm
PIA2-H⁺	$[C_{18}H_{18}N_5O_4]^+$	368.13533	368.13443	-2.854
PIA1-H⁺	$[C_{22}H_{27}N_4O_2]^+$	379.21285	379.21251	-0.903
BIA1-H⁺	$[C_{20}H_{33}N_2O_2]^+$	333.25365	333.25316	-1.820
BIA2-H⁺	$[C_{16}H_{23}N_3O_4]^+$	322.1761	322.1753	-1.685
SI-H⁺	$[C_{22}H_{23}N_4S_2]^+$	407.13586	407.13531	-1.362

Nevertheless, the mass expected for the ionophores from Sydney University did not match the MS spectra obtained which suggests that these structures might have undergone chemical changes. For instance, $m/z = 359.16838$ ($z = +1$) fits to mono-Lys TU when S in the thiourea is substituted by two hydrogens which explains the lack of response in the presence of sulfate.

A.3. Conclusions and Future plan

The key findings of initial studies into development of a sensor prototype for sulfate detection are:

- NPOE has been found to be the best organic solvent to employ for the organic phase of the liquid-liquid electrochemical cell; the sulfate-ionophore I is soluble in this solvent and a wide potential window is achieved.
- Facilitated sulfate anion transfer across the interface has been achieved with the commercially-available ionophore with the formation of a 1:1 ionophore:sulfate interfacial complex at W/NPOE interfaces. For different sulfate concentrations and fixed ionophore concentration, the half-wave potential of transfer decreases by 28.4 mV per 10-fold concentration of sulfate, which corresponds to a $z = -2$ and in agreement with a 1:1 complex formation.
- Evaluation of different concentrations of sulfates (as either sodium salt and sulphuric acid) was determined via CV and both responded to the neutral ionophore in the organic phase.
- A hydrophobic salt (TEA^+TPBCl^-) was synthesised by metathesis of TEA^+Cl^- and K^+TPBCl^-, to be used as an internal reference in order to enable calibration of the transfer potential (x axis of voltammograms). TEA^+TPBCl^- was incorporated in the organic phase (NPOE) and showed no interference in the SO_4^{2-} detection.
- ESI-MS analysis was performed to probe the ionophore-sulfate 1:1 complexation at the W/NPOE interface. Mass data for the 1:1 complex was obtained in aqueous media (methanol:water) and also when the ionophore is in the organic phase (NPOE) and emulsified with methanol:water for ionisation. In both cases, the spectra showed clear peaks at m/z of ca. 503 which corresponds to $[C_{22}H_{23}N_4S_3O_4]^-$, ionophore-$HSO_4^-$, with a maximum deviation from the theoretical mass of 1.1 ppm.
- Cyclic voltammetry (CV) and differential pulse voltammetry (DPV) showed LODs of 1.3 µM. A pre-concentration step of 60 s at a fixed potential where sulfate transfers in combination with DPV, also known as differential pulse stripping voltammetry (DPSV), further lowered the LOD down to 0.6 µM sulfate with the commercially available sulfate ionophore. Intensive data analysis to evaluate the sensitivity of the sensor prototype, such as background subtraction, was implemented.
- Plastic tips were shown to provide an alternative to silicon membranes for a sulfate sensor prototype. Also, PVC was incorporated into the organic phase which reduced the current measured for the sulfate transfer, probably as it decreased the diffusion rate of the ionophore within the PVC-gelled organic phase.
- Selectivity studies for a range of anions (PO_4^{3-}, $H_2PO_4^-$, SO_3^{2-}, NO_3^-, CH_3COO^-, OH^-, Cl^- and SCN^-) were carried out which showed potential interferences by the ions PO_4^{3-}, NO_3^-, OH^-, Cl^-.

- Real samples (pre-RO and post-RO) collected in the Beenyup groundwater replenishment trial plant were studied via CV and DPSV. The data revealed a significant larger increase of current than that expected for sulfate. This was further demonstrated by conductivity and ion chromatography measurements. Chloride (Cl^-) and nitrate (NO_3^-) were found via ion chromatography to be present in at concentrations of 0.2 and 0.1 mM, respectively, in the post-RO samples collected in the Beenyup groundwater replenishment trial plant. These concentrations interfered in the sensor response to sulfate.
- Chloride removal strategies have been undertaken and proposed, such as electrolysis of $Ag_{(s)}$ in the presence of $Cl^-_{(aq)}$ to form $AgCl_{(s)}$. A preliminary study showed 73% removal at a 2×10^{-6} mol·s^{-1} rate.
- A range of new neutral ionophores (9) provided by two research groups, from University of Sydney and University of Murcia were received. These were screened to assess their potentiality for binding of the ligand to sulfate. Two of the acyclic isophthalamide based ionophores with aminomethylpyrrole groups (PIA-1 and PIA-2) donated by University of Murcia showed a reduction in the potential of transfer of sulfate (*ca.* 27 and 75 mV) in comparison to the commercial ionophore.
- Further analysis should be undertaken with the new ionophores and the addition of an ion-exchange membrane and/or removal of chloride and nitrate from the water samples, in order to overcome the interferences observed in dealing with real samples.

The commercially available ionophore for sulfate enables detection of sulfate based on ion-transfer electrochemistry. However the selectivity is not sufficient for applications to real samples and hence development of new ionophores is crucial to realising a suitable sulfate sensor for water recycling applications.

Appendix B. Novel online sensors for RO validation

B.1. Introduction

B.1.1. Background

S::CAN spectrometers are a viable tool for online continuous monitoring of critical process parameters such as monochloramine, TOC, ammonia, temperature, pH, nitrate and total suspended solids. S::CAN probes also offer the option of reliable trigger alarms (e.g. plant shut down, coagulant dose, sampling and analysis) in response to changes of water quality parameters within the membrane treatment process. S::CAN spectrometers could potential replace existing traditional TOC, pH and other analytical instrumentation installed at Advanced Water Recycling Plants (AWRP). The S::CAN unit can also be used as a performance monitoring and management tool to assess each process continuously in the membrane filtration process at an AWRP.

The integration of S::CAN units into the Beenyup AWRP was achieved following a three-week investigative process in consultation with industry experts from DCM and UF/RO process specialists at Water Corporation. To understand variability in source water quality and chemical removal through the RO treatment processes, weekly microbial and chemical sampling of the feed water and product water at the Beenyup AWRP were performed. The data initially demonstrates approximately 92 - 97% organic matter removal through the RO treatment process. During the initial trial, a vast array of data was captured from the S::CAN units. A preliminary review of the data by DCM experts and Water Corporation process specialists identified suitable trends (in particular TOC profiling) which warranted further investigations on the applicability and on the limitation of S::CAN probes for online monitoring of Beenyup AWRP process.

In this context, the ability of S::CAN to detect target chemicals and surrogates was also of particular interest. Various μ-pollutants belonging to different chemical classes such as pesticides (e.g. simazine, metolachlor, trifluralin), hormones (e.g. ethinylestradiol, estrone), pharmaceuticals (metformin, diclofenac, carbamazepine), industrial chemicals (triethylphosphate, tolyltriazole) and nitrosamines (NMOR, NDMA) were initially chosen as potential candidates. These chemicals were selected based on: 1) prior knowledge of their occurrence in wastewater inflow and outflow to the Beenyup AWRP; 2) existing studies of recycled water and surface waters from previous surveys and the literature (Drewes *et al.*, 2008; Van Buynder *et al.*, 2009b; Linge *et al.*, 2012; Tang *et al.*, 2014). Following this, a literature review was conducted by DCM experts on the potential to detect specific pharmaceuticals, hormones, pesticides and pollutants using Ultra Violet/Visible (UV/Vis) absorption spectroscopy. In particular, the capability of UV/Vis spectrophotometry to detect concentrations at a level which may realistically be found in recycled water was investigated.

B.1.2. Sensor theory

The S::CAN spectrometer probe operates using UV/Vis spectrometry. The analyte/parameter to measure contained in the water weakens a light beam emitted by a lamp that moves through the liquid. After contact with the water, light intensity is measured by a detector over a range of wavelengths specific to the application. The spectrometer probe measures optical spectra from 200 to 720 nm. Depending on the application, Spectro::lyser™ UV/Vis can monitor TSS, turbidity, NO_3-N, COD, BOD, TOC, DOC, UV_{254}, colour, BTX, O_3, H_2S, AOC, fingerprints and spectral-alarms, temperature and pressure (Figure 65). S::CAN spectrometer probes can operate in different water types including surface water, groundwater, drinking water and wastewater. With the S::CAN spectrometer, up to 8 major parameters can be measured at once. On this system there is also room for expansion of the range of parameters for future applications not included above. For special applications (e.g. detection of a specific compound in water) a spectral range that correlates with the substance/parameter of interest needs first to be identified. Additional spectral calibrations are also required to accurately detect the substance. A large number of individual substances can be identified against a fluctuating background matrix and separately quantified with the application of chemometric methods (e.g. BTX, phenols, solvents, flavouring agents, etc.). In "event detection" mode, the intelligent "spectral alarm" of the Spectro::lyser™ probe permits detection of deviations from a normal composition providing an associated alarm signal. (More information is available at http://www.s-can.at/text.php?kat=5&id=21&langcode or downloading the instruction manual of the Spectro::lyser™ probe).
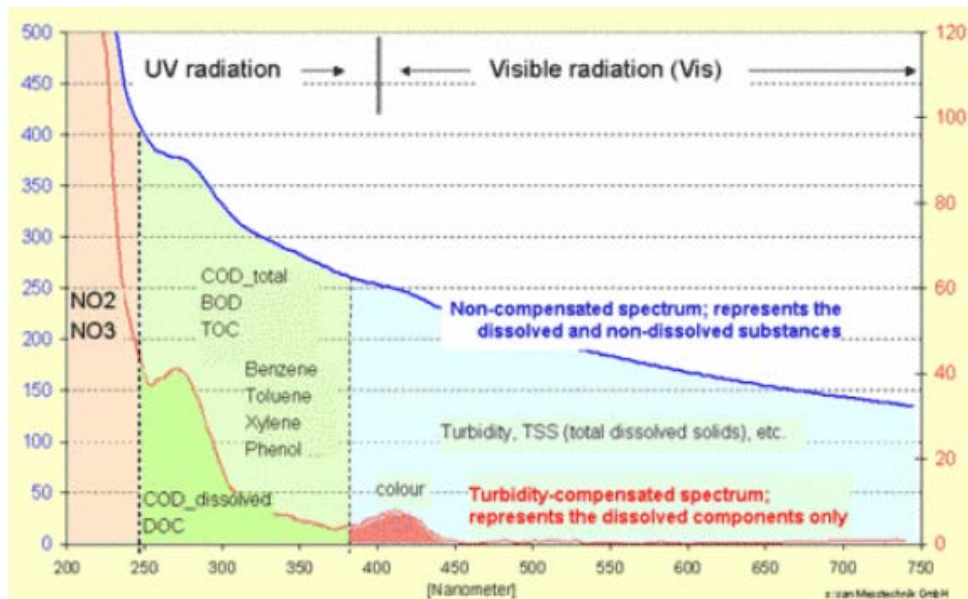
Figure 65. Parameters found in the UV/Vis region for the S::CAN instrument.

For a given compound to be detected directly by UV/Vis absorption spectrometer methods it must have a distinct UV/Vis absorption spectra and absorb strongly enough to be detected against the background water matrix absorption variability. The presence of unusual compounds is likely to be detectable against this background matrix if they are present in sufficient concentration to cause a UV/Vis absorption of a similar or greater magnitude to the usual variability at a given frequency/s (as opposed to the magnitude of the absorption itself). Detection of specific compounds is usually accomplished by derivative spectroscopy. Deviations from normal background water matrix conditions are detected by increases or decreases in the derivative spectra at different wavelengths. In real time operation, in the event an expedience is detected a water sample must be drawn for a laboratory forensic analysis in order to accurately determine the responsible chemical. The instrument would directly drive such auto sampling. The sensitivity of this method depends on (1) the variation in the background water matrix when no contaminants are present and (2) the contaminant concentration and absorption pattern.

B.1.3. Aims of the project

The aims of this work package were to:

- Conduct offline tests on the sensitivity and selectivity of the S::CAN probe toward the detection of target chemicals and surrogates including simazine, metolachlor, trifluralin, metformin, carbamazepine and N-Nitrosodimethylamine in RO water
- Conduct preliminary offline Fluorescence Excitation-Emission matrix tests on a benchtop fluorimeter to assess the detection of selected target chemicals against the RO water background
- Conduct online-S::CAN measurements of the parameter TOC at Beenyup AWRP and assess whether the probe can be used to substitute a cabinet Sievers TOC analyser
- Conduct offline measurements using S::CAN to assess R-WT rejection during challenge tests at Beenyup AWRP

B.2. Materials and Methods

B.2.1. Waterworks at Beenyup WWTP - AWRP

The Advanced Water Recycling Plant (AWRP) is located at Beenyup Wastewater Treatment Plant (WWTP, Perth, Western Australia). The AWRP treats secondary effluent from the Beenyup WWTP which receives predominately urban residential sewage. Briefly, at the WWTP, raw wastewater is treated with screening, grit removal and this wastewater is passed slowly through primary sedimentation tanks. The treated wastewater which leaves the primary sedimentation tanks (primary wastewater) undergoes aeration, activated sludge treatment and clarification (secondary wastewater). The majority of the resulting secondary wastewater is discharged into the Indian Ocean, while a small portion (7 ML·day^{-1}) is fed into the AWRP. Treatment at the AWRP consists of chloramination to preserve membranes, ultrafiltration, reverse osmosis, and UV disinfection for virus inactivation. A schematic of the treatment

process at Beenyup WWTP-AWRP is shown in Figure 66. The S::CAN probes are installed in the following points along the treatment plant: (1) raw wastewater influent; (2) post-ultrafiltration; (3) post-reverse osmosis.
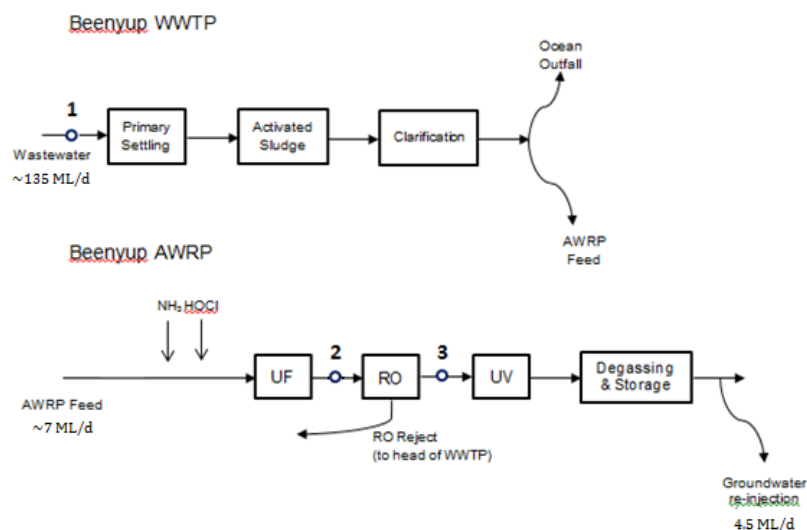
Figure 66. Schematic of the WWTP and the AWTP located at Beenyup. Locations of S::CAN probes (1-3) are also indicated.

B.2.2.   Chemicals and preparation of solutions

Metolachlor PESTANAL® (analytical standard purity > 97.6%), trifluralin (analytical standard purity > 99.9%), simazine PESTANAL® (analytical standard purity > 99.8%), carbamazepine (analytical standard purity > 99.0%), metformin hydrochloride (United States Pharmacopeia (USP) Reference Standard purity > 99.8%), N-Nitrosodimethylamine solution 200 µg·mL^{-1} in methanol (analytical standard purity > 99.9%) were supplied by Sigma–Aldrich (Sydney, Australia); methanol (MeOH) (ChromAR HPLC grade) were purchased from Mallinckrodt Baker (Phillipsburg, NJ, USA). Stock solutions of individual chemicals were prepared by weighting a specified amount of neat chemical and transferring it into a 1 L volumetric flask which was then filled up to the mark with DI water. Due to solubility issues, the pesticide trifluralin was firstly dissolved in 1 mL of MeOH and then the volume was brought up to 1 L with DI water under stirring. Corresponding blanks were also prepared as reference. The mix solutions containing the 6 test chemicals were prepared by sequential dilution of the stock solutions (Mix Conc. A, B, C). Table 34 summarizes the concentrations of single compound stock and mix solutions prepared. All solutions were kept refrigerated at 4°C to prevent degradation.

Table 34. Concentrations of stock solutions and mixtures.

Compound	DWG (µg·L^{-1})	S::CAN Estimated Alarm Limit (µg·L^{-1})	Stock solution (µg·L^{-1})	Mix Conc. A (µg·L^{-1})	Mix Conc. B (µg·L^{-1})	Mix Conc. C (µg·L^{-1})
Metolachlor	300**	2000	4000	400	4000	40
N-Nitrosodimethylamine	100**	50/3000	200	20	200	2
Trifluralin	50**	150/250/1000	2000	200	2000	20
Simazine	20**	30 / 250	1000	100	1000	10
Carbamazepine	100**	1000	2000	200	2000	20
Metformin HCl	250**	50	1000	100	1000	10

**Water Corporation Memorandum of Understanding with the Health Department of WA

B.2.3. S::CAN offline tests to assess the detection of target pollutants at Beenyup AWRP

Offline tests on the sensitivity and selectivity of the S::CAN probe toward the detection of the 6 target chemicals and surrogates were conducted. Following DCM recommendation, a range of µ-pollutants relevant to Water Corporation including pesticides (e.g. simazine, metolachlor, trifluralin), pharmaceuticals (metformin, carbamazepine) and nitrosamines (N-Nitrosodimethylamine, NDMA) were selected for testing. The matrix used for these experiments constituted of laboratory DI water from CWQRC laboratory. DCM recommended avoiding using ultrapure water (e.g. RO water or MQ water) to prepare the solutions. DCM had previously found that some RO units produced RO water containing residual RO resin/fibres that could interfere with the measurements. Therefore DI water was preferred to record the chemical fingerprints in S::CAN. Absorbance measurements were set to be taken at a 2 min interval; measurement time for each sample was 30 s (real measurement: 10 s, software calculations: 20 s). As per DCM instructions, the cleaning of the sensor and of the sample sleeve was carried out before and after each measurement according to DCM "Shore Cleaning/Zero Check Instructions – 35 mm" standard procedure using DI water. The absence of contamination/memory effects was verified by acquiring 2 consecutive blank samples constituted of DI water after each measurement with spiked solutions.

B.2.4. Fluorescence Excitation-Emission matrix experiments

A quinine stock solution (1 g·L^{-1}) was prepared by adding 0.258 g of quinine in 250 mL of sulphuric acid (0.05 M). Other stock solutions of individual chemicals were prepared according to Section B.2.2. Compounds tested for fluorescence excitation-emission experiments were metolachlor, trifluralin, simazine and carbamazepine. Single compound solutions were prepared in DI water and in RO water at concentrations corresponding to the DWG. A mix solution containing the 4 test chemicals were prepared by sequential dilution of the stock solutions in DI water and RO water at concentration corresponding to the DWG. Fluorescence excitation-emission spectra of DI water and RO water blanks were also acquired as reference. Table 35 summarizes the concentrations of single compound stock and mix solutions prepared. All solutions were kept refrigerated at 4°C to prevent degradation.

Table 35. Concentrations of stock solutions and mixtures in DI water and RO water used for the fluorescence excitation-emission matrix experiments.

Compound	DWG (µg·L^{-1})	Stock solution in DI water (µg·L^{-1})	Single compound working solution in DI water (µg·L^{-1})	Single compound working solution in RO water (µg·L^{-1})	Mix in DI water (µg·L^{-1})	Mix in RO water (µg·L^{-1})
Metolachlor	300**	4000	300	300	300	300
Trifluralin	50**	2000	50	50	50	50
Simazine	20**	1000	20	20	20	20
Carbamazepine	100**	2000	100	100	100	100

**Water Corporation Memorandum of Understanding with the Health Department of WA

Fluorescence EEMs were collected using a Hitachi F-7000 spectrophotometer (Hitachi, Sidney, Australia) with a Xenon flash lamp using the method of Cory *et al.* (2010) with modification in the scan range of excitation wavelength of 240 - 450 nm and emission wavelength of 320 - 550 nm. EEM were collected by measuring the fluorescence intensity across excitation wavelength of 200 - 400 nm (in increments of 5 nm) and emission wavelength of 280 - 500 nm (in increments of 2 nm). All samples were measured in triplicate using a 1 cm quartz fluorescence cuvette (Starna, Australia). Listed below are the instrument parameters used to collect the fluorescence excitation- emission matrix of blanks and samples: Excitation - Excitation start: 200 nm; Excitation stop: 400 nm; Excitation Data Interval: 5 nm. Emission - Emission start: 280 nm; Emission stop: 500 nm; Emission Data Interval: 2 nm. Slit width: 5 nm for both excitation and emission; PMT Voltage: High; Scan Rate: 1200 nm·min^{-1}. The EEM data were corrected for Raman and Raleigh scattering using the associated UV/Vis spectra, a solvent blank and two correction factors. The correction was applied using a Matlab program, which also produces a contour plot of relative fluorescence intensity and a spreadsheet containing the corrected EEM data for each scan.

B.2.5. Comparison of the parameter TOC at Beeyup AWRP using online-S::CAN measurements and a Sievers TOC analyser

A 35 mm path length S::CAN UV/Vis spectrometer and a Sievers TOC were installed on a bypass system drawing water from the feedwater side of the Beenyup WWTP RO system. This effectively represents secondary WW which has been passed through ultrafiltration membranes. A 100 mm path length S::CAN UV/Vis spectrometer and a second Sievers TOC analyser were installed on a bypass line drawing water from the permeate side of the Beenyup WWTP RO system. This effectively represents post-UF water which has been passed through reverse osmosis membranes. The S::CAN system was operated in total isolation from each other and each discrete measurement made by each instrument (made here every 2 minutes) is isolated from the previous and successive measurement. That is, there is no averaging, smoothing or other mathematical link between successive measurements. The only potential averaging or smoothing that can occur can be via a lack of flow to the sensing system causing a hydraulic averaging or smoothing. The S::CAN spectrometers were programmed to provide a TOCeq (eq: equivalent) estimate based on mathematical relationship between UV/Vis measurements and accredited laboratory testing of a variety of different drinking water sources. DCM have developed such algorithm for measurements of TOC in drinking water applications and therefore it was unknown how such algorithm would perform in the context of treated wastewater passed through UF and RO membranes. Such molecular sieving is expected to exclude most larger molecules and those having double bonds which are typically those causing the absorptions in drinking waters (Fulvics/humics and various biologically created ring structures). It is however expected that since drinking water is the source water to which waste components were added before entering Beenyup WWTP, these components are likely to be present in at least the RO feedwater. Whether enough of these components pass through the RO membrane to allow detection by the post-RO S::CAN was a question which this work attempts to answer. The S::CAN UV/Vis derived TOC will be referred to as TOCeq where eq is an assumed equivalent based on drinking water matrices.

B.2.6. Challenge tests for R-WT removal at Beenyup AWRP

Challenge tests were conducted at Beenyup AWRP on the 20th of August 2014. Rhodamine WT (R-WT) was spiked in a holding tank at 1000 $\mu g \cdot L^{-1}$. This solution was used as feed water into the RO train while the plant was on by-pass. Samples were taken at different treatment stages including: feed Stage 1, Permeate Stage 1, Feed Stage 2, Permeate Stage 2, Combined Permeate and Concentrate Stage 2. The concentration of R-WT was assessed using S::CAN and the rejection calculated.

B.3. Results and Discussion

B.3.1. S::CAN offline tests to assess the detection of target pollutants at Beenyup AWRP

The list of chemicals to be tested was finalised by DCM experts in conjunction with Water Corporation based on DW guidelines as well as estimated alarm limits (Table 36). For example, according to the data in Table 36, the Drinking Water Guideline (DWG) for pharmaceutical diclofenac is 1.8 $\mu g \cdot L^{-1}$ and the alarm warning limit with UV/Vis methods is estimated as 150 $\mu g \cdot L^{-1}$. This means that UV/Vis is probably not suitable to provide warnings about the compound diclofenac at the maximum allowable composite value in the reuse water. On the other hand, the DWG for metformin is 250 $\mu g \cdot L^{-1}$, while the estimated alarm warning limit is 50 $\mu g \cdot L^{-1}$. This means it may be possible to provide warning for the compound metformin in the post-RO Beenyup location. However, according to DCM, the estimated alarm limits for the S::CAN probe needed to be tested.
.

Table 36. Drinking water guidelines, estimated UV/Vis alarm and spectroscopic properties of the compounds.

Substance	DWG $(\mu g \cdot L^{-1})$	Estimated alarm $(\mu g \cdot L^{-1})$	MW $(g \cdot mol^{-1})$	λ max (nm)	E $(L \cdot mol^{-1} \cdot cm^{-1})$	Abs/m per 1 mg·L^{-1}	µg·L^{-1} per 1Abs/m	Solution type	Reference
Carbamazepine	100*	1000	236.27	290	12000	5.09	1970	No record	Lang, 1996
Diclofenac	1.8*	150	296.15	275	11000	3.71	270	Phosphate buffer pH 6.8-7	Jabłońska *et al.*, 2008
E1	0.03*	750 750	270.37	282 282	2120 2250	0.784 0.832	1280 1200	MeOH, n-BuOH	Chan *et al.*, 2012
EE2	0.0015*	750	296.40	278	2060	0.695	1440	aqueous	Mazellier *et al.*, 2008
Metformin	250*	50	129.16	232	12300	9.5	100	Phosphate buffer pH 6.8-7	Khouri *et al.*, 2004
Metholachlor	0.3* 300**	>2000	283.79	290-330	<750	<0.264	>3790	H$_2$O	Kochany et., 1994
NDMA	0.01* 100**	50 3000	74.08	228 332	7400 110	9.99 0.148	100 6760	Distilled H$_2$O	Farre' *et al.*, 2010
NMOR	0.001* 5**	75 7000	116.14	237 346	7943 85	6.84 0.0732	150 13660	H$_2$O	Druckrey *et al.*, 1967
Simazine	0.02* 20**	30 250	201.66	223.9 264.8	36800 3500	18.2 1.74	60 570	EtOH/H$_2$O (1% v:v)	Spinelli *et al.*, 2014
Tolytriazole	0.007* 20**	…	133.17	…	…	…	…	…	…
Triethylphosphate	n.a.* 1**	…	182.15	…	…	…	…	…	…
Trifluralin	0.05* 50**	150 250 1000	335.28	231 274 431	9800 6700 1930	2.92 2.00 0.576	340 500 1740	ACN/H$_2$O (0.02%)	Tagle *et al.*, 2005
4-cumylphenol	0.35* 0.35**	1000	212.29	290	1800	0.85	1200	…	…

* Environment Protection and Heritage Council, National Health and Medical Research Council & Natural Resource Management Ministerial Council. (2008). Australian Guidelines for Water Recycling - Augmentation of Drinking Water Supplies. Canberra: Biotext Pty Ltd.
**Water Corporation Memorandum of Understanding with the Health Department of WA.

The S::CAN unit used for all measurements had a 35 mm path length for increased sensitivity. The S::CAN unit is installed in the post-RO sampling panel (Figure 67). The probe was disconnected from the unit, and a sample sleeve was installed (Figure 68).
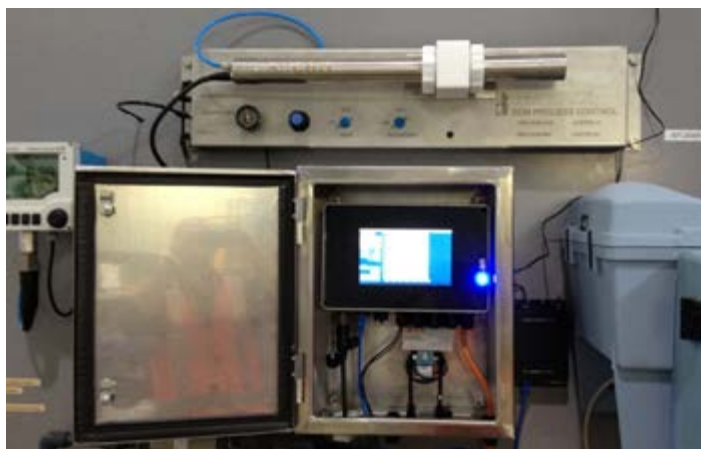
Figure 67. S::CAN probe installed on the post-RO panel at Beenyup AWRP.
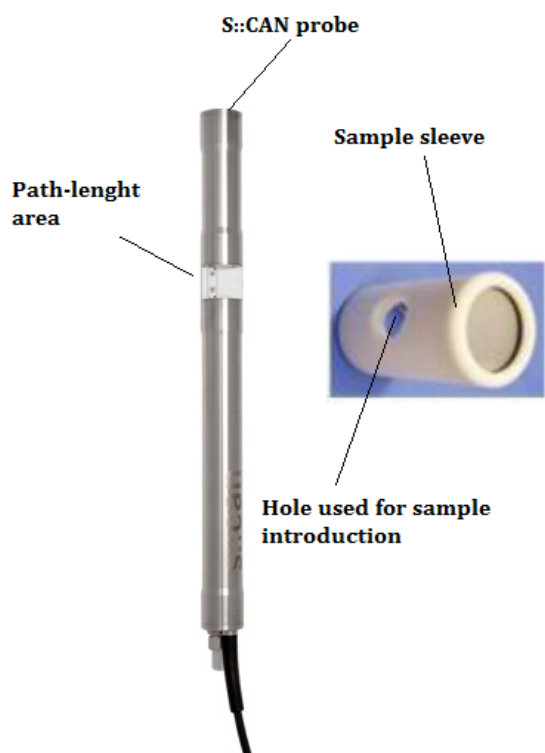
Figure 68. Sample sleeve used on the S::CAN probe. The sample sleeve is slided over the spectro::lyser so that it is covering the path-length area. The hole is used to load the liquid to measure in the path-length area.

The sample sleeve allows offline measurements of small amount of samples to be taken without the need for a constant flow of solution to be pumped through the UV/Vis cell of the S::CAN unit. Baseline/blank measurements were conducted in triplicate on laboratory/AWRP RO water, DI water with MeOH and DI water. Single compound stock solutions as well as mixtures at different concentrations were measured in duplicate.

B.3.1.1. Procedure to estimate alarm limit values

Mathematical analysis was performed by DCM staff to produce the alarm limit estimate values for each of the compounds for which the UV/Vis spectra was measured experimentally at Beenyup AWRP. According to DCM, the procedure to estimate the alarm limit values is the following:

- Determine targ*et al*arm wavelength- corresponds to the UV/Vis spectra at a local maximum gradient near a specific peak.
- Determine variation in Beenyup RO permeate water UV/Vis derivative spectra at the same wavelength.
- Determine minimum priority contaminant concentration which would be detectable against the background variability.
- Compared this concentration to the correspondent drinking water guidelines value, to determine if S::CAN has the required sensitivity to detect the indicator compound at the DW guideline value.

This procedure is summarised in figure 5 using carbamazepine as an example:
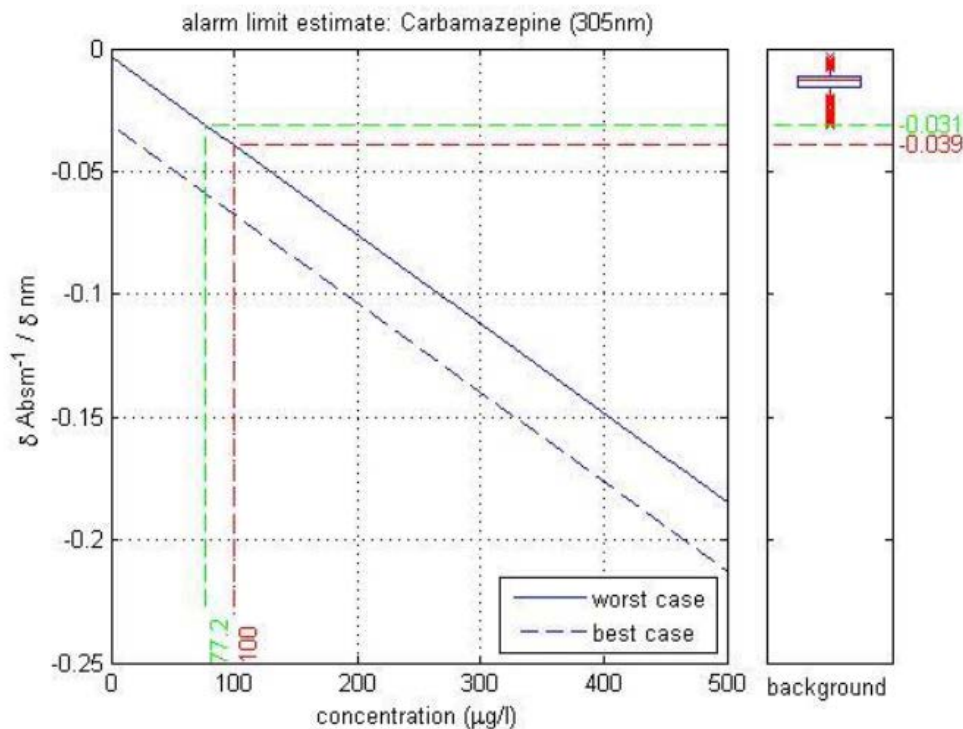
Figure 69. Estimate alarms limits for carbamazepine at 305 nm.

This chart provides a graphical estimation of the detection of Carbamazepine at 305 nm against the Beenyup RO permeate variability. The box and whisker plot at the top in the right hand panel give the variability of the background permeate (very low, from 0 to -0.03 Abs·m^{-1}). The green line gives the minimum concentration of carbamazepine required to always generate a more pronounced gradient and hence trigger an alarm (< -0.03 Abs·m^{-1}·nm^{-1} = 77 µg·L^{-1}). For comparison he DWG limit is also plotted (100 µg·L^{-1} results in a minimum deviation of -0.039 Abs·m^{-1}·nm^{-1}). Since 77 µg·L^{-1} is lower than the DWG (100 µg·L^{-1}) it is expected that the contamination at the DWG could be detected with S::CAN. The results for each compound tested are summarised in the following paragraphs in more details.

B.3.1.2. Discussion of alarm limit values

CARBAMAZEPINE

Carbamazepine is a prescription drug widely used as an anticonvulsant for neuropathic pain, to treat seizures and for bipolar disorder (Busetti *et al*., 2009). Carbamazepine is effectively rejected by RO treatment and it has not been detected previously post-RO/post-UV treatment at Beenyup AWRP (Busetti *et al*., 2009; Van Buynder *et al*., 2009a; Tang *et al*., 2014; Busetti *et al*., 2015).

Molecular Formula: C$_{15}$H$_{12}$N$_2$O
Molecular Weight: 236 g·mol^{-1}
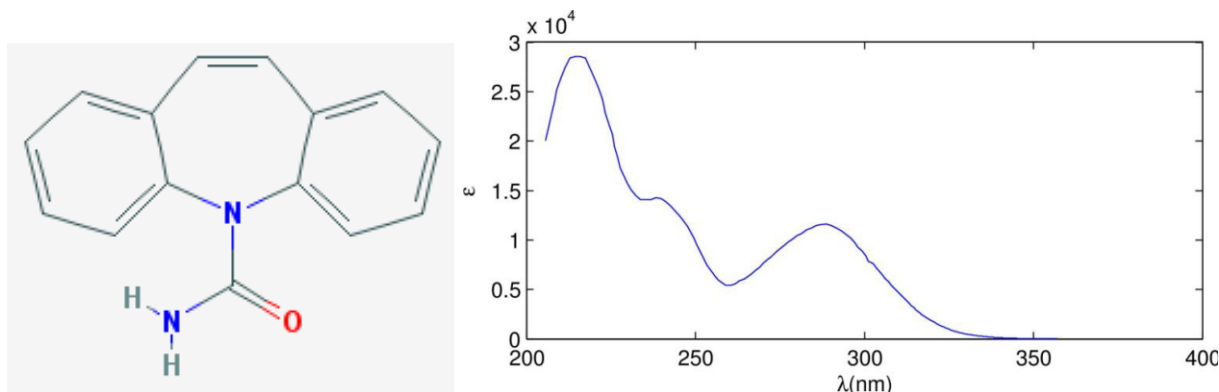
Figure 70. UV adsorption spectra of carbamazepine.

Due to its cyclic unsaturated ring structure, carbamazepine possesses a quite distinctive UV/Vis Abs spectra, showing a strong UV/Vis absorption with an extinction coefficient of 12 000 $M^{-1} \cdot cm^{-1}$. Carbamazepine possesses adsorption maxima at 290 nm, which is the most promising spectral region to be compared against the fluctuating background of RO water (e.g. background water matrix also have strong absorption near 220 nm). Figure 71 show an example of the UV/Vis spectra of the indicator compound carbamazepine spiked at 20, 200, 2000 $\mu g \cdot L^{-1}$ in DI water against the Beenyup RO permeate baseline (blank).
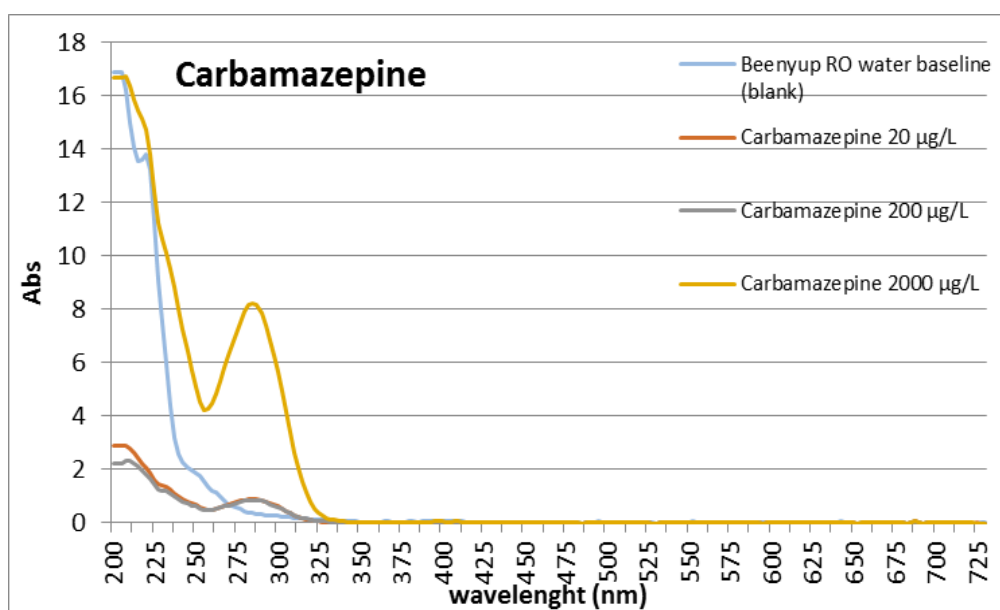
Figure 71. UV/Vis spectra recorded with S::CAN in RO water (blank) and for carbamazepine at 20-2000 $\mu g \cdot L^{-1}$ in DI water.

The target alarm wavelengths (showing a local maximum gradient near a peak) were identified by DCM to be 220, 275 and 305 nm. The variation in Beenyup RO permeate water UV/Vis derivative spectra at the same wavelengths was also determined to produce the following plots. In the worst case scenario, at 305 nm carbamazepine can be detected at a concentration of 77.2 $\mu g \cdot L^{-1}$ (green dotted line) in RO permeate. The red dash line represents the DWG of carbamazepine (100 $\mu g \cdot L^{-1}$).
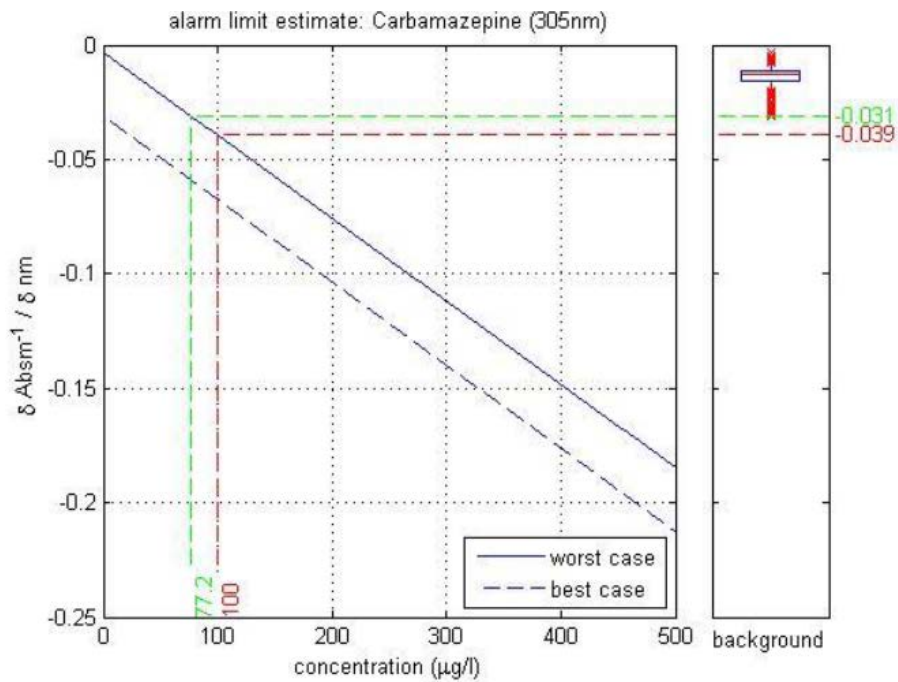
Figure 72. Detection limits for carbamazepine at 305 nm.

At the other wavelength tested (202 nm) by DCM, carbamazepine cannot be detected as the green line never crosses the "worst case" continuous line. The red dash line represents the DWG of carbamazepine.
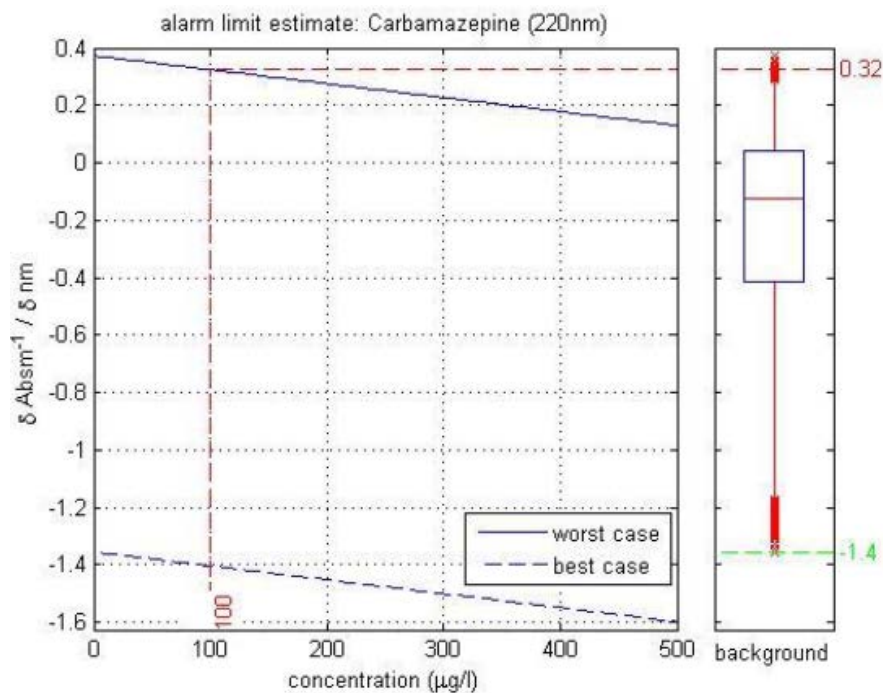
Figure 73. Detection limits for carbamazepine at 220 nm.

In the worst case scenario, at 275 nm carbamazepine can be detected at a concentration of 445 $\mu g \cdot L^{-1}$ (green dotted line) in RO permeate (Figure 74). The red dash line represents the DWG of carbamazepine (100 $\mu g \cdot L^{-1}$). Therefore, also at this wavelength S::CAN cannot detect carbamazepine in RO water, as the alarm estimate limit is approximately 4.5 times higher than the DWG value.
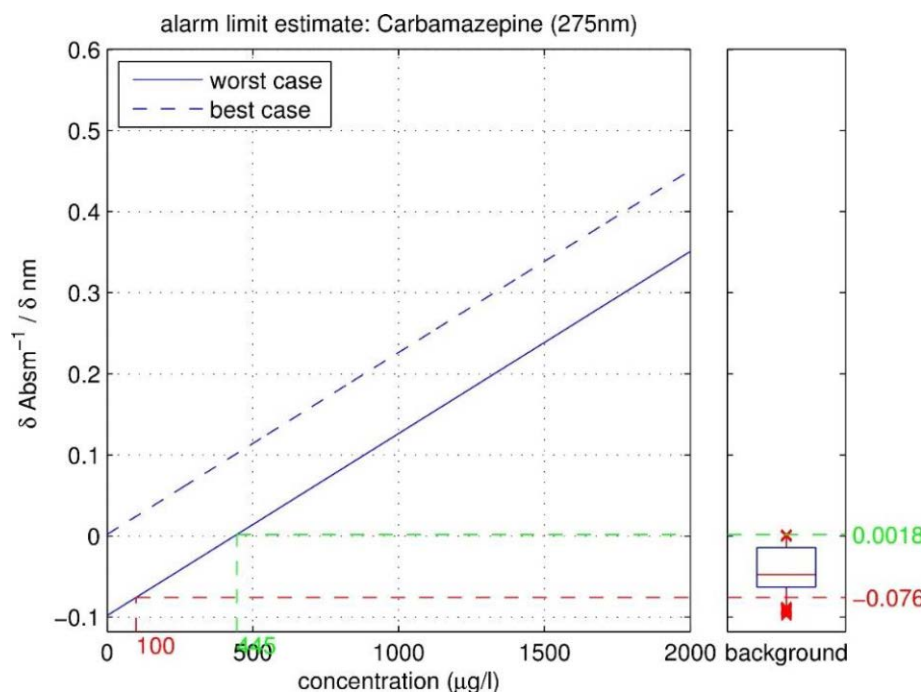
Figure 74. Detection limits for carbamazepine at 275 nm.

In conclusion, carbamazepine can be detected at 77.3 µg·L^{-1} at 305 nm using S::CAN. This value is about 30% below the DWG for carbamazepine of 100 µg·L^{-1}.

METOLACHLOR

Metolachlor is a member of the chloroacetanilide family of herbicides. It has been detected previously in RO water at Beenyup in the concentration range <1 – 7.5 ng·L^{-1} (median 3.75 ng·L^{-1}) while post-UV treatment resulted in the concentration range <0.5 – 5 ng·L^{-1} (median 2.5 ng·L^{-1}) (Busetti *et al.*, 2015). Metolachlor displays a relatively weak absorption of UV/Vis radiation (Dimou *et al.*, 2005). The extinction coefficient of Metolachlor remains lower than 750 M^{-1}·cm^{-1} between 290 nm and 330nm across a range of pH values (Kochany and Maguire, 1994).

Molecular Formula: $C_{15}H_{22}ClNO_2$
Molecular Weight: 283.8 g·mol^{-1}
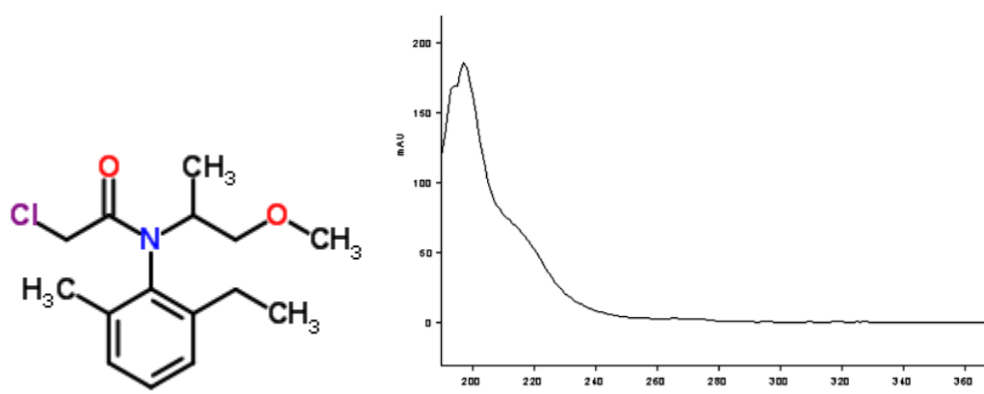
Figure 75. UV adsorption spectra of metolachlor.

Figure 75 show an example of the UV/Vis spectra of the indicator compound metolachlor spiked at 40, 400, 4000 µg·L^{-1} against the Beenyup RO permeate baseline (blank).
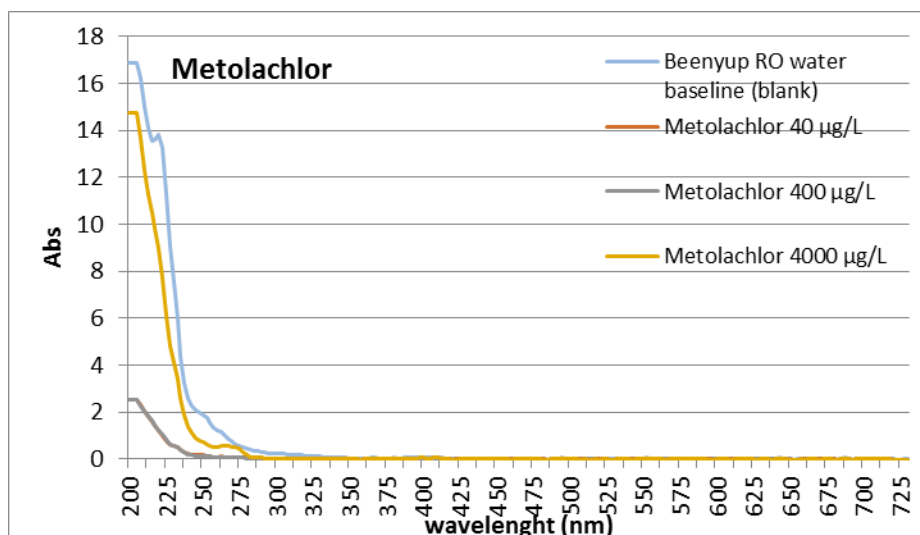
Figure 76. UV/Vis spectra recorded with S::CAN in RO water (blank) and for metolachlor at 40-4000 µg/L in DI water.

The targ*et al*arm wavelength was identified by DCM to be 220 nm. The variation of Beenyup RO permeate water UV/Vis derivative spectra at 220nm was also determined. The following figure was produced to estimate the detection limits of metolachlor in Beenyup RO permeate at 220 nm.

In the worst case scenario, metolachlor cannot be detected in RO permeate as the green line never crosses the "worst case" continuous line (Figure 77). The red dash line represents the DWG of metholachlor (300 µg·L^{-1}). For this compound no additional wavelengths were investigated by DCM.
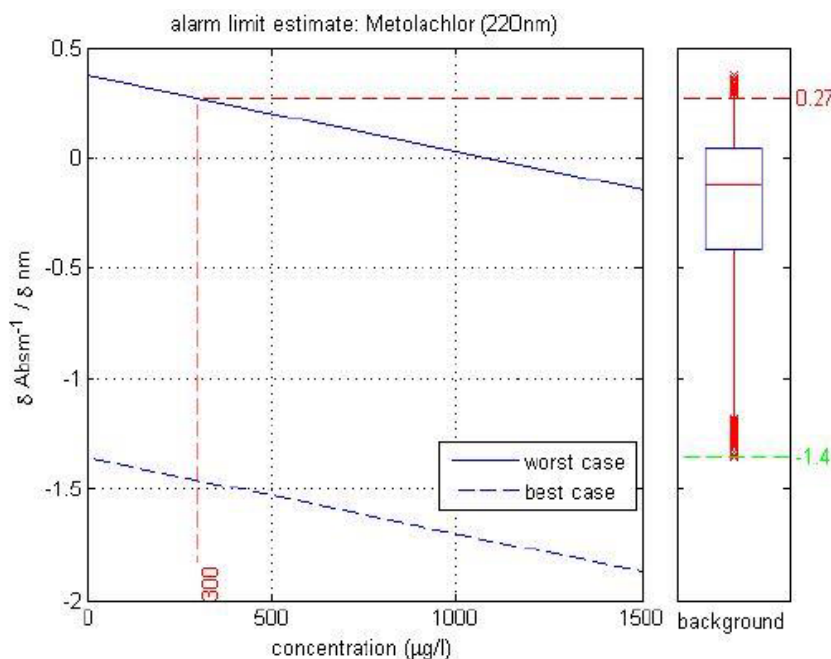
Figure 77. Detection limits for metolachlor at 220 nm.

METFORMIN

Metformin is a very common antihyperglycaemic drug for treatment of type 2 diabetes in obese and overweight people and it is listed as one (of only two) oral antidiabetics in the World Health Organization Model List of Essential Medicines (Tsai *et al.*, 2006). It has been detected previously in RO water at Beenyup in the concentration range 65 - 105 ng·L^{-1} (median 99 ng·L^{-1}) (Busetti *et al.*, 2015).

Molecular Formula: $C_4H_{11}N_5$
Molecular Weight: 129.2 g·mol^{-1}
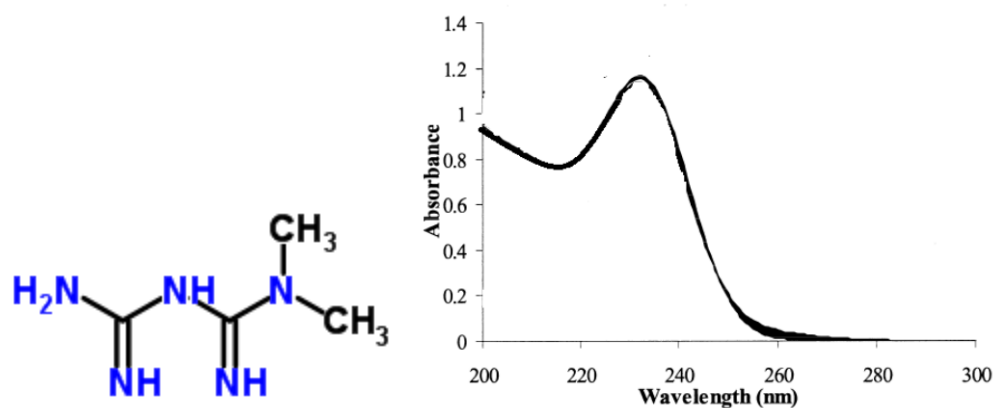
Figure 78. UV adsorption spectra of metformin.

Khouri *et al*. (2004) reported a relatively strong UV/Vis absorption spectra under neutral pH conditions likely to be found in recycled water. The absorption spectrum is due to the resonance structure of the Biguanides and the extinction coefficient in their work was reported to be 12300 $M^{-1} \cdot cm^{-1}$ at 232 nm. Figure 79 shows an example of the UV/Vis spectra of the indicator compound metformin spiked at 10, 100, 1000 $\mu g \cdot L^{-1}$ against the Beenyup RO permeate baseline (blank).
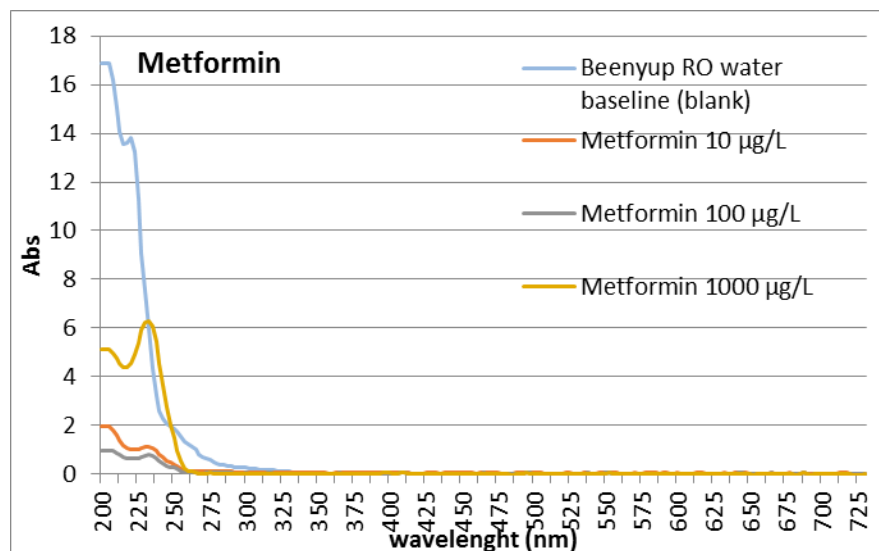
Figure 79. UV/Vis spectra recorded with S::CAN in RO water (blank) and for metformin at 10-1000 µg/L in DI water.

The targe*t al*arm wavelengths were identified by DCM to be 230 and 250 nm. The variation of Beenyup RO permeate water UV/Vis derivative spectra at 230 and 250 nm were also determined. The following figures were produced to estimate the detection limits of metformin in Beenyup RO permeate at 230 and 250 nm.

In the worst case scenario, metformin can be detected at 230 nm at a concentration of 7850 $\mu g \cdot L^{-1}$ (green dotted line) in RO permeate. The red dash line represents the DWG of metformin (250 $\mu g \cdot L^{-1}$).
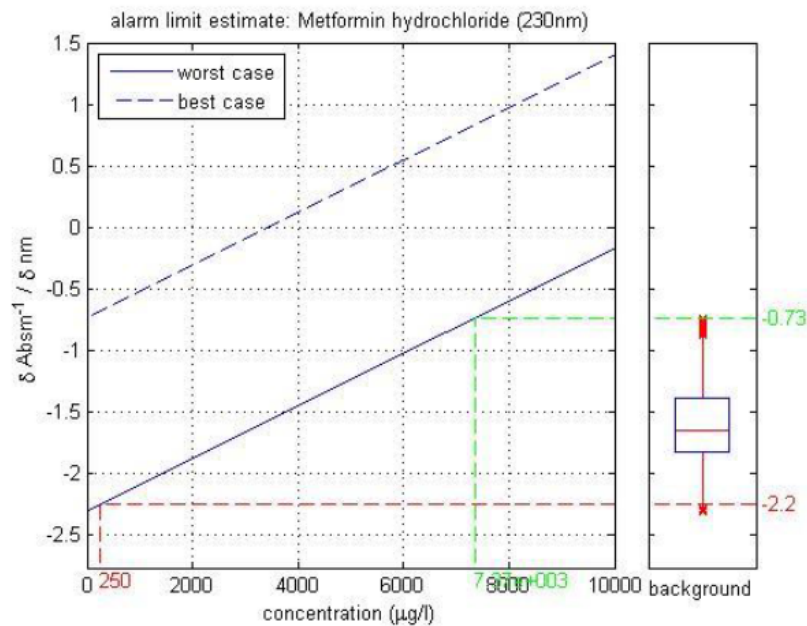
Figure 80. Detection limits for metformin at 230 nm.

At the other wavelength tested (250 nm) by DCM, metformin can be detected at a concentration of 278 µg·L^{-1} (green dotted line) in RO permeate. The red dash line represents the DWG of metformin (250 µg·L^{-1}).
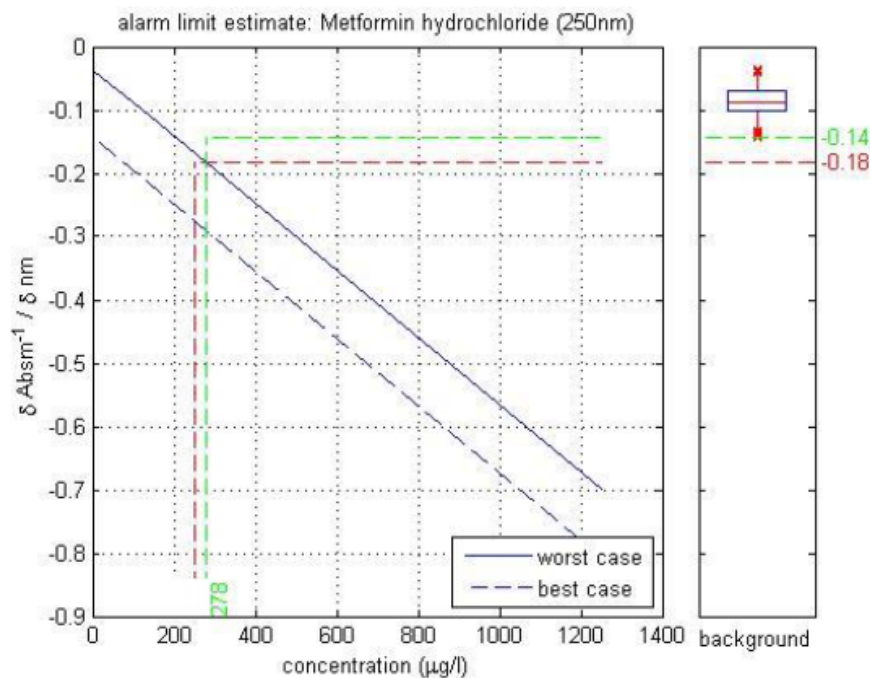
Figure 81. Detection limits for metformin at 250 nm.

N-NITROSODIMETHYLAMINE (NDMA)

N-Nitrosodimethylamine (NDMA) is a semivolatile disinfection by-products known to form during disinfection of water to prevent biofouling of UF/RO membranes. Due to its physic-chemical properties (i.e. low polarity and low MW) NDMA is not effectively rejected by UF/RO treatment. NDMA concentrations in the low ng/L range are typically detected post-RO treatment (Linge *et al.*, 2012). NDMA is susceptible to degradation by UV radiation indicating a strong UV absorption spectra. NDMA displays two main regions of absorption, with maximum absorption wavelengths at 228 nm and 332 nm. The corresponding extinction coefficients are approximately 7400 M^{-1}·cm^{-1} and 110 M^{-1}·cm^{-1} respectively (Farré *et al.*, 2010). NDMA is removed from recycled water by UV/H$_2$O$_2$ treatment.

Molecular Formula: $C_2H_6N_2O$
Molecular Weight: 74.1 g·mol^{-1}
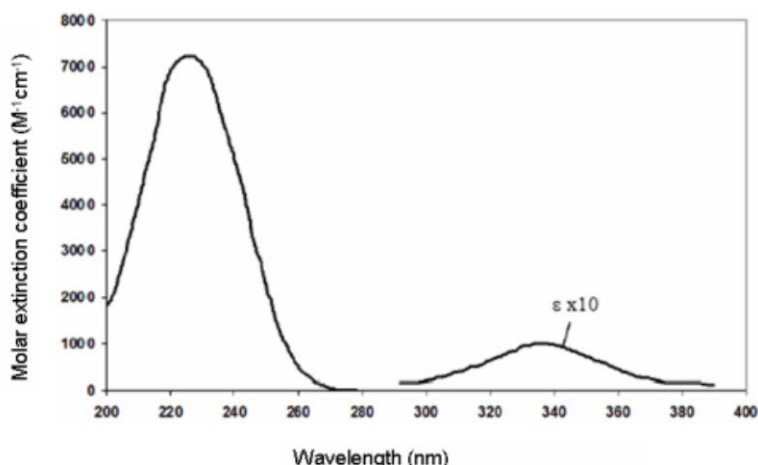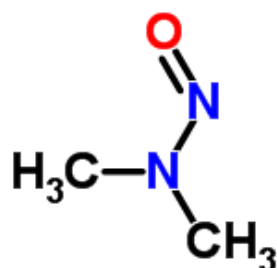

Figure 82. UV adsorption spectra of NDMA.
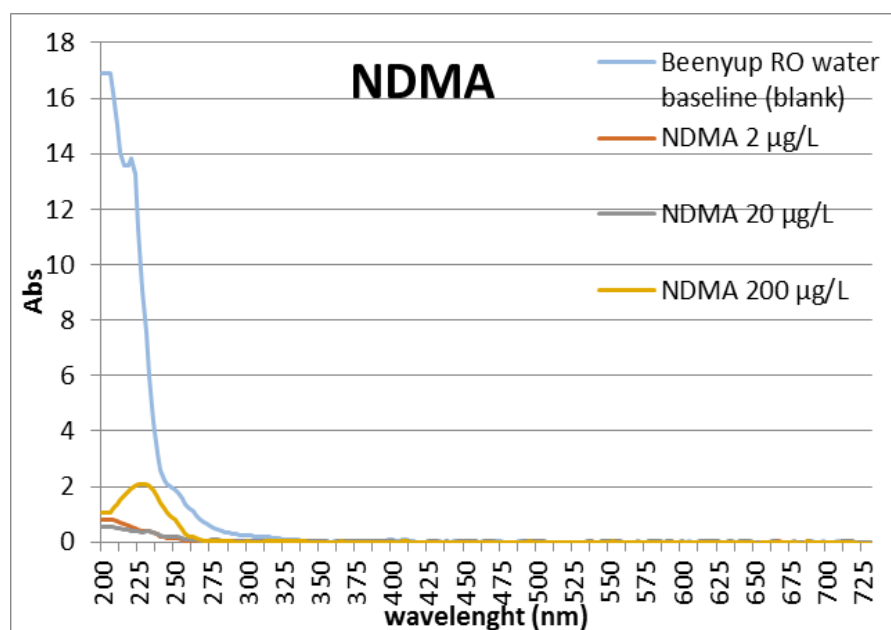
Figure 83. UV/Vis spectra recorded with S::CAN in RO water (blank) and for NDMA at 2-200 µg/L in DI water.

The targe*t al*arm wavelength was identified by DCM to be 245 nm. The variation of Beenyup RO permeate water UV/Vis derivative spectra at 245 nm was also determined. The following figure was produced to estimate the detection limits of NDMA in Beenyup RO permeate at 245 nm.

In the worst case scenario, NDMA can be detected at 245 nm (green dotted line) at a concentration of 241 µg·L^{-1} in RO permeate well above the DWG. The red dash line represents the DWG of NDMA (250 µg·L^{-1}).
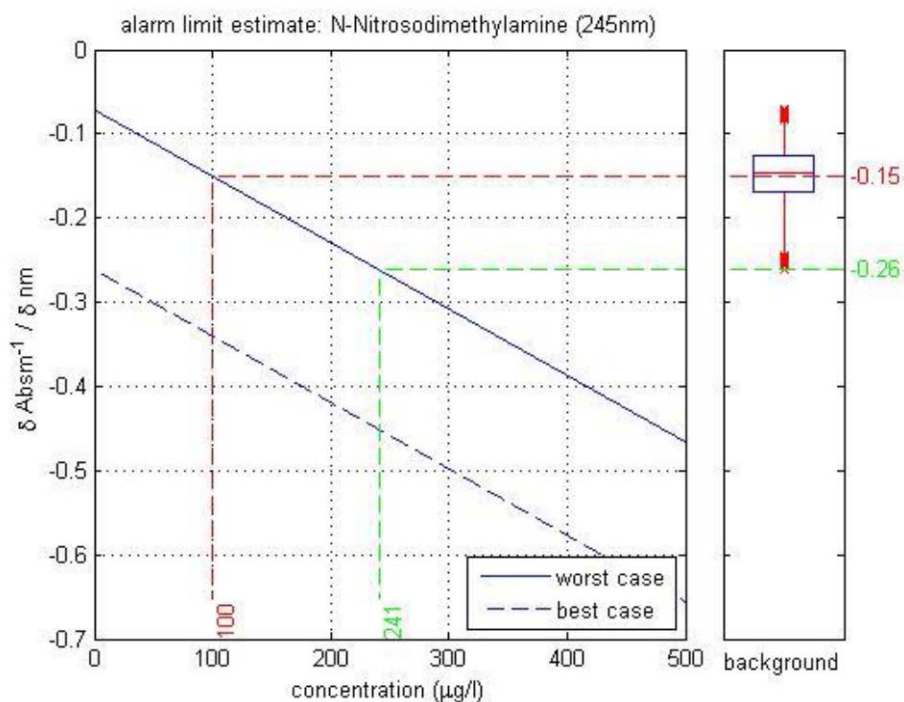
Figure 84. Detection limits for NDMA at 245 nm.

SIMAZINE

Simazine is an herbicide belonging to the triazine class of pesticides. The compound broadly is used to control weeds. In two recent studies conducted at Beenyup AWRP, simazine resulted below detection in RO permeate (Tang *et al.*, 2014; Busetti *et al.*, 2015). However this compound occasionally passes through RO/UV treatment in the low ng/L range. Simazine has been found to display a maximum absorption peak at 223.9 nm and 264.8 nm when an EtOH/H_2O (1% v/v) solution containing 4.9 mg·L^{-1} was tested using a path length of 10 mm (Spinelli *et al.*, 2007). Using the absorbance measurements of 0.894 and 0.085, which correspond respectively to the wavelengths 223.9 nm and 264.8 nm, the extinction coefficients may be calculated using the Beer-Lambert Law.

Molecular Formula: $C_7H_{12}ClN_5$
Molecular Weight: 201.6 g·mol^{-1}
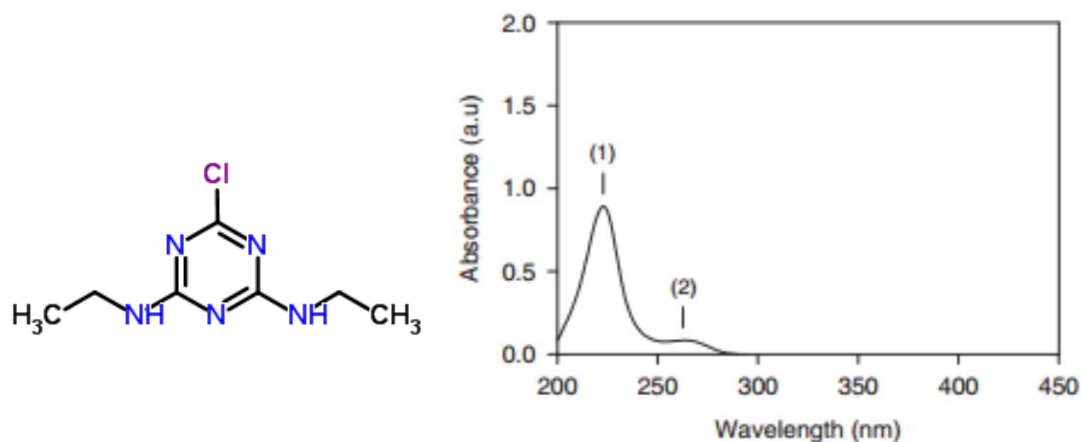
Figure 85. UV adsorption spectra of Simazine.
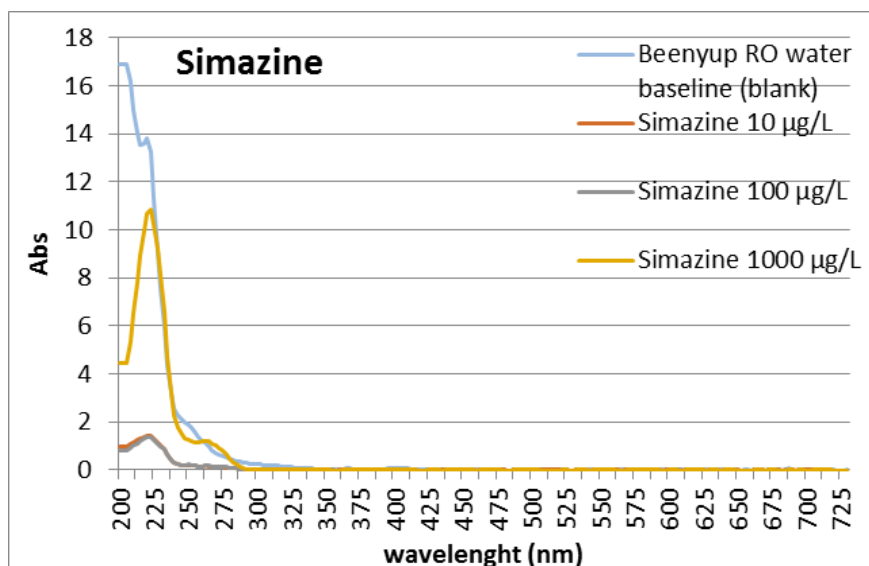
Figure 86. UV/Vis spectra recorded with S::CAN in RO water (blank) and for simazine at 10 - 1000 µg·L^{-1} in DI water.

The target alarm wavelengths were identified by DCM to be 235 and 275 nm. The variation of Beenyup RO permeate water UV/Vis derivative spectra at 235 and 275 nm were also determined. The following figure was produced to estimate the detection limits of NDMA in Beenyup RO permeate at 235 nm. In the worst case scenario, Simazine cannot be detected in RO permeate as the green line never crosses the "worst case" continuous line (Figure 87). The red dash line represents the DWG of Simazine (20 µg·L^{-1}).
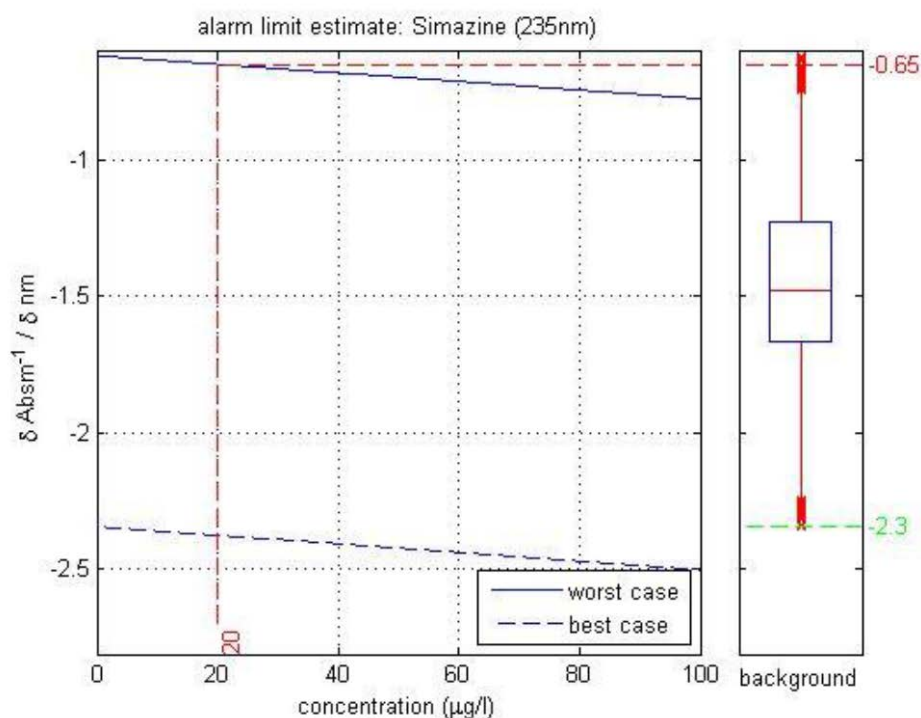
Figure 87. Detection limits for simazine at 235 nm.

Similarly, at the other wavelength tested (275 nm) by DCM, simazine can be detected in RO permeate as the green line never crosses the "worst case" continuous line (Figure 88). The red dash line represents the DWG of Simazine (20 µg·L^{-1}).
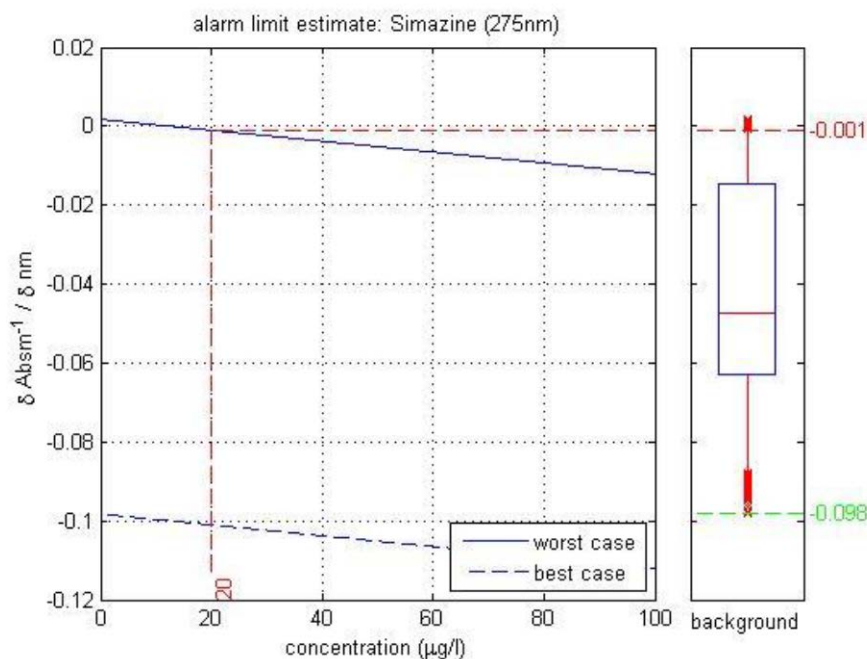
Figure 88. Detection limits for simazine at 275 nm.

TRIFLURALIN

Trifluralin is among one of the most widely used herbicide. In two recent studies conducted at Beenyup AWRP, trifluralin resulted below detection in RO permeate (Tang *et al.*, 2014; Busetti *et al.*, 2015). Trifluralin, undergoes direct aqueous photolysis. With a half-life of approximately 0.4 days (Durkin, 2011) the degradation of trifluralin by light is reasonably fast. In 2005 a study by Sarmiento Tagle *et al.* (2005) investigated the UV/Vis absorbency of Trifluralin and its photolytic degradation products in deionized water and acetonitrile.

The results showed multiple absorption peaks with the most intense peak having a maximum absorbance wavelength of 231 nm and an extinction coefficient of approximately $0.98 \times 10^{-4} \cdot M^{-1} \cdot cm^{-1}$.

Molecular Formula: $C_{13}H_{16}F_3N_3O_4$
Molecular Weight: $335.3 \ g \cdot mol^{-1}$
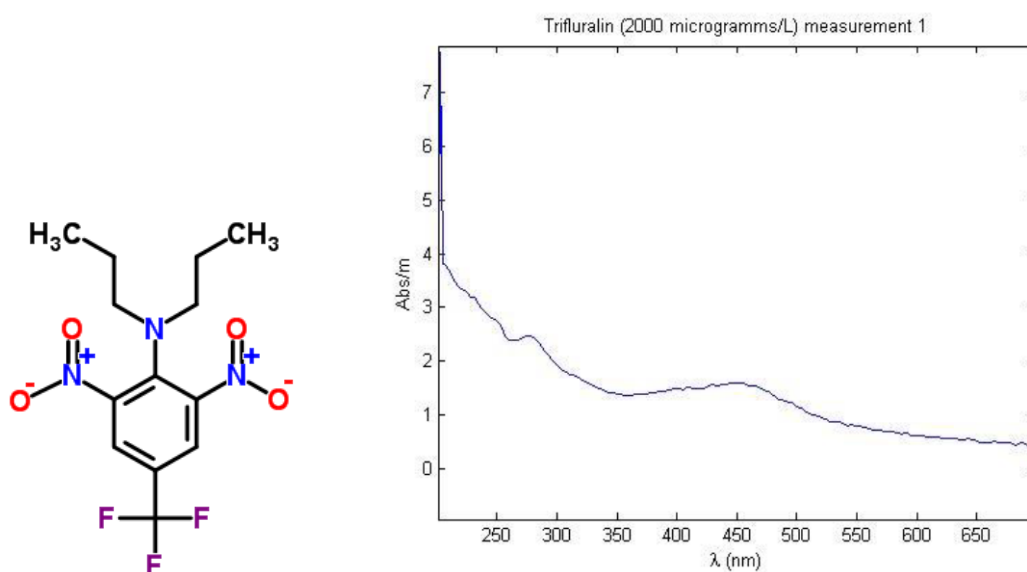
*Figure 89. UV adsorption spectra of trifluralin.*
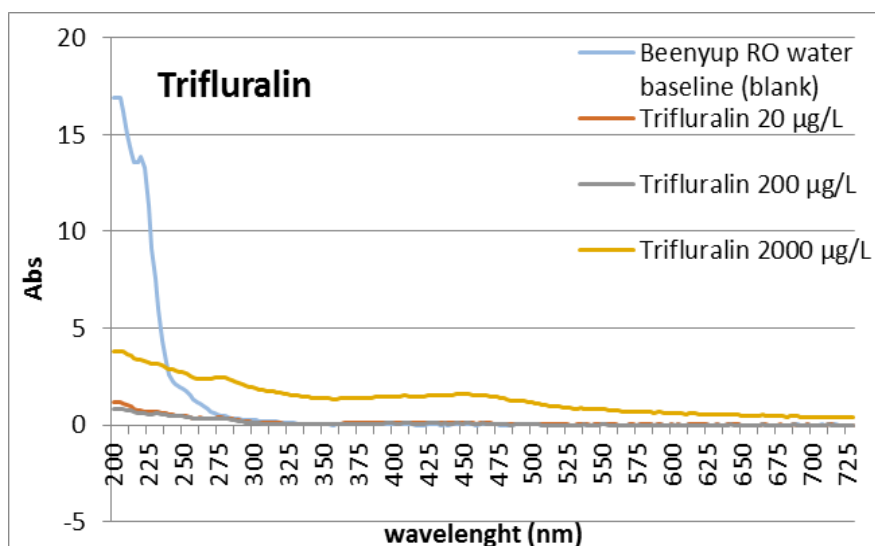
Figure 90. UV/Vis spectra recorded with S::CAN in RO water (blank) and for trifluralin at 20 - 2000 µg·L⁻¹ in DI water.

The target alarm wavelengths were identified by DCM to be 240, 300 and 275 nm. The variation of Beenyup RO permeate water UV/Vis derivative spectra at 240, 300 and 275 nm were also determined. The following figure was produced to estimate the detection limits of NDMA in Beenyup RO permeate at 240 nm.

In the worst case scenario, trifluralin can be detected at 240 nm in RO permeate at 2690 µg·L⁻¹ which is more than 50 times the DWG. The red dash line represents the DWG of trifluralin (50 µg·L⁻¹).
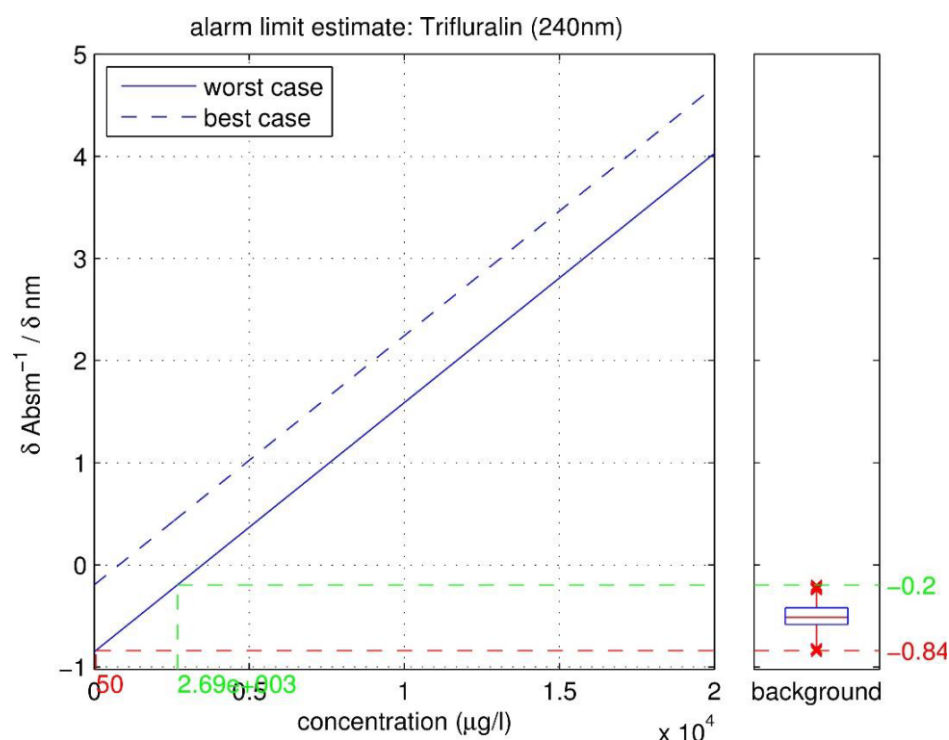
Figure 91. Detection limits for trifluralin at 240 nm.

Similarly, at the other wavelength tested (300 and 275 nm) by DCM, trifluralin can be detected in RO permeate only at concentration well above the DWG (Figure 92 and Figure 93).
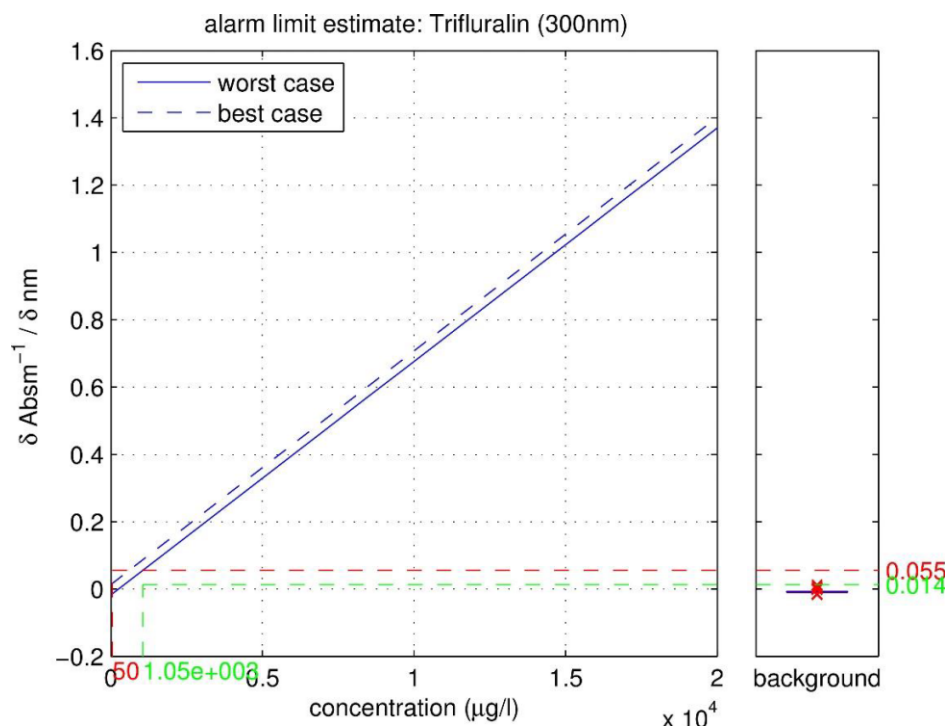
Figure 92. Detection limits for trifluralin at 300 nm.
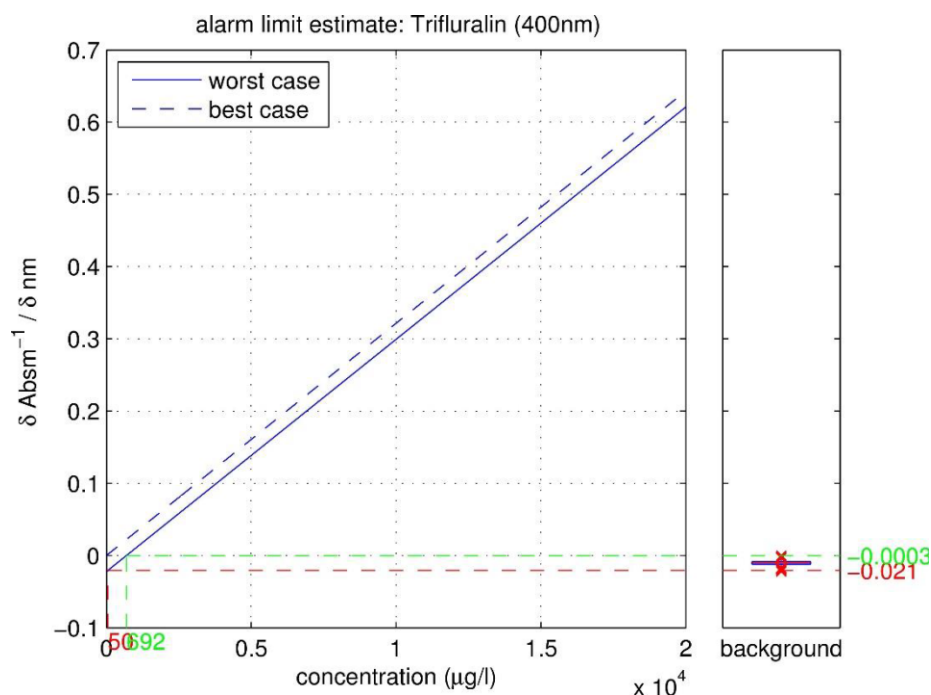
Figure 93. Detection limits for trifluralin at 400 nm.

For the remaining compounds, N-Nitrosomorpholine, estrone, ethinyl estradion, tolyltriazole, triethylphosphate and 4-cumylphenol DCM have not attempted to estimate the alarm limits as either 1) the compounds were not absorbing UV-Light (triethylphosphate); 2) the DWG was deemed to be too low compared to the estimated alarm limits based on the UV/Vis adsorption properties of the compound (4-culylphenol, tolyltriazole, diclofenac) or expected concentrations in post-RO water were too low compared to the estimated alarm limits based on the UV/Vis adsorption properties of the compound (N-Nitrosomorpholine, estrone, ethinyl estradiol). Table 37 summarizes the results from this experimental part.

Substance	DWG ($\mu g \cdot L^{-1}$)	Estimated Alarm, UV/Vis ($\mu g \cdot L^{-1}$)	Estimated detection limits UV/Vis	Suitability of S::CAN
Carbamazepine	100*	1000	77.2 $\mu g \cdot L^{-1}$ @ 305 nm	YES***
Diclofenac	1.8*	150	Not available	NO
E1	0.03*	750 750	Not available	NO
EE2	0.0015*	750	Not available	NO
Metformin	250*	50	7850 $\mu g \cdot L^{-1}$ @ 230 nm 278 $\mu g \cdot L^{-1}$ @ 250 nm	NO
Metolachlor	0.3* 300**	>2000	No detectable	NO
NDMA	0.01* 100**	50 3000	241 $\mu g \cdot L^{-1}$ @ 245nm	NO
NMOR	0.001* 5**	75 7000	Not available	NO
Simazine	0.02* 20**	30 250	No detectable	NO
Tolytriazole	0.007* 20**	…	Not available	NO
Triethylphosphate	n.a.* 1**	…	Not available	NO
Trifluralin	0.05* 50**	150 250 1000	2690 $\mu g \cdot L^{-1}$ @ 240 nm 1050 $\mu g \cdot L^{-1}$ @ 300 nm 692 $\mu g \cdot L^{-1}$ @ 400 nm	NO
4-cumylphenol	0.35* 0.35**	1000	Not available	NO

* Environment Protection and Heritage Council, National Health and Medical Research Council & Natural Resource Management Ministerial Council. (2008). Australian Guidelines for Water Recycling - Augmentation of Drinking Water Supplies. Canberra: Biotext Pty Ltd.

**Water Corporation Memorandum of Understanding with the Health Department of WA.

*** selectivity has not been verified by DCM and therefore the suitability of S::CAN to measure such compound against the interfering matrix cannot be confirmed.

The alarm limits listed in Table 37 indicate the concentration of a primary pollutant which could be detected against the fluctuating post-RO background causing to trigger a non-specific warning. However, a number of different organic chemicals with similar UV/Vis adsorption properties could also trigger this warning meaning any alarms would be non-specific. In the case where an alarm is triggered, further investigation would be required to identify the cause of the alarm including sampling the post–RO water for target/non-target analysis by high resolution mass spectrometry.

B.3.2. EEM Fluorescence

Fluorescence EEM is a synchronised fluorescence scan which can be used for the fingerprinting of water sources. Fluorescence EEM was chosen for characterisation of as it required little or no pre-treatment and is a non-destructive analytical method and it is generally more selective and sensitive when compared to UV/Vis spectrophotometry. Only preliminary tests were conducted where fluorescence excitation-emission spectra were recorded for metolachlor, trifluralin, simazine and carbamazepine present as a single compound and as in a mixture at DWG values in DI and RO water. The aims of this preliminary test were to assess whether or not these chemicals could be detected against the RO background as single compounds and in a mixture. Figure 95 to Figure 99 show the EEM spectra recorded. Pure Milli-Q water was used for background subtraction. Fluorescence excitation-emission matrix scans have two scattering lines not related to the sample, one from Raleigh scattering and the other from Raman Scattering (Hudson *et al.*, 2007). Raleigh scattering is caused by a small proportion of the incident light that is being reflected off the sides of the cuvette and it occurs when excitation and

emission are around the same (Hudson *et al.*, 2007). Raman scattering is caused by scattering of radiation when Raman active molecule such as water is hit by a large amount of radiation (Walrafen *et al.*, 1986). Both Raman scattering line (top left hand corner) and Raleigh scattering line (bottom right hand corner) can be seen clearly in Figure 94.

RO water has been through an intense molecular sieving which is expected to remove most large molecules such as fulvics/humics acids. The typical FLD signatures from these classes of compounds (Table 38) do not appear in RO treated water (Figure 94).

Table 38. List of known fluorophores and their sources, adapt from (Coble, 1996) and (Chen et al., 2003).

Excitation	Emission (nm)	Association
240 - 260	380 - 465	Humic like Terrestrial Inputs (soil Sediments)
300 - 370	400 - 500	Humic like
310 - 315	380 - 400	Marine Humic like
275	340	Tryptophan like Protein like
240 - 280	320 - 330	Amino Acid: Tyrosine, associated with microbial activity
200 - 240	280 - 330	Aromatic Protein-like I
200 - 240	330 - 380	Aromatic Protein-like II
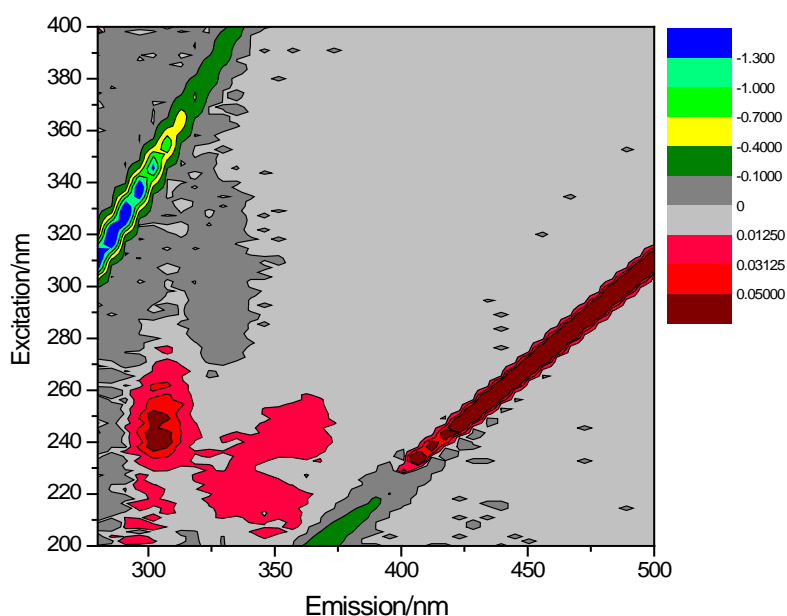
Figure 94. EEM spectra of RO water blank from Beenyup AWRP.
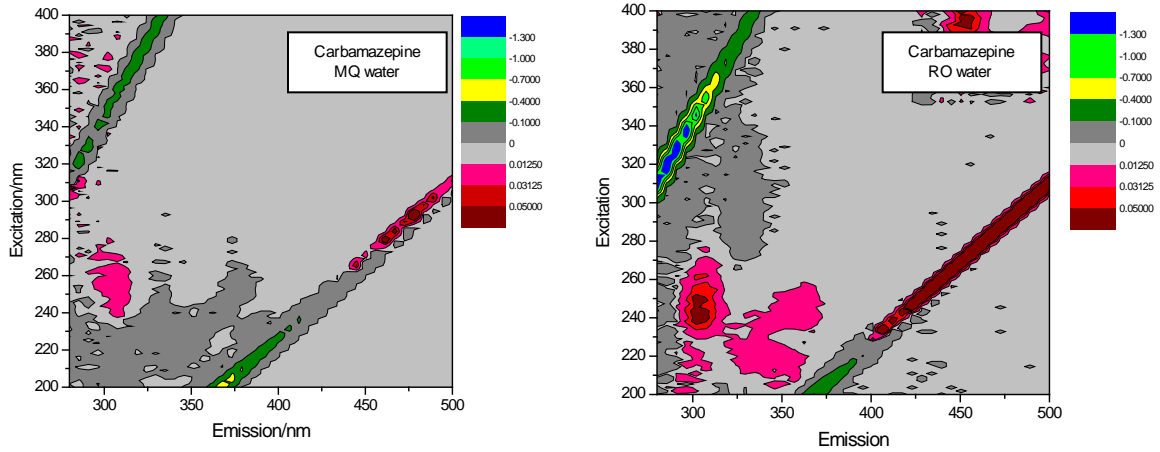
Figure 95. Carbamazepine in MQ water (1) and RO water (2) at DWG concentration.
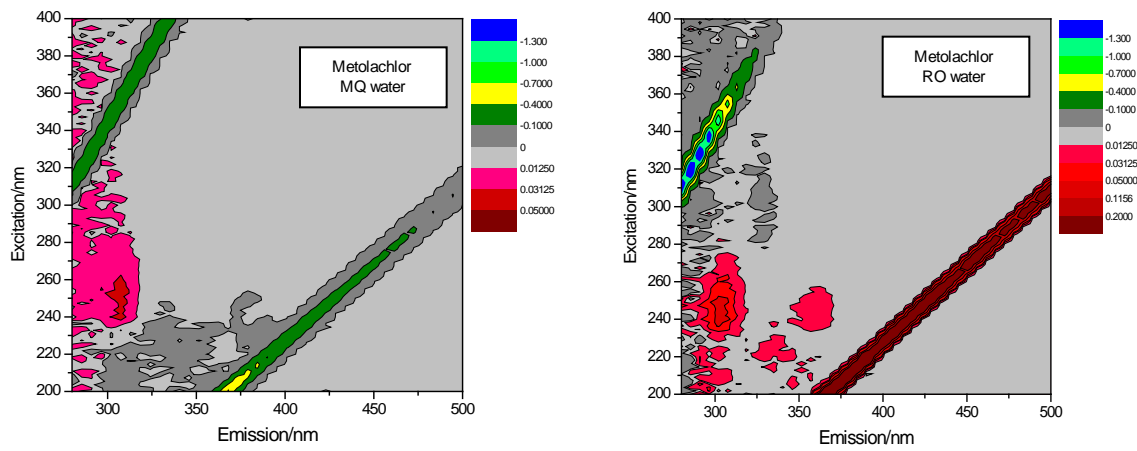
Figure 96. Metolachlor in MQ water (1) and RO water (2) at DWG concentration.
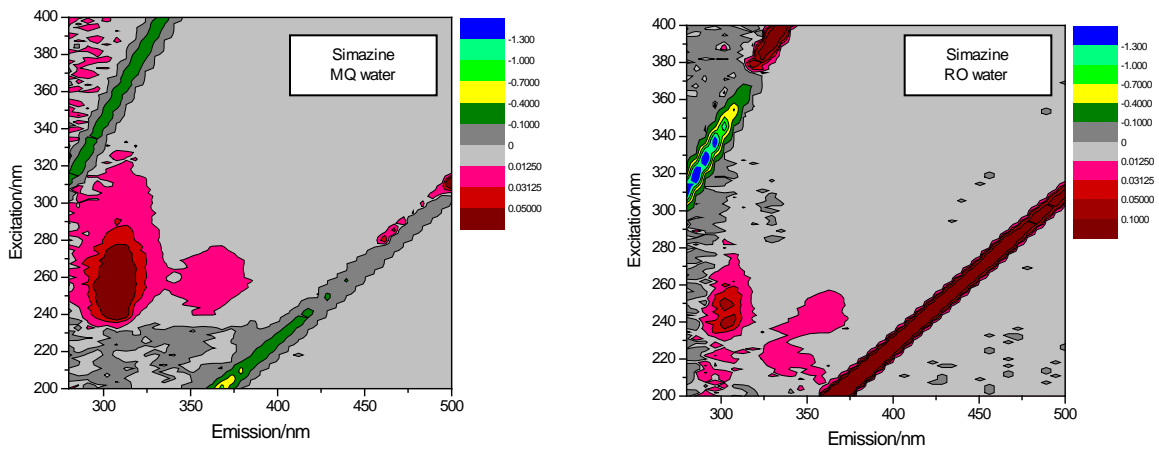
Figure 97. Simazine in MQ water (1) and RO water (2) at DWG concentration.
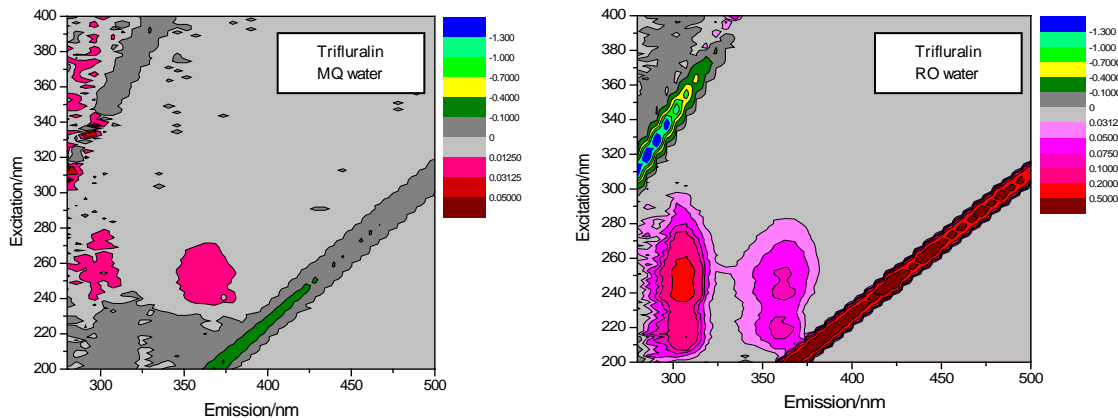
Figure 98. Trifluralin in MQ water (1) and RO water (2) at DWG concentration.
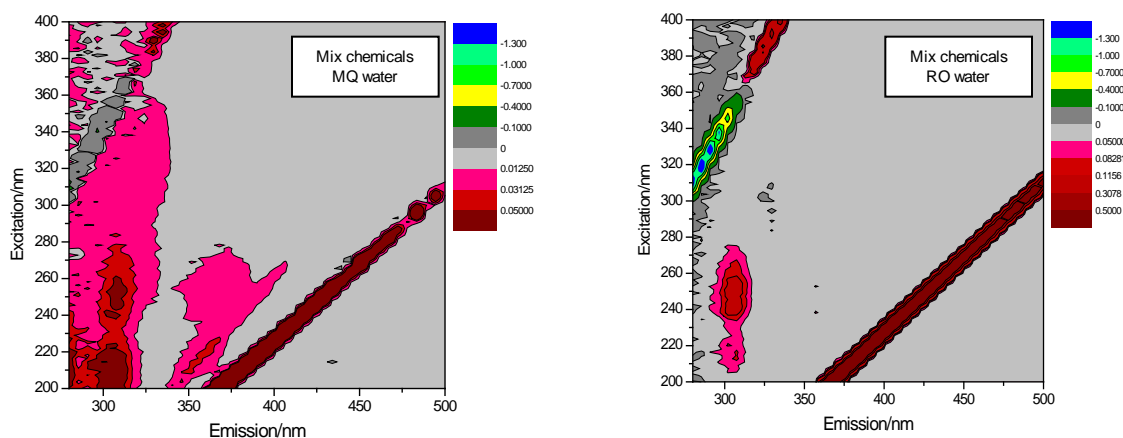
Figure 99. Mixture of carbamazepine, metolachlor, simazine, trifluralin in MQ water (1) and RO water (2) at DWG concentration.

When RO water is spiked for example with the test compound carbamazepine at DWG value, it is not possible to distinguish its EEM fluorescence from the RO background. This situation is very similar for the other compounds tested. When test chemicals are all mixed together at DWG value in RO water (Figure 94 –Figure 99) and compared to the RO background, the situation becomes even worst as most of EEM Fluorescence regions typical of RO water are overlapping with the EMM regions of the chemicals making not possible to distinguish them from the RO background. In analytical chemistry, this is typically achieved by adding an "extra dimension" to the analytical assay by for example adding a LC column to chromatographically separate the different species.

B.3.3. Correlation between TOC measured by S::CAN and Sievers TOC analyzer at Beenyup AWRP

The S::CAN spectrometer probe operates measuring UV/Vis absorbance from 200 to 720 nm. S::CAN spectrometers are a viable tool for online continuous monitoring of critical process parameters such as TSS, turbidity, ammonia, pH, Temp, NO_3-N, COD, BOD, TOC, DOC, UV_{254}, colour, BTX, O_3, H_2S, AOC.

In particular, TOC is a critical control parameter at Beeyup AWRP. This advanced treatment plant uses Beenyup WWTP secondary treated effluent as the source water to produced highly treated water for reinjection in a local aquifer. Currently at Beenyup AWRP TOC is monitored through a conventional TOC cabinet analyser (Sievers) which uses chemical oxidation followed by spectrophotometric detection for analysis of total organic carbon. In order to ease operations and reduce costs, WCWA was interested in assessing whether a spectroscopic technique such S::CAN could effectively replace a traditional TOC analyser to determine TOC concentrations in the feed and permeate water at Beenyup AWRP.

At Beenyup AWRP, the RO feedwater (and to a greater extent RO permeate) have been through extensive biological and physical (MF/RO) removal processes. Therefore residual concentration of solutes and particulate are expected to be very low.

Despite the extensive biological and physical removal processes, both locations exhibit significant UV/Vis absorption levels as recorded by the 35 mm path length S::CAN unit on the RO feedwater and the 100 mm path length S::CAN unit on the RO permeate. These units are often being over ranged (absorption outside the calibration range) rather than being limited by lack of absorbing compounds (absorption below the detection limit). This means high resolution measurement is achievable in both locations.

Figure 100 and Figure 101 show the comparison between the TOC monitored using the Sievers TOC analyser and S::CAN probe in the RO feed and RO permeate water over a period of six weeks (January – March 2013). Figure 102 and Figure 103 show additional comparison data collected in the same points on the Beenyup AWRP over a period of six additional weeks (March – May 2013).
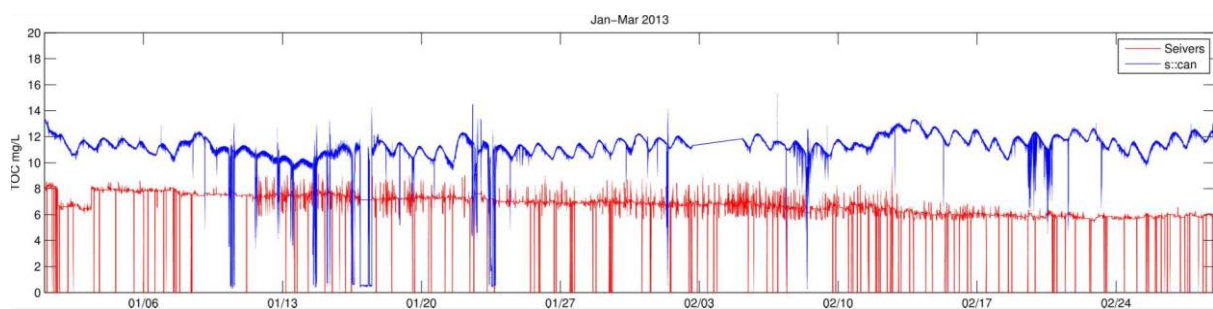
Figure 100. RO feed comparison plot over a six weeks (Jan-March 2013) TOC data. Red line: Sievers TOC analyser; blue line: S::CAN probe.
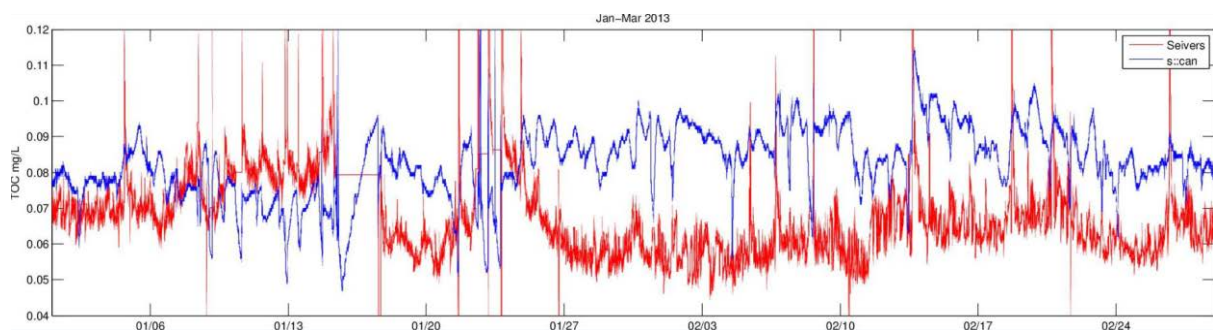
Figure 101. RO permeate TOC comparison plot for the corresponding six weeks period (Jan-March 2013). Red line: Sievers TOC analyser; blue line: S::CAN probe.
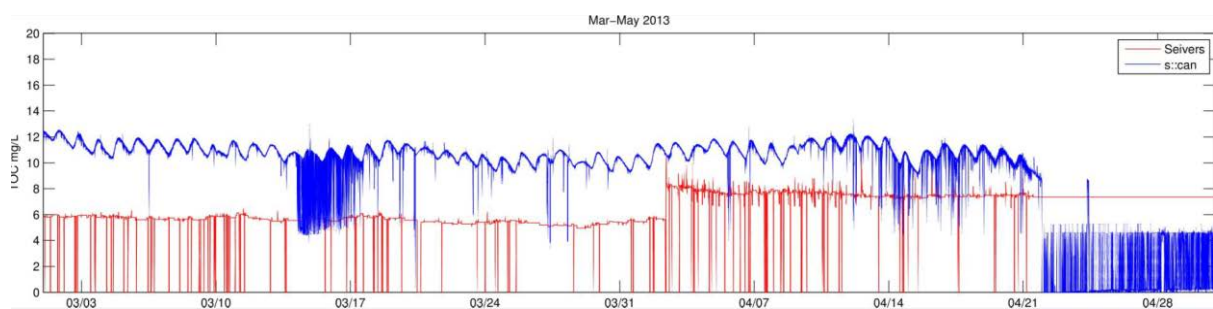
Figure 102. RO feed comparison plot over a six weeks (March-May 2013) TOC data. Red line: Sievers TOC analyser; blue line: S::CAN probe.
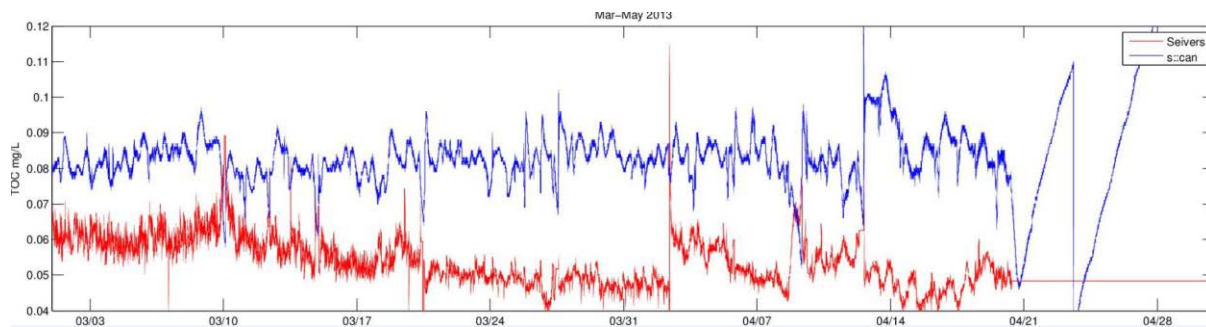
Figure 103. RO permeate TOC comparison plot for the corresponding six weeks period (March-May 2013). Red line: Sievers TOC analyser; blue line: S::CAN probe.

From an analysis of the TOC data in RO feed water, the Sievers TOC analyser is generally reading about 33 – 50% lower TOC compared to the S::CAN. Moreover, the S::CAN exhibits a diurnal TOC pattern in RO feedwater while this is less clear for Sievers TOC analyser. DCM has reported that at the RO feedwater location, the Sievers TOC may have encountered technical difficulty through much of the work. For example after a recalibration of the Sievers TOC which happened between 03/31 and 04/14 (Figure 104) the TOC measured by Sievers TOC jumps from an average of 6 to 8 mg·L^{-1}. The Sievers TOC analyser also shows a diurnal pattern more similar to the S::CAN after the recalibration attempt.
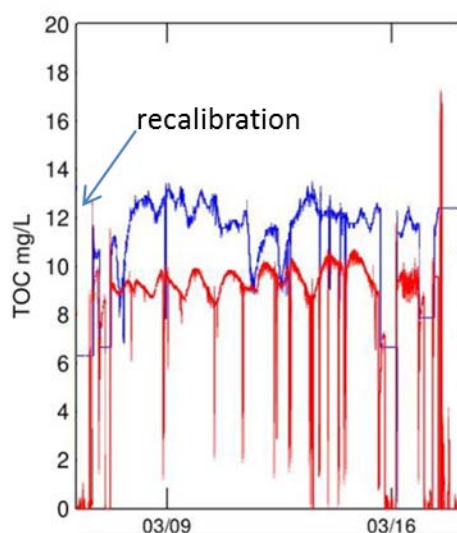
Figure 104. RO feed comparison plot over 1 weeks (March 2013) TOC data. Red line: Sievers TOC analyser; blue line: S::CAN probe. The Sievers TOC analyser shows a diurnal pattern more similar to the S::CAN after a recalibration attempt.

Due to the lack of corroborating evidence to indicate whether the varying offsets between the trends are a function of instrument, substrate or calibration issues, DCM concluded that a correlation between the Sievers TOC and the S::CAN UV/Vis TOCeq could not be determined. No attempt to validate either the Sievers or S::CAN TOC against the lab was attempted constituting a great limitation in the interpretation of the trends observed.

According to DCM, the only observation that can be made is that at times both instruments show a nearly identical diurnal numerical shift in TOC in both the feedwater and permeate locations. In the feedwater location the peaks and troughs are concurrent while in the permeate location the peaks and hollows are sometimes concurrent but most of the time the mirror image of each other. According to DCM, this indicates that the S::CAN system is "reacting" differently to a component of the wastewater and that an adjustment of the algorithm used to define the TOCeq to compensate for the particular compound groups is required. Such adjustment was never attempted due to the additional costs required by DCM to refine the algorithm. In general the S::CAN indicates the TOCeq value and diurnal concentration shift are consistent over long periods of time.

The effective TOCeq rejection is of interest and this can be determined by comparing the S::CAN TOCeq feedwater and permeate values which use exactly the same mathematical algorithm to derive the TOCeq from their respective raw spectra. The S::CAN indicates a TOCeq rejection of approximately 99.3%

based on a feedwater TOCeq of approximately 12 mg·L^{-1} and a permeate TOCeq of approximately 0.08 mg·L^{-1}. The Siever TOC analyser indicates a TOC rejection of approximately 99.2% based on a feedwater TOC of approximately 8 mg/L and a permeate TOC of approximately 0.06 mg·L^{-1}. It is expected that TOC rejection varies through the diurnal cycle with different components of TOC in the feed RO having different rejection rates.

B.3.4. Challenge tests for R-WT removal at Beenyup AWRP

Challenge tests were conducted on the 20th of August 2014 at Beenyup AWRP by spiking the rhodamine WT (R-WT) in the RO feed water while the plant was on by-pass.

Spiked concentration in the feed stage 1 was 1000 µg·L^{-1}. Table 39 summarizes the theoretical concentrations of R-WT in permeate stages 1 and 2 as well as in the combined permeate to achieve a 3 LRV and a 4 LRV of R-WT.

Table 39. Theoretical R-WT concentrations along the RO plant to achieve 3 LRV and 4 LRV.

Sample Location	4 LRV (µg·L^{-1})	3 LRV (µg·L^{-1})
Feed Stage 1	1000	1000
Permeate Stage 1	0.10	1.0
Feed Stage 2	~2000	~2000
Permeate Stage 2	0.20	2
Combined Permeate	0.10	1.0
Concentrate Stage 2	~4000	~4000

Calibration curves of R-WT in the concentration range 0.1 to 1000 µg·L^{-1} were acquired in RO water and DI water using S::CAN. Moreover calibrations curves were acquired in the concentration range 1000 to 4000 µg·L^{-1} in RO feed. R-WT data acquired by S::CAN data was not commissioned to DCM for processing. Therefore R-WT removal was preliminary calculated by comparing samples with calibration curves. For this, UV absorbance was initially assessed at λ = 557.5 nm. This wavelength was chosen as 1) R-WT shows an adsorption maxima and 2) the background absorption of MF/RO water in this region is very low.

As shown in Figure 107, the calibrations curve for R-WT in the concentration range 1 - 1000 µg·L^{-1} is linear with a R^2 of 0.9999. At higher concentrations (e.g. 2000 and 4000 µg·L^{-1}) the calibration curve reach a plateau meaning the relationship between Abs/m and concentration is no longer linear (data not shown). Therefore, measurements of R-WT at high concentrations (e.g. Feed Stage 2 and Concentrate Stage 2) at λ = 557.5 nm would require at least 1:2 v/v and 1:4 v/v dilution followed by re-measurement which it is not possible during an online measurement with S::CAN. Alternatively, different wavelengths showing lower sensitivity were tentatively chosen for these high concentration samples. For example at λ = 460 nm, the calibration curve for R-WT in the concentration range 1000 - 4000 µg·L^{-1} is linear with R^2 = 0.995 but the reading at low concentrations (e.g. Permeate Stage 2 and Combined Permeate) are likely to be quite inaccurate due to the decreased sensitivity of the measurement at this wavelength.

Figure 105 summarizes all the measurements taken during the R-WT challenge test, while Figure 106 focuses only on the few measurements directly relevant to the challenge test all the measurements taken during the R-WT challenge test.
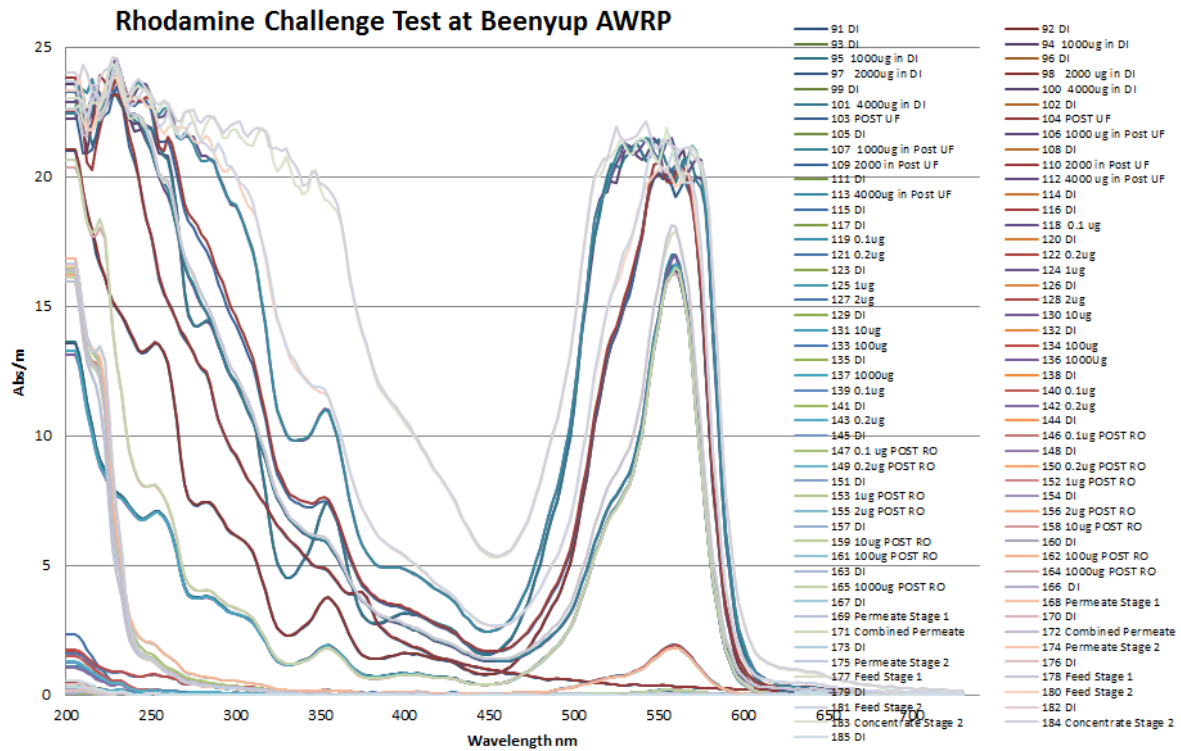
Figure 105. Summary of all measurements taken with S::CAN for the R-WT challenge test.
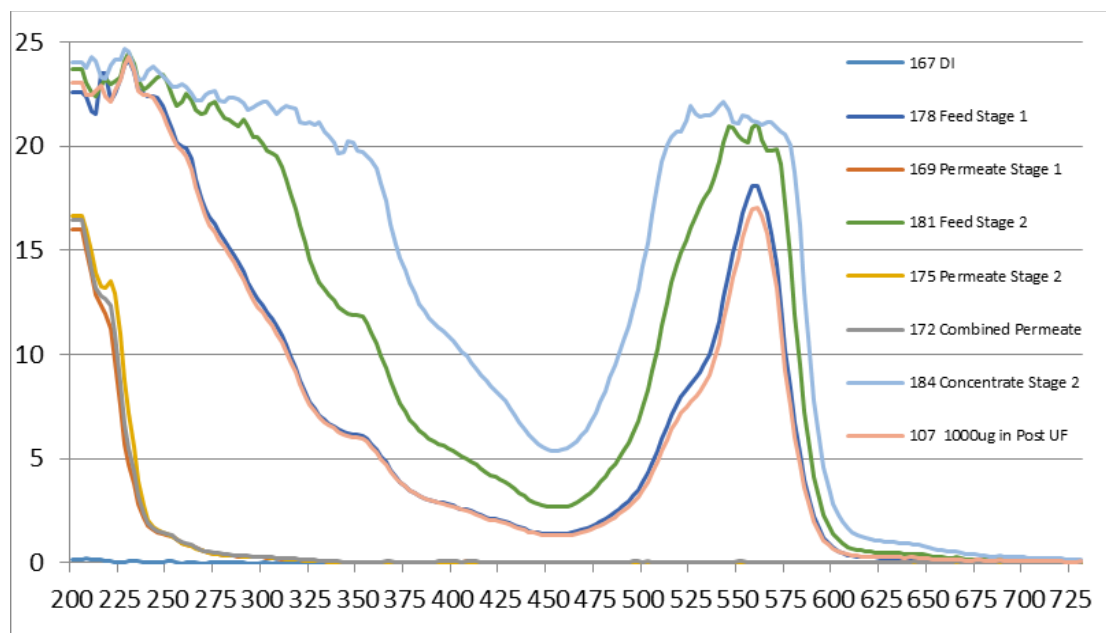
Figure 106. UV/Vis scan at λ = 200 - 725 nm in RO feed stage 1 and 2, RO permeate stage 1 and 2, combined permeate, concentrate stage 2. DI water is also reported as a blank. A 1000 µg·L^{-1} post-UF spike is also reported for comparison.
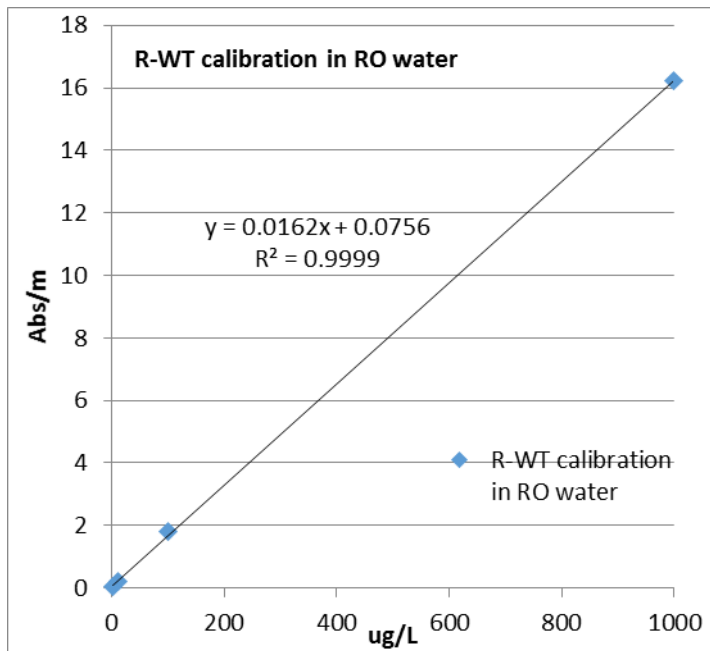
Figure 107. Calibration (1 - 1000 µg·L^{-1}) of R-WT in RO water (λ = 557.5 nm).
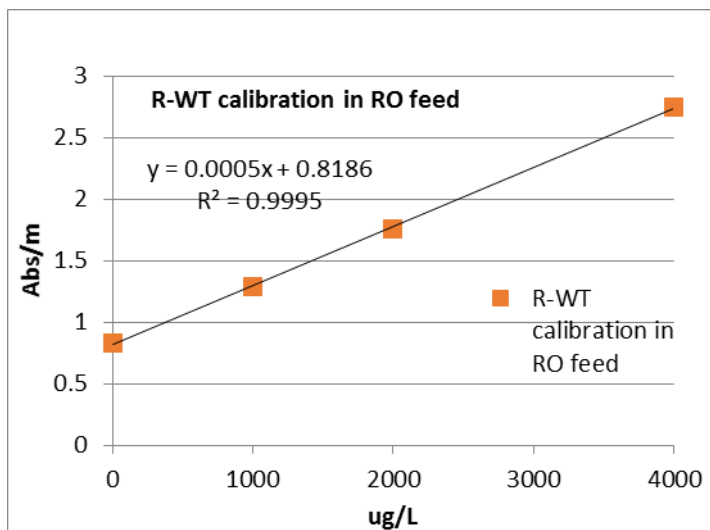
Figure 108. Calibration (1000 - 4000 µg·L^{-1}) of R-WT in RO water (λ = 460 nm) in RO feed water.

Following calibrations, the rejection of R-WT was found to be the following:
Feed stage 1: concentration found = 1125 µg·L^{-1}
Permeate stage 1: concentration found = 1.67 µg·L^{-1}
Removal= (1100 - 1.67)/1100 * 100 = 99.85%

The theoretical rejection needed to demonstrate 3 LRV with a feed stage 1 concentration of 1000 µg·L^{-1} and a permeate stage 1 concentration of 1.0 µg·L^{-1} is given by Equation *(17*.

$$3\ LRV = \frac{(1000-1.0)}{1000} \times 100 = 99.90\%$$ (17)

The removal of R-WT calculated using S::CAN is just below the required value of 99.90%. Therefore S::CAN seems to be suited to demonstrate 3 LRV of R-WT. However, S::CAN seems not to have the adequate sensitivity to read concentrations of R-WT at 0.1 - 0.2 µg·L^{-1} or below to demonstrate 4 LRV. For this, a fluorescence probe is likely to be more suited as characterised by better selectivity and sensitivity.

B.4. Conclusions

- The alarm limits established for a range of test compounds using S::CAN either a) exceed drinking water guidelines or 2) could not be determined. The only exception is for the compound carbamazepine with an estimated alarm limit of 77 μg·L^{-1} in post-RO water.
- The alarm limits of S::CAN indicate the concentration of a primary pollutant which could be detected against the fluctuating post-RO background causing to trigger a non-specific warning. A number of different organic chemicals with similar UV/Vis adsorption properties could also trigger this warning meaning any alarms would be non-specific.
- In the case where an alarm is triggered, further investigation would be required to identify the cause of the alarm including sampling the post–RO water for target/non-target analysis by high resolution mass spectrometry.
- Preliminary EEM matrix tests indicate that the RO background EEM Fluorescence regions typical of RO water are overlapping with the EMM regions of the tested chemicals making not possible to distinguish them from the RO background itself.
- A correlation between the Sievers TOC and the S::CAN UV/Vis TOCeq could not be determined by DCM due to the lack of corroborating evidence to indicate whether the varying offsets between the trends are a function of instrument, substrate or calibration issues.
- The S::CAN system is "reacting" differently to a component of the wastewater compared to the Siever TOC analyser and an adjustment of the algorithm used to define the TOCeq could compensate for the discrepancy observed.
- S::CAN seems to be able to demonstrate 3 LRV of R-WT. The removal of R-WT calculated using S::CAN is just below the required value of 99.90%.
- S::CAN seems not to have the adequate sensitivity to read concentrations of R-WT at 0.1 - 0.2 μg·L^{-1} or below to demonstrate 4-log removal. For this, a fluorescence probe is likely to be more suited as characterised by better selectivity and sensitivity.

References

Adham S, Gagliardo P, Smith D, Ross D, Gramith K, Trussell R. 1998a. Monitoring the integrity of reverse osmosis membranes. Desalination 119:143-150.

Adham S, Trussell S, Gagliardo P, Trussell R. 1998b. Rejection of MS-2 virus by RO membranes. Journal AWWA 90:130-135.

Adham SS, Gagliardo P, Smith D, Ross D, Gramith K, Trussell R. 1998c. Monitoring the integrity of reverse osmosis membranes. Desalination 119:143-150.

Adham SS, Jacangelo JG. 1994. Assessing the reliability of low pressure membrane systems for microbial removal. In: Proceedings of National Conference on Environmental Engineering on Critical Issues inWater andWastewater Treatment, American Society of Civil Engineers, NewYork, pp. 313–319. ed. Boulder, CO, USA: Publ by ASCE. p 313-319.

Adham SS, Trussell RS, Gagliardo PF, Trussell RR. 1998d. Rejection of MS-2 virus by RO membranes. Journal of Americal Water Works Association 90:130-135.

Amjad Z. 1993. Reverse osmosis: membrane technology, water chemistry & industrial applications. New York: Van Nostrand Reinhold.

Antony A, Blackbeard J, Angles M, Leslie G. 2014. Non-microbial indicators for monitoring virus removal by ultrafiltration membranes. Journal of Membrane Science 454:193-199.

Antony A, Blackbeard J, Leslie G. 2012. Removal Efficiency and Integrity Monitoring Techniques for Virus Removal by Membrane Processes. Critical Reviews in Environmental Science and Technology 42:891-933.

Antony A, Fudianto R, Cox S, Leslie G. 2010. Assessing the oxidative degradation of polyamide reverse osmosis membrane—Accelerated ageing with hypochlorite exposure. Journal of Membrane Science 347:159-164.

Antony A, Leslie G. 2011. Chapter 22: Degradation of polymeric membranes in water and wastewater treatment. In: Nunes ABaSP, editor. Advanced Membrane Science and Technology for Sustainable Energy and Environmental Applications. Cambridge, UK: Woodhead Publishing Limited. p 718-745.

Arkhangelsky E, Kuzmenko D, Gitis V. 2007. Impact of chemical cleaning on properties and functioning of polyethersulfone membranes. Journal of Membrane Science 305:176-184.

ASTM. 2010. D6908-06 Standard practice for integrity testing water filtration membrane systems. In: Book of Standards Volume: 11.02. West Conshohocken, PA: ASTM International.

Baghoth SA, Sharma SK, Amy GL. 2011. Tracking natural organic matter (NOM) in a drinking water treatment plant using fluorescence excitation-emission matrices and PARAFAC. Water Research 45:797-809.

Bard AJ, Faulkner LR. 2001. Electrochemical methods : fundamentals and applications, 2nd ed. New York: Wiley.

Bargeman G, Vollenbroek JM, Straatsma J, Schroën CGPH, Boom RM. 2005. Nanofiltration of multi-component feeds. Interactions between neutral and charged components and their effect on retention. Journal of Membrane Science 247:11-20.

Bartels C, Franks R, Rybar S, Schierach M, Wilf M. 2005. The effect of feed ionic strength on salt passage through reverse osmosis membranes. Desalination 184:185-195.

Behrens H, Beims U, Dieter H, Dietze G, Eikmann T, Grummt T, Hanisch H, Henseling H, Käß W, Kerndorff H, Leibundgut C, Müller-Wegener U, Rönnefahrt I, Scharenberg B, Schleyer R, Schloz W, Tilkes F. 2001. Toxicological and ecotoxicological assessment of water tracers. Hydrogeology Journal 9:321-325.

Ben Amar N, Saidani H, Deratani A, Palmeri J. 2007. Effect of Temperature on the Transport of Water and Neutral Solutes across Nanofiltration Membranes. Langmuir 23:2937-2952.

Berg P, Hagmeyer G, Gimbel R. 1997. Removal of pesticides and other micropollutants by nanofiltration. Desalination 113:205-208.

Braghetta A. 1995. The influence of solution chemistry and operating conditions on nanofiltration of charged and uncharged organic macromolecules. Chapel Hill: University of North Carolina.

Busetti F, Linge KL, Heitz A. 2009. Analysis of pharmaceuticals in indirect potable reuse systems using solid-phase extraction and liquid chromatography-tandem mass spectrometry. J Chromatogr, A 1216:5807-5818.

Busetti F, Ruff M, Linge KL. 2015. Target screening of chemicals of concern in recycled water. Environmental Science: Water Research & Technology.

Chang S, Waite TD, Schäfer AI, Fane AG. 2003. Adsorption of the Endocrine-Active Compound Estrone on Microfiltration Hollow Fiber Membranes. Environmental Science & Technology 37:3158-3163.

Chellam S, Taylor JS. 2001. Simplified Analysis of Contaminant Rejection During Ground- and Surface Water Nanofiltration Under the Information Collection Rule. Water Research 35:2460-2474.

Chen W, Westerhoff P, Leenheer JA, Booksh K. 2003. Fluorescence excitation-emission matrix regional integration to quantify spectra for dissolved organic matter. Environmental Science and Technology 37:5701-5710.

Clesceri LS, Greenberg AE, Eaton AD. 1998. Standard Methods for Examination of Water & Wastewater, 20th Edition: American Public Health Association.

Coble PG. 1996. Characterization of marine and terrestrial DOM in seawater using excitation-emission matrix spectroscopy. Marine Chemistry 51:325-346.

Cory RM, Miller MP, McKnight DM, Guerard JJ, Miller PL. 2010. Effect of instrument-specific response on the analysis of fulvic acid fluorescence spectra. Limnology and Oceanography: Methods 8:67-78.

Cran MJ, Bigger SW, Gray SR. 2011. Degradation of polyamide reverse osmosis membranes in the presence of chloramine. Desalination 283:58-63.

Cuartero M, García MS, Ortuño JA. 2013. Differential dynamic potentiometric responses obtained with anion-selective electrodes for perchlorate, thiocyanate, iodide, nitrate, sulfate, picrate and bis(trifluoromethylsulfonyl) imide. Electrochim Acta 93:272-278.

Davidson MG, Deen WD. 1988. Hydrodynamic theory for the hindered transport of flexible macromolecules in porous membranes. Journal of Membrane Science 35:167-192.

Dewettinck T, Van Houtte E, Geenens D, Van Hege K, Verstraete W. 2001. HACCP (Hazard Analysis and Critical Control Points) to guarantee safe water reuse and drinking water production - A case study. Water Science & Technology 43:31-38.

Dimou AD, Sakkas VA, Albanis TA. 2005. Metolachlor photodegradation study in aqueous media under natural and simulated solar irradiation. Journal of Agricultural and Food Chemistry 53:694-701.

Do VT, Tang CY, Reinhard M, Leckie JO. 2012a. Effects of hypochlorous acid exposure on the rejection of salt, polyethylene glycols, boron and arsenic(V) by nanofiltration and reverse osmosis membranes. Water Res 46:5217-5223.

Do VT, Tang CY, Reinhard M, Leckie JO. 2012b. Effects of hypochlorous acid exposure on the rejection of salt, polyethylene glycols, boron and arsenic(V) by nanofiltration and reverse osmosis membranes. Water Research 46:5217-5223.

Doederer K. 2014. Disinfection by-products in high quality recycled water production with high pressure membranes. In: School of chemical engineering: The University of Queensland. p 209.

Doederer K, Farré MJ, Pidou M, Weinberg HS, Gernjak W. 2014. Rejection of disinfection by-products by RO and NF membranes: Influence of solute properties and operational parameters. Journal of Membrane Science 467:195-205.

Donose BC, Sukumar S, Pidou M, Poussade Y, Keller J, Gernjak W. 2013a. Effect of pH on the ageing of reverse osmosis membranes upon exposure to hypochlorite. Desalination 309:97-105.

Donose BC, Sukumar S, Pidou M, Poussade Y, Keller J, Gernjak W. 2013b. Effect of pH on the ageing of reverse osmosis membranes upon exposure to hypochlorite. Desalination 309:97-105.

Drewes JE, Sedlak D, Snyder S, Dickenson E. 2008. Development of Indicators and Surrogates for Chemical Contaminant Removal during Wastewater Treatment and Reclamation. In: WRF03-014, editor. Alexandria: WateReuse Foundation.

Durkin PR. 2011. Trifluralin - human health and ecological risk assessment. In: USDA Forest Service.

Elimelech M, Chen WH, Waypa JJ. 1994. Measuring the zeta (electrokinetic) potential of reverse osmosis membranes by a streaming potential analyzer. Desalination 95:269-286.

Elmes RBP, Yuen KKY, Jolliffe KA. 2014. Sulfate-Selective Recognition by Using Neutral Dipeptide Anion Receptors in Aqueous Solution. Chem-Eur J 20:7373-7380.

Ettori A, Gaudichet-Maurin E, Schrotter J-C, Aimar P, Causserand C. 2011. Permeability and chemical analysis of aromatic polyamide based membranes exposed to sodium hypochlorite. Journal of Membrane Science 375:220-230.

Farré MJ, Keller J, Gernjak W, Weinberg HS, Lyon B, Poussade Y. 2010. Fate of disinfection by-products & their precursors across reverse osmosis membranes when producing high quality recycled water. In: Water Quality Technology Conference and Exposition 2010. p 757-765.

Filmtec. 1998. Product information: Factors affecting RO membrane performance. In: DOW, editor. www.dow.com.

Freger V, Gilron J, Belfer S. 2002. TFC polyamide membranes modified by grafting of hydrophilic polymers: an FT-IR/AFM/TEM study. Journal of Membrane Science 209:283-292.

Frenkel VS, Cohen Y, Rahardianto A, Suruwanvijit S, Thompson J, Cummings G. 2014. WRRF09-06b: New Techniques for Real-Time Monitoring of Membrane Integrity for Virus Removal: Pulsed-Marker Membrane Integrity Monitoring System. In: WRRF, editor. Research report. Alexandria, VA.

Fujioka T, Khan SJ, Poussade Y, Drewes JE, Nghiem LD. 2012a. N-nitrosamine removal by reverse osmosis for indirect potable water reuse – A critical review based on observations from laboratory-, pilot- and full-scale studies. Separation and Purification Technology 98:503-515.

Fujioka T, Nghiem LD, Khan SJ, McDonald JA, Poussade Y, Drewes JE. 2012b. Effects of feed solution characteristics on the rejection of N-nitrosamines by reverse osmosis membranes. Journal of Membrane Science 409–410:66-74.

Furiga A, Pierre G, Glories M, Aimar P, Roques C, Causserand C, Berge M. 2011. Effects of ionic strength on bacteriophage MS2 behavior and their implications for the assessment of virus retention by ultrafiltration membranes. Applied and Environmental Microbiology 77:229-236.

Gerba CP. 1984. Applied and Theoretical Aspects of Virus Adsorption to Surfaces. In: Allen IL, editor. Advances in Applied Microbiology: Academic Press. p 133-168.

Golmohammadi R, Valegård K, Fridborg K, Liljas L. 1993. The Refined Structure of Bacteriophage MS2 at 2·8 Å Resolution. Journal of Molecular Biology 234:620-639.

Grygolowicz-Pawlak E, Sohail M, Pawlak M, Neel B, Shvarev A, de Marco R, Bakker E. 2012. Coulometric Sodium Chloride Removal System with Nafion Membrane for Seawater Sample Treatment. Anal Chem 84:6158-6165.

Guo H, Wyart Y, Perot J, Nauleau F, Moulin P. 2010. Low-pressure membrane integrity tests for drinking water treatment: A review. Water Research 44:41-57.

Hambly AC, Henderson RK, Storey MV, Baker A, Stuetz RM, Khan SJ. 2010. Fluorescence monitoring at a recycled water treatment plant and associated dual distribution system - Implications for cross-connection detection. Water Research 44:5323-5333.

Her N, Amy G, Chung J, Yoon J, Yoon Y. 2008. Characterizing dissolved organic matter and evaluating associated nanofiltration membrane fouling. Chemosphere 70:495-502.

Herath G, Yamamoto K, Urase T. 1999. Removal of viruses by microfiltration membranes at different solution environments. Water Science and Technology 40:331-338.

Hoang T, Stevens G, Kentish S. 2010. The effect of feed pH on the performance of a reverse osmosis membrane. Desalination 261:99-103.

Hu D, Wang H, Gao K, Jiang X, Wang M, Long Y, Chen Y. 2014. Anion transfer across "anion channels" at the liquid/liquid interface modified by anion-exchange membrane. Rsc Adv 4:57035-57040.

Hu JY, Jin X, Ong SL. 2007. Rejection of estrone by nanofiltration: Influence of solution chemistry. Journal of Membrane Science 302:188-196.

Hu JY, Ong SL, Song LF, Feng YY, Liu WT, Tan TW, Lee LY, Ng WJ. 2003. Removal of MS2 bacteriophage using membrane technologies. Water Science and Technology 47:163-168.

Huang H, Young TA, Schwab KJ, Jacangelo JG. 2012. Mechanisms of virus removal from secondary wastewater effluent by low pressure membrane filtration. Journal of Membrane Science 409–410:1-8.

Hudson N, Baker A, Reynolds D. 2007. Fluorescence analysis of dissolved organic matter in natural, waste and polluted waters - A review. River Research and Applications 23:631-649.

Hydranautics. 2001. What is membrane performance normalization? Technical Service Bulletin January.

IAWPRC. 1991. Bacteriophages as model viruses in water quality controlag. Water Research 25:529-545.

Irwin R, van Herk, M., Smith, D. September 2014. Validation of UF Membrane Plants for Water Recycling in Victoria. Journal of the Australian Water Association 41:66-72.

ISO. 1995a. Water quality—detection and enumeration of bacteriophages—part 1: enumeration of F-specific RNA bacteriophages. In: EN ISO 10705-1. International Organization of Standardization, Geneva, Switzerland.

ISO. 1995b. Water quality - detection and enumeration of bacteriophages. In: Part 1: enumeration of F-specific RNA bacteriophages. Geneva, Switzerland: International Organisation of Standardization.

Israelachvili JN. 1985. Intermolecular and Surface Forces: With Applications to Colloidal and Biological Systems: Academic Press.

Jacangelo JG, Adham SS, Laine J-M. 1995. Mechanism of Cryptosporidium, Giardia, and MS2 Virus Removal by MF and UF. Journal of Americal Water Works Association 87:107-121.

Jacangelo JG, Laine J-M, Carns KE, Cummings EW, Mallevialle J. 1991. Low-pressure membrane filtration for removing Giardia and microbial indicators. Journal of Americal Water Works Association 83:97-106.

Jacangelo JG, Madec A, Schwab KJ, Huffman DE, Mysore CS. 2005. Advances in the use of low-pressure, hollow fiber membranes for the disinfection of water. Water Science and Technology: Water Supply 5:109-115.

Jin X, Hu J, Ong SL. 2010. Removal of natural hormone estrone from secondary effluents using nanofiltration and reverse osmosis. Water Research 44:638-648.

Kamide K, Iijima H. 1994. Recent advances in cellulose membranes. In: Gilbert RD, editor. Polymers, Blends and Composites. Munich: Carl Hanser Verlag. p 189-207.

Kelle Zeiher EH, Ho B, Williams KD. 2003. Novel antiscalant dosing control. Desalination 157:209-216.

Khouri H, Collin F, Bonnefont-Rousselot D, Legrand A, Jore D, Gardès-Albert M. 2004. Radical-induced oxidation of metformin. European Journal of Biochemistry 271:4745-4752.

Kim YK, Lee SY, Kim DH, Lee BS, Nam SY, Rhim JW. 2010. Preparation and characterization of thermally crosslinked chlorine resistant thin film composite polyamide membranes for reverse osmosis. Desalination 250:865-867.

Kimura K, Amy G, Drewes JE, Heberer T, Kim T-U, Watanabe Y. 2003. Rejection of organic micropollutants (disinfection by-products, endocrine disrupting compounds, and pharmaceutically active compounds) by NF/RO membranes. Journal of Membrane Science 227:113-121.

Kiso Y, Nishimura Y, Kitao T, Nishimura K. 2000. Rejection properties of non-phenylic pesticides with nanofiltration membranes. Journal of Membrane Science 171:229-237.

Kiso Y, Sugiura Y, Kitao T, Nishimura K. 2001. Effects of hydrophobicity and molecular size on rejection of aromatic pesticides with nanofiltration membranes. Journal of Membrane Science 192:1-10.

Kitis M, Lozier JC, Kim J-H, Mi B, Marinas BJ. 2003a. Microbial removal and integrity of RO and NF membranes. Journal AWWA 95:105-119.

Kitis M, Lozier JC, Kim JH, Mi B, Marinas BJ. 2003b. Microbial removal and integrity monitoring of RO and NF membranes. Journal of Americal Water Works Association 95:105-119.

Kitis M, Lozier JC, Kim JH, Mi B, Mariñas BJ. 2003c. Evaluation of biologic and non-biologic methods for assessing virus removal by and integrity of high pressure membrane systems. In. p 81-92.

Kochany J, Maguire RJ. 1994. Sunlight photodegradation of metolachlor in water. Journal of Agricultural and Food Chemistry 42:406-412.

Košutić K, Kaštelan-Kunst L, Kunst B. 2000. Porosity of some commercial reverse osmosis and nanofiltration polyamide thin-film composite membranes. Journal of Membrane Science 168:101-108.

Kruithof JC, Kamp PC, Folmer HC, Nederlof MM, Van Hoof SCJM. 2001a. Development of a membrane integrity monitoring strategy for the UF/RO Heemskerk drinking water treatment plant. In. p 261-271.

Kruithof JC, Kamp PC, Folmer HC, Nederlof MM, Van Hoof SCJM. 2001b. Development of a membrane integrity monitoring strategy for the UF/RO Heemskerk drinking water treatment plant. Water Science and Technology: Water Supply 1:261-271.

Kruithof JC, Kamp PC, Folmer HC, Nederlof MM, Van Hoof SCJM. 2001c. Development of a membrane integrity monitoring strategy for the UF/RO Heemskerk drinking water treatment plant. Water Science and Technology: Water Supply 1:261-271.

Kumar M, Adham S, DeCarolis J. 2007. Reverse osmosis integrity monitoring. Desalination 214:138-149.

Kwon Y-N, Leckie JO. 2006. Hypochlorite degradation of crosslinked polyamide membranes. Journal of Membrane Science 283:21-26.

Langlet J, Gaboriaud F, Duval JFL, Gantzer C. 2008a. Aggregation and surface properties of F-specific RNA phages: Implication for membrane filtration processes. Water Research 42:2769-2777.

Langlet J, Gaboriaud F, Gantzer C, Duval JFL. 2008b. Impact of Chemical and Structural Anisotropy on the Electrophoretic Mobility of Spherical Soft Multilayer Particles: The Case of Bacteriophage MS2. Biophysical Journal 94:3293-3312.

Lapworth DJ, Kinniburgh DG. 2009. An R script for visualising and analysing fluorescence excitation–emission matrices (EEMs). Computers & Geosciences 35:2160-2163.

Lawaetz AJ, Stedmon CA. 2009. Fluorescence Intensity Calibration Using the Raman Scatter Peak of Water. Applied Spectroscopy 63:936-940.

Lawler W, Antony A, Cran M, Duke M, Leslie G, Le-Clech P. 2013. Production and characterisation of UF membranes by chemical conversion of used RO membranes. J Membr Sci 447:203-211.

Lee J-H, Chung JY, Chan EP, Stafford CM. 2013. Correlating chlorine-induced changes in mechanical properties to performance in polyamide-based thin film composite membranes. Journal of Membrane Science 433:72-79.

Leenheer JA, Croue JP. 2003. Characterizing dissolved aquatic organic matter. Environmental Science and Technology January 1:19A-26A.

Li Q, Song J, Yu H, Li Z, Pan X, Yang B. 2014. Investigating the microstructures and surface features of seawater RO membranes and the dependencies of fouling resistance performances. Desalination 352:109-117.

Linge KL, Blair P, Busetti F, Rodriguez C, Heitz A. 2012. Chemicals in reverse osmosis-treated wastewater: occurrence, health risk and contribution to residual dissolved organic carbon. Journal of Water Supply: Research and Technology - AQUA 61:494-505.

López-Muñoz MJ, Sotto A, Arsuaga JM, Van der Bruggen B. 2009. Influence of membrane, solute and solution properties on the retention of phenolic compounds in aqueous solution by nanofiltration membranes. Separation and Purification Technology 66:194-201.

Lovins III WA, Taylor JS, Hong SK. 2002. Micro-organism rejection by membrane systems. Environmental Engineering Science 19:453-465.

Lovins WA, Taylor JS, Hong SK. 2002. Micro-Organism Rejection by Membrane Systems. Environmental Engineering Science 19:453-465.

Lozier J, Kitis M, Colvin CK, Kim J-H, Mi B, Marinas B. 2004. Microbial Removal and Integrity Monitoring of High-Pressure Membranes. In: IWA Publishing.

Lozier JC, Kitis M, Colvin CK, Kim JH, Mi B, Marinas BJ. 2003. Microbial removal and integrity monitoring in high-pressure membranes. Denver, CO: AWWA research foundation.

Lukasik J, Scott TM, Andryshak D, Farrah SR. 2000. Influence of Salts on Virus Adsorption to Microporous Filters. Applied and Environmental Microbiology 66:2914-2920.

Lytle CD, Routson LB. 1995. Minimized virus binding for tests of barrier materials. Applied and Environmental Microbiology 61:643-649.

Macca C, Wang J. 1995. Experimental Procedures for the Determination of Amperometric Selectivity Coefficients. Anal Chim Acta 303:265-274.

Madireddi K, Babcock Jr RW, Levine B, Huo TL, Khan E, Ye QF, Neethling JB, Suffet IH, Stenstrom MK. 1997a. Wastewater reclamation at Lake Arrowhead, California: An overview. Water Environment Research 69:350-362.

Madireddi K, Babcock RW, Levine J, B. , Huo L, Khan E, Ye QF, Neethling JB, Suffet IH, Stenstrom MK. 1997b. Wastewater reclamation at Lake Arrowhead, California: an overview. Water Environment Research 69:350-362.

Maruf SH, Ahn DU, Pellegrino J, Killgore JP, Greenberg AR, Ding Y. 2012. Correlation between barrier layer Tg and a thin-film composite polyamide membrane's performance: Effect of chlorine treatment. Journal of Membrane Science 405-406:167-175.

Mas-Montoya M, Cuartero M, Curiel D, Ortuno JA, Soledad Garcia M, Tarraga A. 2015. Binding studies and anion-selective electrodes with neutral isophthalamide-based receptors. Analyst 140:287-294.

Mattaraj S, Phimpha W, Hongthong P, Jiraratananon R. 2010. Effect of operating conditions and solution chemistry on model parameters in crossflow reverse osmosis of natural organic matter. Desalination 253:38-45.

Meares P. 1976. The physical chemistry of transport and separation by membranes. In: Meares P, editor. Membrane Separation Processess. Amsterdam: Elsevier.

Mi B, Eaton CL, Kim JH, Colvin CK, Lozier JC, Marinas BJ. 2004. Removal of biological and non-biological viral surrogates by spiral-wound reverse osmosis membrane elements with intact and compromised integrity. Water Research 38:3821-3832.

Michen B, Graule T. 2010. Isoelectric points of viruses. Journal of Applied Microbiology 109:388-397.

Murphy KR, Butler KD, Spencer RGM, Stedmon CA, Boehme JR, Aiken GR. 2010. Measurement of Dissolved Organic Matter Fluorescence in Aquatic Environments: An Interlaboratory Comparison. Environmental Science and Technology 44:9405-9412.

MWH. 2007. City of San Diego Advanced Water Treatment Research Studies. In: MWH, editor.

Negaresh E, Antony A, Cox S, Lucien FP, Richardson DE, Leslie G. 2013. Evaluating the impact of recycled fiber content on effluent recycling in newsprint manufacture. Chemosphere 92:1513-1519.

Nghiem LD, Schäfer AI, Elimelech M. 2005. Pharmaceutical retention mechanisms by nanofiltration membranes. Environmental Science and Technology 39:7698-7705.

NHMRC, NRMMC. 2011. Australian Drinking Water Guidelines 6. In: National Health and Medical Research Council NRMMC, editor. Version 3.0 Updated December 2014. Canberra: Commonwealth of Australia,.

NRMMC, EPHC, NHMRC. 2006. Australian guidelines for water recycling: Managing health and environmental risks (phase 1). In. Canberra, Australia: Biotext Pty Ltd.

NRMMC, EPHC, NHMRC. 2008. Australian guidelines for water recycling: managing health and environmental risks (phase 2). Augmentation of water supplies. In. Canberra, Australia: Biotext Pty Ltd.

Ochando-Pulido JM, Rodriguez-Vives S, Hodaifa G, Martinez-Ferez A. 2012. Impacts of operating conditions on reverse osmosis performance of pretreated olive mill wastewater. Water Research 46:4621-4632.

Ong SL, Zhou W, Song L, Ng WJ. 2002. Evaluation of feed concentration effects on salt/ion transport through RO/NF membranes with the Nernst-Planck-Donnan model. Environmental Engineering Science 19:429-439.

Onwuegbuzie AJ, Daniel L, Leech NL. 2007. Pearson Product-Moment Correlation Coefficient. In: Salkind. NJ, editor. Encyclopedia of Measurement and Statistics. Thousand Oaks, CA: SAGE Reference. p 750-755.

Ottoson J, Hansen A, Björlenius B, Norder H, Stenström TA. 2006. Removal of viruses, parasitic protozoa and microbial indicators in conventional and membrane processes in a wastewater pilot plant. Water Research 40:1449-1457.

Overby LR, Barlow GH, Doi RH, Jacob M, Spiegelman S. 1966. Comparison of two serologically distinct ribonucleic acid bacteriophages. I. Properties of the viral particles. Journal of Bacteriology 91:442-448.

Peeters JMM, Boom JP, Mulder MHV, Strathmann H. 1998. Retention measurements of nanofiltration membranes with electrolyte solutions. Journal of Membrane Science 145:199-209.

Peiris RH, Budman H, Moresoli C, Legge RL. 2010a. Understanding fouling behaviour of ultrafiltration membrane processes and natural water using principal component analysis of fluorescence excitation-emission matrices. Journal of Membrane Science 357:62-72.

Peiris RH, Hallé C, Budman H, Moresoli C, Peldszus S, Huck PM, Legge RL. 2010b. Identifying fouling events in a membrane-based drinking water treatment process using principal component analysis of fluorescence excitation-emission matrices. Water Research 44:185-194.

Penrod SL, Olson TM, Grant SB. 1995. Whole Particle Microelectrophoresis for Small Viruses. Journal of Colloid and Interface Science 173:521-523.

Petersen RJ. 1993. Composite reverse osmosis and nanofiltration membranes. Journal of Membrane Science 83:81-150.

Polatides C, Dortsiou M, Kyriacou G. 2005. Electrochemical removal of nitrate ion from aqueous solution by pulsing potential electrolysis. Electrochim Acta 50:5237-5241.

Pontius FW, Crimaldi JP, Amy GL. 2011. Virus passage through compromised low-pressure membranes: A particle tracking model. Journal of Membrane Science 379:249-259.

Portillo M. 2015. Monitoring reverse osmosis membrane integrity for direct potable reuse applications. In: WateReuse conference. Texas, USA: WateReuse.

Pype M-L. 2013a. Monitoring reverse osmosis membrane integrity and virus rejection in water reuse. In: The university of Queensland and Université de Montpellier II. p 200.

Pype M-L. 2013b. Monitoring reverse osmosis membrane integrity and virus rejection in water reuse. In: School of Chemical Engineering & Ecole Doctorale Science des Procédés – Science des Aliments: The University of Queensland (Australia) & Université de Montpellier II (France). p 199.

Pype M-L, Patureau D, Wery N, Poussade Y, Gernjak W. 2013. Monitoring reverse osmosis performance: Conductivity versus fluorescence excitation–emission matrix (EEM). Journal of Membrane Science 428:205-211.

R Regel CH, A Keegan. 2012. Full-scale MS2 testingof the Glenelg RWTP UF membrane process. Water Journal 1:69.

Sarmiento Tagle MG, Salum ML, Buján EI, Argüello GA. 2005. Time evolution and competing pathways in photodegradation of trifluralin and three of its major degradation products. Photochemical and Photobiological Sciences 4:869-875.

Shan JH, Hu JY, Ong SL. 2009. Adsorption of neutral organic fractions in reclaimed water on RO/NF membrane. Separation and Purification Technology 67:1-7.

Sharma RR, Agrawal R, Chellam S. 2003. Temperature effects on sieving characteristics of thin-film composite nanofiltration membranes: pore size distributions and transport parameters. Journal of Membrane Science 223:69-87.

Sharma RR, Chellam S. 2006. Temperature and concentration effects on electrolyte transport across porous thin-film composite nanofiltration membranes: Pore transport mechanisms and energetics of permeation. Journal of Colloid and Interface Science 298:327-340.

Shields PA, Farrah SR. 1987. Determination of the electrostatic and hydrophobic character of enteroviruses and bacteriophages. In: Proceedings of the 87th Annual Meeting on American Society of Microbiology Washington.

Simon AR. 2014. Effects of hypochlorite exposure on morphology and trace organic. Univeristy of Wollongong.

Singh S, Henderson RK, Baker A, Stuetz RM, Khan SJ. 2009. Distinguishing stage 1 and 2 reverse osmosis permeates using fluorescence spectroscopy. Water Science and Technologie 60:2017-2023.

Singh S, Henderson RK, Baker A, Stuetz RM, Khan SJ. 2012. Characterisation of reverse osmosis permeates from municipal recycled water systems using fluorescence spectroscopy: Implications for integrity monitoring. Journal of Membrane Science 421–422:180-189.

Smart PL, Laidlaw IMS. 1977. An evaluation of some fluorescent dyes for water tracing. Water Resources Research 13:15-33.

Soice NP, Greenberg AR, Krantz WB, Norman AD. 2004a. Studies of oxidative degradation in polyamide RO membrane barrier layers using pendant drop mechanical analysis. Journal of Membrane Science 243:345-355.

Soice NP, Greenberg AR, Krantz WB, Norman AD. 2004b. Studies of oxidative degradation in polyamide RO membrane barrier layers using pendant drop mechanical analysis. J Membr Sci 243:345-355.

Soice NP, Maladono AC, Takigawa DY, Norman AD, Krantz WB, Greenberg AR. 2003. Oxidative degradation of polyamide reverse osmosis membranes: Studies of molecular model compounds and selected membranes. J Appl Polym Sci 90:1173-1184.

Sorber CA, Malina JF, Sagik BP. 1972. Virus rejection by the reverse osmosis-ultrafiltration processes. Water Research 6:1377-1388.

Spiegler KS, Kedem O. 1966. Thermodynamics of hyperfiltration (reverse osmosis): criteria for efficient membranes. Desalination 1:311-326.

Spinelli S, Gonzalez C, Thomas O. 2007. Chapter 11 UV spectra library. In: Techniques and Instrumentation in Analytical Chemistry. p 267-356.

Steinle-Darling E, Salveson A, Sutherland J, Yoon SH, Morrison C. 2015. Online integrity monitoring for reverse osmosis in potable reuse. In: Worldwater Water Reuse & Desalination. London, UK: WEF. p 16-18, 33.

Strutwolf J, Arrigan DWM. 2010. Optimisation of the conditions for stripping voltammetric analysis at liquid-liquid interfaces supported at micropore arrays: a computational simulation. Anal Bioanal Chem 398:1625-1631.

Surawanvijit S, Thompson J, Rahardianto A, Frenkel V, Cohen Y. 2015. Pulsed marker method for real-time detection of reverse osmosis membrane integrity loss. Desalination 370:25-32.

Tang CY, Kwon Y-N, Leckie JO. 2009. Effect of membrane chemistry and coating layer on physiochemical properties of thin film composite polyamide RO and NF membranes: I. FTIR and XPS characterization of polyamide and coating layer chemistry. Desalination 242:149-167.

Tang JYM, Busetti F, Charrois JWA, Escher BI. 2014. Which chemicals drive biological effects in wastewater and recycled water? Water Res 60:289-299.

Tansel B, Sager J, Rector T, Garland J, Strayer RF, Levine L, Roberts M, Hummerick M, Bauer J. 2006. Significance of hydrated radius and hydration shells on ionic permeability during nanofiltration in dead end and cross flow modes. Separation and Purification Technology 51:40-47.

Tödtheide V, Laufenberg G, Kunz B. 1997. Waste water treatment using reverse osmosis: real osmotic pressure and chemical functionality as influencing parameters on the retention of carboxylic acids in multi-component systems. Desalination 110:213-222.

Tsai AG, Wadden TA, Berkowitz RI. 2006. Pharmacotherapy for overweight adolescents. Obesity Management 2:98-102.

Tu KL, Nghiem LD, Chivas AR. 2010. Boron removal by reverse osmosis membranes in seawater desalination applications. Separation and Purification Technology 75:87-101.

UNESCO, WRQA. 2009. Virus particle removal by membrane based water recycling plants: Development of testing protocols and understanding long-term operational performance. Phase1: Literature review. In.

Urase T, Yamamoto K, Ohgaki S. 1994. Effect of pore size distribution of ultrafiltration membranes on virus rejection in crossflow conditions. Water Science and Technology 30:199-208.

Urase T, Yamamoto K, Ohgaki S. 1996. Effect of pore structure of membranes and module configuration on virus retention. Journal of Membrane Science 115:21-29.

USEPA. 2005a. Membrane filtration guidance manual. In: EPA.815-R-06-009. Cincinnati, OH: United States Environmental Protection Agency.

USEPA. 2005b. Membrane Filtration Guidance Manual. EPA815-R-09-009.

Uyak V, Koyuncu I, Oktem I, Cakmakci M, Toroz I. 2008. Removal of trihalomethanes from drinking water by nanofiltration membranes. Journal of Hazardous Materials 152:789-794.

Valent O, Koryta J, Panoch M. 1987. Voltammetric study of ion transfer across the water/o-nitrophenyloctyl ether interface: Part I. Reversible process. Journal of Electroanalytical Chemistry and Interfacial Electrochemistry 226:21-25.

Van Buynder P, Lugg R, Rodriguez C, Bromley M, Filmer J, Blair P, Handyside M, Higginson S, Turner N, Lord O, Taylor P, Courtney K, Newby C, Heitz A, Linge K, Blythe J, Busetti F, Toze S. 2009a. Premier's Collaborative Research Program (2005-2008): Characterising Treated Wastewater For Drinking Purposes Following Reverse Osmosis Treatment. Technical Report. In: Department of Health, Western Australia. p 370.

Van Buynder P, Lugg R, Rodriguez C, Bromley M, Filmer J, Blair P, Handyside M, Higginson S, Turner N, Lord O, Taylor P, Courtney K, Newby C, Heitz A, Linge K, Blythe J, Busetti F, Toze S. 2009b. Premier's Collaborative Research Program (2005–2008). Characterising Treated Wastewater For Drinking Purposes Following Reverse OsmosisTreatment. In: Technical Report. Western Australia: Department of Health.

Van der Bruggen B, Schaep J, Maes W, Wilms D, Vandecasteele C. 1998. Nanofiltration as a treatment method for the removal of pesticides from ground waters. Desalination 117:139-147.

Van der Bruggen B, Schaep J, Wilms D, Vandecasteele C. 1999. Influence of molecular size, polarity and charge on the retention of organic molecules by nanofiltration. Journal of Membrane Science 156:29-41.

van Voorthuizen EM, Ashbolt NJ, Schäfer AI. 2001. Role of hydrophobic and electrostatic interactions for initial enteric virus retention by MF membranes. Journal of Membrane Science 194:69-79.

Vasudevan D, Fimmen RL, Francisco AB. 2001. Tracer-Grade Rhodamine WT: Structure of Constituent Isomers and Their Sorption Behavior. Environmental Science & Technology 35:4089-4096.

VDoH. 2013. Guidelines for validating treatment processes for pathogen reduction. Supporting Class A recycled water schemes in Victoria. In: State of Victoria DoH, editor. Melbourne: Victorian Government.

Walrafen GE, Hokmabadi MS, Holmes NC. 1986. Raman spectrum and structure of thermally treated silica aerogel. The Journal of Chemical Physics 85:771-776.

Wang D-X, Su M, Yu Z-Y, Wang X-L, Ando M, Shintani T. 2005. Separation performance of a nanofiltration membrane influenced by species and concentration of ions. Desalination 175:219-225.

Wiesner MR, Buckley CA. 1996. Principles of rejection in pressure driven membrane process. New York: McGraw Hill.

Wilf M, editor. 2010. The Guidebook to Membrane Technology for Wastewater Reclamation.

Williams ME. 2003. A Review of Reverse Osmosis Theory. In. http://www.eetcorp.com/heepm/RO_TheoryE.pdf: Williams Engineering Services Company, Inc.

Williams ME, Hestekin JA, Smothers CN, Bhattacharyya D. 1999. Separation of Organic Pollutants by Reverse Osmosis and Nanofiltration Membranes: Mathematical Models and Experimental Verification. Industrial & Engineering Chemistry Research 38:3683-3695.

Xu J, Wang Z, Wei X, Yang S, Wang J, Wang S. 2013. The chlorination process of crosslinked aromatic polyamide reverse osmosis membrane: New insights from the study of self-made membrane. Desalination 313:145-155.

Zazpe R, Hibert C, O'Brien J, Lanyon YH, Arrigan DWM. 2007. Ion-transfer voltammetry at silicon membrane-based arrays of micro-liquid-liquid interfaces. Lab Chip 7:1732-1737.

Zornes GE, Jansen E, Lozier JC. 2010. Validation testing of the reverse osmosis system at Gippsland water factory. In: WRA conference. Sydney, Australia: WateReuse Association.